# Development of a Unified Lipidomics LC-$MS^2$ Method with Automated Online Extraction

---

Dissertation

zur

Erlangung der naturwissenschaftlichen Doktorwürde
(Dr. sc. nat.)

vorgelegt der

Mathematisch-naturwissenschaftlichen Fakultät

der

Universität Zürich

von

**Regula Andrea Steiner**

von

Schwyz SZ und Dietikon ZH

**Promotionskommission**

Prof. Dr. Arnold von Eckardstein (Vorsitz, Leitung der Dissertation)
Prof. Dr. Thorsten Hornemann
Prof. Dr. Michael Arand
Prof. Dr. Bruno Stieger
Prof. Dr. Nicola Zamboni

**Zürich, 2018**

# Table of content

# I Zusammenfassung

Die *de novo* Synthese von Sphingolipiden startet mit der Konjugation von L-Serin und Palmitoyl-CoA durch die Serin-Palmitoyltransferase (SPT). SPT kann unter gewissen Bedingungen auch kürzere und längere Fettsäure-CoA ($C_{12}$ bis $C_{18}$) sowie auch andere Aminosäuren verstoffwechseln, was zur Bildung einer Reihe von atypischen Sphingolipiden führt. Im Speziellen kann SPT auch L-Alanin oder Glycin verwenden, was zur Bildung von 1-Deoxysphingolipiden respektive 1-Deoxymethylsphingolipiden führt. Mehrere Mutationen in der SPT sind mit der hereditären sensorischen und autonomen Neuropathie Typ 1 (HSAN1) assoziiert, welche zu einer permanenten Verschiebung der Substratspezifität von L-Serin zu L-Alanin und Glycin führt, was in einer erhöhten Produktion von 1-Deoxysphingolipiden und 1-Deoxymethylsphingolipiden resultiert. 1-Deoxysphingolipiden und 1-Deoxymethylsphingolipiden fehlt die $C_1$-Hydroxylgruppe der Sphingolipide und sie können darum weder im kanonischen Stoffwechselweg weiter verstoffwechselt noch abgebaut werden. Darum werden 1-Deoxysphingolipide und 1-Deoxymethylsphingolipide typischerweise als metabolische Sackgasse angesehen, wobei sonst wenig über deren Metabolismus bekannt ist.

Während dieser Promotionsarbeit haben wir uns auf zwei Aspekte der Sphingolipidbiologie fokussiert. Auf der einen Seite haben wir die Struktur von atypischen 1-Deoxysphingosine charakterisiert und den Metabolismus von 1-Deoxymethylsphingolipiden studiert. Auf der anderen Seite haben wir eine Flüssig-Chromatographie-Methode gekoppelt mit Massenspektrometrie (LC-MS) für die Detektion und Quantifizierung von typischen und atypischen Sphingolipiden entwickelt und validiert sowie die Möglichkeit für die Nutzung einer online-Probenextraktion von Sphingolipiden mit turbulenter Flüssigchromatographie ausprobiert.

In Kapitel eins haben wir gezeigt, dass die Position der Doppelbindung im nativen 1-Deoxysphingosine bei (14*Z*) ist und nicht wie beim kanonischen Sphingosine bei (4*E*), was zu einer anderen Struktur im Grundgerüst von 1-Deoxysphingosine führt. Darum haben wir über die Existenz einer weiteren Sphingolipid Desaturase spekuliert, die im Stoffwechsel von

Sphingolipiden involviert ist. Im Kapitel zwei haben wir den Stoffwechsel von 1-Deoxymethylsphingolipiden genauer untersucht. Neben den schon bekannten 1-Deoxymethylsphinganine und 1-Deoxymethylsphingosine, haben wir fünf weiter Abbauprodukte von 1-Deoxymethylsphinganine identifiziert. Mehrere Enzyme des kanonischen Sphingolipid-Stoffwechsels sind in der Bildung von ungesättigten (DES 1/2) oder mono-hydroxylierten (DES 2) Spezies involviert. Zudem werden 1-Deoxymethylsphingolipide über einen bis jetzt unbekannten Weg di-hydroxyliert, eine wohl für 1-Deoxymethylsphingolipide spezifische Reaktion.

Im Kapitel drei haben wir angeschaut, ob eine online-Extraktion mit turbulentem Fluss für eine effiziente Extraktion von Lipiden genutzt werden kann. Unsere Resultate legten nahe, dass eine online-Extraktion mit turbulentem Fluss für Lipide aus biologischen Proben nur von begrenztem Nutzen ist. Die online Extraktion zeigte eine tiefe Wiederfindungsrate zwischen 12 % (1-Deoxyceramide) und 93 % (S1P) für die verschiedenen Sphingolipidklassen im Vergleich zu den Standard flüssig-flüssig-Extraktionen für Lipide. Im vierten Kapitel zeigen wir eine LC-$MS^2$ Methode für die umfassende Analyse von Sphingolipiden (inkl. freie sphingoid Base, Ceramid, Sphingomyelin, Hexosylceramid und Sphingosin-1-Phosphat, aber auch die atypischen 1-Deoxysphingolipide) in verschiedenen Matrizen. Die Methode erlaubt auch eine Analyse von anderen Lipidklassen in der gleichen Messung, wie Glycerphospholipide oder Sterole.

Im fünften Kapitel haben wir die neu entwickelte Methode bei verschiedenen biomedizinischen Fragestellungen angewandt, was eine Validierung der Methode im biologischen Kontext ermöglichte. Als Erstes haben wir das Sphingolipidprofil in Plasmen von Patienten mit einer Mutation in der Sphingosin-1-Phosphat Lyase (SGPL1) analysiert. Diese Mutationen im SGPL1-Gen verursachen eine hereditäre sensorische Neuropathie, was eine bis jetzt unbekannte Verbindung zwischen dem gestörten Abbau von S1P und einer Neuropathie aufzeigt. Zweitens haben wir die Änderungen im Sphingolipidom in Plasmen von Mäusen nach einer Magen-Bypass-Operation untersucht. Weiter haben wir die Sphingolipide in ORMDL3 KO Mäusen untersucht. ORMDL3 fungiert als Aktivitätsregulator

des eukariotischen SPT-Komplexes und zeigt in genomweiten Assoziierungsstudien eine Korrelation mit Asthma. Als Letztes haben wir eine allgemeine Lipidanalyse in einem Mausmodell für altersbedingte Macula Degeneration (ADM) angewendet, um den Effekt der Lipidtransporter ABCA1 und ABCG1 und die damit verbundene Akkumulation von Lipiden im Augengewebe im Kontext der ADM zu betrachten.

Zusammenfassend haben wir Techniken der Flüssigchromatographie in Kombination mit Massenspektrometrie angewendet, um die Struktur von 1-Deoxysphingosine aufzuklären, den Stoffwechselweg von 1-Deoxymethlsphinganine zu bestimmen und eine LC-$MS^2$ Analysemethode entwickelt, mit welcher ein exaktes Sphingolipidprofil nicht nur für typische und relativ häufige Sphingolipide, sondern auch für atypische und seltene Sphingolipid-Spezies ermittelt werden kann.

# II Abstract

Sphingolipid *de novo* synthesis is initiated by the conjugation of L-serine and palmitoyl-CoA, a reaction catalysed by serine-palmitoyltransferase (SPT). Under certain conditions, SPT also metabolises other acyl-CoA ($C_{12}$ to $C_{18}$) and other amino acids, leading to the formation of a diverse group of atypical sphingolipids. Especially, SPT can use L-alanine but also glycine as alternative substrates, leading to atypical 1-deoxysphingolipids and 1-deoxymethylsphingolipids respectively. Several mutations in SPT are associated with hereditary sensory and autonomic neuropathy type 1 (HSAN1) that lead to a permanent shift in the substrate preference from L-serine to L-alanine and glycine resulting in increased production of 1-deoxysphingolipids and 1-deoxymethylsphingolipids. 1-Deoxysphingolipids lack the $C_1$ hydroxyl group and as such are not metabolized or degraded over the canonical sphingolipid pathway. Thus, 1-deoxysphingolipids and 1-deoxymethylsphingolipids have typically been regarded as “dead-end” metabolites with little else known about their metabolism.

During the course of my PhD thesis, we focused on two aspects of the sphingolipid biology. On one hand, we characterized the structure of the atypical 1-deoxysphingosine, as well as the metabolism of 1-deoxymethylsphingolipids. On the other hand, we developed and validated a liquid-chromatography and mass spectrometry (LC-MS) method to detect and quantify typical and atypical sphingolipids and elaborated the possibility of online sample extraction of sphingolipids using online turbulent flow chromatography.

In chapter one, we showed, that the double bond position of native 1-deoxysphingosine is at the (14*Z*) position, compared to the (4*E*) double bond of the canonical sphingosine, which results in a different backbone structure for 1-deoxysphingosine. Therefore, we speculated about the existence of another sphingoid base desaturase, involved in the metabolism of 1-deoxysphingolipids. In chapter two, we investigated the metabolism of 1-deoxymethylsphingolipids. Besides the already known 1-deoxymethylsphinganine and 1-deoxymethylsphingosine, we identified five novel downstream metabolites of 1-

deoxymethylsphinganine. Several enzymes of the canonical sphingolipid metabolism are involved in the formation of desaturated (DES 1/2) or mono-hydroxylated (DES 2) 1-deoxymethylsphingolipid species. Additionally, they are di-hydroxylated over a yet unknown pathway, which seems to be specific for 1-deoxymethylsphingolipid.

In chapter three, we investigated whether a turbulent flow online extraction system can be efficiently used for lipid extraction. Our results indicated that turbulent flow online extraction of lipids from biological samples is of limited use. The online extraction showed poor recovery, ranging from 12 % (1-deoxyceramides) to 93 % (S1P) for different sphingolipid classes compared to standard liquid-liquid extraction procedures. In chapter four, we report an LC-$MS^2$ method for a comprehensive analysis of sphingolipids (including free sphingoid base, ceramide, sphingomyelin, hexsosylceramide and sphingosine-1-phosphate, but also the atypical 1-deoxysphingolipids) in different matrices. The method also allows the analysis of other lipid classes such as glycerophospholipids or sterols within the same run.

In chapter five, we applied the newly developed method to several biomedical questions, which allowed validating the method in a biological context. First, we analysed the sphingolipid profile in plasma of patients with mutations in sphingosine-1-phosphate lyase (SGPL1). The mutations in the SGPL1 gene cause a hereditary sensory neuropathy, which showed a hitherto unknown connection between the degradation of S1P and neuropathy. Second, we studied the sphingolipidome in plasma of mice undergoing gastric bypass surgery. Further, we evaluated the sphingolipidome of ORMDL3 KO mice. ORMDL3 is an activity regulator of the eukaryotic SPT complex, which was linked to asthma in genome wide association studies. Finally, we applied an unbiased lipidomics approach to a mouse model for age-related macula degeneration (AMD) to study the effect of the lacking lipid transporters ABCA1 and ABCG1 on the accumulation of lipids in eye tissue of these mice.

In summary, we used liquid chromatography coupled to mass spectrometry techniques to elucidate the structure of 1-deoxysphingosine, unravel the metabolism of 1-deoxymethylsphinganine, and developed a LC-$MS^2$ for the comprehensive quantification of

sphingolipidome for not only typical and relatively abundant sphingolipids as well as the minor and atypical sphingolipid species.

# III Introduction

Derived from the Greek word 'lipos', which essentially means Fat, lipids are described as molecules of biological origin that are soluble in organic solvents, with only little to no solubility in water. The international lipid classification and nomenclature committee describes lipids as hydrophobic or amphiphilic molecules that may originate, entirely or in part by carbanion-based condensation of thio-ester and or by carbocation-based condensation of isoprene units [1, 2]. In reality, the lipids are a very diverse class of metabolites consisting of many sub-types, which are distinguished by physical and chemical properties as well as their source of synthesis and underlying chemical units. Evolutionary, delimiting lipid membranes ensured the integrity of cells as exchangeable functional units but also allowing the co-evolution of genetic material and the metabolic systems [3]. Lipids constitute one of the most abundant and diverse molecules in living organisms across all kingdoms of life. Lipids constitute about 50% of animal cell membranes, and are the most abundant small molecules found in human plasma [4]. Given their diverse physiological functions, this structural diversity of lipids is not surprising. As storage lipids, mainly in the form of triacylglycerol's, they form the most strongly concentrated source of energy. Phospholipids (PL), such as phosphatidylcholine and phosphoethanolamine are the major structural lipid components of eukaryotic membranes. These PL maintain the quasi-fluid state of the membranes and regulate protein functions [5]. Distinct sterols are the major non-polar lipid constituents of the cellular membranes in yeast, plants, and mammals, which mainly differ in desaturation and the position of methylation within the sterol nucleus [6]. Sphingolipids, on the other hand, contain a specific amino –alcohol backbone, which is amide linked to a fatty acid to form a ceramide. This ceramide can be modified, such as with phosphocholine to form sphingomyelin, or glycans to form glycosphingolipids [7]. Sphingomyelins associate with sterols to form ordered lipid domains within the plasma-membrane which are termed lipid rafts, which are essential for signal transduction, protein sorting and trafficking [8]. In addition to this, phosphorylated forms of sphingosine, (sphingosine-1-phosphate) and ceramide (ceramide-1-phosphate) are essential lipid signalling molecules which aid in cell survival and

apoptosis [9]. Although the combinatorial permutations of substrates allow the generations of tens of thousands of different lipid molecules, just close to a thousand have been identified in cells and membranes so far. The number of identified and characterized lipids is increasing by the time, due to the availability of better standards and the development of more sensitive detection methods [10]. There is still a need for further development.

## III.1 Lipid classification

The diverse group of lipids can be classified as hydrophobic or amphipathic small molecules that originate entirely or in part by carbanion-based condensations of ketoacyl subunits (as fatty acids, glycerolipids, glycerophospholipids, sphingolipids, saccharolipids and polyketides) and/or by carbocation-based condensations of isoprene subunits (sterol and prenol lipids) [1, 11]. The Lipid maps consortium published a classification system, where lipids can be classified as fatty acyls, glycerolipids, glycerophospholipids, sphingolipids, sterol lipids, prenol lipids, and saccharolipids [1, 11] (Figure I-1).

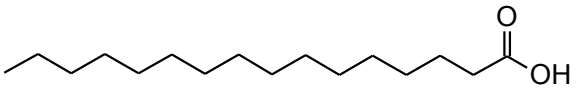

Fatty acid, palmitic acid (16:0)

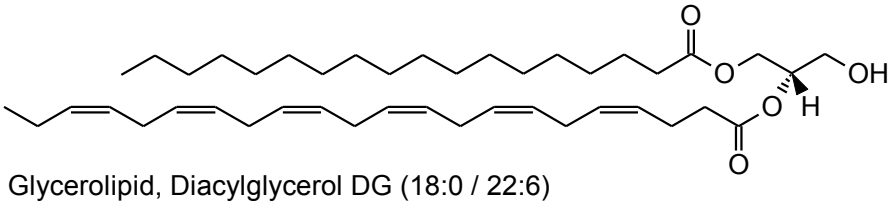

Glycerolipid, Diacylglycerol DG (18:0 / 22:6)

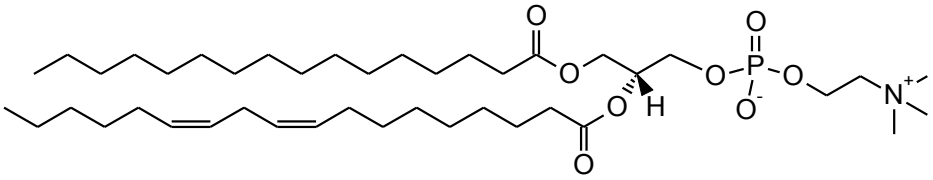

Glycerpphospholipid, Phosphatidylcholine PC (16:0 / 18:2)

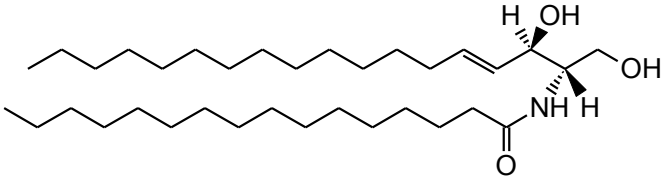

Sphingolipid, Ceramide (d18:1 / 16:0)

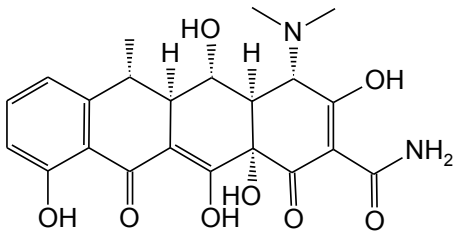

Polyketide, Doxycycline

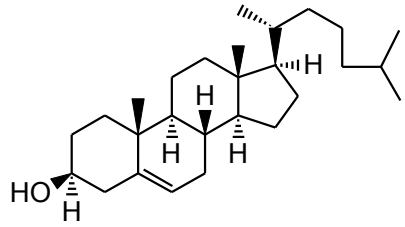

Sterol lipid, Cholesterol

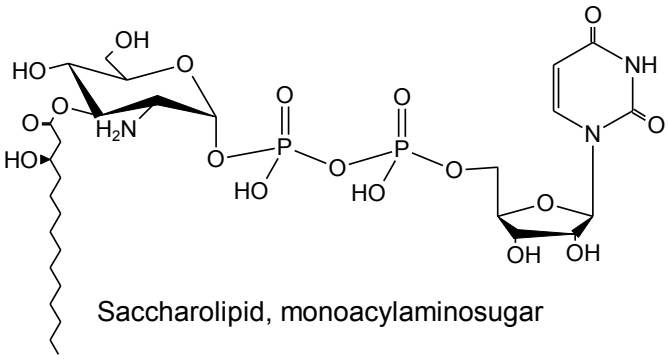

Saccharolipid, monoacylaminosugar

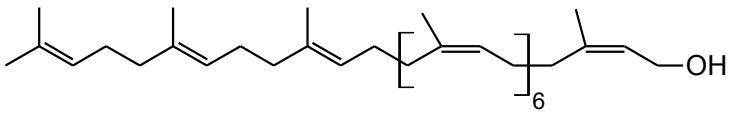

Prenol lipid, decaprenol

Figure I-1: Representative structures for each lipid category.

### III.1.1. Fatty Acids

The simplest lipids are free fatty acids. Commonly they are monocarboxylic acids with a long and unbranched hydrocarbon chains with a single carboxyl group at the end. Most of the fatty acids have an even number of carbon atoms between 14 and 22. This carbon chain can be saturated or desaturated, containing one or multiple double bonds, typically in a *cis* configuration. In polyunsaturated species, these double bonds are always separated by three carbons [12-15]. Fatty acids are significant sources of energy and essential building components of membrane lipids. They are either derived from food or are synthesized from acetyl-coenzyme A (acetyl-CoA) through complex sets of reactions. Intermediary products of glycolysis and citric acid cycle contribute to the formation of the backbone carbons of fatty acids and glycerols for the synthesis of lipids [16, 17].

Fatty acids represent the primary building block of complex lipids. For most of the complex lipids, one or multiple fatty acids are connected to a glycerol backbone by ester bounds. Because of the repetition of methylene groups, fatty acids are hydrophobic, and these hydrophobic properties are responsible for most of the characteristics of the more complex lipids [18, 19].

### III.1.2. Glycerolipids

The group of glycerolipids composes of all glycerol-linked lipids. Three different functional groups can be attached to the glycerol backbone, differentiating between neutral glycerolipids and glycerophospholipids [1].

Neutral glycerolipids are mostly acylglycerols, where fatty acids are esterified with a glycerol backbone, forming mono-, di- or triacylglycerol. These lipids are mainly used for energy storage [20-22]. Next to fatty acid linkage, also sugar residues can be conjugated over glycosidic linkage on the *sn*-3 position [23].

Glycerophospholipids consist of two fatty acids bound to a glycerol backbone (at the *sn-1* and *sn-2* position) and to a polar phosphate-containing head group attached to the third carbon of the glycerol backbone (*sn-3* position). With the phosphate group, other small

molecules such as choline, serine, ethanolamine or inositol can be conjugated leading to different subclasses of phospholipids, dependent on the head group attached. Phospholipids, therefore, have a hydrophobic tail and a hydrophilic head, which is an essential property for the formation of membranes [4, 24].

### III.1.3. Prenol lipids

The prenol lipids are subdivided primarily by biological function. Sterols, with cholesterol as the most studied species, are composed of four carbon rings instead of a linear carbon chain. Sterols are essential parts of biological membranes [25-27], whereas steroids (which also contain the same fused four-ring core structure) play a role as hormones and signalling molecules [28].

### III.1.4. Sphingolipids

Sphingolipids are not based on a glycerol backbone but a sphingoid base formed by the condensation of L-serine with a fatty acid [29]. The sphingoid base can be N-acetylated, and head groups like carbohydrates (glycosphingolipids) or phosphocholine (as in sphingomyelin) can be attached [30, 31].

Sphingolipids form the most heterogeneous lipid class with the largest number of different species [32]. Sphingolipids have been reported to play a role in senescence, inflammation, and apoptosis and are relevant for diseases like Alzheimer's, diabetes and atherosclerosis [33-37].

## III.2 Lipids in human plasma

The plasma lipidome consist of more than 500 lipid species distributed among six classes of lipids, including fatty acids, glycerolipids, glycerophospholipids, sphingolipids, and prenol lipids [32]. The number of identified species is so far limited by the sensitivity of available analytical technologies and will probably grow in the future with the advance of mass spectrometry. After sterol lipids, glycerophospholipids represent the second major component of the plasma lipidome, counting for ~32% of plasma lipids (Figure I-2A). Plasma glycerophospholipids comprise of more than 160 individual molecular species with the PCs and PEs being the most abundant lipids (Figure I-2B). In addition, plasma contains

considerable amounts of LPCs, LPEs and PIs as well as minor amounts of PC-derived and PE-derived plasmalogens [32]. Plasma sphingolipids comprise more than 200 molecular species. Total sphingolipids were determined about ~4% of total lipids in the plasma (Figure I-2A). This diversity results from the attachment of different sphingoid base backbones to different fatty acids to form diverse ceramides, which can be further combined with different head groups to form complex sphingolipids. Sphingomyelins (SM) are the major sphingolipids, representing ~95% of total sphingolipids, followed by Ceramides (Cer) (~3.5%) and monohexosylCeramides (hexCer) (<1%) (Figure I-2C) [32, 38]. Among the sphingoid bases, $C_{18}$ sphingosine is the most abundant backbone, representing ~60% of total sphingoid bases. $C_{18}$ Sphingadiene, $C_{18}$ Sphinganine and $C_{16}$ Sphingosine represent 20%, 10% and 10% respectively. Other sphingoid bases are present to a minor amount (< 5%) [4, 32]. 1-deoxysphingolipids (1-deoxySL) are present in the plasma of healthy individual but account for less than 1% of the total plasma sphingolipids [39, 40].

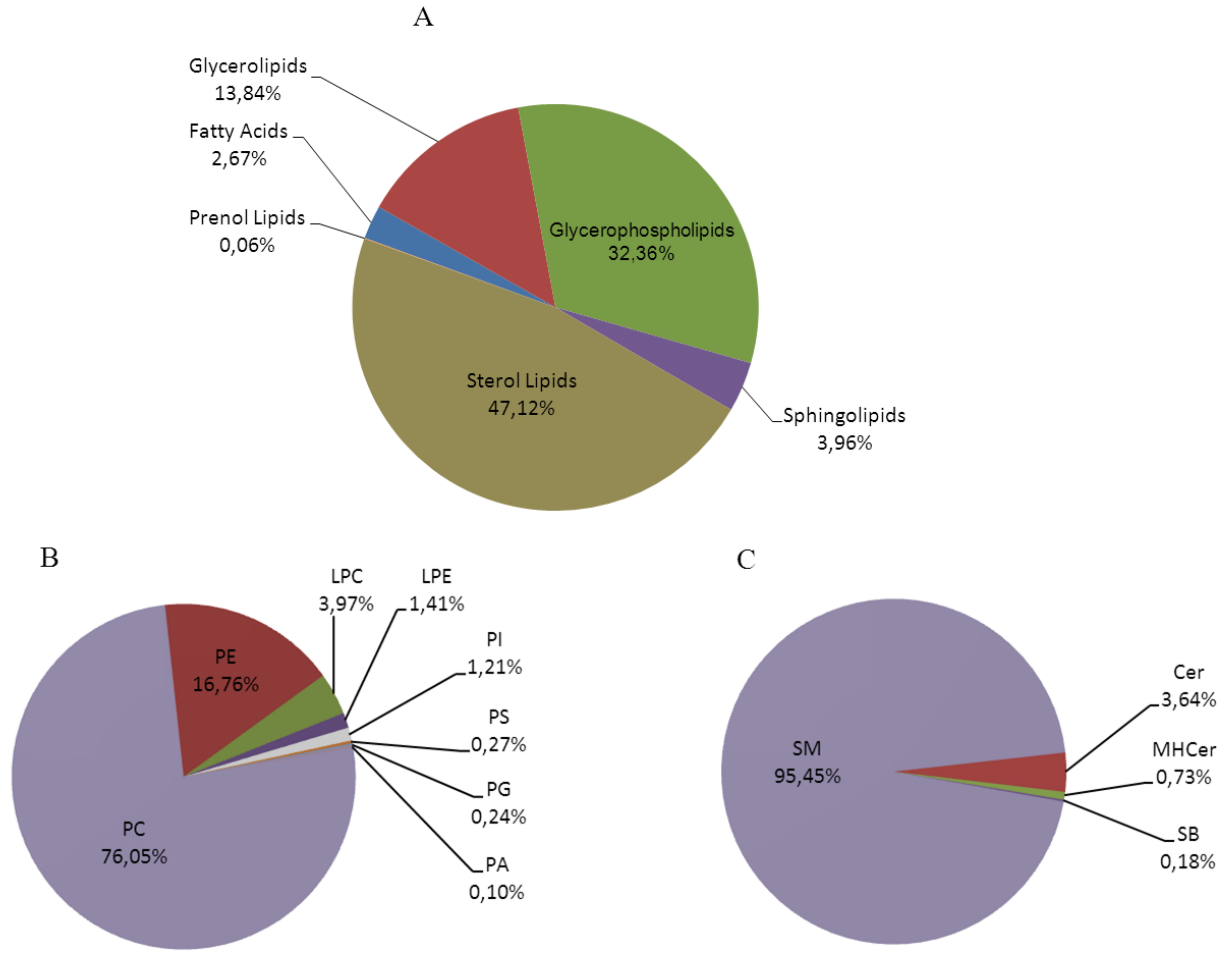


Figure I-2: A: Distribution of plasma lipids, B: glycerophospholipids and C: sphingolipids. The figure is reproduced from the data reported by Quehenberger and colleagues [32]. Cer stands for ceramide; MHCer, monohexosyl ceramide; LPC, lysophosphatidylcholine; LPE, lysophosphatidylethanolamine; PA, phosphatidic acid; PC, phosphatidylcholine; PE, phosphatidylethanolamine; PG, phosphatidylglycerol; PI, phosphatidylinositol; PS, phosphatidylserine; SB, sphingoid base; SM, sphingomyelin.

Plasma glycerophospholipids, triacylglycerol, sterols and sphingolipids are associated with lipoproteins [41-43]. Glycerophospholipids and sphingolipids are not equally distributed among different plasma lipoproteins. Specifically, high-density lipoproteins (HDL) carry larger proportions of PC, PE and PE-based plasmalogens [41, 43]. VLDL and LDL contain higher amounts of the plasma sphingomyelin and ceramides compared to HDL [38]. Interestingly, plasma 1-deoxySLs are found only in the VLDL and LDL but not in the HDL fraction of plasma of healthy subjects [39].

## III.3 Sphingolipid metabolism

### III.3.1. Canonical sphingolipids

*De novo* sphingolipid synthesis is initiated in the ER by the condensation of palmitoyl-CoA and L-serine, a reaction that is catalysed by Serine-Palmitoyltransferase (SPT) [44-46] (Figure I-3). This first reaction by SPT is the rate-limiting step in the biosynthesis of sphingolipids. SPT is a pyridoxal 5'-phosphate (PLP)-dependant enzymes in the subfamily of α-oxolamine synthases. SPT is a multimeric protein complex, consisting of three subunits, SPTLC1, SPTLC2 and SPTLC3 [44-48]. Besides the canonical substrates (L-serine and palmitoyl-CoA), SPT can also metabolize different acyl-CoA with chain lengths of $C_{12}$-$C_{18}$, as well as other amino acids like L-alanine or glycine, thereby forming a variety of atypical sphingolipid metabolites [34]. The reaction of L-serine with palmitoyl-CoA generates $C_{18}$ based sphingolipids, whereas the reaction with other acyl-CoA results in the formation of different chain length sphingolipids. With the use of L-alanine or glycine, atypical 1-deoxysphingolipids and 1-deoxymethylsphingolipids respectively are formed, which lack the $C_1$-hydroxyl group [40, 49, 50].

The condensation of L-serine with palmitoyl-CoA by SPT generates 3-ketosphinganine, which is rapidly reduced to sphinganine (SA) by the NADPH-dependant 3-keto-sphinganine reductase enzyme (KDHR) [51]. SA is N-acetylated by Ceramide synthase (CerS) to form dihydro-ceramides [52]. CerS is a family of six enzymes (CerS1-6) with different tissue distribution and specificities for certain fatty acid chain length as substrates [53]. The formed dihydro-ceramides are converted to ceramides by the introduction of a double bond at (4*E*) by the dihydroceramide Δ4-desaturase [54]. Dihydroceramide Δ4-desaturase is present in two isoforms, DES1 and DES2. DES1 primarily introduces the (4*E*) double bond. DES2 reacts in a two-step reaction forming phyto-sphingosine intermediate, a hydroxylated product at Δ4, and then, introduces a (4*E*) double bond as second step [55, 56]. All of these reactions in the *de novo* formation of sphingolipids take place in the ER. For further metabolism, ceramides have now to be transported from the ER to the Golgi compartment through vesicular or non-vesicular transport [57].

By the attachment of a phosphocholine group to the $C_1$ hydroxyl group of (dihydro-) ceramides, sphingomyelin synthase produces sphingomyelin [58, 59]. By the attachment of glucose and galactose to the $C_1$-hydroxy group, glycosphingolipids are formed by the ceramide-glucosyltransferase or ceramide-galactosyltransferase respectively. With the addition of further glucose or galactose molecules, more complex glycosphingolipids are built [60-64]. In the Golgi, but also in the ER, plasma membrane ceramides are converted into membrane sphingolipids, by the formation of complex phosphosphingolipids or catabolized in salvage pathways [57].

Catabolism of sphingolipids starts by the degradation of sphingomyelins and glycosphingolipids to ceramides. This process involves dedicated catabolic enzymes, such as glycohydrolases and sphingomyelinases that reside in the Nucleus, the ER, Golgi, and lysosomes. Sphingomyelins are degraded by the sphingomyelinases (SMase). Isoforms of SMase act in acidic, alkaline or neutral pH environment depending on their localization, pH optimum, and the microenvironment in the cell [31, 65-68.] Glycosphingolipids are degraded by the sequential removal of sugar molecules and are finally degraded to ceramides by glucosylceramidase [69]. Ceramides are deacylated by ceramidase to release a second sphingoid backbone, sphingosine (SO), which bears a double bond at (4*E*) compared to sphinganine [70-72]. Sphingosine is either recycled to ceramides by ceramide -synthase or phosphorylated at $C_1$ hydroxyl group by sphingosine kinase (SK1/SK2) [73-76]. S1P, once formed, can again be converted back to SO through the action of S1P phosphatases, (S1PPase 1/2), or hydrolyzed to trans-2-hexadecenal and ethanolamine phosphate in the ER by Sphingosine-1-Phosphate Lyase (SGPL1) [77, 78]. This last reaction is irreversible and the only exit point of the pathway.

Next, to the most abundant backbone structures, sphinganine (SA) and sphingosine (SO) and the low abundant backbone structure phyto-sphingosine, another backbone called sphingadiene, bearing two double bonds, is known for sphingolipids. Sphingadiene bears the sphingosine (4*E*) double bond and an additional double bond, which was reported to be at (14*Z*) in human plasma. This sphingadiene is the second most abundant backbone structure

found in human plasma. Although the structure of plasma sphingadiene was published in 1969 by Renkonen et al. the responsible enzyme for second double bond insertion at (14*Z*) is still unknown [79]. The complete metabolic pathway of sphingolipids can be seen in Figure I-3.

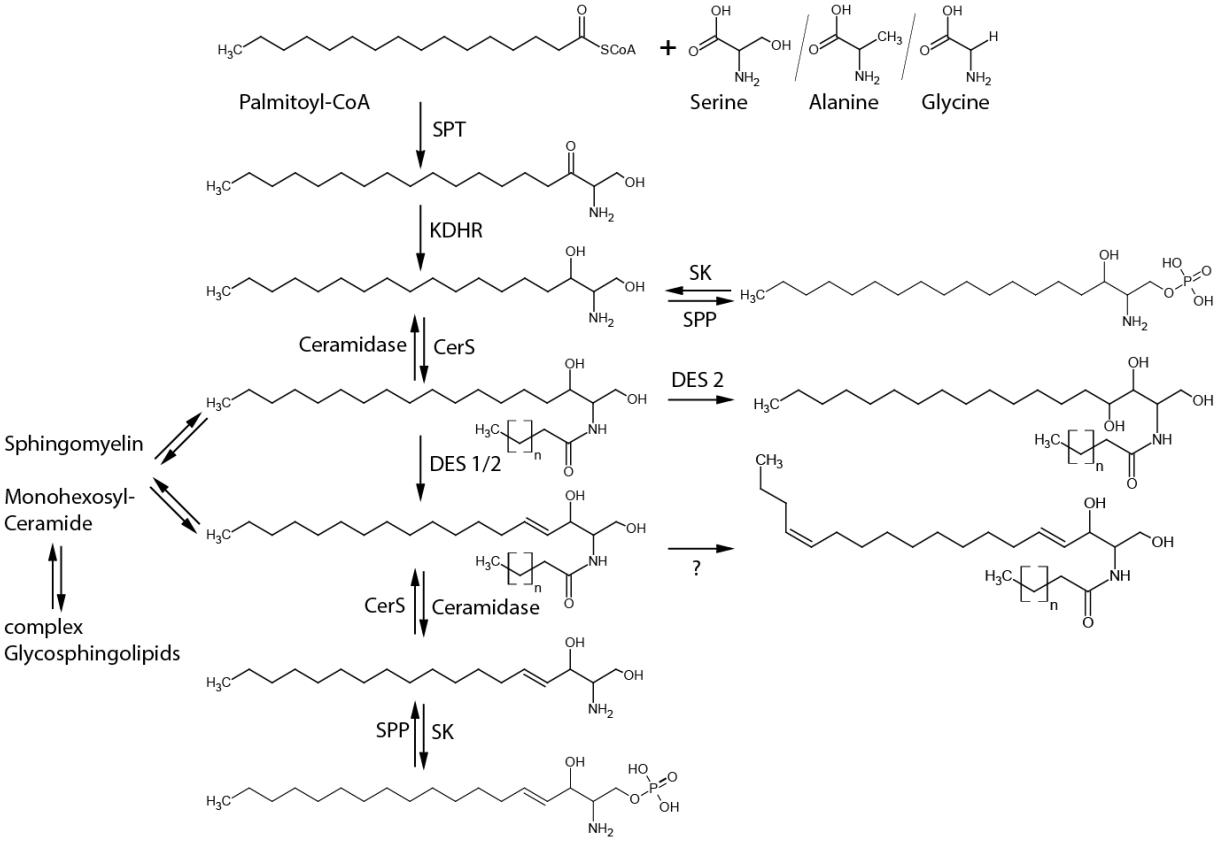


Figure I-3: Overview of sphingolipid metabolism with the essential enzymes and reactions in normal sphingolipid metabolism using the canonical substrates (L-serine and palmitoyl-CoA ). SPT: L-serine palmitoyltransferase, KDHR: 3-Ketodihydrosphingosine Reductase, CerS: ceramide synthase, DES: Dihydroceramide Δ4-desaturase, SK: sphingosine kinase, SPP: sphingosine phosphate phosphatase.

### III.3.2. Atypical chain length sphingolipids

Although palmitoyl-CoA is the preferred acyl-CoA for SPT, it can also use other acyl-CoAs in the condensation reaction. The use of myristoyl and stearoyl-CoA results in the formation of sphingolipids with $C_{16}$ and $C_{20}$ backbones, respectively, while the use of pentadecanoyl and heptadecanoyl-CoA gives rise to $C_{17}$ and $C_{19}$-based sphingolipids [49, 80, 81].

SPT is composed of the three subunits: SPTLC1 (53-kDa), SPTLC2 (63-kDa) and SPTLC3 (62-kDa). While SPTLC1 and SPTLC2 are ubiquitously expressed, SPTLC3 is restricted to

certain tissues primarily placenta, liver, heart, kidney and skin [48]. SPT it is believed to be an octameric complex with four SPTLC1/SPTLC2 or SPTLC1/SPTLC3 dimers forming a dynamic complex [47, 82]. Moreover, while SPTLC2 prefers palmitoyl-CoA, SPTLC3 can use $C_{14}$-$C_{18}$ acyl-CoAs [83]. Overexpression of SPTLC3 in HEK293 cells resulted in the generation of short-chain ($C_{16}$) and long chain ($C_{19}$, $C_{20}$) sphingoid bases [83].

### III.3.3. Atypical 1-deoxy-sphingolipids

In 2000, an atypical sphingoid base which lacked the $C_1$-hydroxyl group of canonical sphingolipids was isolated from the marine organism, *Spisula polynyma*, and was therefore named spisulosine [84]. This compound was found to be cytotoxic through inducing a characteristic loss of actin stress fibres [84] and was therefore tested as ES-285 in an experimental anticancer drug trial [85-87]. Interestingly, almost a decade letter, the same compound was identified in mammals, including humans, by two independent lines of study and was renamed as 1-deoxysphinganine (1-deoxySA) [40, 50].

Besides the canonical substrate L-serine and palmitoyl-CoA, SPT can use other acyl-CoA's as well as L-alanine or glycine as the substrates. The use of alternative amino acids generates a category of atypical 1-deoxysphingolipids (1-deoxySL) and 1-deoxymethylsphingolipids (1-deoxymethylSL) which lack the $C_1$-OH group of canonical sphingolipids [7, 50].

Several missense mutations in SPT that are associated with the rare inherited neuropathy HSAN1 (Hereditary sensory and autonomic neuropathy type 1) induce a permanent shift in the substrate specificity of the enzyme resulting in increased 1-deoxySL formation [40, 88]. Penno et al. [40] was the first who discovered 1-deoxySA and its downstream metabolites in the context of HSAN1. Since then, a number of mutations in the SPTLC1 and SPTLC2 subunits have been found to shift the substrate preference of SPT from L-serine to L-alanine and to cause the disease [40, 89-91].

HSAN1 is a rare autosomal and dominantly inherited axonopathy and clinically characterized by a progressive loss of pain and temperature sensation. It is often accompanied by

neuropathic pain attacks and skin ulcers [40]. Clinical symptoms start typically in the 2nd to 3rd decade of life with the loss of sensations for pain, temperature and vibration in the feet and hands. The disease is slowly progressing in a stocking-and-glove distribution. Sensory loss leads to ulcers and mutilations, which might require amputations. Positive sensory symptoms such as parasthesias or lancinating pain, motor or autonomic symptoms are also frequently present [92, 93] .

1-DeoxySL are toxic to primary sensory neurons in culture and lead to neurite retraction and the disruption of the neuronal cytoskeleton structure in a dose-dependent manner [40, 94]. They also interfere with the survival and insulin secretory capacity of pancreatic beta cells, and 1-deoxySL plasma levels have been found to be prospective biomarkers for the risk to develop type 2 diabetes mellitus (T2DM) [95-97]. Zitomer et al. [50] found that 1-deoxySA accumulates when cells in culture or animals are treated with the ceramide synthase inhibitor Fumonisin B1 (FB1). This lipid was shown to be produced by wild-type SPT, as the production of 1-deoxySA was not present in CHO-LYB cells which are lacking a functional SPT, but reappeared when the normal SPTLC1 subunit was restored [50]. Wild-type SPT can in fact produce considerable amounts of 1-deoxySA. After four days in culture, RAW264.7 cells had approximately equal levels of 1-deoxydihydroceramides (1-deoxyDHCer) and ceramides [98]. These cells are known to deplete L-serine in the medium while accumulating L-alanine [99].

So far, no explanation exists as to why SPT is not faithful to one amino acid. The side chain of L-alanine is smaller than the hydroxymethyl-group of L-serine, and could therefore fit into the same binding pocket. The side chain hydroxyl of L-serine interacts with the 5'- phosphate of the PLP domain, which appears to be optimal for both substrate binding and catalytic efficiency [100]. Interestingly, the SPT reaction interconnects lipid and amino acid metabolism, which is further upstream connected to carbohydrate metabolism. This connection suggests that metabolic changes in carbohydrate or fatty acid metabolism also influence sphingolipid formation [34].

1-Deoxysphinganine (1-deoxySA) can be converted to 1-deoxy-dihydroceramides (1-deoxy-DHCer). These 1-deoxy-dihydroceramides are desaturated to 1-deoxyceramides (1-deoxyCer) by the introduction of a double bond but not further converted to complex sphingolipids because of the missing $C_1$-OH group. During catabolism, 1-deoxyCer are degraded by ceramidase to form 1-deoxysphingosine (1-deoxySO) but cannot be phosphorylated to form the catabolic intermediate sphingosine-1-P (S1P). This prevents its cleavage to hexadecenal by S1P-lyase implying that 1-deoxySL cannot be degraded by the canonical catabolic pathway [50]. Apart from this, it was assumed that 1-deoxySA is metabolized by the same set of enzymes as canonical sphingoid bases [7].

## III.4 Principles of lipidomics

The term “omics” derives from Latin “ome” which means some or many. It refers to analytical methods which record a large number of analytes within one sample and within one process [101]. Lipidomics describes techniques to study the structure and function of the entire set of lipids (the lipidome) formed in a cell or organism. With lipidomics, interactions of lipids with other lipids, proteins, and metabolites are investigated. Lipidomics focuses specifically on the profiling of lipids, whereas metabolomics is typically an unbiased approach to measure metabolites and metabolic changes in biological systems [102].

### III.4.1. Lipidomics Workflow

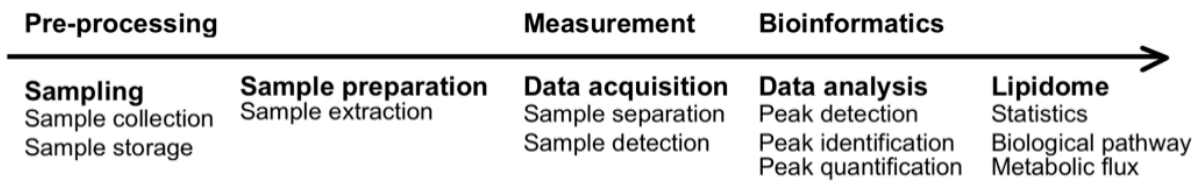


Figure I-4: A workflow for lipidomics analysis.

A lipidomics experiment consists of several steps, which are depicted in Figure I-4. The experimental design includes protocols for each step in the process, that is sample collection and storage, sample preparation and the data acquisition techniques (the actual measurement). After sample collection and storage, the sample needs to be processed for

the exact measurement. Lipids can be measured with mass spectrometry detectors either directly or after separation with different techniques such as thin-layer, gas- or liquid-chromatography [2]. Mass spectrometry-based tools are nowadays the most widely used technique for lipid profiling and quantification [103], as new developments like electrospray ionization and high-resolution accurate mass spectrometry allow the analysis of a broad set of lipids. Additionally, new bio-informatics tools have been developed and implemented for the analysis of the big datasets from mass spectrometry-based lipidomics [2].

### III.4.2. Sample preparation

The selection of the right preparation method is a critical step, as it can influence the observed lipid profile [104]. The goal of pre-treatment is to extract the analytes of interest without bias due to degradation or the introduction of contamination [105]. Sample pre-treatment targets the enrichment of analytes of interest and the removal of impurities, like proteins, salts, sugars, or amino acids, which interfere with the analysis. The solvent system should be capable of effectively extracting lipids representative of the sample under study without the mentioned biases. The performance of the lipid extraction for a given sample (tissue, cell, or fluid) with a particular solvent system depends on the partitioning of the different lipids between the polar and apolar phases of the extraction system used and consequently on the sample lipid composition [105]. For lipidomics studies, sample preparation techniques are required, which are reproducible, fast and therefore suitable for high throughput approaches, which cover a broad range of lipids with different polarities. At the same time, preparation methods need to be compatible with the instrument techniques used for the analysis [106]. Lipids in native samples are usually not in their free form but bound to proteins. Chromatographic separation techniques, which are commonly coupled to mass spectrometry analysis, do not tolerate proteins during the (lipid) analysis as they interact with the stationary phase, interfere with the retention of analytes, form precipitates blocking or binding analytes, and interfere with most of the detectors. Therefore, proteins have to be efficiently removed from the sample prior to the analysis with mass spectrometry [107].

Currently, several strategies are used, like simple protein precipitation, liquid-liquid extraction or solid phase extraction before LC-MS analysis [106, 108]. So far, all of these traditional extraction methods result in optimal extraction for some but not all lipid classes. According to literature, it appears that it would be best to use a specific and optimal extraction method for each lipid class [32, 109]. The most commonly used methods for liquid-liquid extraction where introduced by Folch [110] in 1957 or Bligh and Dyer [111] in 1959 and modified and improved over time. The two methods are based on a two-phase liquid-liquid extraction, which uses methanol (MeOH) and chloroform. Over the years, protocols containing other organic solvents, such as methyl-tert-butyl-ether (MTBE) [112] or butanol [113] were tested, trying to get rid of the toxic chloroform.

Iverson et al. [114] compared the Folch method and the Bligh and Dyer method and showed similar recoveries in the extraction of the predominant phospholipid classes [114], and similar conclusions were reported in other studies comparing the Folch method with alternative extraction solvent systems, such as MTBE [112] or butanol [113]. MTBE has become particularly popular for sphingolipidomics studies and the extraction of lipids from fluids [38, 41]. Generally, the alternative solvent systems were not reported to present significant differences in the extraction of most abundant lipid classes when compared with the traditional solvent systems. Rather, the advantage of these extraction systems lies in the avoidance of chlorinated solvents, which are environmental hazards [105]. Reis et al. [105] compared the efficiency of several methods of liquid extraction  for the efficiency to extract major as well as minor species (phosphatidylinositols, lyso-lipids, ceramides, and cholesterol sulfates) from LDL. They found, that extraction of less abundant lipids was greatly influenced by the solvent system used, whereas solvent composition had a small effect on the extraction of predominant lipid classes (triacylglycerides, cholesterol esters, and phosphatidylcholines). Overall, the Folch method was most effective for the extraction of a broad range of lipid classes from LDL, although the hexane-isopropanol method was best for apolar lipids and the MeOH-MTBE method was suitable for hexosylceramides [105].

Further, a sample can also be prepared by precipitating the proteins and extract the containing lipid with a one-phase extraction method. Different organic solvents, like methanol, acetonitrile or isopropanol or a combination of methanol / chloroform / methyl-tert-butyl-ether were tested and compared towards their utility in lipidomics [109]. These solvents will lead to the denaturation of proteins to which lipids are bound. The denatured proteins can be easily removed by centrifugation after lipids had been released from protein binding and solubilized in the extraction solvent. Single phase protein precipitation is more comfortable in handling and less time consuming, compared to two-phase extraction protocols, making them applicable for the handling of larger numbers of samples [109, 115].

Turbulent flow chromatography is another technique for sample preparation, which was established for the analysis of small molecule [116] including metabolites [117]. It allows automation, as the sample can be directly injected into the chromatographic system. This reduces the manual sample preparation steps but also allows high throughput approaches [118-122].

### III.4.3. Separation based techniques for lipidomics

For data acquisition, two strategies are currently used. Samples are either chromatographically separated before detection or directly infused to the detector without prior separation in a so-called shotgun approach. Both procedures have their advantages and disadvantages [2].

In a shotgun analysis, lipid extracts are directly infused to the detector. As there is no separation before detection, the shotgun analysis is rather fast and reproducible, but it does not allow differentiation between isobaric / isomeric compounds. Furthermore, ion suppression by matrix components during detection happens to all analytes, in the same manner, and thereby interferes with the quantification of low abundant compounds. Ion suppression can be seen as a competition for ionization between molecules introduced into the MS source at the same time. However, quantification is more accurate with shotgun

approaches, as ion suppression applies in the same manner to the analyte and the corresponding internal standard [2, 123-125].

**Thin-layer chromatography**

Thin-layer chromatography (TLC) was the earliest chromatographic method used to separate lipids. Separation is achieved on a solid stationary phase, typically a silica gel plate, due to the polarity of the analytes. Analytes are loaded onto the TLC plate and eluted over the plate with a liquid mobile phase. TLC is a rather inexpensive and fast technique, delivering useful information with little effort and allows separation of a mixture of lipids with different polarities in a single run. The use of variations of mobile phase and stationary phases, even enables the separation of complex lipid mixtures. As a new TLC plate is used for every analysis, carry over from previous samples can be avoided and also suspicious samples can be analysed without risk of destroying the stationary phase. However, oxidation of lipids might occur during storage of the examined plates, and preparative applications are quite limited. Further, TLC shows low resolution and low sensitivity [101, 124, 126, 127].

**Gas chromatography**

Gas chromatography (GC) uses a solid stationary phase and a gas mobile phase. Hydrogen is preferred as the carrier gas as it has a lower elution temperature that allows for shorter times of analysis and less risk of thermal degradation of samples [127]. GC is widely applied in the study of fatty acids, where it provides a simple, fast and reliable tool for isobaric separation and quantification. For the analysis of fatty acids with GC, fatty acids need to be derivatized to fatty acid methyl esters, which makes the sample preparation process somewhat time-consuming. GC has limited applications because compounds must be thermally stable compounds, as separation occurs in the gas phase at high temperature and pressure. Although derivatization can solve the volatility problems, this is usually just applicable for simple molecules. As for complex biomolecules, derivatization might involve several reaction steps or eliminate crucial structural information [101, 124].

**High-performance liquid chromatography**

In high-performance liquid chromatography (HPLC) analytes are separated on a solid stationary phase and eluted with liquid mobile phase. For HPLC separation, two strategies are used to separate lipid on a stationary phase. In reversed-phase liquid chromatography (RPLC), the lipid species are separated on a C18 or lately also C30 column. The separation of lipids by RPLC is based on lipophilicity, where the lipids elute according to their carbon-chain length and the number of double bonds (in the fatty acid). Thus, lipid species containing longer acyl chains are eluted from the LC column later than shorter chain lipids, and saturated acyl structures are eluted after polyunsaturated species. Normal phase (NPLC) or hydrophilic interaction liquid chromatography (HILIC) separates lipids according to hydrophilic functionalities, such as the polar head groups [128-130].

HPLC is somewhat time-consuming, moreover internal standards are frequently not eluted at the same time as the corresponding analytes, so that it is difficult to control for ion suppression and thereby guarantee accurate quantification [101, 124].

### III.4.4. Mass spectrometry techniques for lipidomics

Lipids can be analysed by mass spectrometry either with direct infusion of the sample to the mass spectrometer or by pre-separation for example with liquid chromatography. With the combination of separation and mass spectrometry, it is possible to annotate not only the different lipid classes but also the individual lipid species [101, 131].

Nowadays, there are three different mass filter techniques used in lipidomics with mass spectrometry, namely triple quadrupole, time-of-flight, (TOF), and orbitraps. Triple quadrupoles are usually used for targeted quantification of lipids, whereas TOF and orbitrap instruments also allow untargeted analysis by their higher resolution of masses (Table I-1)[132, 133].

Table I-1: Several mass spectrometry analytical methods used in lipidomics, adopted from Taguchi et al. [132]

| Analytical method | Sensitivity | Advantages |
|---|---|---|
| Untargeted<br>• Data dependant product ion scan<br>• Data independent product ion scan | For high content molecules with low sensitivity | Possible to find unexpected molecules, re-analysis possible |
| Focused<br>• Neutral loss scan<br>• Precursor ion scan | For medium content molecules with medium sensitivity | Possible to find small amounts of molecules within focused classes |
| Targeted<br>• Multiple reaction monitoring | For low content molecules with high sensitivity | Possible to find new low abundant structural isomers, but just within predefined species |

By the use of high-resolution accurate mass spectrometry, it is possible to determine the exact mass of lipid molecules and to resolve isobars with different atomic composition or isotopic interferences.

For all of the mentioned techniques, it is possible to acquire full *m/z* (mass over charge ratio) but also measure on the tandem-MS ($MS^2$) level. The fundamental principle of $MS^2$ is to select a precursor ion, fragment it and measure the *m/z* ratio of the formed product ions. With $MS^2$, any selected lipid ion can be further fragmented and characterized giving information about building its blocks, like the fatty acid chain length of isomeric compounds [2, 134]. Isobaric lipids might be separated by elution time upon liquid chromatography, high-resolution accurate mass spectrometry and because of specific fragmentation pattern of different building blocks, also by the use of $MS^2$ technique [134].

**Triple quadrupoles**

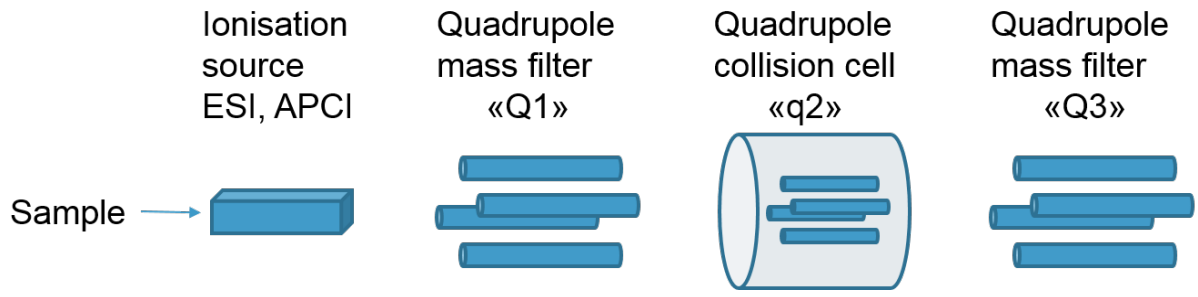


Figure I-5: Principle of triple quadrupole mass spectrometer

A triple quadrupole consists of two quadrupole mass analysers (Q1 and Q3) and a quadrupole collision cell (q2), as shown in Figure I-5. By coupling two quadrupoles with a collision cell, it is possible to perform different types of scans on the $MS^2$ level. They are typically operated in single-reaction monitoring (SRM) mode (also called multiple-reaction monitoring (MRM)). In SRM mode, the precursor ion is monitored in Q1, fragmented in q2 and the transitions of the precursor ion to multiple fragments are monitored in Q3. This provides a significant gain in sensitivity compared with the acquisition of full spectral data. Other operating modes with triple quadrupole analyzers, are product-ion, precursor-ion and neutral-loss scan [135, 136]. The different types of $MS^2$ experiments are shown in Figure I-6.

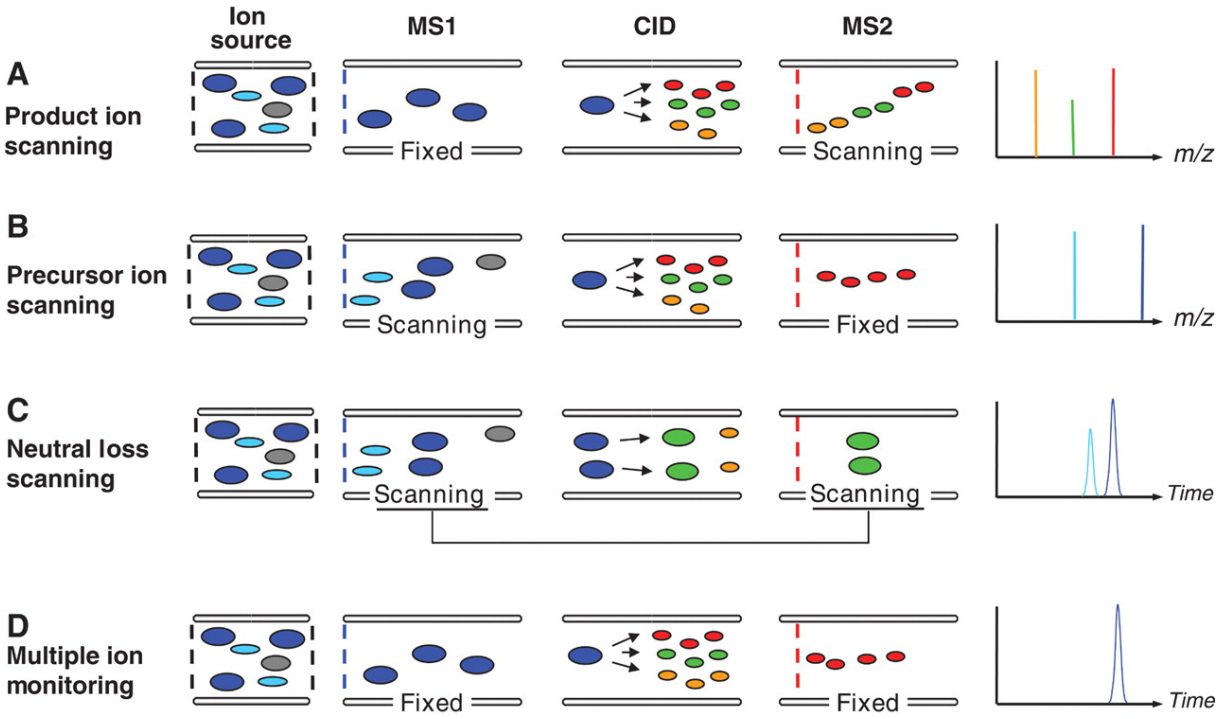


Figure I-6: Schematic representation of various types of tandem mass spectrometry experiments. (A) Product ion scanning is the most common $MS^2$ experiment. In this experiment, the first analyser ($MS^1$) is set to a value that selects one specific precursor ion at a time. The selected ion undergoes CID in the collision cell, and the all resulting fragments are analysed by the second analyser ($MS^2$). This process is repeated for different precursors. (B) Precursor ion scanning sets the second analyser ($MS^2$) to transmit only one specific fragment ion to the detector. $MS^1$ is scanned to detect all the precursor ions that generate this fragment. (C) Neutral loss scanning scans both analysers in a synchronized manner, so that the mass difference of ions passing through $MS^1$ and $MS^2$ remains constant. The mass difference corresponds to a neutral fragment that is lost from the ion in the collision cell. (D) MRM consists of a series of short experiments in which one precursor ion and one specific fragment characteristic for that precursor are selected by $MS^1$ and $MS^2$, respectively. Typically, the instrument cycles through a series of transitions (precursor-fragment pair) and records the signal as a function of time (chromatographic elution). MRM is used for the detection of a specific analyte with known fragmentation properties in complex samples. Figure taken from Domon et al. [137]

Further, rapid polarity switching and moving from detection of positive and negative ions allows a wide range of compounds to be incorporated into one method [135].

Triple quadrupole MS is the preferred technique for targeted sensitive and quantitative analysis of a limited amount of lipids. However, triple quadrupoles have certain limitations. Because of limited resolution, they are less suitable for untargeted discovery, but a good option for targeted sensitive and quantitative analysis of a limited amount of lipids. Also, because of pre-defined transition monitoring in SRM mode, the reprocessing of data to search for unknown compounds is not possible [125, 135, 138, 139].

**Time-of-flight**

A time-of-flight mass analyzer uses the differences in transit time through a drift region of ions with different masses to separate them. In a time-of-flight analyzer, a group of ions is accelerated in a flight tube and sent to the detector. The ions are accelerated by getting an identical high-voltage pulse. Because equally charged ions have the same kinetic energy, molecules with lower masses achieve higher velocity and reach the detector first [135] (Figure I-7.

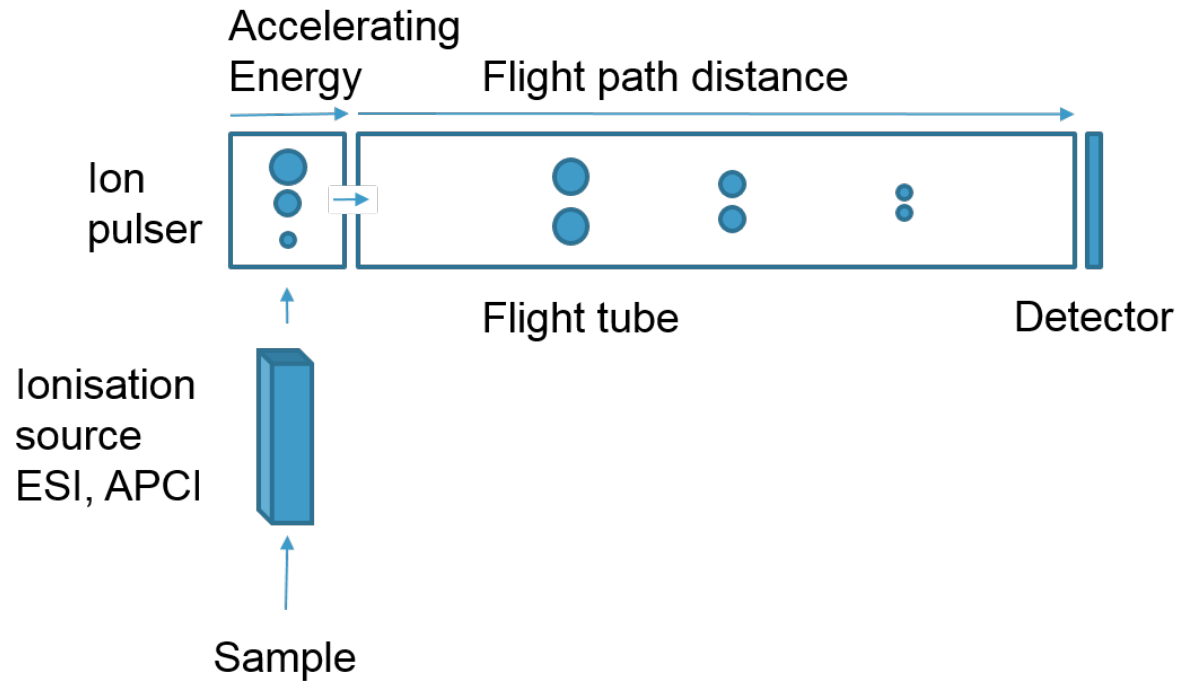


Figure I-7: Principle of Time-of-flight mass spectrometer

Time-of-flight mass spectrometry offers high resolution and mass accuracy and provides the possibility to analyse elemental composition and whit this, high specificity in the analysis [125, 138, 139].

**Orbitrap**

In the Orbitrap analyser, a group of ions is injected into a small electrostatic device. Their ions circle around a central, spindle-shaped electrode at high energies. The axial motion of the ions is followed and picked up by the detector, and this signal is Fourier transformed (FT)

for high-resolution mass spectra. Ions can be sent out to a collision cell for fragmentation and fragments are sent back to the orbitrap for mass analysis (Figure I-8).

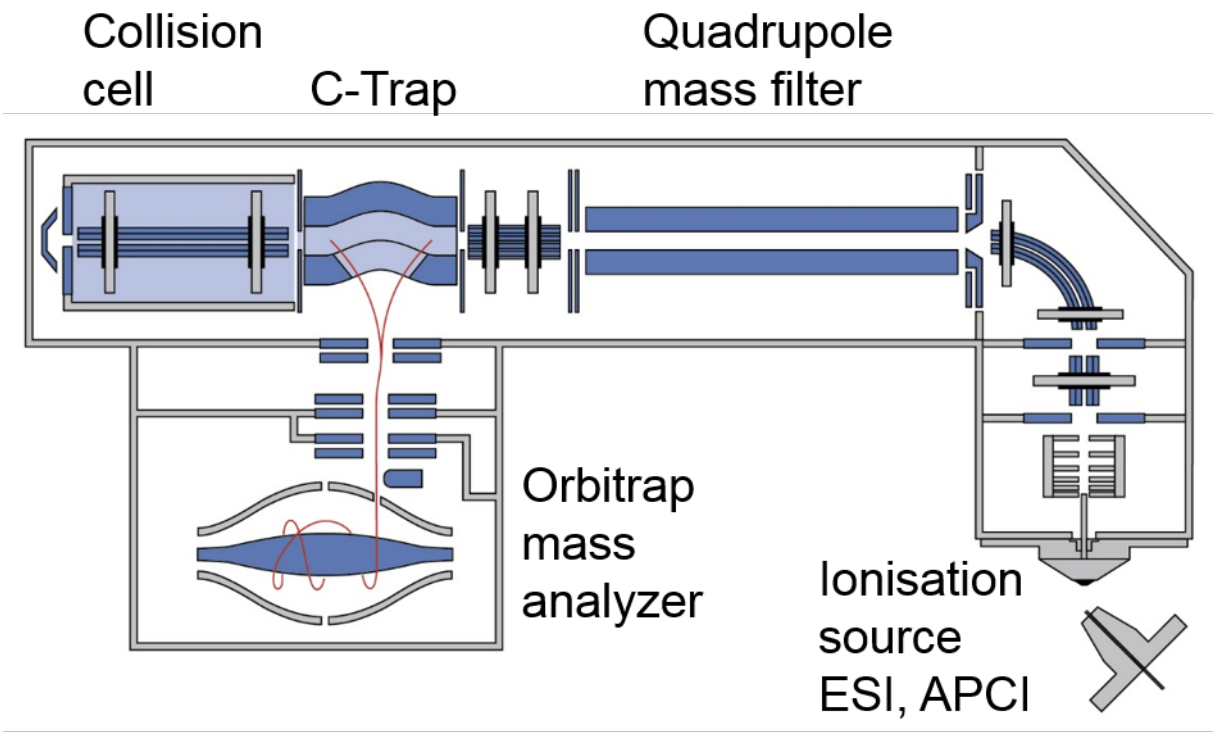


Figure I-8: Principle of Orbitrap mass spectrometer. Figure adopted from Thermo scientific (planetorbitrap.com)

Orbitrap analysers operate at a different mass resolution that is proportional to acquisition time and inversely proportional to the square root of the *m/z* ratio. Thus, we expect resolution values for the orbitrap to be highest at low masses. This is different to time-of-flight analysers, where resolution is consistent across the mass range. Orbitraps offer scan filters with a very high resolution, which allows determining the exact mass of a molecule and to couple this information with fragmentation data [123, 135, 140].

### III.4.5. Data analysis

Lipidomics generates large amounts of data, which are processed by various bioinformatics methods to detect and quantify metabolite peaks and annotate compound names [2]. Although liquid chromatography and mass spectrometry techniques have been evolved rapidly to allow high-throughput lipidomics, the processing of the generated data and elucidation of lipid structures is not as trivial. There are combinatorial challenges when it comes identification,

quantification, and interpretation of the diversity of lipid structures. Detailed structural annotation requires a sophisticated $MS^2$ approach, which combines information from retention time, high-resolution accurate mass data, and fragmentation pattern in different analysis polarities. The analytical progress in the structural elucidation of lipid led to novel challenges for bioinformatics [141, 142].

The first step in data processing is to collect as many valid compound signals from a data set as possible, while at the same time, minimizing the number of detected artefact peaks and noise. High abundant species usually give strong and distinct signals, but as the metabolite concentrations are close at the detection limit, it becomes difficult to identify and quantify the peaks automatically. Software solutions need to be developed for the automatic identification and quantification of lipids in high-throughput lipidomics experiments, which also cover the low abundant compounds [2, 142].

The second step is to incorporate this analysed and quantified data into a biological context and combine it with other data for example from different "omics" techniques. Therefore, further downstream analysis such as statistics, biological pathway or metabolic flux analysis can be performed [2, 142].

## III.5 Aim of the study

With our previous analytical workflows for lipid analysis, the individual lipid classes like phosphoglycerates, sphingosine-1-phosphates, and sphingolipids were each analysed by separate methods for sample preparation and extraction, but also for LC-MS analysis. One aim of this project was to unify and further expand our existing LC-$MS^2$ based methods into a more comprehensive lipidomics analysis, which includes a single and fast sample preparation protocol and a unique LC-MS analysis.

Moreover, the atypical 1-deoxysphingosine was structurally characterized, and the metabolic pathway of atypical 1-deoxymethylsphingolipids was further investigated.

## III.6 References

[1] Fahy, E, Subramaniam, S, Brown, HA, et al., A comprehensive classification system for lipids, J Lipid Res, 2005;46:839-861.
[2] Vaz, FM, Pras-Raves, M, Bootsma, AH, et al., Principles and practice of lipidomics, J Inherit Metab Dis, 2015;38:41-52.
[3] Lombard, J, Lopez-Garcia, P and Moreira, D, The early evolution of lipid membranes and the three domains of life, Nat Rev Microbiol, 2012;10:507-515.
[4] Quehenberger, O and Dennis, EA, The human plasma lipidome, N Engl J Med, 2011;365:1812-1823.
[5] van Meer, G, Voelker, DR and Feigenson, GW, Membrane lipids: where they are and how they behave, Nat Rev Mol Cell Bio, 2008;9:112-124.
[6] Dufourc, EJ, Sterols and membrane dynamics, J Chem Biol, 2008;1:63-77.
[7] Merrill, AH, Jr., Sphingolipid and glycosphingolipid metabolic pathways in the era of sphingolipidomics, Chem Rev, 2011;111:6387-6422.
[8] Simons, K and Sampaio, JL, Membrane organization and lipid rafts, Cold Spring Harb Perspect Biol, 2011;3:a004697.
[9] Chalfant, CE and Spiegel, S, Sphingosine 1-phosphate and ceramide 1-phosphate: expanding roles in cell signaling, J Cell Sci, 2005;118:4605-4612.
[10] Wenk, MR, The emerging field of lipidomics, Nat Rev Drug Discov, 2005;4:594-610.
[11] Fahy, E, Subramaniam, S, Murphy, RC, et al., Update of the LIPID MAPS comprehensive classification system for lipids, J Lipid Res, 2009;50 Suppl:S9-14.
[12] Rambold, AS, Cohen, S and Lippincott-Schwartz, J, Fatty acid trafficking in starved cells: regulation by lipid droplet lipolysis, autophagy, and mitochondrial fusion dynamics, Dev Cell, 2015;32:678-692.
[13] Calhoon, EA, Ro, J and Williams, JB, Perspectives on the membrane fatty acid unsaturation/pacemaker hypotheses of metabolism and aging, Chem Phys Lipids, 2015;191:48-60.
[14] Lee, H and Park, WJ, Unsaturated fatty acids, desaturases, and human health, J Med Food, 2014;17:189-197.
[15] Wallis, JG, Watts, JL and Browse, J, Polyunsaturated fatty acid synthesis: what will they think of next?, Trends Biochem Sci, 2002;27:467.
[16] Wakil, SJ and Abu-Elheiga, LA, Fatty acid metabolism: target for metabolic syndrome, Journal of lipid research, 2009;50 Suppl:S138-143.
[17] Wakil, SJ, Fatty acid synthase, a proficient multifunctional enzyme, Biochemistry, 1989;28:4523-4530.
[18] Leekumjorn, S, Cho, HJ, Wu, Y, et al., The role of fatty acid unsaturation in minimizing biophysical changes on the structure and local effects of bilayer membranes, Biochim Biophys Acta, 2009;1788:1508-1516.
[19] Mattson, FH and Grundy, SM, Comparison of effects of dietary saturated, monounsaturated, and polyunsaturated fatty acids on plasma lipids and lipoproteins in man, J Lipid Res, 1985;26:194-202.
[20] Ahmadian, M, Duncan, RE, Jaworski, K, et al., Triacylglycerol metabolism in adipose tissue, Future Lipidol, 2007;2:229-237.
[21] Takase, H, Metabolism of diacylglycerol in humans, Asia Pac J Clin Nutr, 2007;16 Suppl 1:398-403.
[22] Chon, SH, Zhou, YX, Dixon, JL, et al., Intestinal monoacylglycerol metabolism: developmental and nutritional regulation of monoacylglycerol lipase and monoacylglycerol acyltransferase, J Biol Chem, 2007;282:33346-33357.
[23] Krasnova, L and Wong, CH, Understanding the Chemistry and Biology of Glycosylation with Glycan Synthesis, Annu Rev Biochem, 2016;85:599-630.
[24] van Meer, G, Voelker, DR and Feigenson, GW, Membrane lipids: where they are and how they behave, Nat Rev Mol Cell Biol, 2008;9:112-124.
[25] Yu, RK, Suzuki, Y and Yanagisawa, M, Membrane glycolipids in stem cells, FEBS Lett, 2010;584:1694-1699.
[26] Sandhoff, K, van Echten, G, Schroder, M, et al., Metabolism of glycolipids: the role of glycolipid-binding proteins in the function and pathobiochemistry of lysosomes, Biochem Soc Trans, 1992;20:695-699.
[27] Grouleff, J, Irudayam, SJ, Skeby, KK, et al., The influence of cholesterol on membrane protein structure, function, and dynamics studied by molecular dynamics simulations, Biochim Biophys Acta, 2015;1848:1783-1795.
[28] Kliewer, SA, Moore, JT, Wade, L, et al., An orphan nuclear receptor activated by pregnanes defines a novel steroid signaling pathway, Cell, 1998;92:73-82.

[29] Gault, CR, Obeid, LM and Hannun, YA, An overview of sphingolipid metabolism: from synthesis to breakdown, Adv Exp Med Biol, 2010;688:1-23.
[30] Pralhada Rao, R, Vaidyanathan, N, Rengasamy, M, et al., Sphingolipid metabolic pathway: an overview of major roles played in human diseases, J Lipids, 2013;2013:178910.
[31] Bienias, K, Fiedorowicz, A, Sadowska, A, et al., Regulation of sphingomyelin metabolism, Pharmacol Rep, 2016;68:570-581.
[32] Quehenberger, O, Armando, AM, Brown, AH, et al., Lipidomics reveals a remarkable diversity of lipids in human plasma, Journal of lipid research, 2010;51:3299-3305.
[33] Basit, A, Piomelli, D and Armirotti, A, Rapid evaluation of 25 key sphingolipids and phosphosphingolipids in human plasma by LC-MS/MS, Anal Bioanal Chem, 2015;407:5189-5198.
[34] Hla, T and Dannenberg, AJ, Sphingolipid signaling in metabolic disorders, Cell Metab, 2012;16:420-434.
[35] Lahiri, S and Futerman, AH, The metabolism and function of sphingolipids and glycosphingolipids, Cell Mol Life Sci, 2007;64:2270-2284.
[36] Pettus, BJ, Chalfant, CE and Hannun, YA, Ceramide in apoptosis: an overview and current perspectives, Biochim Biophys Acta, 2002;1585:114-125.
[37] Haimovitz-Friedman, A, Kolesnick, RN and Fuks, Z, Ceramide signaling in apoptosis, Br Med Bull, 1997;53:539-553.
[38] Hammad, SM, Pierce, JS, Soodavar, F, et al., Blood sphingolipidomics in healthy humans: impact of sample collection methodology, J Lipid Res, 2010;51:3074-3087.
[39] Bertea, M, Rutti, MF, Othman, A, et al., Deoxysphingoid bases as plasma markers in diabetes mellitus, Lipids Health Dis, 2010;9:84.
[40] Penno, A, Reilly, MM, Houlden, H, et al., Hereditary sensory neuropathy type 1 is caused by the accumulation of two neurotoxic sphingolipids, J Biol Chem, 2010;285:11178-11187.
[41] Wiesner, P, Leidl, K, Boettcher, A, et al., Lipid profiling of FPLC-separated lipoprotein fractions by electrospray ionization tandem mass spectrometry, J Lipid Res, 2009;50:574-585.
[42] Scherer, M, Bottcher, A, Schmitz, G, et al., Sphingolipid profiling of human plasma and FPLC-separated lipoprotein fractions by hydrophilic interaction chromatography tandem mass spectrometry, Biochim Biophys Acta, 2011;1811:68-75.
[43] Dashti, M, Kulik, W, Hoek, F, et al., A phospholipidomic analysis of all defined human plasma lipoproteins, Scientific reports, 2011;1:139.
[44] Weiss, B and Stoffel, W, Human and murine serine-palmitoyl-CoA transferase--cloning, expression and characterization of the key enzyme in sphingolipid synthesis, Eur J Biochem, 1997;249:239-247.
[45] Hanada, K, Hara, T, Nishijima, M, et al., A mammalian homolog of the yeast LCB1 encodes a component of serine palmitoyltransferase, the enzyme catalyzing the first step in sphingolipid synthesis, J Biol Chem, 1997;272:32108-32114.
[46] Buede, R, Rinker-Schaffer, C, Pinto, WJ, et al., Cloning and characterization of LCB1, a Saccharomyces gene required for biosynthesis of the long-chain base component of sphingolipids, J Bacteriol, 1991;173:4325-4332.
[47] Hornemann, T, Wei, Y and von Eckardstein, A, Is the mammalian serine palmitoyltransferase a high-molecular-mass complex?, Biochem J, 2007;405:157-164.
[48] Hornemann, T, Richard, S, Rutti, MF, et al., Cloning and initial characterization of a new subunit for mammalian serine-palmitoyltransferase, J Biol Chem, 2006;281:37275-37281.
[49] Williams, RD, Wang, E and Merrill, AH, Jr., Enzymology of long-chain base synthesis by liver: characterization of serine palmitoyltransferase in rat liver microsomes, Arch Biochem Biophys, 1984;228:282-291.
[50] Zitomer, NC, Mitchell, T, Voss, KA, et al., Ceramide synthase inhibition by fumonisin B1 causes accumulation of 1-deoxysphinganine: a novel category of bioactive 1-deoxysphingoid bases and 1-deoxydihydroceramides biosynthesized by mammalian cell lines and animals, J Biol Chem, 2009;284:4786-4795.
[51] Beeler, T, Bacikova, D, Gable, K, et al., The Saccharomyces cerevisiae TSC10/YBR265w gene encoding 3-ketosphinganine reductase is identified in a screen for temperature-sensitive suppressors of the Ca2+-sensitive csg2 Delta mutant, Journal of Biological Chemistry, 1998;273:30688-30694.
[52] Michel, C, van Echten-Deckert, G, Rother, J, et al., Characterization of ceramide synthesis. A dihydroceramide desaturase introduces the 4,5-trans-double bond of sphingosine at the level of dihydroceramide, J Biol Chem, 1997;272:22432-22437.
[53] Levy, M and Futerman, AH, Mammalian ceramide synthases, IUBMB Life, 2010;62:347-356.
[54] Ternes, P, Franke, S, Zahringer, U, et al., Identification and characterization of a sphingolipid delta 4-desaturase family, J Biol Chem, 2002;277:25512-25518.

[55] Omae, F, Miyazaki, M, Enomoto, A, et al., DES2 protein is responsible for phytoceramide biosynthesis in the mouse small intestine, Biochem J, 2004;379:687-695.
[56] Enomoto, A, Omae, F, Miyazaki, M, et al., Dihydroceramide:sphinganine C-4-hydroxylation requires Des2 hydroxylase and the membrane form of cytochrome b5, Biochem J, 2006;397:289-295.
[57] Hanada, K, Kumagai, K, Yasuda, S, et al., Molecular machinery for non-vesicular trafficking of ceramide, Nature, 2003;426:803-809.
[58] Huitema, K, van den Dikkenberg, J, Brouwers, JF, et al., Identification of a family of animal sphingomyelin synthases, EMBO J, 2004;23:33-44.
[59] Vacaru, AM, Tafesse, FG, Ternes, P, et al., Sphingomyelin synthase-related protein SMSr controls ceramide homeostasis in the ER, J Cell Biol, 2009;185:1013-1027.
[60] Leipelt, M, Warnecke, DC, Hube, B, et al., Characterization of UDP-glucose:ceramide glucosyltransferases from different organisms, Biochem Soc Trans, 2000;28:751-752.
[61] Futerman, AH and Pagano, RE, Determination of the intracellular sites and topology of glucosylceramide synthesis in rat liver, Biochem J, 1991;280 ( Pt 2):295-302.
[62] Schulte, S and Stoffel, W, Ceramide UDPgalactosyltransferase from myelinating rat brain: purification, cloning, and expression, Proc Natl Acad Sci U S A, 1993;90:10265-10269.
[63] Stahl, N, Jurevics, H, Morell, P, et al., Isolation, characterization, and expression of cDNA clones that encode rat UDP-galactose: ceramide galactosyltransferase, J Neurosci Res, 1994;38:234-242.
[64] Kapitonov, D and Yu, RK, Cloning, characterization, and expression of human ceramide galactosyltransferase cDNA, Biochem Biophys Res Commun, 1997;232:449-453.
[65] Adada, M, Luberto, C and Canals, D, Inhibitors of the sphingomyelin cycle: Sphingomyelin synthases and sphingomyelinases, Chem Phys Lipids, 2016;197:45-59.
[66] Tomiuk, S, Hofmann, K, Nix, M, et al., Cloned mammalian neutral sphingomyelinase: functions in sphingolipid signaling?, Proc Natl Acad Sci U S A, 1998;95:3638-3643.
[67] Schuchman, EH, Suchi, M, Takahashi, T, et al., Human acid sphingomyelinase. Isolation, nucleotide sequence and expression of the full-length and alternatively spliced cDNAs, J Biol Chem, 1991;266:8531-8539.
[68] Cheng, Y, Nilsson, A, Tomquist, E, et al., Purification, characterization, and expression of rat intestinal alkaline sphingomyelinase, J Lipid Res, 2002;43:316-324.
[69] Sandhoff, K and Kolter, T, Biosynthesis and degradation of mammalian glycosphingolipids, Philos Trans R Soc Lond B Biol Sci, 2003;358:847-861.
[70] Coant, N, Sakamoto, W, Mao, C, et al., Ceramidases, roles in sphingolipid metabolism and in health and disease, Adv Biol Regul, 2016.
[71] Bikman, BT and Summers, SA, Ceramides as modulators of cellular and whole-body metabolism, J Clin Invest, 2011;121:4222-4230.
[72] Mao, C and Obeid, LM, Ceramidases: regulators of cellular responses mediated by ceramide, sphingosine, and sphingosine-1-phosphate, Biochim Biophys Acta, 2008;1781:424-434.
[73] Kohama, T, Olivera, A, Edsall, L, et al., Molecular cloning and functional characterization of murine sphingosine kinase, J Biol Chem, 1998;273:23722-23728.
[74] Liu, H, Sugiura, M, Nava, VE, et al., Molecular cloning and functional characterization of a novel mammalian sphingosine kinase type 2 isoform, J Biol Chem, 2000;275:19513-19520.
[75] Pulkoski-Gross, MJ, Donaldson, JC and Obeid, LM, Sphingosine-1-phosphate metabolism: A structural perspective, Crit Rev Biochem Mol Biol, 2015;50:298-313.
[76] Wang, E, Norred, WP, Bacon, CW, et al., Inhibition of sphingolipid biosynthesis by fumonisins. Implications for diseases associated with Fusarium moniliforme, J Biol Chem, 1991;266:14486-14490.
[77] Van Veldhoven, PP and Mannaerts, GP, Subcellular localization and membrane topology of sphingosine-1-phosphate lyase in rat liver, J Biol Chem, 1991;266:12502-12507.
[78] Merrill, AH, Jr., Schmelz, EM, Dillehay, DL, et al., Sphingolipids--the enigmatic lipid class: biochemistry, physiology, and pathophysiology, Toxicol Appl Pharmacol, 1997;142:208-225.
[79] Renkonen, O and Hirvisalo, EL, Structure of plasma sphingadienine, J Lipid Res, 1969;10:687-693.
[80] Braun, PE, Morell, P and Radin, NS, Synthesis of C18- and C20-dihydrosphingosines, ketodihydrosphingosines, and ceramides by microsomal preparations from mouse brain, J Biol Chem, 1970;245:335-341.
[81] Hanada, K, Hara, T and Nishijima, M, Purification of the serine palmitoyltransferase complex responsible for sphingoid base synthesis by using affinity peptide chromatography techniques, J Biol Chem, 2000;275:8409-8415.
[82] Hanada, K, Serine palmitoyltransferase, a key enzyme of sphingolipid metabolism, Biochim Biophys Acta, 2003;1632:16-30.
[83] Hornemann, T, Penno, A, Rutti, MF, et al., The SPTLC3 subunit of serine palmitoyltransferase generates short chain sphingoid bases, J Biol Chem, 2009;284:26322-26330.

[84] Cuadros, R, Montejo de Garcini, E, Wandosell, F, et al., The marine compound spisulosine, an inhibitor of cell proliferation, promotes the disassembly of actin stress fibers, Cancer Lett, 2000;152:23-29.
[85] Baird, RD, Kitzen, J, Clarke, PA, et al., Phase I safety, pharmacokinetic, and pharmacogenomic trial of ES-285, a novel marine cytotoxic agent, administered to adult patients with advanced solid tumors, Mol Cancer Ther, 2009;8:1430-1437.
[86] Vilar, E, Grunwald, V, Schoffski, P, et al., A phase I dose-escalating study of ES-285, a marine sphingolipid-derived compound, with repeat dose administration in patients with advanced solid tumors, Invest New Drugs, 2012;30:299-305.
[87] Schoffski, P, Dumez, H, Ruijter, R, et al., Spisulosine (ES-285) given as a weekly three-hour intravenous infusion: results of a phase I dose-escalating study in patients with advanced solid malignancies, Cancer Chemother Pharmacol, 2011;68:1397-1403.
[88] Rotthier, A, Auer-Grumbach, M, Janssens, K, et al., Mutations in the SPTLC2 subunit of serine palmitoyltransferase cause hereditary sensory and autonomic neuropathy type I, Am J Hum Genet, 2010;87:513-522.
[89] Astudillo, L, Sabourdy, F, Therville, N, et al., Human genetic disorders of sphingolipid biosynthesis, Journal of Inherited Metabolic Disease, 2015;38:65-76.
[90] Auer-Grumbach, M, Bode, H, Pieber, TR, et al., Mutations at Ser331 in the HSN type I gene SPTLC1 are associated with a distinct syndromic phenotype, European Journal of Medical Genetics, 2013;56:266-269.
[91] Ernst, D, Murphy, SM, Sathiyanadan, K, et al., Novel HSAN1 Mutation in Serine Palmitoyltransferase Resides at a Putative Phosphorylation Site That Is Involved in Regulating Substrate Specificity, Neuromol Med, 2015;17:47-57.
[92] Auer-Grumbach, M, Hereditary sensory neuropathy type I, Orphanet Journal of Rare Diseases, 2008;3.
[93] Houlden, H, King, R, Blake, J, et al., Clinical, pathological and genetic characterization of hereditary sensory and autonomic neuropathy type 1 (HSAN I), Brain, 2006;129:411-425.
[94] Jun, BK, Chandra, A, Kuljis, D, et al., Substrate Availability of Mutant SPT Alters Neuronal Branching and Growth Cone Dynamics in Dorsal Root Ganglia, J Neurosci, 2015;35:13713-13719.
[95] Zuellig, RA, Hornemann, T, Othman, A, et al., Deoxysphingolipids, novel biomarkers for type 2 diabetes, are cytotoxic for insulin-producing cells, Diabetes, 2014;63:1326-1339.
[96] Othman, A, Bianchi, R, Alecu, I, et al., Lowering plasma 1-deoxysphingolipids improves neuropathy in diabetic rats, Diabetes, 2015;64:1035-1045.
[97] Othman, A, Rütti, MF, Ernst, D, et al., Plasma deoxysphingolipids: a novel class of biomarkers for the metabolic syndrome?, Diabetologia, 2012;55:421–431.
[98] Jimenez-Rojo, N, Sot, J, Busto, JV, et al., Biophysical Properties of Novel 1-Deoxy-(Dihydro)ceramides Occurring in Mammalian Cells, Biophysical Journal, 2014;107:2850-2859.
[99] Sakagami, H, Kishino, K, Amano, O, et al., Cell Death Induced by Nutritional Starvation in Mouse Macrophage-like RAW264.7 Cells, Anticancer Research, 2009;29:343-347.
[100] Montefusco, DJ, Newcomb, B, Gandy, JL, et al., Sphingoid Bases and the Serine Catabolic Enzyme CHA1 Define a Novel Feedforward/Feedback Mechanism in the Response to Serine Availability, Journal of Biological Chemistry, 2012;287:9280-9289.
[101] Jurowski, K, Kochan, K, Walczak, J, et al., Analytical Techniques in Lipidomics: State of the Art, Crit Rev Anal Chem, 2017;47:418-437.
[102] Han, X, Lipidomics for studying metabolism, Nat Rev Endocrinol, 2016;12:668-679.
[103] Hu, T and Zhang, JL, Mass-Spectrometry-Based Lipidomics, J Sep Sci, 2017.
[104] Vuckovic, D, Current trends and challenges in sample preparation for global metabolomics using liquid chromatography-mass spectrometry, Anal Bioanal Chem, 2012;403:1523-1548.
[105] Reis, A, Rudnitskaya, A, Blackburn, GJ, et al., A comparison of five lipid extraction solvent systems for lipidomic studies of human LDL, J Lipid Res, 2013;54:1812-1824.
[106] Jurowski, K, Kochan, K, Walczak, J, et al., Comprehensive review of trends and analytical strategies applied for biological samples preparation and storage in modern medical lipidomics: State of the art, 2016.
[107] Chang, MS, Ji, Q, Zhang, J, et al., Historical review of sample preparation for chromatographic bioanalysis: pros and cons, Drug Develop Res, 2007;68:107-133.
[108] Zhou, J and Yin, Y, Strategies for large-scale targeted metabolomics quantification by liquid chromatography-mass spectrometry, Analyst, 2016;141:6362-6373.
[109] Pellegrino, RM, Di Veroli, A, Valeri, A, et al., LC/MS lipid profiling from human serum: a new method for global lipid extraction, Anal Bioanal Chem, 2014;406:7937-7948.
[110] Folch, J, Lees, M and Sloane Stanley, GH, A simple method for the isolation and purification of total lipides from animal tissues, J Biol Chem, 1957;226:497-509.

[111] Bligh, EG and Dyer, WJ, A rapid method of total lipid extraction and purification, Can J Biochem Physiol, 1959;37:911-917.
[112] Matyash, V, Liebisch, G, Kurzchalia, TV, et al., Lipid extraction by methyl-tert-butyl ether for high-throughput lipidomics, J Lipid Res, 2008;49:1137-1146.
[113] Lofgren, L, Stahlman, M, Forsberg, GB, et al., The BUME method: a novel automated chloroform-free 96-well total lipid extraction method for blood plasma, J Lipid Res, 2012;53:1690-1700.
[114] Iverson, SJ, Lang, SL and Cooper, MH, Comparison of the Bligh and Dyer and Folch methods for total lipid determination in a broad range of marine tissue, Lipids, 2001;36:1283-1287.
[115] Sarafian, MH, Gaudin, M, Lewis, MR, et al., Objective set of criteria for optimization of sample preparation procedures for ultra-high throughput untargeted blood plasma lipid profiling by ultra performance liquid chromatography-mass spectrometry, Anal Chem, 2014;86:5766-5774.
[116] Couchman, L, Jones, DJ and Moniz, CF, The use of turbulent flow chromatography for rapid, on-line analysis of tryptic digests, Rapid Commun Mass Spectrom, 2015;29:2140-2146.
[117] Tecleab, AG, Schofield, RC, Ramanathan, LV, et al., A Simple and Sensitive Method for Quantitative Measurement of Methylmalonic Acid by Turbulent Flow Chromatography and Tandem Mass Spectrometry, J Chromatogr Sep Tech, 2016;7.
[118] Michopoulos, F, Edge, AM, Theodoridis, G, et al., Application of turbulent flow chromatography to the metabonomic analysis of human plasma: comparison with protein precipitation, J Sep Sci, 2010;33:1472-1479.
[119] Bousova, K, Senyuva, H and Mittendorf, K, Multiresidue automated turbulent flow online LC-MS/MS method for the determination of antibiotics in milk, Food Addit Contam Part A Chem Anal Control Expo Risk Assess, 2012;29:1901-1912.
[120] Gorga, M, Insa, S, Petrovic, M, et al., Analysis of endocrine disrupters and related compounds in sediments and sewage sludge using on-line turbulent flow chromatography-liquid chromatography-tandem mass spectrometry, J Chromatogr A, 2014;1352:29-37.
[121] Lim, HK, Chan, KW, Sisenwine, S, et al., Simultaneous screen for microsomal stability and metabolite profile by direct injection turbulent-laminar flow LC-LC and automated tandem mass spectrometry, Anal Chem, 2001;73:2140-2146.
[122] Mueller, DM, Duretz, B, Espourteille, FA, et al., Development of a fully automated toxicological LC-MS(n) screening system in urine using online extraction with turbulent flow chromatography, Anal Bioanal Chem, 2011;400:89-100.
[123] Schwudke, D, Schuhmann, K, Herzog, R, et al., Shotgun lipidomics on high resolution mass spectrometers, Cold Spring Harb Perspect Biol, 2011;3:a004614.
[124] Carrasco-Pancorbo, A, Navas-Iglesias, N and Cuadros-Rodríguez, L, From lipid analysis towards lipidomics, a new challenge for the analytical chemistry of the 21st century. Part I: Modern lipid analysis, TrAC Trends in Analytical Chemistry, 2009;28:263-278.
[125] Kofeler, HC, Fauland, A, Rechberger, GN, et al., Mass spectrometry based lipidomics: an overview of technological platforms, Metabolites, 2012;2:19-38.
[126] Fuchs, B, Suss, R, Teuber, K, et al., Lipid analysis by thin-layer chromatography--a review of the current state, J Chromatogr A, 2011;1218:2754-2774.
[127] Peterson, BL and Cummings, BS, A review of chromatographic methods for the assessment of phospholipids in biological samples, Biomed Chromatogr, 2006;20:227-243.
[128] Cajka, T and Fiehn, O, Comprehensive analysis of lipids in biological systems by liquid chromatography-mass spectrometry, Trends Analyt Chem, 2014;61:192-206.
[129] Narvaez-Rivas, M and Zhang, Q, Comprehensive untargeted lipidomic analysis using core-shell C30 particle column and high field orbitrap mass spectrometer, J Chromatogr A, 2016;1440:123-134.
[130] Merrill, AH, Jr., Sullards, MC, Allegood, JC, et al., Sphingolipidomics: high-throughput, structure-specific, and quantitative analysis of sphingolipids by liquid chromatography tandem mass spectrometry, Methods, 2005;36:207-224.
[131] Dettmer, K, Almstetter, MF, Appel, IJ, et al., Comparison of serum versus plasma collection in gas chromatography--mass spectrometry-based metabolomics, Electrophoresis, 2010;31:2365-2373.
[132] Taguchi, R, Nishijima, M and Shimizu, T, Basic analytical systems for lipidomics by mass spectrometry in Japan, Methods Enzymol, 2007;432:185-211.
[133] Griffiths, WJ and Wang, Y, Mass spectrometry: from proteomics to metabolomics and lipidomics, Chem Soc Rev, 2009;38:1882-1896.
[134] Murphy, RC and Axelsen, PH, Mass spectrometric analysis of long-chain lipids, Mass Spectrom Rev, 2011;30:579-599.
[135] Hird, SJ, Lau, BPY, Schuhmacher, R, et al., Liquid chromatography-mass spectrometry for the determination of chemical contaminants in food, TrAC Trends in Analytical Chemistry, 2014;59:59-72.

[136] Holcapek, M, Jirasko, R and Lisa, M, Recent developments in liquid chromatography-mass spectrometry and related techniques, Journal of Chromatography A, 2012;1259:3-15.
[137] Domon, B and Aebersold, R, Mass spectrometry and protein analysis, Science, 2006;312:212-217.
[138] Han, X, Yang, K and Gross, RW, Multi-dimensional mass spectrometry-based shotgun lipidomics and novel strategies for lipidomic analyses, Mass Spectrom Rev, 2012;31:134-178.
[139] Ekroos, K, Chernushevich, IV, Simons, K, et al., Quantitative profiling of phospholipids by multiple precursor ion scanning on a hybrid quadrupole time-of-flight mass spectrometer, Anal Chem, 2002;74:941-949.
[140] Bird, SS, Marur, VR, Sniatynski, MJ, et al., Lipidomics profiling by high-resolution LC-MS and high-energy collisional dissociation fragmentation: focus on characterization of mitochondrial cardiolipins and monolysocardiolipins, Anal Chem, 2011;83:940-949.
[141] Hartler, J, Tharakan, R, Kofeler, HC, et al., Bioinformatics tools and challenges in structural analysis of lipidomics MS/MS data, Brief Bioinform, 2013;14:375-390.
[142] Pauling, J and Klipp, E, Computational Lipidomics and Lipid Bioinformatics: Filling In the Blanks, J Integr Bioinform, 2016;13:299.

# 1 Chapter 1: Elucidating the chemical structure of native 1-deoxysphingosine

Regula Steiner[1*], Essa M. Saied[2*], Alaa Othman[1,$], Christoph Arenz[3], Alan T. Maccarone[4], Berwyck L. J.Poad[5], Stephen J. Blanksby[5], Arnold von Eckardstein[1] and Thorsten Hornemann[1#]

*Affiliations*

1. Institute of Clinical Chemistry, University and University Hospital of Zurich, Raemistrasse 100, CH-8091 Zurich, Switzerland
2. Institute for Chemistry, Humboldt Universität zu Berlin, Brook-Taylor-Str. 2, 12489 Berlin, Germany and Institute for Chemistry Suez Canal University, Egypt
3. Institute for Chemistry, Humboldt Universität zu Berlin, Brook-Taylor-Str. 2, 12489 Berlin, Germany
4. Mass Spectrometry User Resource and Research Facility, School of Chemistry, University of Wollongong, NSW 2522, Australia
5. Central Analytical Research Facility, Institute for Future Environments, Queensland University of Technology, QLD 4001, Australia

* both authors contributed equally to this work

$ current address: Center of Brain Behaviour and Metabolism(CBBM) Institute of Experimental and Clinical Pharmacology and Toxicology University of Lübeck Ratzeburger Allee 160, 23562 Lübeck

\# corresponding author:

Thorsten Hornemann
Institute of Clinical Chemistry
University and University Hospital of Zurich,
Raemistrasse 100,
CH-8091 Zurich
Switzerland

Published: Steiner, R, Saied, EM, Othman, A, et al., Elucidating the chemical structure of native 1-deoxysphingosine, J Lipid Res, 2016;57:1194-1203.

Author contributions: Steiner R did the cell culture, acquired, analyzed, and interpreted LC-MS based and DMDS adduct data and wrote the manuscript. Saied, EM and Arenz C synthesized 1-deoxysphigosine standards. Othman A contributed to the data interpretation. Maccarone AT, Poad BLJ and Blanksby SJ were responsible for differential mobility spectrometry with ozone-induced dissociation experiments. Von Eckardstein A supervised the study and critically revised the manuscript. Hornemann T supervised the study, was involved in data interpretation, and critically revised the manuscript.

## 1.1 Abstract

1-Deoxysphingolipids (1-deoxySL) are formed by an alternate substrate usage of the enzyme serine-palmitoyltransferase and devoid of the $C_1$-OH-group present in canonical sphingolipids (SL). Pathologically elevated 1-deoxySL levels are associated with the rare inherited neuropathy HSAN1 and diabetes type 2 (T2DM) and might contribute to beta cell failure and the diabetic sensory neuropathy. In analogy to canonical SL it was assumed that also 1-deoxySL bear a (4*E*) double bond which is normally introduced by sphingolipid delta(4)-desaturase 1 (DES1). This, however, was never confirmed. We therefore supplemented HEK293 cells with isotope labeled $D_3$-1-deoxy-sphinganine (1-deoxySA) and compared the downstream formed $D_3$-1-deoxy-sphingosine (1-deoxySO) to a commercial synthetic SPH m18:1(4*E*)(3OH) standard. Both compounds showed the same mass-to-charge ratio (*m/z*) but differed in their RPLC retention time and APCI in-source fragmentation, suggesting that the two compounds are structural isomers. Using dimethyl disulfide (DMDS) derivatization followed by $MS^2$ as well as differential mobility spectrometry combined with ozon-induced dissociation mass spectrometry, we identified the carbon-carbon DB in native 1-deoxySO to be located at (Δ14) position. Comparing the chromatographic behavior of native 1-deoxySO to chemically synthesized SPH m18:1(14*Z*) and (14*E*) stereoisomers assigned the native compound to be SPH m18:1(14*Z*). This indicates that 1-deoxySL are metabolized differently than canonical sphingolipids.

**Keywords**

deoxysphingolipids, 1-deoxysphingosine, double bond position, dimethyl disulfide adducts, mass spectrometry, differential mobility spectrometry, ozone-induced dissociation, structural isomers

## 1.2 Introduction

Sphingolipids are typically formed by the condensation of L-serine and palmitoyl-CoA, a reaction catalyzed by the serine-palmitoyltransferase (SPT) enzyme. Besides these canonical substrates SPT can use other acyl-CoA's but also L-alanine or glycine as substrate which then forms a category of atypical 1-deoxysphingolipids (1-deoxySL) which lack the $C_1$-OH group of canonical sphingolipids [1, 2].

Several missense mutations in SPT, which are associated with the rare inherited neuropathy HSAN1, induce a permanent shift in the substrate specificity of the enzyme resulting in a increased 1-deoxySL formation. HSAN1 is a rare autosomal and dominantly inherited axonopathy and clinically characterized by a progressive loss of pain and temperature sensation often accompanied by neuropathic pain attacks and skin ulcers [3]. 1-DeoxySL are toxic to primary sensory neurons in culture and lead to neurite retraction and the disruption of the neuronal cytoskeleton structure in a dose dependent manner [3, 4]. They also interfere with the survival and insulin secretory capacity of pancreatic beta cells and 1-deoxySL plasma levels have been found to be prospective biomarkers for the risk to develop T2DM [5-7].

The 1-deoxy-sphinganine (1-deoxySA) that is formed by SPT can be converted to 1-deoxy-ceramides (1-deoxyCer) but not to complex sphingolipids because of the missing $C_1$-OH group. During catabolism 1-deoxyCer is degraded by ceramidase to form 1-deoxysphingosine (1-deoxySO) but not phosphorylated to form the catabolic intermediate sphingosine-1-P (S1P). This prevents its cleavage to hexadecenal by S1P-lyase meaning that 1-deoxySL cannot be degraded by the canonical catabolic pathway [2]. Apart from that, it was assumed that 1-deoxySA is metabolized by the same set of enzymes as canonical sphingoid bases and that 1-deoxySO like SO bears a (4*E*) double bond which is introduced by the sphingolipid delta(4)-desaturase 1 (DES1).

However, we observed that natively formed 1-deoxySO showed a different RPLC retention time than a synthetic SPH m18:1(4*E*)(3OH) standard, though the *m/z* was identical for both compounds. This suggested that native 1-deoxySO and the synthetic SPH m18:1(4*E*)(3OH) are

structural isomers probably differing in position and / or configuration of the carbon-carbon double bond. To further elucidate this difference we used a set of tandem mass spectrometry methods in combination with total synthesis to elucidate the real double bond position and configuration of native 1-deoxySO.

## 1.3 Materials and Methods

Unless stated differently all solvents and reagents were purchased from Sigma-Aldrich Chemie GmbH (Buchs, Switzerland) excluding methanol, which was purchased from Honeywell specialty chemicals Seelze GmBH, Germany.

### 1.3.1 Cell extract

HEK293 cells were fed with 1 µM deuterium labelled $D_3$-1-deoxysphinganine (Avanti Polar Lipids, Alabaster, AL) or with the unlabeled 1-deoxysphinganine (Avanti Polar Lipids, Alabaster, AL). Cells were harvested after 24 h and the whole sphingolipid extract was hydrolyzed to get the free sphingoid bases as described previously with some modifications [7, 8]. The cell pellet was dissolved in 100 µL of PBS. 500 µL methanol including $D_7$-sphingosine and $D_7$-sphinganine (Avanti Polar Lipids, Alabaster, AL) as the internal standards were added. Lipids were extracted for one hour under constant agitation at 37°C. Samples were centrifuged to pellet precipitated proteins and the supernatant transferred into a new tube. Lipids were hydrolyzed by adding 75 µL of methanolic HCl (1 N HCl and 10 M $H_2O$ in methanol) and incubated for 16 h at 65°C. HCl was neutralized by adding 100 µL of KOH (10M). Then 625µL chloroform was added followed by 100 µL 2N ammonium hydroxide and 0.5 mL alkaline water to complete phase separation. The sample was vortexed, centrifuged at 16,000 g for 5 min, the upper phase discarded and the lower (organic) phase washed 3 times with alkaline water. The organic phase was finally dried under $N_2$ and stored at −20$^{o}$C until analysis.

Throughout this paper we refer to the extracted 1-deoxySO as *native*.

### 1.3.2 LC-MS Method

A commercial 1-deoxySO standard (SPH m18:1(4*E*)(3OH)) was purchased from Avanti Polar Lipids Inc. (Alabaster, AL). SPH m18:1(14*Z*)(3OH) was synthesized according to the method

described below. The SPH m18:1(*E*)(3OH) standards (5*E*, 8*E*, 12*E*, 13*E,* 14*E*) were synthesized based on an unpublished method that will be issued elsewhere [*]. An LC-MS method described previously [8], was used to compare retention times and in source fragmentation. Sphingoid bases were separated by RPLC on a C18-column (Uptispere 120 Å, 5 µm, 125 × 2 mm; Interchim, Montluçon, France) and analyzed on a TSQ Quantum Ultra or a Q Exactive (Thermo, Reinach, BL, Switzerland) using an atmospheric pressure chemical ionization (APCI) interface. Mobile phases consisted of A: ultra-pure $H_2O$ / MeOH 1/1 v/v with 2.6 mM ammonium acetate and B: MeOH. Gradient was set from 50 % B to 100 % B within 25 min followed by 5 min 100 % B and 5 min of equilibration with a flow rate of 0.3 mL/min. For mass spectral detection, the following parameters were set on the APCI source: discharge current of 4 µA, vaporizer temperature of 450 °C, sheath gas pressure 20 AU, aux gas 5 AU and capillary temperature of 200 °C.

### 1.3.3 DMDS adduct analysis

Dimethyl disulfide (DMDS, 100 µL) and 20 µL of $I_2$ (in diethyl ether, 60 mg/mL) was added to whole cell extracts or 15 nmol SPH m18:1(4*E*)(3OH) standard. Samples were agitated for 16 h in an Eppendorf Thermo Shaker at 1400 rpm and 35°C. The reaction was quenched with 100 µL of 5% aqueous $Na_2S_2O_3$, extracted with 200 µL of hexane and dried under $N_2$. Samples were dissolved in 200 µL isopropanol for further analysis according to the method of Dunkelblum *et al* [9]. The sample was directly injected into the MS at a flowrate of 10 µL/min. The $[M + H]^+$ ion of the DMDS adduct of 1-deoxySO was generated by electrospray ionization (ESI) on a Thermo Fisher Scientific Q-Exactive and both collision-induced dissociation and high-resolution accurate mass analysis were performed. For detection, the following parameters were set on the ESI source: spray voltage of 4.2 kV, vaporizer temperature of 30°C, sheath gas pressure 5 AU, aux gas 0 AU, capillary temperature of 320°C and for fragmentation in-source collision-induced dissociation (CID) was performed at 30 eV and higher-energy collision induced dissociation (HCD) of the ion at *m/z* 378.3 was performed with setting of 25.

[*] Manuscript in preparation

### 1.3.4 Differential Mobility Spectrometry combined with Ozone-Induced Dissociation

A SelexION™ differential mobility spectrometer (DMS) was employed with a QTRAP®5500 triple quadrupole ion-trap mass spectrometer (SCIEX, Ontario, Canada). The instrument has been modified for ozone-induced dissociation (OzID) as previously described [10]. Solutions for analysis were prepared in LC-grade methanol (VWR Scientific, Murrarie, QLD, Australia) with 5 mM UPLC-grade ammonium acetate (Sigma Aldrich, St. Louis, MO); SPH standard concentrations were 0.05 µM. Sample solutions were subjected to ESI in a TurboV™ (SCIEX) and passed through the mobility spectrometer. Compensation voltage (CV) applied across the electrodes was scanned while the separation voltage (SV) was held constant at 4100 V. Ionograms were obtained from scanning CV and represent the sum of five mass spectra at each voltage point and have been smoothed using PeakView® (SCIEX). The ESI source and DMS cell temperatures were 100 and 150°C, respectively; the ESI voltage was set to 5500 V. Nitrogen was set to 20 psi for each of the following: resolving gas in the DMS cell, the nebulizing ESI gas, and the MS curtain gas. Ions exiting the DMS cell into the mass spectrometer were mass selected in first quadrupole prior to isolation in the collision cell with ozone present. Ozone was produced by an external generator (Titan, Absolute Ozone, Alberta, Canada) operating at 220 g/Nm$^3$ (10.3% v/v ozone in oxygen) from which a small portion was mixed into the nitrogen collision gas input to the mass spectrometer through a variable leak valve (Nenion, Lustenau, Austria). The isolation time for ionized lipids in the collision cell was optimized between 100 ms and 15 s depending on the ozone-reactivity of a given ionized lipid [11, 12]. Following ozonolysis, ions were transferred to the third quadrupole region where mass analysis was performed using a trap-scan at 1000 Th/s. OzID spectra obtained at discrete CV values were averaged between 2 to 5 mins.

### 1.3.5 Synthesis of 1-deoxysphingosine (SPH m18:1(14Z)(3OH) or (2S,3R,14Z)-2-aminooctadec-14-en-3-ol)

Eleven intermediate compounds en route to the target SPH m18:1 (14Z)(3OH) were synthesized as described in the supplementary info. A stirred solution of compound **11** (57 mg, 3 mmol) in 1,4- dioxane (1 mL) at 0°C was treated with a solution of 4M HCl-dioxane (2 mL) over a period of 10 min. The resulting reaction mixture was allowed to stir for 1 h at the same conditions, gradually warmed to ambient temperature, and followed by TLC analysis. After being stirred for additional 2 h (as monitored by TLC, Pet. ether/EtOAc 4:1; $R_{f(adduct)}$= 0.5; $R_{f(product)}$=0.0; visualized with $KMnO_4$ solution), the reaction mixture was concentrated under reduced pressure. The resultant residue was dissolved in with $CH_2Cl_2$ (50 mL) and sequentially washed with saturated $NaHCO_3$ solution (40 mL), water (30 mL), and brine solution (40 mL). The organic layer was subsequently dried over anhydrous $Na_2SO_4$, filtered and concentrated *in vacuo* to afford a pale yellow oily residue. Flash column chromatography of the obtained crude amine over silica gel using ethylacetate and isopropanol as eluents (from 0-10% isopropanol in ethylacetate) provided the final compound **12** as colorless oil. Yield: 32 mg (71%). $R_f$: 0.32 (EtOAc/iso-propanol 4:1, visualized with 1.3% ninhydrine). $^1$H NMR (500 MHz, MeOD) δ 5.35 (ddd, *J* = 5.9, 3.6, 2.8 Hz, 2H), 3.70 (ddd, *J* = 8.1, 5.3, 3.0 Hz, 1H), 3.26 (qd, *J* = 6.7, 3.1 Hz, 1H), 2.07 – 1.98 (m, 4H), 1.52 (dt, *J* = 10.3, 8.2 Hz, 1H), 1.47 – 1.41 (m, 2H), 1.41 – 1.28 (m, 18H), 1.21 (d, *J* = 6.8 Hz, 3H), 0.91 (t, *J* = 7.4 Hz, 3H).$^{13}$C NMR (126 MHz, MeOD) δ 131.05, 130.65, 71.71, 52.61, 34.02, 30.86, 30.75, 30.73, 30.69, 30.65, 30.35, 30.31, 28.15, 27.00, 23.98, 14.16, 12.08. HRMS (ESI$^+$) *m/z* calcd for $C_{18}H_{38}NO$ $[M + H]^+$ 284.2953; found 284.2959.

## 1.4 Results

### 1.4.1 1-deoxySO is a downstream metabolite of 1-deoxySA

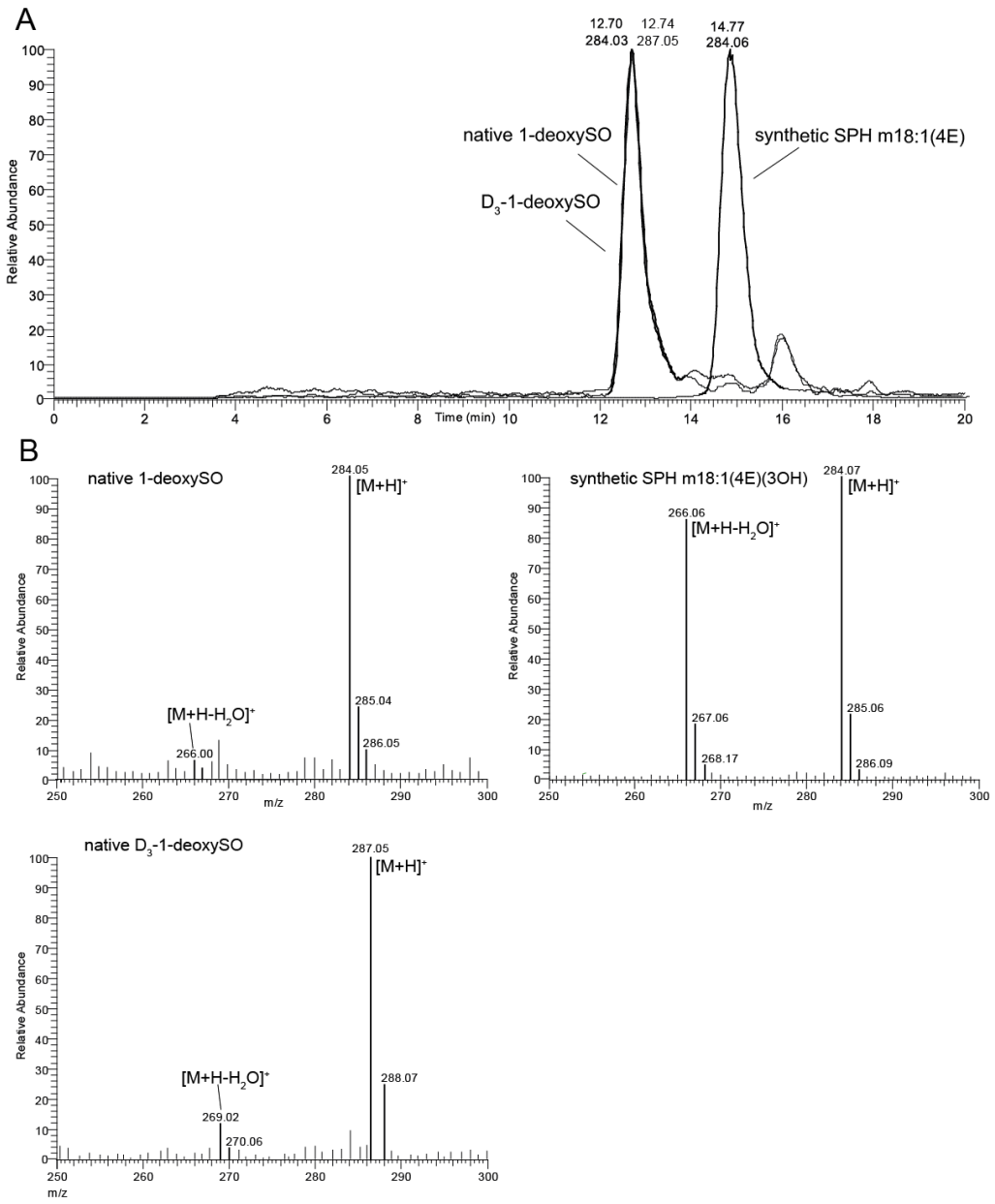


Figure 1-1: (A) Difference RPLC retention time of synthetic SPH m18:1(4E)(3OH) and native 1-deoxySO extracted from HEK293 cells treated with 1-deoxySA or $D_3$-1-deoxySA. (B) APCI in-source fragmentation of a synthetic SPH m18:1(4E)(3OH) standard, native 1-deoxySO and $D_3$-1-deoxySO: the precursor [M + H]+ ion (*m/z* of 284) is identical for SPH m18:1(4E)(3OH) and native 1-deoxySO. However, synthetic SPH m18:1(4E)(3OH) formed an abundant [M + H - H2O]+ product ion (*m/z* 266) which was formed much less from native 1-deoxySO and $D_3$-1-deoxySO at identical conditions. MS spectra were recorded on a triple quad MS (TSQ Quantum Ultra) with APCI ionization.

HEK293 cells were cultured in the presence of deuterium labeled $D_3$-1-deoxySA or unlabeled 1-deoxySA. Cells were harvested after 24 h and the profile of the extracted sphingoid bases analyzed by RPLC-MS. We observed the appearance of $[M + H]^+$ ions with *m/z* 284.3 (unlabeled 1-deoxySO) and of *m/z* 287.3 (labeled $D_3$-1-deoxySO) which both eluted at the same time from the LC column (Figure 1-1A), indicating that 1-deoxySO is a product formed downstream of 1-deoxySA (labeled and unlabeled).

### 1.4.2 Comparison of synthetic SPH m18:1(4*E*) and native 1-deoxySO

Retention time and APCI in-source fragmentation was compared between native 1-deoxySO and a commercially available synthetic SPH m18:1(4*E*)(3OH) standard. The native 1-deoxySO eluted from the C18 column after 12.70 min whereas the synthetic SPH m18:1(4*E*)(3OH) eluted after 14.77 min (Figure 1-1A). $[M + H]^+$ ions formed by APCI showed in-source fragmentation and a significant water loss for the SPH m18:1(4*E*)(3OH) standard which was considerably less pronounced for the native 1-deoxySO (B). As both molecules showed identical *m/z* using high-resolution accurate mass spectrometry (HRAMS, < 2ppm for $[M + H]^+$ and $[M + H - H_2O]^+$ ) the observed deviations in retention time and in-source fragmentation suggested that native 1-deoxySO and the synthetic SPH m18:1(4*E*)(3OH) were structural isomers.

### 1.4.3 Dimethyl disulfide (DMDS) derivatization

As the synthetic SPH m18:1(4*E*)(3OH) and the native 1-deoxySO showed different RPLC properties we aimed to elucidate the carbon-carbon double bond position of native 1-deoxySO by derivatization with dimethyl disulfide (DMDS). The DMDS adducts of 1-deoxySO were analyzed by HRAMS using direct injection and ESI ionization. The $[M + H]^+$ ions from the DMDS adducts of 1-deoxySO were selected at *m/z* 378.3 and subjected to collision-induced dissociation. The CID spectrum showed four abundant but non-specific product ions at *m/z* 330.3 $[M + H - CH_3SH]^+$, 312.3 $[M+H - CH_3SH - H_2O]^+$, 282.3 $[M + H -2CH_3SH]^+$ and 264.3 $[M + H - 2CH_3SH - 2H_2O]^+$ corresponding to the neutral loss of methane thiols and water as indicated (Figure 1-2).

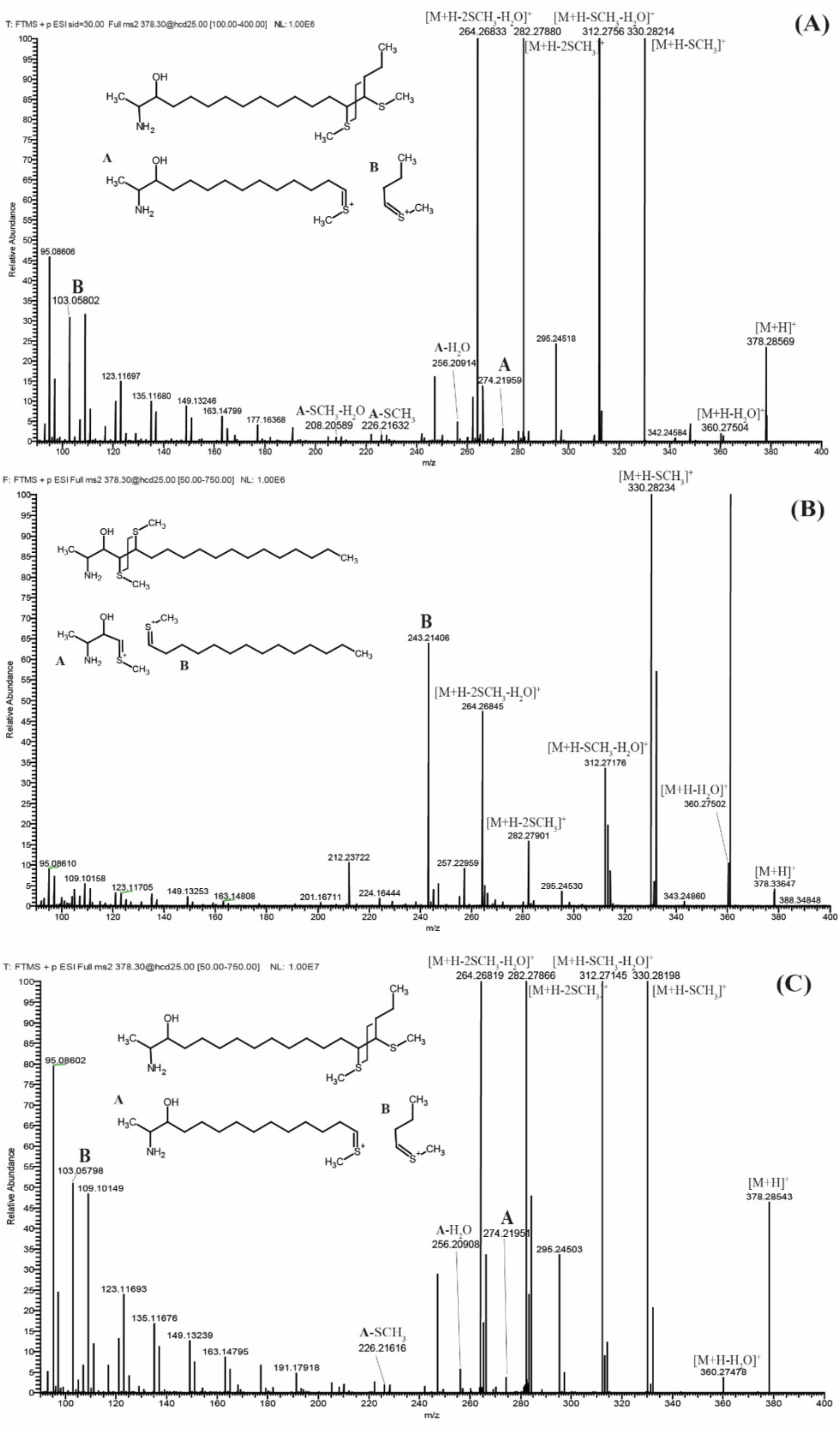


Figure 1-2: (A) Hydrolyzed lipid extract from HEK293 cells was subjected to DMDS derivatization and analyzed on a high-resolution accurate mass spectrometer using ESI ionization and direct injection. The [M + H]+ ion formed from DMDS adduct of native 1-deoxySO (*m/z* of 378.2857) was in excellent agreement (< 1 ppm) with the calculated mass of 378.2859 ($C_{20}H_{44}NOS_2^+$). The precursor ion was selected for collision-induced dissociation yielding to the spectrum shown. Product ions A (*m/z* 274) and B (*m/z* 103) are indicated in the spectrum and are diagnostic for a fragmentation at (Δ14) position. (B) Spectrum from SPH m18:1(4E)(3OH) showing product ion B (*m/z* 243). (C) Spectrum from SPH m18:1(14Z)(3OH) showing product ions A (*m/z* 274) and B (*m/z* 103). Putative structures for the diagnostic product ions are shown as insets in the spectra.

Importantly, two less abundant but structurally diagnostic product ions were observed at *m/z* 274.2 (**A**) and 103.1 (**B**). These product ions were formed by a cleavage of the carbon-carbon bond between the two methyl sulfide moieties. The mass distribution of the two fragments indicated a double bond in (Δ14)-position for native 1-deoxySO. Product ions indicating a fragmentation at the (Δ4)-position (*m/z* 243.2 and 134.1) were not detected.

**Differential-mobility spectrometry (DMS) combined with Ozone-Induced Dissociation**

DMS has previously been deployed successfully for lipid isomer separation prior to mass spectrometric analysis [10, 13]. Here it was combined with OzID which exploits the reaction between mass-selected lipid ions and gaseous ozone inside a mass spectrometer to drive fragmentation diagnostic of the position(s) of carbon-carbon double bonds [12, 14]. In these experiments the $D_3$-labeled hydrolyzed extract from HEK293 cells was spiked with a 1:1 mixture of the unlabeled commercial SPH m18:1(4*E*)(3OH) and synthesized SPH m18:1(14*E*)(3OH) structural isomers and the mixture subjected to electrospray ionization. Figure 1-3A shows DMDS ionograms obtained for *m/z* 284 (black trace) and 287 (red trace) corresponding in mass to the $[M + H]^+$ ions expected from unlabeled and labeled 1-deoxySO, receptively. The black trace shows peaks corresponding to at least two chemically distinct ion populations of *m/z* 284 (*i.e.,* isobars): one with a maximum CV at around 17 V and another peaking at 20 V. Isobars carrying *m/z* 284 in this mixture should be dominated by the protonated forms of the synthetic SPH m18:1(4*E*)(3OH) and SPH m18:1(14*E*)(3OH) isomers. The red trace, corresponding to isobars of *m/z* 287 (Figure 1-3A), showed an analogous pair of peaks at CV 17 and 20 V. These signals could be assigned to $[M + H]^+$ ions arising from native forms of 1-deoxySO present in the cell extract. To interrogate the structure of the ions responsible for each of the two peaks in the ionogram, OzID spectra were acquired for *m/z* 284 and 287 ions using fixed CV settings of 17 V and 20 V. Figure 1-3B shows product ions arising from the synthetic lipids (at *m/z* 284) in black and the corresponding $D_3$-labeled native lipid (at *m/z* 287) in red. Both spectra revealed product ions arising from neutral loss of 40 and 24 Da characteristic of ozonolysis of a carbon-carbon double bond at the (Δ14)-position on the sphingoid backbone [15] (see Supplementary Figure 1A and Supplementary Table 1). Conversely, in the OzID spectra obtained at a CV of 20

V (Figure 1-3C) these product ions were absent, while fragments arising from oxidative cleavage of a (Δ4)-double bond (neutral losses of 180 and 164) were observed at *m/z* 104 and 120 for the unlabeled standard (see Supplementary Figure 1B and supplementary Table 1). Of this pair of ions, the aldehyde is mass-shifted and appears as expected at *m/z* 107 for the $D_3$-isotopologue while the *m/z* 123 is absent in this spectrum: possibly due to the lower abundance of the CV = 20 V feature in the native extract. Interestingly, an abundant water loss was observed in the spectra in Figure 1-3C, which is much diminished in the spectra in Figure 1-3B providing further evidence of the structural difference between the two lipids.

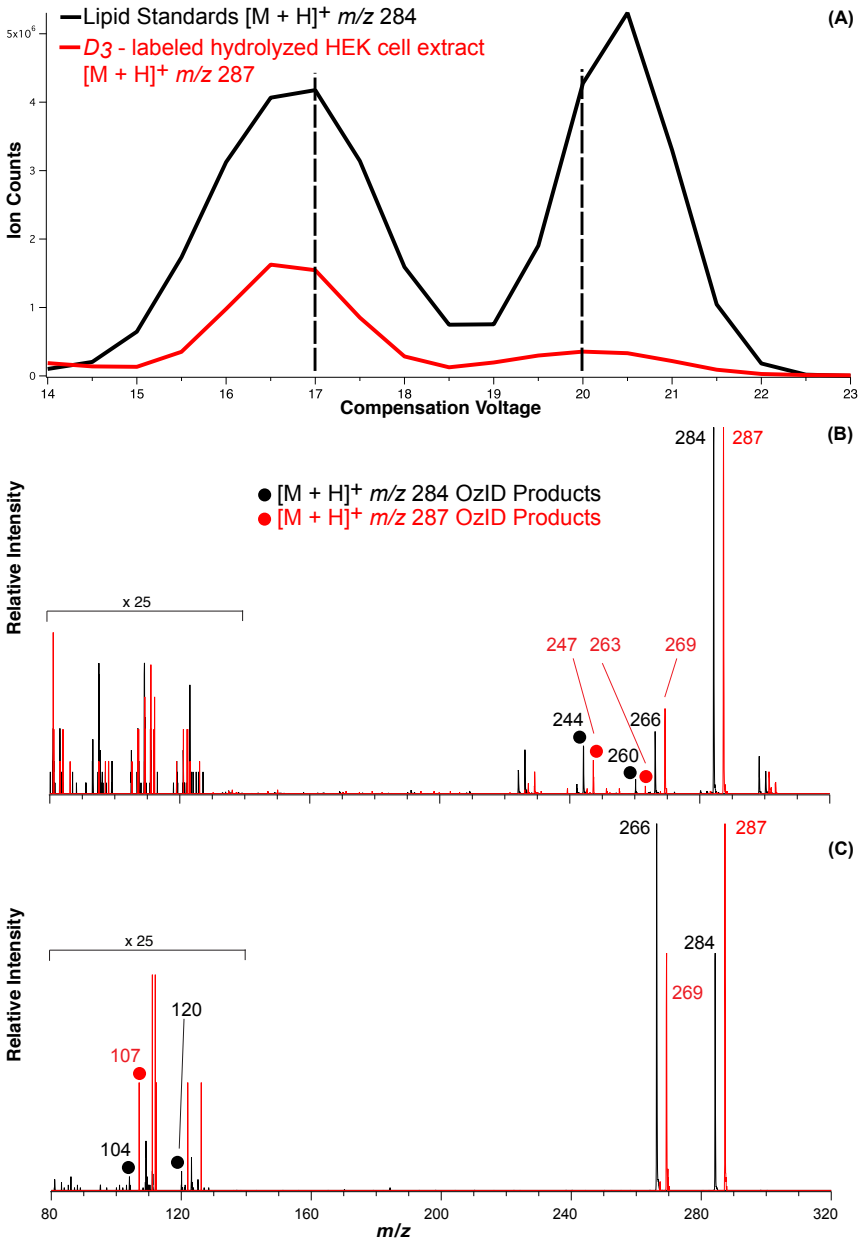


Figure 1-3: ESI(+) was undertaken on a mixture of $D_3$-labeled hydrolyzed HEK293 cell lipid extracts spiked with unlabeled synthetic standards SPH m18:1(4E)(3OH) and SPH m18:1(14E)(3OH). (A) Ionograms showing separation in voltage space of the [M + H]+ ions formed from the two lipid isomers. Each of the synthetic lipids spiked into the extract produced a peak in the black trace (*m/z* 284) and similar features were observed for the labeled HEK293 extract shown in the red trace (*m/z* 287). (B) OzID spectra obtained for synthetic standard (black spectrum) and the $D_3$-labelled extract (red spectrum) corresponding to the first feature in the ionogram (i.e., CV = 17 V ozone reaction time of 100 ms). (C) OzID spectra obtained for synthetic standard (black spectrum) and the $D_3$-labelled extract (red spectrum) corresponding to the second feature in the ionogram (i.e., CV = 20 V ozone reaction time of 15 s). OzID product ions characteristic of the locations of the carbon-carbon double bonds are indicated by closed circles and enable assignment of the position of desaturation to (B) (Δ 14) - position and (C) (Δ4) - position.

DMS-OzID analysis was also performed on non-hydrolyzed lipid extract from HEK293 cells. Four 1-deoxyceramide species could be detected as $[M + H]^+$ ions consistent with the assignments: Cer m18:1/16:0, Cer m18:1/18:0, Cer m18:1/22:0 and Cer m18:1/24:1. As before, the OzID spectra showed a neutral loss of 40 Da as a characteristic signature for 1-deoxySO with a carbon-carbon double bond at the (Δ14)-position (Figure 1-4). These data support the presence of the (Δ14) carbon-carbon double bond in both 1-deoxyceramide and the 1-deoxySO and exclude the possibility that the observed (Δ14) desaturation is formed as an artifact of the hydrolysis reaction.

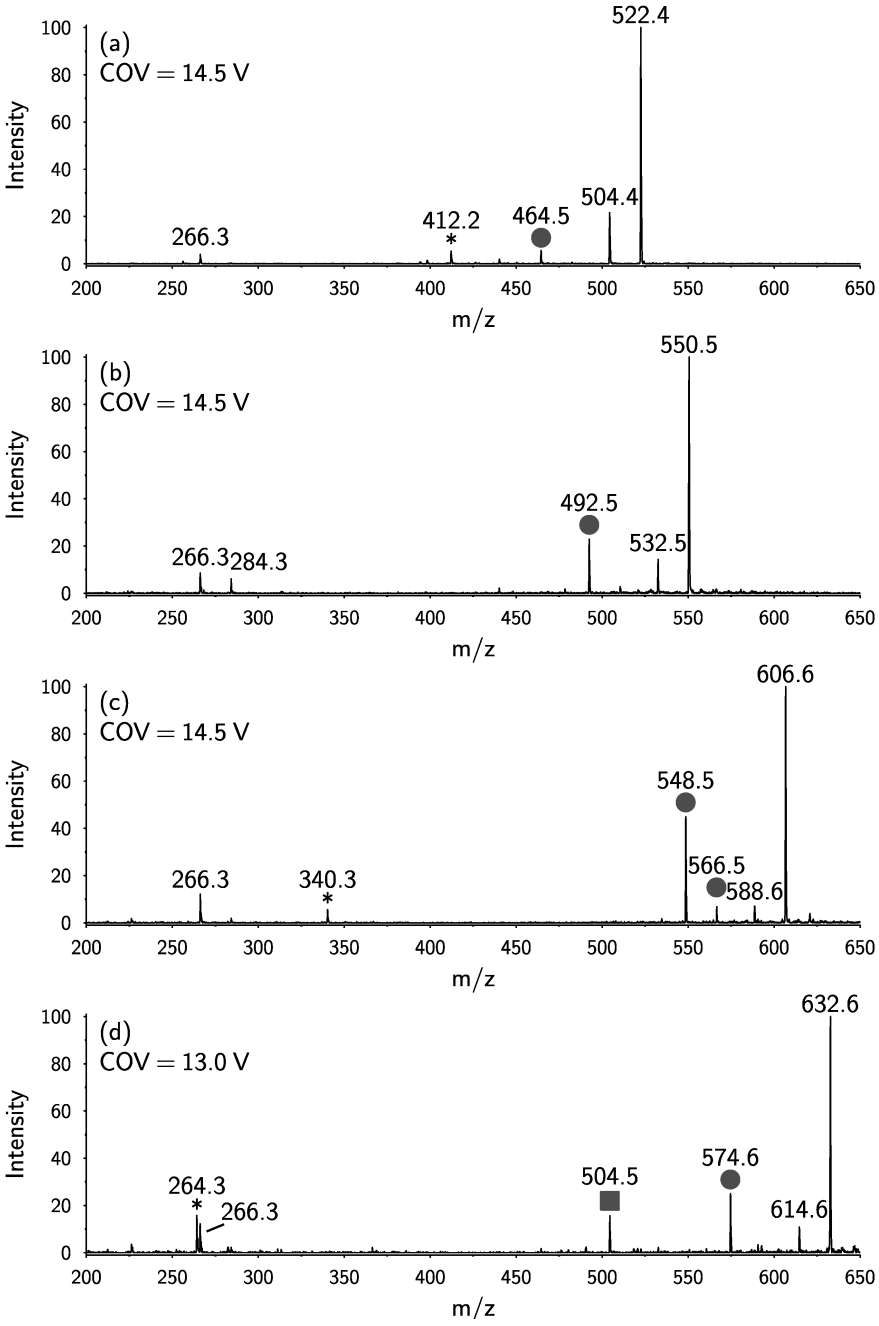


Figure 1-4: ESI(+)-OzID spectra obtained for *m/z* values corresponding to deoxyceramides present in an non-hydrolyzed HEK293 cell lipid extract. All spectra show a product ion at *m/z* 266, which is consistent with the collision-induced dehydration of the backbone followed by cleavage of the amide bond to liberate the acyl chain. Product ions arising from a characteristic neutral loss of 40 Da from the [M+H]+ or [M+H-H2O]+ are marked with circles and are consistent with an n-4 double bond (i.e., a Δ14 double bond in the SPH m18:1 backbone). Product ions arising from a characteristic neutral loss of 110 Da from the [M+H]+ or [M+H-H2O]+ are marked with squares and are consistent with the presence of an n-9 double bond (e.g., 24:1 Δ15 acyl chain). These spectra are consistent with the deoxyceramides (a) Cer m18:1(Δ14)/16:0, (b) Cer m18:1(Δ14)/18:0, (c) Cer m18:1(Δ14)/22:0, (d) Cer m18:1(Δ14)/24:1(Δ15). (See also supplementary Figure 2 and supplementary table 1). Product ions marked with an asterisk (*) showed different mobility characteristics to the OzID peaks and likely arise from isobaric interference.

### 1.4.4 Synthesis of deoxy-Sphingosine standards

Although the previous analysis confirmed the (Δ14) carbon-carbon double bond in native 1-deoxySO they did not unambiguously assign the stereochemistry of the bond. To further confirm the position and configuration of the double bond a number of 1-deoxySO analogues with different double bond positions and confirmations (5*E*, 8*E*, 12*E*, 13*E*, 14*E* and 14*Z*) were synthesized. Here we focus on the synthesis of the SPH m18:1(14*Z*)(3OH) as details on the synthesis of the other derivatives will be published elsewhere[†]. The synthesis of SPH m18:1(14*Z*)(3OH) **12** commenced from commercially available 1,10-decandilol (Figure 1-5). Treatment of 1,10-decanediol with dihydropyran in the presence of a catalytic amount of *p*-toluenesulfonic acid (PTSA) afforded the mono-THP ether **3** in moderate yield. Subsequent conversion of mono-hydroxyl compound **3** to the corresponding bromo derivative **4** was accomplished through treatment of **3** with tetrabromomethane ($CBr_4$) and triphenyl phosphine ($PPh_3$) to provide compound **4**. With intermediate **4** in hand, the coupling with lithiated 1-pentyne was performed following a previously described protocol [16] with some modifications (see supporting information Table 1 for details). Thus, *tert*-butyllithium was added to 1-pentyne at -78°C, and the *in situ* generated 1-lithio-1-pentyne was sequentially reacted with DMPU and bromo substrate **4** to afford compound **5** in a satisfactory yield. Subsequent stereoselective hydrogenation of alkyne **5** was accomplished with Lindlar catalyst after optimization of reaction conditions to afford the desired *Z*-configuration of the alkene **6** as a sole isomer (see supporting information Table 2 for more details). It is noteworthy, that initial attempts to furnish alkene **6** led to a product that was contaminated (10-15%) with inseparable by-products. Careful analysis of $^1$H-NMR spectra of the crude mixture identified these by-products as the *E*-configured alkene and the over reduced-product 1-bromopentadecane. Cleavage of the THP-protecting group in **6** under acid-catalyzed ethanol treatment proceeded smoothly to provide the hydroxyl alkene **7** which was subsequently subjected to Appel reaction with $CBr_4$/$PPh_3$ to furnish the *Z*-bromo-alkene **8**.

[†] Manuscript in preparation

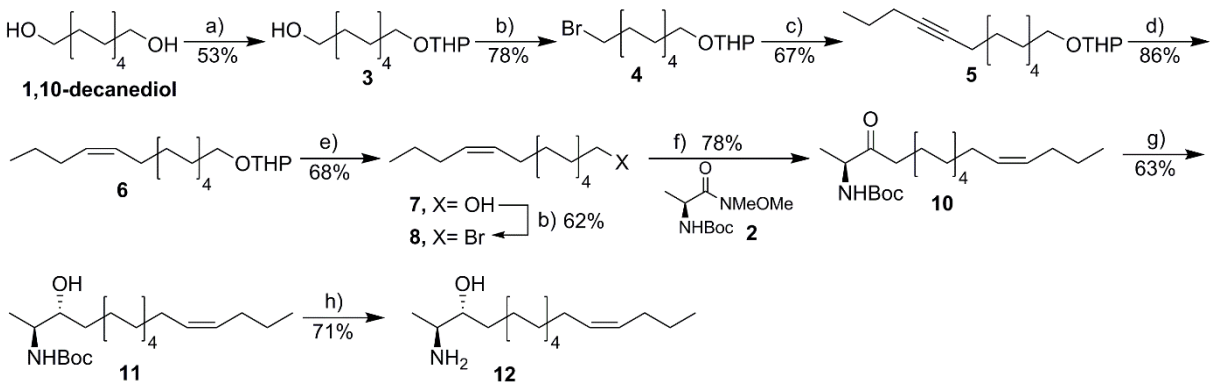


Figure 1-5: Synthesis of the 14Z-deoxy-sphingosine analogue. Reagents and conditions: a) DHP, PTSA (cat.), THF:DCM, 0°C-rt, 12 h. b) CBr4, PPh3, DCM, 0°C-rt, 4 h. c) (i) 1-Pentyne, tert-BuLi, toluene, -78°C, 1 h, and then (ii) DMPU, 4, THF, -78°C-rt, 7 h d) H2, EDA, Lindlar catalyst, 5% DMF in EtOAc, 0°C, 6 h. e) PPTS (cat.), EtOH, 62°C, 2 h. f) (i) Mg, 1,2-DBE (drops), Et2O, reflux, 2 h, and then (ii) 2, MeMgBr, DCM:Et2O; reflux, 2 h. g) TBLAH, EtOH, -78°C, 1 h  h) 4M HCl-Dioxane, 0°C, 3 h.

Next, the obtained bromo-alkenyl chain **8** was converted into the corresponding Grignard reagent **9** and subsequently coupled to the Weinreb amide **2** (prepared from L-alanine in two steps, see the supporting information for details). Toward this end, Weinreb amide **2** was reacted with 0.9 equivalent of methylmagnesium bromide (as sacrificial base), followed by addition the Grignard reagent **9** to afford ketone **10** in 78% isolated yield. The subsequent diastereoselective reduction of the carbonyl group in **10** with lithium tri-(*tert*-butoxy)-aluminum hydride (TBLAH) (1.7 equiv.) in absolut ethanol at -78°C was accomplished without reduction of the double bond to furnish the desired *anti*-amino alcohol **11** as a mere stereoisomer. Acidic hydrolysis of the *tert*-butyl carbamate protecting group of **11** with 4M HCl-dioxane solution yieled the corresponding hydrochloric salt of SPH m18:1(14*Z*)(3OH) (.HCl). The desired product **12** was finally obtained after neutralization workup in 71% yield.

### 1.4.5 Retention-time correlation of native lipids with synthetic standards

The RPLC retention times of the synthetic SPH m18:1(*E*)(3OH) standards with double bonds in positions 5*E*, 8*E*, 12*E* and14*E*, were compared. We observed an inverse logarithmic correlation ($R^2$=0.96) between retention times and the double bond position (Figure 1-6A). The more the DB was positioned towards the *omega* end the earlier the molecule eluted from the column. The closest match in retention time between native 1-deoxySO and the synthetic standards was

seen again for SPH m18:1(14*E*)(3OH) although the elution time between the two compounds still differed by about 30 seconds (Figure 1-6B).

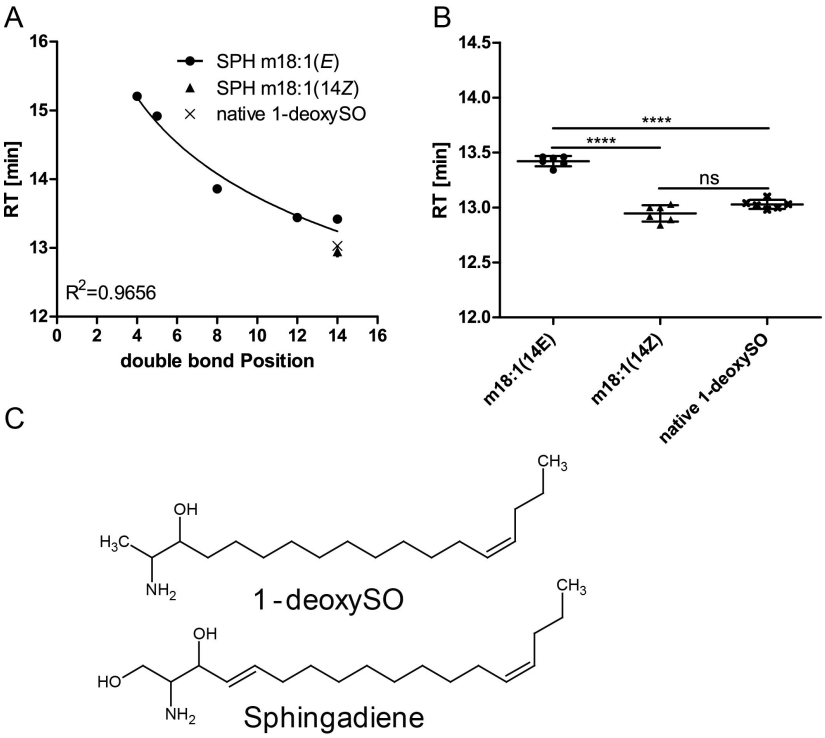


Figure 1-6: (A) RPLC retention times for a set of synthetic SPH m18:1 standards having double bonds in positions (4E), (5E), (8E), (12E) and (14E). The position of the double bond within the alkyl chain showed a logarithmic correlation to the retention times (B) Comparing the retention times of native 1-deoxySO to the synthetic standards SPH m18:1 (14Z) and SPH m18:1 (14E) identified native 1-deoxySO as SPH m18:1 (14Z) ( **** p< 0.0001). (C) Comparison of the chemical structures of 1-deoxySO and Sphingadiene

To further elucidate the DB configuration, we compared the retention times of native 1-deoxySO with the synthetic standard in (14*Z*) configuration (Figure 1-6B and supplementary Figure 3). The SPH m18:1(14*Z*) eluted at 13.0 min and was therefore coinciding with the elution time of native 1-doxySO. From these results we conclude that native 1-deoxySO bears a (14*Z*) double bond.

## 1.5 Discussion

1-deoxySO is an atypical sphingolipid, lacking the $C_1$-hydroxylgroup of canonical sphingosine. It is a downstream metabolite of 1-deoxySA, which is formed by SPT due to its alternative activity with L-alanine. Because of the missing $C_1$-hydroxyl group, 1-deoxySO cannot be phosphorylated to sphingosine 1-phosphate and therefore also not degraded by S1P-lyase [2].

Pathologically elevated 1-deoxySL play an important role in the inherited neuropathy HSAN1 but were also found in other conditions like the metabolic syndrome and type 2 diabetes [3, 7]. However, the metabolism of 1-deoxySLs and their molecular structures has not been investigated in detail yet. Comparing native 1-deoxySO to a synthetic SPH m18:1(4*E*) standard by RPLC we observed a significant deviation in retention time although *m/z* was identical for both molecules. Analyzing the DMDS derivatized adducts of native 1-deoxySO by $MS^2$ revealed two specific fragments which indicated the double bond position at (Δ14) and therefore distinct to that of the canonical (Δ4)-position. The (Δ14)-position was further confirmed using differential mobility spectrometry combined with ozone-induced dissociation. Comparing retention times of native 1-deoxySO to a set of synthetic SPH m18:1 standards finally confirmed a (14*Z*) DB in native 1-deoxySO.

During the sphingolipid *de novo* synthesis, the sphingolipid delta(4)-desaturase 1 (DES1) normally introduces a (4*E*) double bond into the sphingoid base backbone of dihydro-ceramide to form ceramide. The observation that native 1-deoxySO bears a (14*Z*) instead of (4*E*) DB, indicates that the metabolism of 1-deoxySL deviates from that of canonical sphingolipids. Interestingly, sphingadiene (SAdiene) a polyunsaturated downstream product of sphingosine [17] has double bonds at both, (4*E*) and (14*Z*) positions (Figure 1-6C). The presence of a (14*Z*) double bond in both, SAdiene and native 1-deoxySO suggests that both metabolites are substrates of the same desaturase although the responsible enzyme is unknown so far [18]. The fact that exogenously added $D_3$-lableled 1-deoxySA is converted to $D_3$-labeled 1-deoxySO also showed that the double bond is introduced downstream of 1-deoxySA and not formed by an SPT mediated incorporation of an desaturated acyl-CoA. Interestingly, 1-deoxymethylsphingosine (1-deoxymethSO), the corresponding downstream product of 1-deoxymethylsphinganine which is formed by the condensation with glycine, seems to contain a (3*E*) DB. The *m/z* as well as RPLC retention time of native 1-deoxymethSO matched that of an synthetic m17:1 (3*E*)(2OH) standard (supplementary Figure 4). As 1-deoxymethSO contains only 17 carbons this equals the (4*E*) DB position of canonical SL.

In conclusion we provide strong evidences from multiple, orthogonal analytical techniques to unambiguously assign native 1-deoxySO as it is formed in HEK293 cells to be a SPH m18:1(14*Z*)(3OH) structure. This furthermore implies that 1-deoxy-ceramides are metabolized distinct from canonical sphingolipids. However, more detailed studies are needed to further investigate the enzymatic pathways and metabolic steps involved in the conversion of these lipids.

## 1.6 Acknowledgments

RS, AO, AVE and TH want to thank the following funding sources for support: The 7th Framework Program of the European Commission ("RESOLVE", Project number 305707), the Swiss National Foundation SNF (Project 31003A_153390/1); the Hurka Foundation, the Novartis Foundation and the Rare Disease Initiative Zurich ("radiz", Clinical Research Priority Program for Rare Diseases, University of Zurich). SJB and ATM would like to thank Assoc. Prof. Todd W. Mitchell for insightful discussion regarding the DMS-OzID experiments. SJB is supported by project funding through the Australian Research Council*via* the Discovery and Linkage programs (DP150101715and LP110200648;the latter is an industry partnership with SCIEX, Ontario, Canada).

## 1.7 References

[1] Merrill, AH, Jr., Sphingolipid and glycosphingolipid metabolic pathways in the era of sphingolipidomics, Chem Rev, 2011;111:6387-6422.
[2] Zitomer, NC, Mitchell, T, Voss, KA, et al., Ceramide synthase inhibition by fumonisin B1 causes accumulation of 1-deoxysphinganine: a novel category of bioactive 1-deoxysphingoid bases and 1-deoxydihydroceramides biosynthesized by mammalian cell lines and animals, J Biol Chem, 2009;284:4786-4795.
[3] Penno, A, Reilly, MM, Houlden, H, et al., Hereditary sensory neuropathy type 1 is caused by the accumulation of two neurotoxic sphingolipids, J Biol Chem, 2010;285:11178-11187.
[4] Jun, BK, Chandra, A, Kuljis, D, et al., Substrate Availability of Mutant SPT Alters Neuronal Branching and Growth Cone Dynamics in Dorsal Root Ganglia, J Neurosci, 2015;35:13713-13719.
[5] Zuellig, RA, Hornemann, T, Othman, A, et al., Deoxysphingolipids, novel biomarkers for type 2 diabetes, are cytotoxic for insulin-producing cells, Diabetes, 2014;63:1326-1339.
[6] Othman, A, Bianchi, R, Alecu, I, et al., Lowering plasma 1-deoxysphingolipids improves neuropathy in diabetic rats, Diabetes, 2015;64:1035-1045.
[7] Othman, A, Rütti, MF, Ernst, D, et al., Plasma deoxysphingolipids: a novel class of biomarkers for the metabolic syndrome?, Diabetologia, 2012;55:421–431.
[8] Othman, A, Benghozi, R, Alecu, I, et al., Fenofibrate lowers atypical sphingolipids in plasma of dyslipidemic patients: A novel approach for treating diabetic neuropathy?, J Clin Lipidol, 2015;9:568-575.
[9] Dunkelblum, E, Tan, SH and Silk, PJ, Double-bond location in monounsaturated fatty acids by dimethyl disulfide derivatization and mass spectrometry: Application to analysis of fatty acids in pheromone glands of four lepidoptera, J Chem Ecol, 1985;11:265-277.
[10] Maccarone, AT, Duldig, J, Mitchell, TW, et al., Characterization of acyl chain position in unsaturated phosphatidylcholines using differential mobility-mass spectrometry, J Lipid Res, 2014;55:1668-1677.
[11] Pham, HT, Maccarone, AT, Campbell, JL, et al., Ozone-induced dissociation of conjugated lipids reveals significant reaction rate enhancements and characteristic odd-electron product ions, J Am Soc Mass Spectrom, 2013;24:286-296.
[12] Poad, BL, Pham, HT, Thomas, MC, et al., Ozone-induced dissociation on a modified tandem linear ion-trap: observations of different reactivity for isomeric lipids, J Am Soc Mass Spectrom, 2010;21:1989-1999.
[13] Shvartsburg, AA, Isaac, G, Leveque, N, et al., Separation and classification of lipids using differential ion mobility spectrometry, J Am Soc Mass Spectrom, 2011;22:1146-1155.
[14] Thomas, MC, Mitchell, TW, Harman, DG, et al., Ozone-induced dissociation: elucidation of double bond position within mass-selected lipid ions, Anal Chem, 2008;80:303-311.
[15] Brown, SH, Mitchell, TW and Blanksby, SJ, Analysis of unsaturated lipids by ozone-induced dissociation, Biochim Biophys Acta, 2011;1811:807-817.
[16] Chen, J, Li, Y and Cao, XP, First stereoselective synthesis of serinol-derived malyngamides and their 1 '-epi-isomers, Tetrahedron-Asymmetr, 2006;17:933-941.
[17] Zhang, T, Barclay, L, Walensky, LD, et al., Regulation of mitochondrial ceramide distribution by members of the BCL-2 family, J Lipid Res, 2015;56:1501-1510.
[18] Renkonen, O and Hirvisalo, EL, Structure of plasma sphingadienine, J Lipid Res, 1969;10:687-693.
[19] Fyrst, H and Saba, JD, Sphingosine-1-phosphate lyase in development and disease: sphingolipid metabolism takes flight, Biochim Biophys Acta, 2008;1781:448-458.
[20] Alecu, I, Othman, A, Penno, A, et al., Cytotoxic 1-deoxysphingolipids are metabolized by a cytochrome P450-dependent pathway, J Lipid Res, 2017;58:60-71.
[21] Stockmann-Juvala, H and Savolainen, K, A review of the toxic effects and mechanisms of action of fumonisin B1, Hum Exp Toxicol, 2008;27:799-809.
[22] Rahmaniyan, M, Curley, RW, Jr., Obeid, LM, et al., Identification of dihydroceramide desaturase as a direct in vitro target for fenretinide, J Biol Chem, 2011;286:24754-24764.
[23] Cingolani, F, Casasampere, M, Sanllehi, P, et al., Inhibition of dihydroceramide desaturase activity by the sphingosine kinase inhibitor SKI II, J Lipid Res, 2014;55:1711-1720.
[24] Steiner, R, Saied, EM, Othman, A, et al., Elucidating the chemical structure of native 1-deoxysphingosine, J Lipid Res, 2016;57:1194-1203.
[25] Ternes, P, Franke, S, Zahringer, U, et al., Identification and characterization of a sphingolipid delta 4-desaturase family, J Biol Chem, 2002;277:25512-25518.
[26] Omae, F, Miyazaki, M, Enomoto, A, et al., DES2 protein is responsible for phytoceramide biosynthesis in the mouse small intestine, Biochem J, 2004;379:687-695.
[27] Enomoto, A, Omae, F, Miyazaki, M, et al., Dihydroceramide:sphinganine C-4-hydroxylation requires Des2 hydroxylase and the membrane form of cytochrome b5, Biochem J, 2006;397:289-295.

[28] Weiss, B and Stoffel, W, Human and murine serine-palmitoyl-CoA transferase--cloning, expression and characterization of the key enzyme in sphingolipid synthesis, Eur J Biochem, 1997;249:239-247.
[29] Hanada, K, Hara, T, Nishijima, M, et al., A mammalian homolog of the yeast LCB1 encodes a component of serine palmitoyltransferase, the enzyme catalyzing the first step in sphingolipid synthesis, J Biol Chem, 1997;272:32108-32114.
[30] Fabrias, G, Munoz-Olaya, J, Cingolani, F, et al., Dihydroceramide desaturase and dihydrosphingolipids: debutant players in the sphingolipid arena, Prog Lipid Res, 2012;51:82-94.

# 2 Chapter 2: The Metabolism of 1-Deoxymethylsphingolipids

*Regula Steiner*

## 2.1 Abstract

Canonical sphingolipids are formed by the condensation of palmitoyl-CoA and L-serine catalysed by serine palmitoyltransferase (SPT). Besides L-serine, SPT can also metabolize L-alanine and glycine. The conjugation with L-alanine forms 1-deoxysphingolipids, which lack the $C_1$-OH group, whereas the conjugation with glycine forms 1-deoxymethylsphingolipids (1-deoxymethylSL), which are devoid of the $C_1$-methanolic group (R-$C_1$-OH). They are natural lipids found in mammalian cells and human plasma but their biological role is not yet clear. Pathologically elevated 1-deoxySL and 1-deoxymethylSL cause the rare hereditary sensory neuropathy type 1 (HSAN1). 1-DeoxySL are toxic to primary sensory neurons in culture, lead to neurite retraction, and might contribute to beta cell failure and diabetic sensory neuropathy.

1-DeoxymethylSL are assumed to be metabolised by the same enzymes as canonical sphingolipids, although they can neither be degraded nor converted to complex sphingolipids due to the missing $C_1$-methanolic group. Here, we elucidated the metabolism of 1-deoxymethylSL in comparison to the canonical sphingolipid pathway.

HEK293 cells were supplemented with isotopic labelled 1-deoxymethylSA to study the metabolism of these lipids. Five new downstream metabolites of 1-deoxymethylSA were identified. 1-deoxymethylSL are converted to either mono- or di-desaturated species or alternatively are mono- or di-hydroxylated. The chemical structures were elucidated using liquid chromatography and high-resolution accurate mass spectrometry. Several enzymes of the canonical sphingolipid metabolism are involved in the formation of the desaturated or mono-hydroxylated species. The di-hydroxylated form is generated by a not yet known enzyme, which seems to be specific for 1-deoxymethylSL.

In summary, we demonstrated that 1-deoxymethySL follow partly the same but also other metabolic routes as canonical sphingolipids but also 1-deoxySL.

## 2.2 Introduction

The *de novo* synthesis of sphingolipids (SL) typically starts by the condensation of L-serine and palmitoyl-CoA, a reaction catalyzed by serine-palmitoyltransferase (SPT). Besides these canonical substrates, SPT can use other acyl-CoAs but also glycine or L-alanine as alternative substrates and thereby generate a category of atypical 1-deoxysphingolipids (1-deoxySL) and 1-deoxymethylsphingolipids (1-deoxymethylSL). These metabolites lack the $C_1$-OH or even the $C_1$-methanolic group of canonical sphingolipids [1, 2].

Several missense mutations in SPT are associated with the inherited neuropathy HSAN1, a rare autosomal dominant inherited axonopathy which is clinically characterized by a progressive loss of pain and temperature sensation often accompanied by neuropathic pain attacks and skin ulcers [3]. The missense mutations induce a permanent shift in the substrate specificity from L-serine to L-alanine and/or glycine resulting in increased 1-deoxySL and 1-deoxymethylSL formation [3]. 1-DeoxymethylSL have been found in mammalian cells and human plasma but their biological role is unknown so far.

When following the canonical SL metabolic pathway, the condensation of glycine and palmitoyl-CoA trough SPT forms 1-deoxymethylSA which is converted to the N-acetylated form by ceramide synthases (CerS) and 1-deoxymethyldihydroCeramide is finally converted to 1-deoxymethylCeramide by the introduction of a double bond. From that stage the lipids are not metabolized further because of the missing $C_1$-OH group. During catabolism, 1-deoxymethylCeramdies are degraded by ceramidase to form 1-deoxymethylsphingosine (1-deoxymethylSO) which in contrast to canonical SL cannot be phosphorylated to form the catabolic intermediate sphingosine-1-phosphate (S1P) [4]. This prevents its cleavage to hexadecenal by S1P-lyase so that 1-deoxymethylSL cannot be degraded by the canonical catabolic pathway [1, 2].

Previous studies showed that 1-deoxysphinganine (1-deoxySA), which arises from the condensation with L-alanine, has a different metabolism than canonical sphingolipids and that enzymes in the canonical sphingolipid pathway play a minor role in their metabolism.

Instead, a set of downstream metabolites were identified, which appear to be formed by of CYP 4F enzymes [5]. For 1-deoxymethylSL it is currently unclear, whether they follow the canonical or an alternative pathway.

We therefore compared the metabolism of the SPT products, which were formed by either the conjugation of L-serine, L-alanine or glycine.

## 2.3 Material and Methods

Unless stated differently, all solvents and reagents were purchased from Sigma-Aldrich Chemie GmbH (Buchs, Switzerland) excluding methanol, which was purchased from Honeywell specialty chemicals Seelze GmBH, Germany.

### 2.3.1 Cell culture

HEK293 cells were grown and maintained in DMEM (Sigma) with 10 % FBS (Fisher Scientific; FSA15-043) and 1 % penicillin / streptomycin (100 units per mL / 0.1 mg/mL, Sigma) at 37 °C and 5 % $CO_2$. HEK293 cells were harvested in PBS.

### 2.3.2 Transfection of DES 1/2 cells

HEK293 wild type cells were transfected with plasmids containing wild type DES1 or DES2 cDNAs. Stable cell lines were generated by propagating cells under geneticine (G418) selection. Expression of the DES1 or DES2 was confirmed by western blotting.

### 2.3.3 Metabolic labelling assay

$D_7$-Sphingosine, $D_7$-Sphinganine, $D_3$-deoxysphinganine, $D_5$-deoxymethylsphinganine and 1-deoxymethylsphingosine were dissolved in ethanol (1mM). All sphingolipid standards were purchased from Avanti polar lipids (Avanti Polar Lipids, Alabaster, AL).

HEK293 cells were fed with 0.5 µM of each lipid for kinetic assays or with 1 µM for inhibitor assays as indicated in the results section. In pulse-chase experiments, cells were fed with the specific lipid for 1 h, medium was exchanged to fresh medium without lipid supplement containing the respective inhibitor and cells were harvested up to 48 hours after medium change at different time points.

In steady state experiments, cells were fed with 1 µM lipid and the respective inhibitor and cells were harvested up to 48 hour after medium change at different time points.

The following inhibitors were used: Fumonisine B1 [6] (FB1, Sigma, 35 µM), Fenretinide [7] (4-HPR, Tocris Bioscience, 2 µM), 4-[[4-(4-Chlorophenyl)-2-thiazolyl]amino]phenol [8] (SK I II, 20 µM), HET0016 (Santa Cruz Biotechnology, 5 µM).

HEK293 cells were harvested in PBS, counted (Z2 Coulter counter; Beckman Coulter, Brea, CA) and pelleted (1200 rpm, 5 min at 4 °C, Eppendorf 5424R).

### 2.3.4 Cell extract

From the harvested pellet, the whole sphingolipids were extracted and hydrolyzed to get the free sphingoid bases as described previously with some modifications [9-11]. The cell pellet was dissolved in 100 µL of PBS. 500 µL methanol containing the internal standard $D_3$-threo-1-deoxySA (Avanti Polar Lipids, Alabaster, AL) was added to the dissolved pellet. Lipids were extracted for one hour under constant agitation at 37 °C in an Eppendorf Thermomixer. Samples were centrifuged at 16000 rpm for 5 min to pellet precipitated proteins and 500 µL of the supernatant was transferred into a new tube. Lipids were hydrolyzed by adding 75 µL of methanolic HCl (1 M HCl and 10 M $H_2O$ in methanol) and incubated for 16 h at 65 °C. By adding 100 µL of KOH (10 M) HCl was neutralized. 625 µL chloroform were added followed by 100 µL 2 M ammonium hydroxide and 0.5 mL alkaline water to reach phase separation. The sample was vortexed, centrifuged at 16000 rpm for 5 min, the upper phase discarded and the lower (organic) phase washed 3 times with alkaline water. The organic phase was finally dried under $N_2$ and stored at −20 $^{o}$C until analysis.

### 2.3.5 LC-MS Method

An LC-MS method described previously [10] was used to detect and quantify the hydrolyzed sphingolipid profile in the samples. Sphingoid bases were separated by RPLC on a C18-column (Uptispere 120 Å, 5 µm, 125×2 mm; Interchim, Montluçon, France) and analyzed on a Q Exactive (Thermo, Reinach, BL, Switzerland) using an atmospheric pressure chemical ionization (APCI) interface. Mobile phases consisted of A: ultra-pure $H_2O$ / methanol 1/1 v/v

with 2.6 mM ammonium acetate and B: methanol. A linear gradient was set from 50 % B to 100 % B within 25 min followed by 5 min 100 % B and 5 min of equilibration with 50 % B at a flow rate of 0.3 mL/min. For mass spectral detection, the following parameters were set on the APCI source: discharge current of 4 µA, vaporizer temperature of 450 °C, sheath gas pressure 20 AU, aux gas 5 AU and capillary temperature of 200 °C. The measured area under the peak curve was normalized to $D_3$-threo-1-deoxySA and lipid concentrations were calculated by comparison to $D_3$-threo-1-deoxySA and quantification was reported as pmol per million cells.

### 2.3.6 Diol synthesis with potassium permanganate

100 nmol 1-deoxymethylSO (m17:1 (3E)(2OH)) was dissolved in 10 µL ethanol. 100 µL 2 mM $KMnO_4$ (in $H_2O$) and 75 µL 10 M NaOH was added to the tube, which was cooled to 4 °C on ice. After the solution changed the colour from purple to brown, 500 µL chloroform were added and the mixture was vortexed for 20 seconds. The chloroform phase was transferred into another tube and the water phase was re-extracted with another 500 µL of chloroform. The chloroform phases were combined and dried under $N_2$.

### 2.3.7 Statistical Analysis

Experiments were always carried out in triplicates. Statistical significance was calculated using GraphPad Prism 6 software using a two-tailed t test or ANOVA.

## 2.4 Results

### 2.4.1 Identification of downstream metabolites

To identify potential $D_5$-1-deoxmethSA downstream products, HEK293 cells were fed with $D_5$-1-deoxymethylSA (1 µM) or vehicle (ethanol) for 24 h. As $D_5$-1-deoxymethlSA cannot be degraded via the S1P lyase, all metabolites bearing a $D_5$ label were assumed to be formed downstream of $D_5$-1-deoxymethylSA and should not be present in the ethanol treated control samples. With the help of Sieve™, but also with manual data review, high-resolution accurate mass patterns were identified bearing a $D_5$ label.

Besides the already known downstream metabolite $D_5$-1-deoxymethylSO, five additional metabolites were identified. Based on mass differences, one of the metabolites appeared to have a second double bond (1-deoxymethylsphingadiene), which would correspond to the canonical sphingadiene (SAdiene), a downstream product of SO which contains a (4*E*) and a (14*Z*) double bond. Additionally, four mono- or di-hydroxylated species were identified. We found a mono-hydroxylated and a di-hydroxylated metabolite of 1-deoxymethylSA but also 1-deoxymethylSO. The di-hydroxylated metabolites were more abundant than the mono-hydroxylated ones. The most abundant metabolite after 48 h was di-hydroxyl-1-deoxymethylSA (SPH t17:0) having two additional hydroxyl groups. The exact position of the hydroxyl groups has not yet been unravelled.

Among canonical sphingolipids the downstream metabolism of sphinganine requires N-acylation of the free base. To test if the hydroxylated downstream products of 1-deoxymethylspinganine are formed on the free base rather than on the N-acyl form, HEK293 cells were supplemented with $D_5$-1-deoxymethylSA (1 µM) for 24 h in the presence of Fumonisine B1 (FB1, 35 µM) a potent inhibitor of ceramide synthase (CerS). As seen in Figure 2-1, all identified downstream metabolites of $D_5$-1-deoxymethylSA were less abundant in the presence of FB1 indicating that not the free base but the N-acyl form is metabolized. Therefore, the precursor of all downstream metabolites is the N-acetylated form for both the canonical SL and atypical SL.

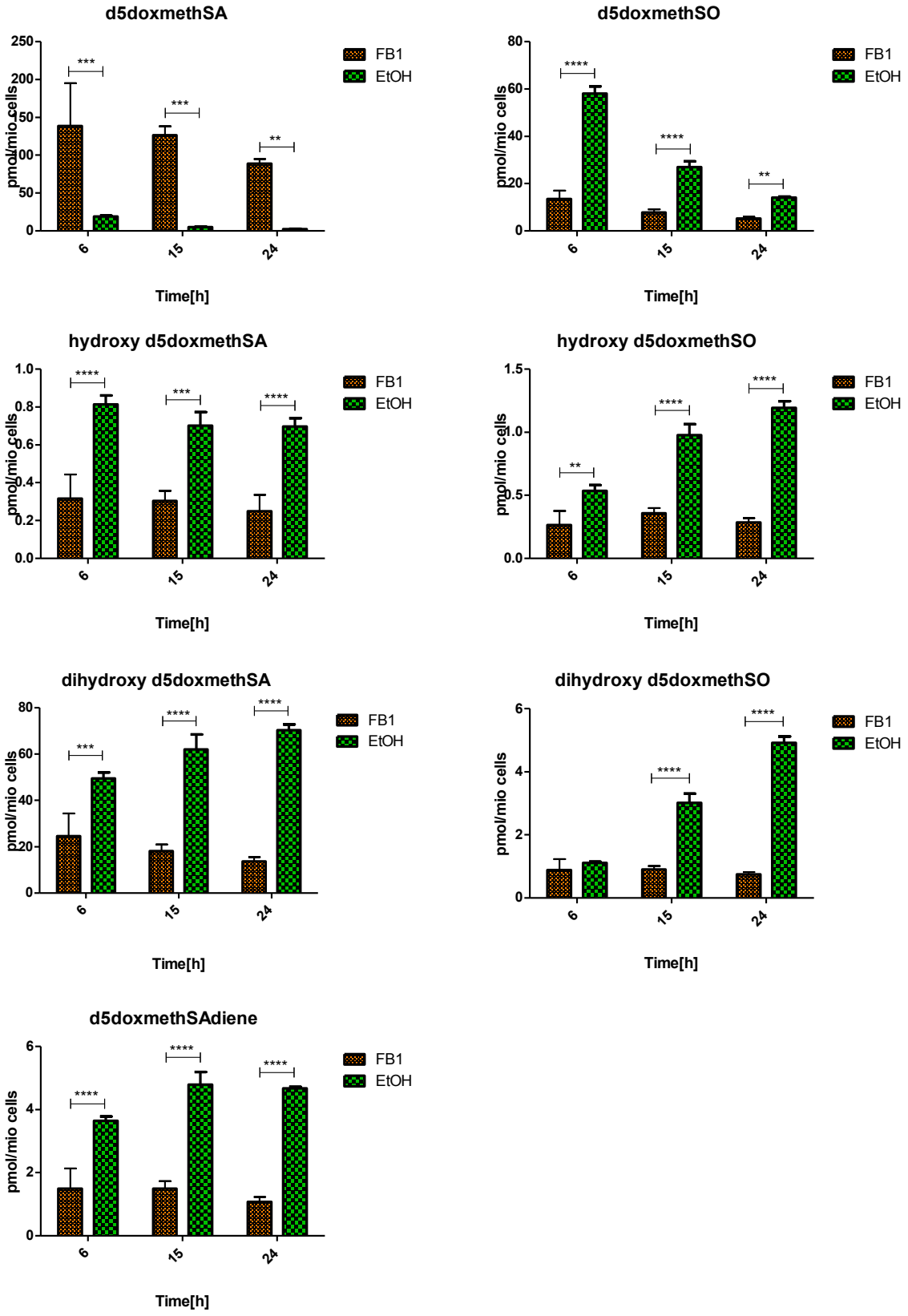


Figure 2-1: HEK293 wells were fed with $D_5$-1-deoxymethylSA for 24 h with and without FB1. Formation of downstream metabolites is drastically reduced with FB1. Statistical significance was tested using ANOVA. **= P < 0.01, ***= P < 0.001, ****=P < 0.0001.

### 2.4.2 Kinetics

To compare the metabolism and elimination of canonical sphinganine and 1-deoxysphingolipids and 1-deoxymethylsphingolipids (formed from L-alanine and glycine, respectively), HEK293 cells were supplemented with a 1 h pulse of $D_7$-sphinganine ($D_7$-SA), $D_3$-1-deoxysphinganine ($D_3$-1-deoxySA) and $D_5$-1-deoxymethylsphinganine ($D_5$-1-deoxymethylSA) (1 h, 0.5 µM each) followed by a 48 h chase. The formation of various isotopicly labeled downstream products was followed over time (Figure 2-2). Concentrations of the isotopic labeled lipids at time point zero was measured after medium exchange at the start of the chase period.

The uptake of supplemented sphingoid bases was fast. Already a few minutes after addition of the isotopic labeled compounds an increase in the intercellular levels was detectable. At time point 0 h, $D_3$-1-deoxySA levels were about two times higher than those of $D_7$-SA or $D_5$-1-deoxymethylSA. Assuming that the uptake of all three LCBs was similar, this difference is likely explained by different velocity in the metabolic conversion during the 1 h pulse (Figure 2-2A).

For $D_7$-SA this metabolic conversion was quite fast. Already 2 h after the medium exchange, more than 50 % of the initial pulse was converted into $D_7$-SO or degraded (Figure 2-2B). Also, $D_7$-SAdiene was mostly degraded after 24 h (Figure 2-2C). This rapid decrease in $D_7$-SA and its downstream metabolites can be explained by its conversion into sphingosine-1-phosphate (S1P), which is then terminally degraded to hexadecenal by S1P lyase.

In contrast, 1-deoxySA conversion was much slower. The maximum level of $D_3$-1-deoxySO was only reached after 15 h (Figure 2-2B). Levels of the di-desaturated $D_3$-1-deoxySAdiene were still increasing after 48 h. (Figure 2-2C). This, however, was different for $D_5$-1-deoxymethylSA. Surprisingly, we observed a faster conversion rate than for 1-deoxySA, similar to the one of $D_7$-SA (Figure 2-2).

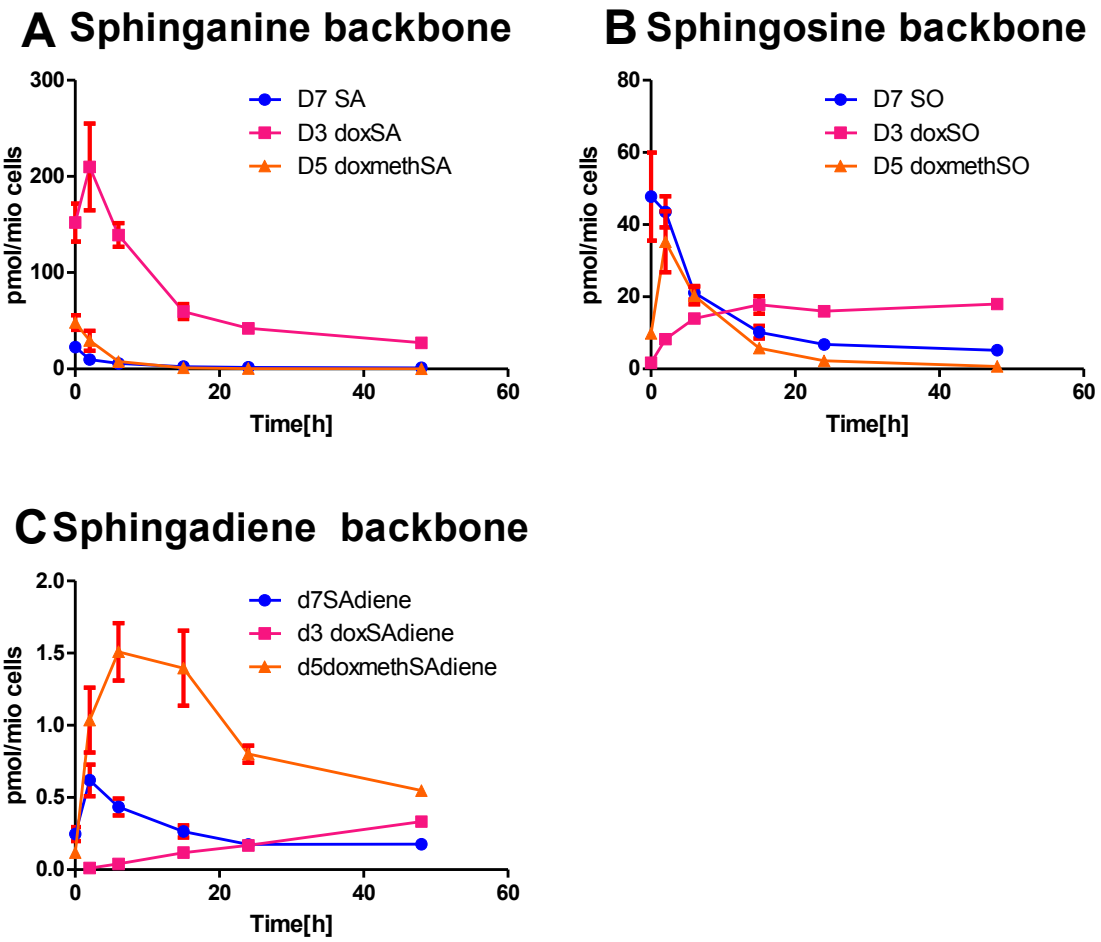


Figure 2-2: HEK293 cells were fed with $D_7$-SA, $D_3$-1-deoxySA and $D_5$-1-deoxymethylSA (0.5 µM each) for 1 h, after 1 h the medium was replaced by un-supplemented medium and cells were cultured for 0 h, 2 h, 6 h, 15 h, 24 h or 48 h. Cells were harvested and total sphingolipids were extracted and hydrolyzed as described. Kinetics of $D_7$-SA and its downstream metabolites $D_7$-SO or $D_7$-sphingadiene was compared to the kinetics of $D_3$-1-deoxySA or $D_5$-1-deoxymethylSA and their respective downstream metabolites.

### 2.4.3 Double bond position and the role of DES1 and DES2 in the metabolism of 1-deoxymethylSA

**Double bond position**

For the conversion of sphinganine to sphingosine, dihydroceramides are converted to ceramides by the introduction of a double bond at (4*E*) by the dihydroceramide Δ4-desaturase [12] which is expressed in two isoforms, DES1 and DES2. Whereas DES1 primarily introduces the (4*E*) double bond, DES2 catalyses a two-step reaction by first adding a

hydroxyl group at Δ4 position thereby forming phytosphingosine and introducing a (4*E*) double bond similar to DES1 [13, 14].

However, 1-deoxySO contains a (14*Z*) double bond in contrast to the canonical (4*E*) and was shown not to be formed by DES1 or DES2. However the role of DES1/2 in metabolising 1-deoxymethylSA is not known. We first wanted to see whether 1-deoxymethylSO contains a canonical or a differently positioned double bond. We supplemented HEK293 cells with isotope labeled $D_5$-1-deoxymethylSA and compared the formed $D_5$-1-deoxymethylSO to a commercially available synthetic SPH m17:1(3*E*)(2OH) standard. Both compounds had the same mass-to-charge ratio (*m/z*) and also and overlapping retention time indicating that both compounds have the identical structure (Figure 2-3). This means, that in contrast to 1-deoxySO, 1-deoxymethylSO contains a canonical double bond position.

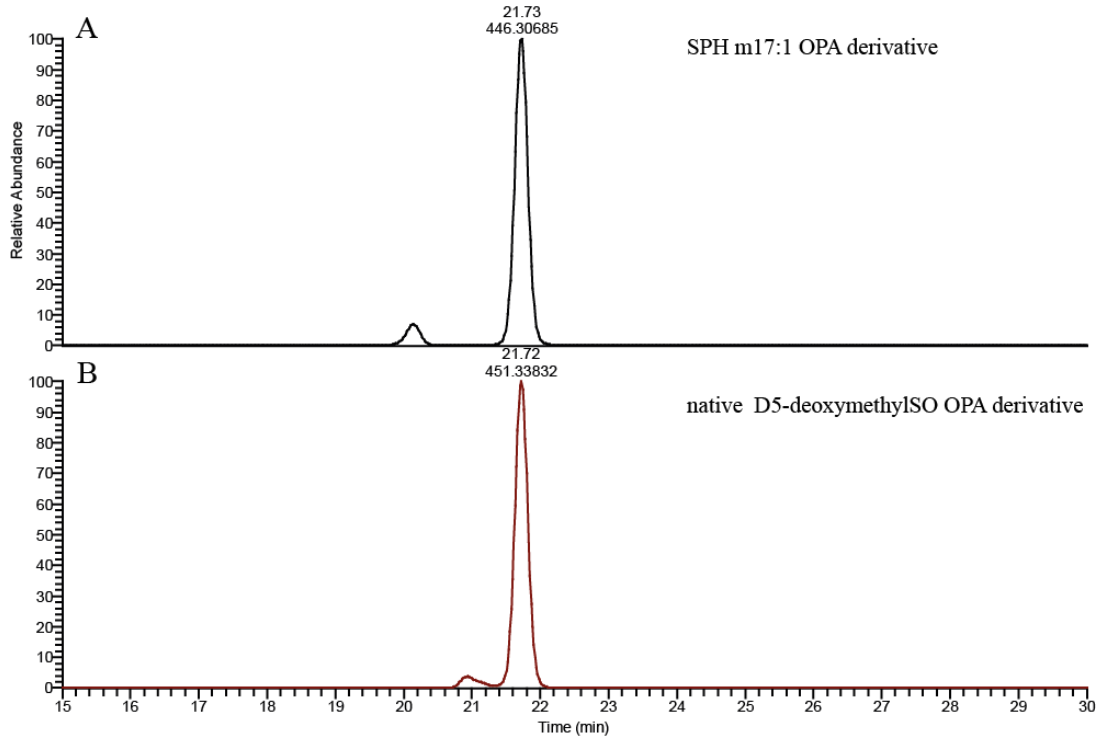


Figure 2-3: HEK293 cells were fed with labeled $D_5$-1-deoxymethylSA (Avanti Polar Lipids, Alabaster, AL). Cells were harvested after 24 h and the whole sphingolipid extract was hydrolyzed to get the free sphingoid bases. Extract was treated with o-phthalaldehyde (OPA) to get the OPA derivative of sphingoid bases. Sphingoid bases were separated on a C18 column and detected on an HRAMS Q Exactive. Retention time and *m/z* of deuterium labeled $D_5$-1-deoxymethylSO were compared to synthetic SPH m17:1(3E). Retention time of native $D_5$-1-deoxymethylSO was 21.73 min (B) and for SPH m17:1(3E) 21.73 min (A). *m/z* of native $D_5$-1-deoxymethylSO was 451.33832 (calculated 451.34011, < 5 ppm) and for SPH m17:1(3E) 446.30685 (calculated 446.30872, < 5 ppm) [11].

This indicates that the double bond in both canonical SO and 1-deoxymethSO is also introduced by DES1/2 [12]. To proof that, we added 4-HPR, a potent inhibitor for DES1/2 together with $D_5$-1-deoxymethSO to HEK293 cells (24 h) and analyzed the labelled downstream metabolites. Supporting our hypothesis, the conversion of $D_5$-1-deoxymethylSA to $D_5$-1-deoxymethylSO was inhibited by 4-HPR. The concentration of $D_5$-1-deoxymethylSA was significantly higher in cells treated with 4-HPR compared to controls. In contrast, $D_5$-1-deoxymethylSO was significantly lower for all time points in the presence of 4-HPR (Figure 2-4A).

Next, we overexpressed DES1 and DES2 in HEK293 cells and compared the conversion of $D_5$-1-deoxymethylSA to $D_5$-1-deoxymethylSO in the overexpressing cells to that in wild type (WT) cells. The concentration of $D_5$-1-deoxymethylSO was not changed in the overexpressing cells. This might be due to the rapid degradation of 1-deoxymethylSO after increased formation in DES1/2 overexpressing cells (Figure 2-4B).

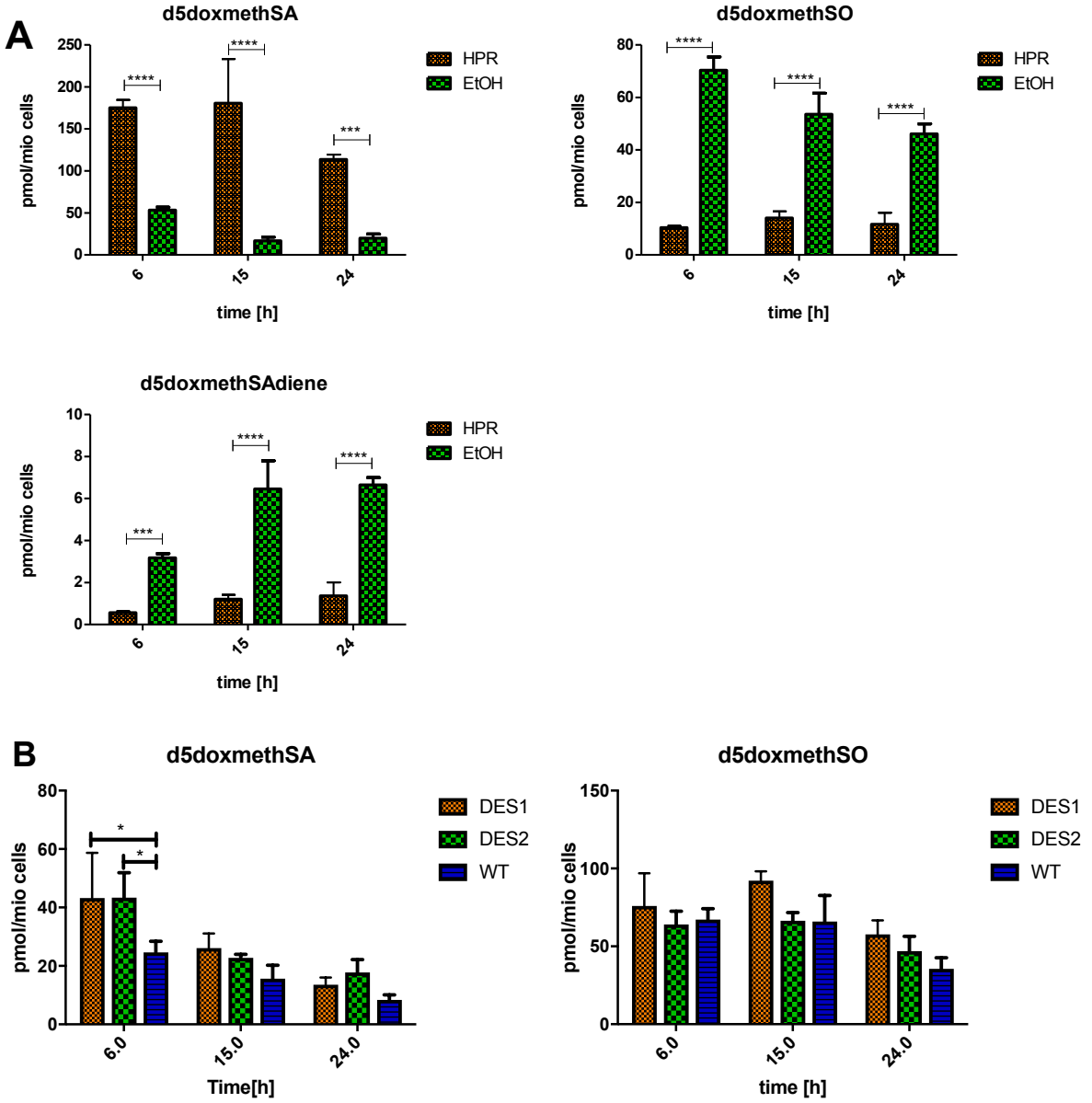


Figure 2-4: A: HEK293 cells were fed with $D_5$-1-deoxymethylSA (1 µM) and DES was inhibited with HPR. Conversion of $D_5$-1-deoxymethylspinganine to $D_5$-1-deoxymethylSO is reduced with 4-HPR. Additionally, the conversion to the downstream metabolite of $D_5$-1-deoxymethylSO, 1-deoxymethylsphingadiene is also inhibited with 4-HPR. B: HEK293 overexpressing DES 1 and DES 2 and HEK293 WT cells as control were fed with $D_5$-1-deoxymethylSA (1 µM). Levels of $D_5$-1-deoxymethylSO were compared between cells overexpressing DES1 or DES2 and wild type cells. Formation of $D_5$-1-deoxymethylSO is not changed in DES1 or in DES2 overexpressing cells compared to WT. Statistical significance was tested using ANOVA. **= P< 0.01, ***= P < 0.001, ****=P < 0.0001.

### Mono-hydroxylation

Whereas DES1 introduces the Δ4 double bond in a single step reaction, DES2 acts in a two step reaction by first introducing a Δ4 hydroxylgroup, forming phytosphingosine (SPH t18:0), which can then be further converted to a (4*E*) double bond or released as hydroxylated species. Therefore, we also wanted to confirm, if DES2 is responsible for the formation of the newly identified mono-hydroxylated species of 1-deoxymethylSL. As it is not known from literature, if 4-HPR inhibits both of the DES isoforms, we also added SKI II, a sphingosine kinase inhibitor, which was published to also inhibit DES enzymes. With the inhibition of DES, the levels of hydroxyl-$D_5$-1-deoxymethylSA and hydroxyl-$D_5$-1-deoxymethylSO are significantly decreased at all time points (Figure 2-5A with 4-HPR, Figure 2-5B with SKI II). Therefore, the desaturase is involved in the formation of mono-hydroxylated species of 1-deoxymethylSL.

To exclude an unspecific effect of the two tested inhibitors, we finally overexpressed DES1 and DES2 in HEK293 cells and supplemented the cells with $D_5$-1-deoxymethylSA for 24 h and the hydroxylated downstream product was measured in the overexpressing cells. The formation of hydroxyl-$D_5$-1-deoxymethylSA was significantly increased in cells overexpressing DES2 enzyme for all time points, whereas the formation of hydroxyl-$D_5$-1-deoxymethylSO was only increased after 24 hours in DES overexpressing cells (Figure 2-5C). Therefore DES2 is most probably forming a mono-hydroxyl-1-deoxymethylSA, comparable to the Phyto-Sphingosine (t18:0) formed by DES2 from sphinganine by adding a hydroxyl-group at Δ4-C. The position for hydroxylation of 1-deoxymethylSA is not known, but can be assumed to be inserted at Δ3, which corresponds to the position in canonical hydroxyl-sphinganine (Phyto-Sphingosine t18:0). The formation of hydroxyl-1-deoxymethylSO needs two independent reactions - the insertion of the alternative double bond (most probably (13*Z*)) and the Δ3-hydroxylation by DES2 - therefore hydroxyl-$D_5$-1-deoxymethylSO is not increased rapidly in cells overexpressing DES2. In Figure 2-5D the proposed structures are shown.

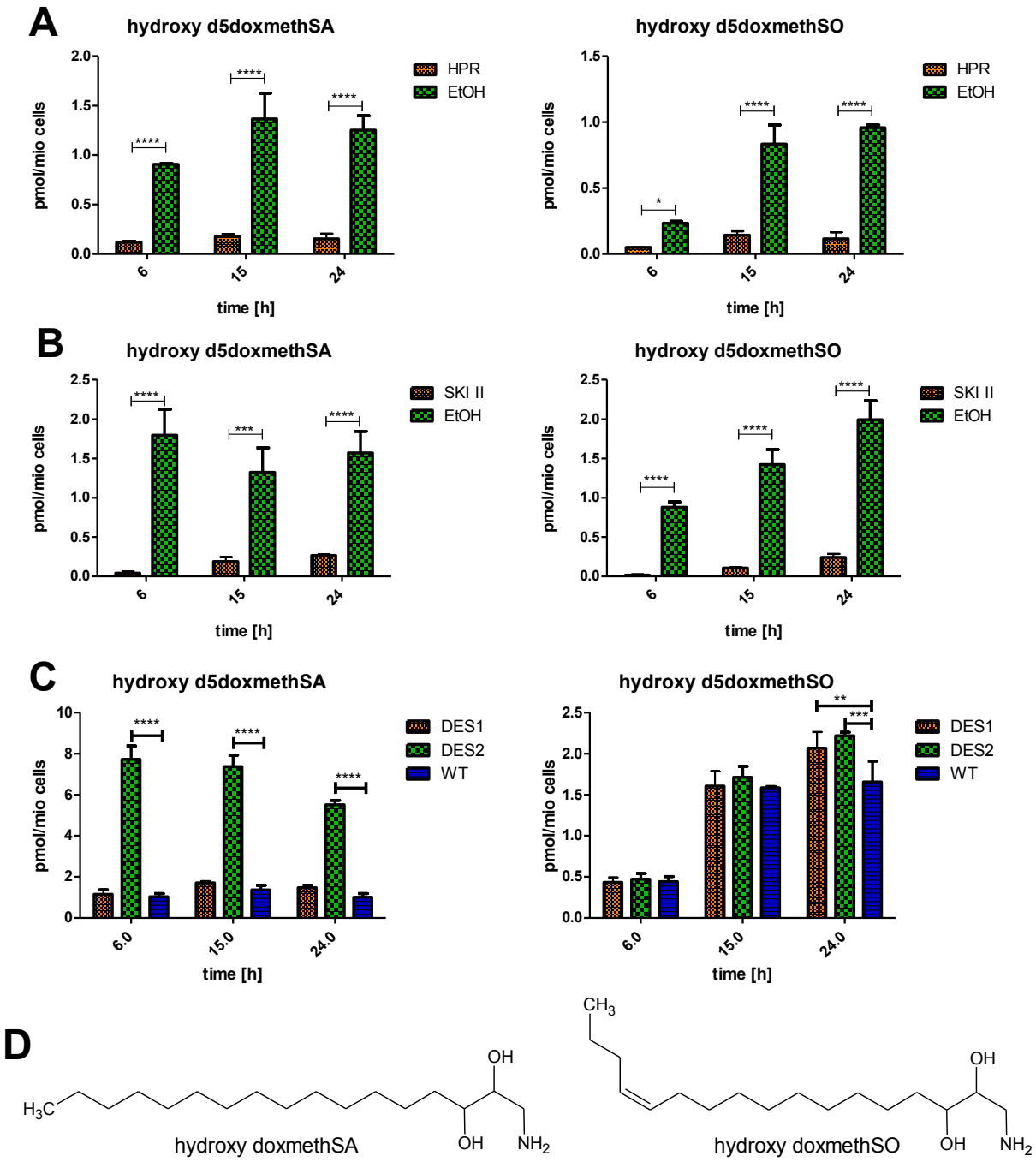


Figure 2-5: A: HEK293 were fed with $D_5$-1-deoxymethylSA (1 µM) and DES1/2 was inhibited with 4-HPR. Formation of mono-hydroxylated metabolites is clearly inhibited by 4-HPR. B: HEK293 were fed with $D_5$-1-deoxymethylSA (1 µM) and DES1/2 was inhibited with SK I II, which was reported to also inhibit DES enzyme. Formation of mono-hydroxylated metabolites is clearly inhibited by SK I II. C: HEK293 overexpressing DES 1 and DES 2 and HEK293 WT cells as control were fed with $D_5$-1-deoxymethylSA (1 µM). Levels of mono-hydroxylated $D_5$-1-deoxymethylSL species were compared between cells overexpressing DES 1 or DES 2 to wild type cells. Formation of hydroxyl-$D_5$-1-deoxymethylSA is increased in cells overexpressing DES 2 in all time points; formation of hydroxyl-$D_5$-1-deoxymethlSO is increased after 24 hours in cells overexpressing any desaturase enzyme. Statistical significance was tested using ANOVA. **= P< 0.01, ***= P < 0.001, ****=P < 0.0001. D: Proposed structure for hydroxyl-1-deoxymethylspinganine (hydroxyl doxmethSA) and hydroxyl-1-deoxymethylSO (hydroxy doxmethSO )

### 2.4.4 Alternative double bond insertion over unknown desaturase

For sphinganine it is known that in addition to the (4*E*) double bond, a (14*Z*) double bond can be introduced. Further, 1-deoxysphingosine does not containing a (4*E*) but a (14*Z*) double bond. This (14*Z*) seems to be an alternative pathway, next to the desaturation by DES1 or DES2, but the corresponding enzyme is still unknown. Therefore, it was investigated, if this alternative double bond also exists in 1-deoxymethylSL.

After feeding cells with $D_5$-1-deoxymethylSA, we observed a small peak eluting before 1-deoxymethylSO (Figure 2-3B). This peak has the same *m/z* as 1-deoxymethylSO and also contains a $D_5$-label, suggesting the presence of an alternative form of 1-deoxymetSO, possibly containing a (13*Z*) double bond. 1-DeoxySL metabolism differs between cell types. The metabolism of 1-deoxySLs is faster and more diverse in MEF cells compared to HEK293 cells. Also in MEF cells, this alternative peak was observed.

Therefore, we tested in HEK293 and in MEF cells, if 4-HPR has an effect on the formation of this alternative 1-deoxymethylSO. In either cells line, a second 1-deoxymethylSO was formed and this alternative peak was increased in 4-HPR treated HEK293 (Figure 2-6A) and MEF (Figure 2-6B) cells indicating that the formation of this variant is increased after inhibition of DES1/2. This compensatory mechanism was not seen for 1-deoxySL, as they are no substrate for DES1/2 and therefore, only the (14*Z*) position is formed over the alternative pathway, but none of the (4*E*) form.

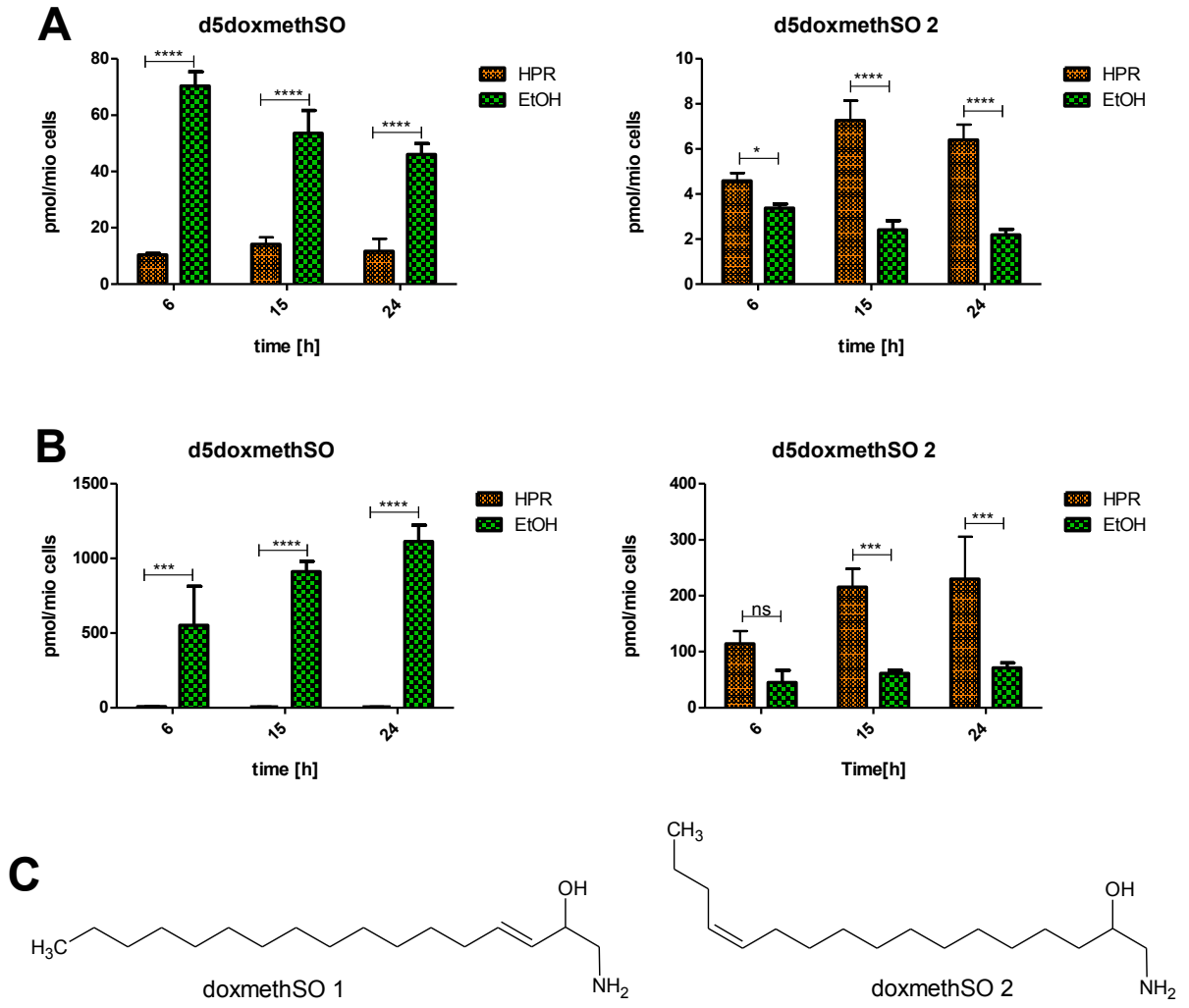


Figure 2-6: A: HEK293 cells were fed with $D_5$-1-deoxymethylSA and DES was inhibited with 4-HPR. There were two different 1-deoxymethylSO identified and quantified. B: MEF cells were fed with $D_5$-1-deoxymethylSA and DES was inhibited with 4-HPR. There were two different 1-deoxymethylSO identified and quantified. For both HEK293 and MEF cells, the formation of the alternative 1-deoxymethylSO was increased with the inhibition of DES, whereas the formation of the (3*E*) form was decreased. C. Proposed structures for 1-deoxymethylspinhosine (3*E*) (doxmethSO 1) and 1-deoxymethylSO (13*Z*) (doxmethSO 2)

**1-deoxymethylSAdiene**

We also identified a 1-deoxymethSA downstream metabolite which by mass bears two double bonds (1-deoxymethylSAdiene). This 1-deoxymethylSAdiene likely corresponds to the canonical SO metabolite Sphingadiene (SAdiene). In analogy to SAdiene we hypothesized that the two double bonds in 1-deoxymethylSAdiene are located in (3*E*) and (13*Z*) position. As demonstrated in Figure 2-4 the insertion of the (3*E*) double bond depends on DES1/2 whereas the second double bond is introduced independently of DES (Figure 2-6). Based on our previous observations it is likely that the two double bonds are introduced in a sequential reaction by fist introducing the (3*E*) (by DES1/2) followed by the (13*Z*) (by an unknown desaturase) or vice versa.

### 2.4.5 Di-hydroxylated 1-deoxymethylsphingolipids are formed by an unknown enzyme

**Di-hydroxylation downstream of 1-deoxymethylsphingosine**

Di-hydroxylation was not described for canonical sphingolipids [15], but it was seen in 1-deoxySL, although in very low amounts [5]. For 1-deoxymethylSLs, it is one of the most abundant downstream metabolites. Di-hydroxylated 1-deoxymethylSL could be formed directly from 1-deoxymethylSA or further downstream, e.g. as a sequential reaction after mono-hydroxylation or by the conversion of the double bond of 1-deoxymethylSO to a vicinal diol. To test if di-hydroxylation is downstream of 1-deoxymethylSA or 1-deoxymethylSO, we inhibited the conversion from fed $D_5$-1-deoxymethylSA to $D_5$-1-deoxymethylSO with 4-HPR to see if di-hydroxylated 1-deoxymethylSL were still formed.

4-HPR inhibits the desaturation of added $D_5$-1-deoxymethylSA, the levels of formed $D_5$-1-deoxymethylSO are significantly reduced with 4-HPR. Furthermore, di-hydroxylated 1-deoxymethylSL are significantly decreased in presence of the 4-HPR inhibitor (Figure 2-7A). This might be explained by reduced formation of precursor metabolite $D_5$-1-deoxymethylSO though inhibition of DES1/2. However, HEK293 cells which overexpress DES1 or DES2 were fed with $D_5$-1-deoxymethylSA formation showed an increased formation of di-hydroxylated 1-

deoxymethylSL species. There was no change seen in 1-deoxymethylSO formation after feeding $D_5$-1-deoxymethylSA, but the di-hydroxylated forms were increasing after 15 hours in DES 2 overexpressing cells and after 24 h also in DES1 overexpressing cells compared to WT form (Figure 2-7B).

As the di-hydroxylated 1-deoxymethylSL forms were increased in DES overexpressing cells and decreased with DES inhibition with 4-HPR they were formed most likely downstream of 1-deoxymethylSO (Figure 2-7A and Figure 2-7B). For a proof, HEK293 cells were supplemented with synthetic 1-deoxymethylSO (1 µM) for up to 24 h in a steady state manner. As there was no deuterium labeled 1-deoxymethylSO available, also natively formed downstream metabolites are present in the cells. Levels of downstream metabolites formed from exogenous 1-deoxymethylSO have to be compared to endogenously formed levels of 1-deoxymethylSL (Figure 2-7C). All downstream metabolites are formed on the 1-deoxymethylCer forms but not on the free base. To block the conversion of the free base 1-deoxymethylSO to 1-deoxymethylCer ceramide synthase (CerS) inhibitor FB1 was added together with 1-deoxymethylSO. With the addition of FB1, exogenous 1-deoxymethylSO should not get converted further.

Di-hydroxylation of 1-deoxymethySL and also 1-deoxymethylSAdiene were formed after feeding cells with 1-deoxymethylSO. With the addition of the CerS inhibitor FB1, the formation of 1-deoxymethylSAdiene, but also the di-hydroxylated species was significantly reduced and the exogenous 1-deoxymethylSO accumulated in the cell. In conclusion, the di-hydroxylated forms were formed downstream of 1-deoxymethylSO. This reaction seems to be a unique reaction during 1-deoxymethylSL metabolism, as di-hydroxylated species of L-serine based SL were not yet reported. Di-hydroxylated 1-deoxySL were formed but in much less than di-hydroxylated 1-deoxmethylSL.

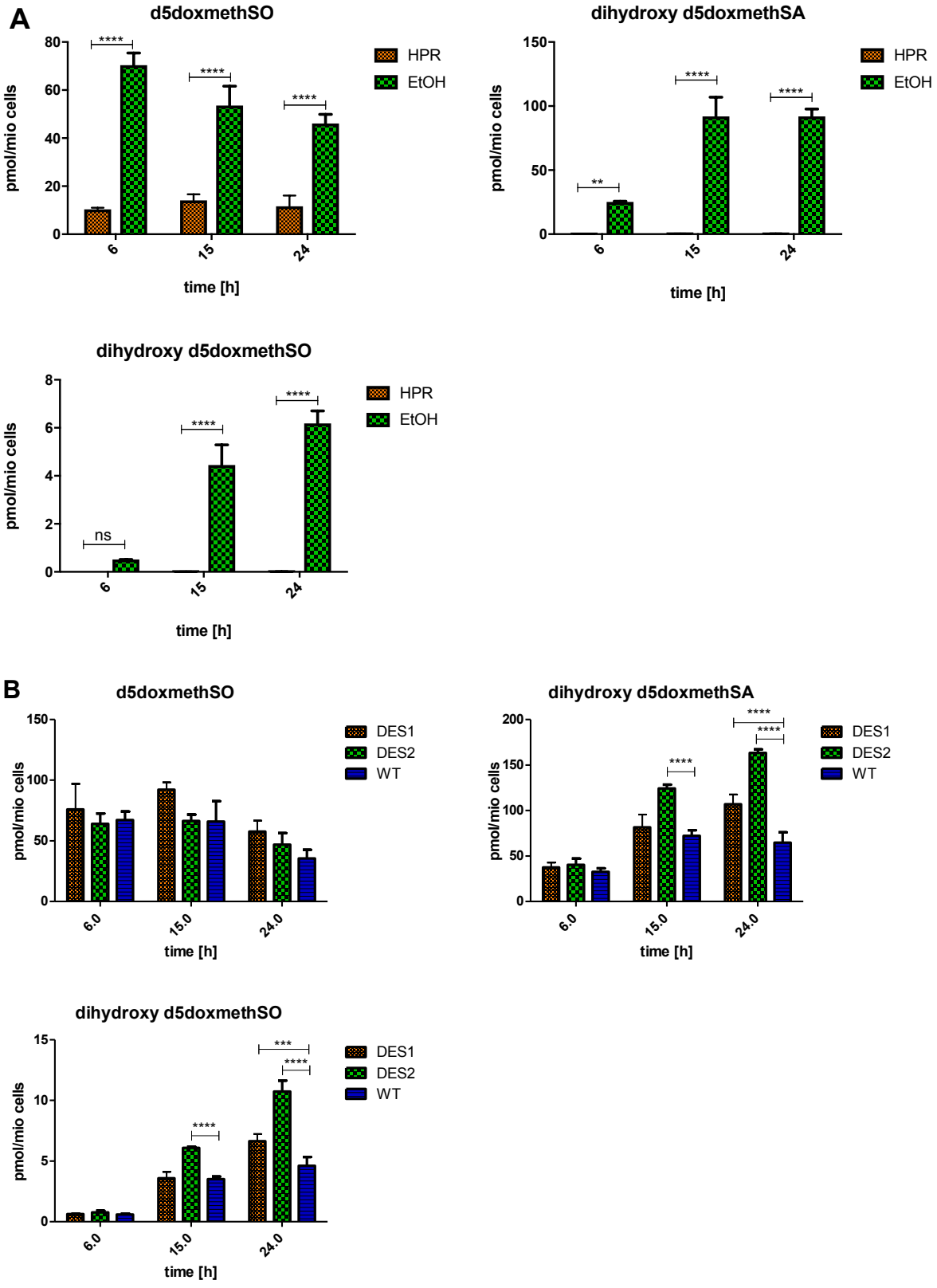
A
d5doxmethSO
pmol/mio cells
time [h]
HPR
EtOH
dihydroxy d5doxmethSA
dihydroxy d5doxmethSO
ns
B
DES1
DES2
WT
6.0
15.0
24.0

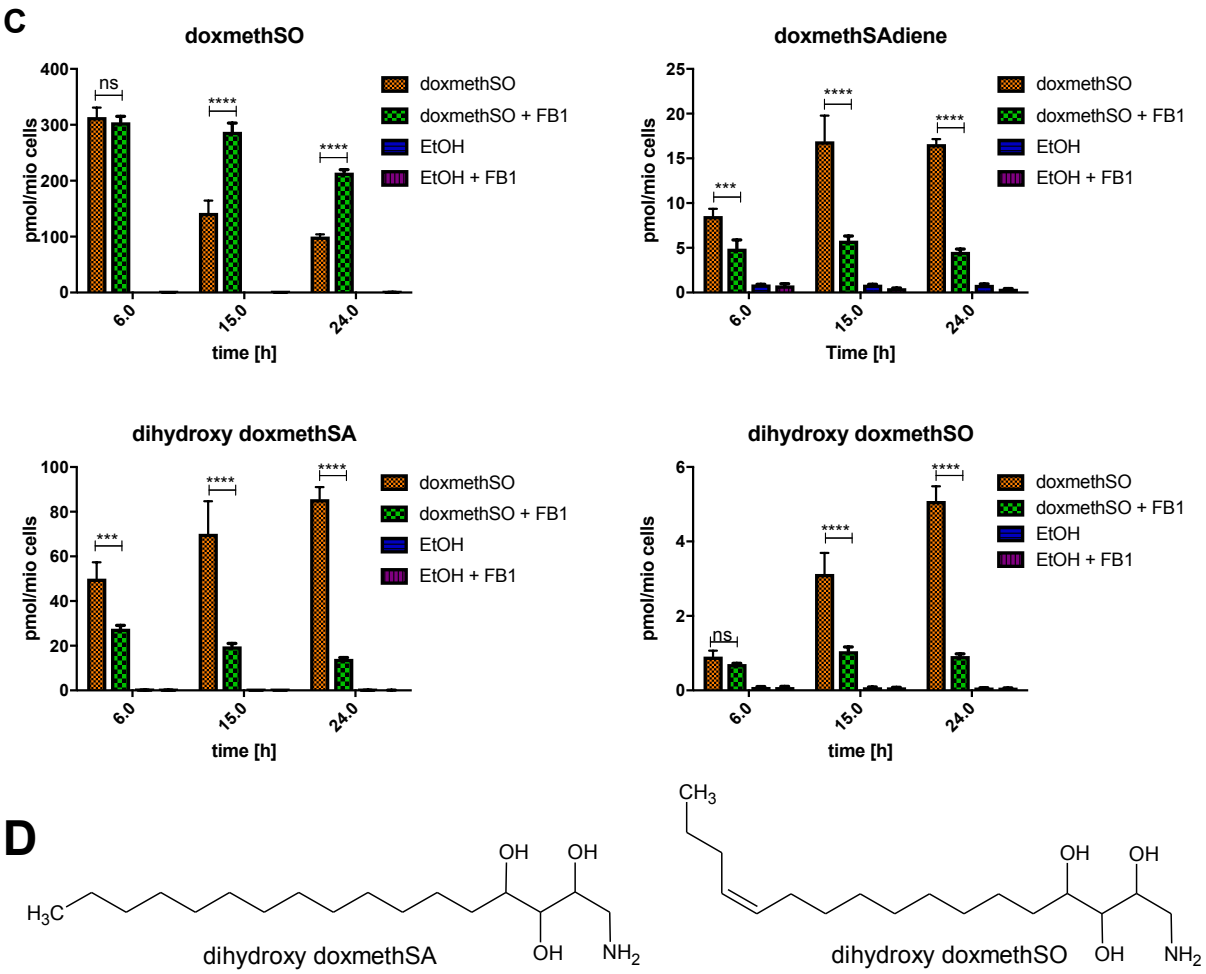


Figure 2-7: A: HEK293 cells were fed with $D_5$-1-deoxymethylSA for 24 h and DES1/2 inhibitor 4-HPR or ethanol as control was added. The formation of di-hydroxylated 1-deoxymethylSL species is reduced with 4-HPR, as the conversion to precursor 1-deoxymethylSO is blocked. B: Concentration of di-hydroxylated 1-deoxymethylSL after $D_5$-1-deoxymethylSA treatment for 24 h in DES 1 or DES2 overexpressing HEK293 cells compared to WT cells. C: HEK293 cells were fed with 1-deoxymethylSO (1 µM) for up to 24 h and CerS was inhibited with FB1 as a control. To control for natively formed 1-deoxymethySL formed by the cells, cells were treated with Ethanol with and without FB1 only. Di-hydroxylated 1-deoxymethylSL are significantly elevated in cells fed with 1-deoxymethylSO, whereas FB1 inhibits the formation of di-hydroxylated species. Statistical significance was tested using ANOVA. **= P< 0.01, ***= P < 0.001, ****=P < 0.0001. D: Proposed structure for di-hydroxyl-1-deoxymethylspinganine (di-hydroxyl doxmethSA) and di-hydroxyl-1-deoxymethylSO (di-hydroxy doxmethSO )

It is suspected that 1-deoxySL are metabolized to their mono-hydroxylated forms by the 4F family of cytochrome P 450 (CYP) enzymes, an enzyme family with mostly monooxygenase activity. However, CYP 4F enzymes seem not to be involved in the canonical sphingolipid metabolism. We therefore tested, whether CYP 4F enzymes also contribute to the metabolism of 1-deoxymethylSL. As MEF cells metabolize 1-deoxySL more actively, we supplemented MEF cells with $D_5$-1-deoxymethylSA in combination with the CYP 4A/F pan-

inhibitor HET0016. In the presence of HET0016, the formation of di-hydroxyl forms was clearly reduced, whereas the levels of $D_5$-1-deoxymethylSO, $D_5$-1-deoxymethylSAdiene and mono-hydroxylated $D_5$-1-deoxymethylSA was increased (Figure 2-8). With CYP 4A/F inhibition, $D_5$-1-deoxymethylSO was accumulating but also converted to $D_5$-1-deoxymethylSAdiene. Also $D_5$-1-deoxymethylSA was accumulated and converted to mono-hydroxylated species. This indicated that CYP 4F reaction occurs downstream of 1-deoxymethylSO. In Figure 2-7D, the proposed structures of di-hydroxy-1-deoxymethylSA and di-hydroxy-1-deoxymethylSO are shown.

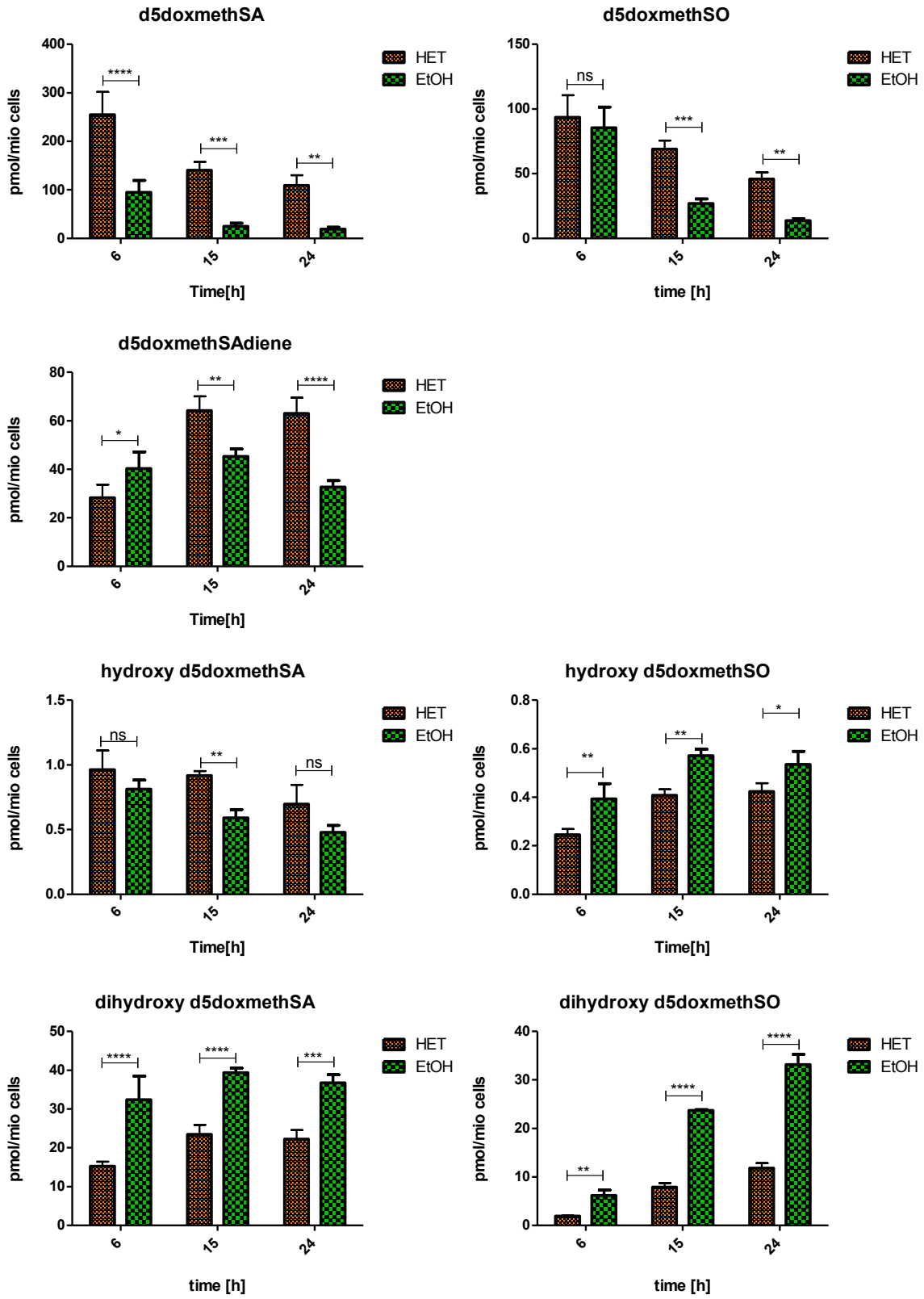


Figure 2-8: MEF cells were fed with $D_5$-1-deoxymethylSA for 24 h and CYP 4F family was inhibited with HET0016 (or ethanol as control was added). Statistical significance was tested using ANOVA. **= P< 0.01, ***= P < 0.001, ****=P < 0.0001.

### 2.4.6 Structural elucidations of di-hydroxy-1-deoxymethylsphinganine

As di-hydroxyl-1-deoxymethylSA is formed downstream of 1-deoxymethylSO, it is likely that the double bond is cleaved and a vicinal diol is formed. To elucidate its structure, we tried to oxidize the double bond of 1-deoxymethylSO with potassium permanganate to form a vicinal diol (di-hydroxyl-1-deoxymethylSA m17:0 (2OH)(3OH)(4OH) and we compared the retention time in RPLC to the native formed di-hydroxyl-1-deoxymethylSA. Two different reaction products were formed (Figure 2-9B), corresponding to the two possible syn diols that can be formed from 1-deoxymethylSO. Figure 2-9A displays the native product formed from feeding HEK293 cells with $D_5$-1-deoxymethylSA. The retention times of the different diols and the native product do not match possibly due to the fact that the native product could be an anti-diol. The position of hydroxylation therefore remains elusive.

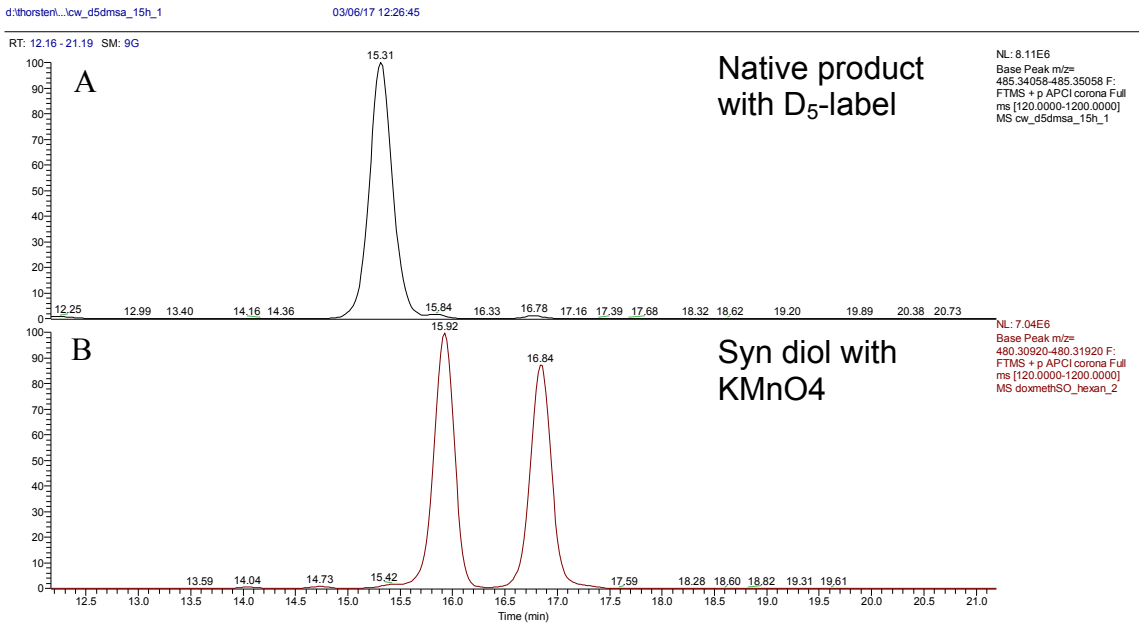


Figure 2-9: Chromatogram of A natively formed di-hydroxyl-$D_5$-1-deoxymethylSA and B the two syn-diols formed after the oxidation with potassium permanganate

## 2.5 Discussion

Based on the structural similarities it was assumed, that also atypical 1-deoxysphingolipids and 1-deoxymethylsphingolipids follow the same metabolic rout as canonical sphingolipids, except that, they cannot be converted to complex sphingolipids or phosphorylated to sphingosine-1-phosphate for degradation by sphingosine-1-phosphate-lyase, because of the

missing $C_1$-hydroxyl group [1, 4]. However, this assumption was not correct for 1-deoxySL which are formed from L-alanine and metabolized by a different enzyme as canonical sphingolipids [5]. Here we showed that the metabolism of 1-deoxymethylSL partly but not entirely follows the canonical sphingolipid pathway. In Figure 2-10 we show the proposed metabolic pathway for canonical and atypical sphingolipids with all likely branching points.

The metabolism starts with palmitoyl-CoA, which is either conjugated to L-serine, L-alanine or glycine. All three reactions are catalyzed by the enzyme serine-palmitoyl-transferase (SPT) [16, 17]. After the sphingoid backbone is formed, the canonical sphinganine (SA) is N-acetylated to dihydroceramide and converted to ceramide by DES1 and DES2.

For L-serine and glycine based sphingolipids, a desaturation at (4*E*) and (3*E*) respectively over DES1/2 is possible which leads to the second major sphingoid backbone sphingosine (SO) [12]. For L-alanine based 1-deoxySL, this desaturation does not occur, but a double bond is introduced at (14*Z*) [11]. This reaction also occurs for L-serine or glycine based sphingolipids, but seems to be a less frequently used alternative pathway of desaturation for these lipids. The two possibilities for desaturation in L-serine or glycine based sphingolipids lead to the formation of di-unsaturated sphingoid backbone sphingadiene (SAdiene) [18], which corresponds to the a downstream metabolite of sphingosine with (4*E*) and (14*Z*) double bond. As glycine based sphingolipids are based on 17 carbons, the corresponding 1-deoxymethylSAdiene presumably contains a (3*E*) and a (13*Z*) double bond. The enzyme involved in the formation of the (14*Z*) double bond is as yet unknown.

In addition to the three major sphingoid bases, SA, SO and SAdiene, sphingolipids can be converted to quantitatively minor backbone structures. SA can be hydroxylated by DES2 to phytosphingosine (t18:0) [12, 14]. DES2, which is involved in the canonical sphingolipid pathway, is not involved in the metabolism of atypical 1-deoxysphingolipds, as mono-hydroxyl-1-deoxySA is formed by CYP 4F enzymes [5].

It remains the question on the involvement of DES in the double bond formation of atypical sphingolipids. SO and 1-deoxymethylSO but not 1-deoxySO are substrates for DES.

Therefore it is probably not the $C_1$-hydroxylgroup which is responsible for the DES recognition and desaturation or hydroxylation of $\Delta 4$ [19] except if 1-deoxySA is locally separated from DES within the cell compartments. Previous studies showed the different localization of the canonical sphingolipids and 1-deoxySL, the latter of which seems to be mostly located in mitochondria [20].

As seen in Figure 2-10 the metabolism of canonical sphingolipids as well as atypical 1-deoxysphingolipids and 1-deoxymethylsphingolipids follow the same central metabolic pathway involving SPT, CerS, and Ceramidase. Furthermore, DES1 and DES2 metabolize canonical SL and 1-deoxymethylSL, but not 1-deoxySL, although, mono-desaturated 1-deoxySO and mono-hydroxylated 1-deoxySA exist, however, they are metabolized by different enzymes than DES1/2.

As 1-deoxySL and 1-deoxymethylSL are missing the $C_1$-hydroxyl group, they can be neither converted to complex sphingolipids, nor phosphorylated and degraded via SK and SGPL. For 1-deoxySL, there seems to be an alternative downstream metabolic pathway involving CYP 4F enzymes. 1-Deoxymethylsphingolipids are di-hydroxylated by a reaction, which is not known for canonical sphingolipids.

In summary, we showed, that despite some overlap the metabolism of glycine based 1-deoxymethylsphingolipids differs from that of both canonical sphingolipids as well as atypical L-alanine based sphingolipids.

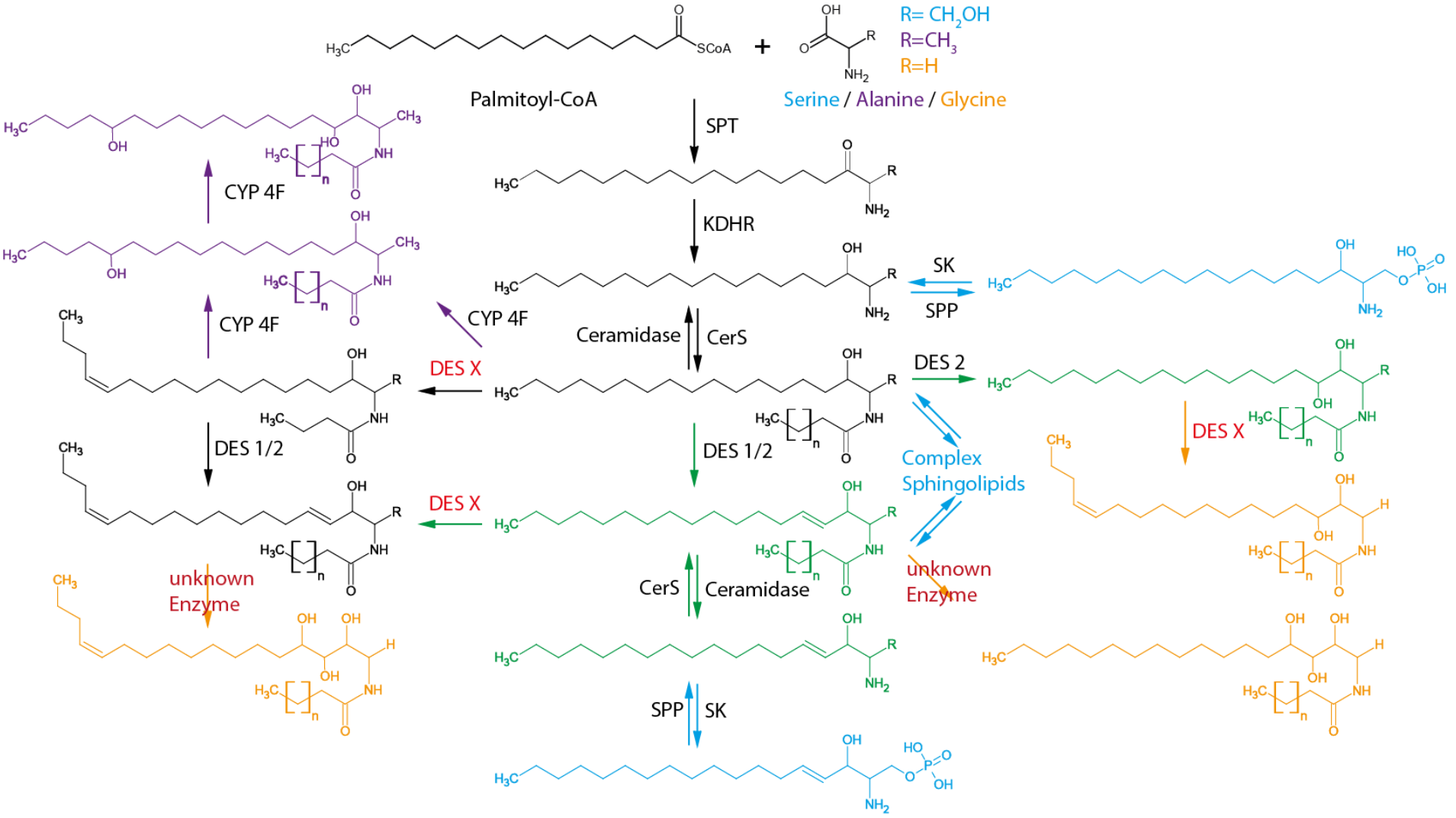


Figure 2-10: Proposed metabolic pathway for sphingolipids with different amino acid starting points. Structures in black: Route for L-serine, L-alanine and glycine based sphingolipids. Structures in green: Route for L-serine and glycine based sphingolipids. Structures in blue: route only possible for L-serine based sphingolipids. Structures in violet: route only possible for L-alanine based 1-deoxysphingolipids. Structures in yellow: route only possible for glycine based 1-deoxymethylsphingolipids.

## 2.6 References

[1] Merrill, AH, Jr., Sphingolipid and glycosphingolipid metabolic pathways in the era of sphingolipidomics, Chem Rev, 2011;111:6387-6422.
[2] Zitomer, NC, Mitchell, T, Voss, KA, et al., Ceramide synthase inhibition by fumonisin B1 causes accumulation of 1-deoxysphinganine: a novel category of bioactive 1-deoxysphingoid bases and 1-deoxydihydroceramides biosynthesized by mammalian cell lines and animals, J Biol Chem, 2009;284:4786-4795.
[3] Penno, A, Reilly, MM, Houlden, H, et al., Hereditary sensory neuropathy type 1 is caused by the accumulation of two neurotoxic sphingolipids, J Biol Chem, 2010;285:11178-11187.
[4] Fyrst, H and Saba, JD, Sphingosine-1-phosphate lyase in development and disease: sphingolipid metabolism takes flight, Biochim Biophys Acta, 2008;1781:448-458.
[5] Alecu, I, Othman, A, Penno, A, et al., Cytotoxic 1-deoxysphingolipids are metabolized by a cytochrome P450-dependent pathway, J Lipid Res, 2017;58:60-71.
[6] Stockmann-Juvala, H and Savolainen, K, A review of the toxic effects and mechanisms of action of fumonisin B1, Hum Exp Toxicol, 2008;27:799-809.
[7] Rahmaniyan, M, Curley, RW, Jr., Obeid, LM, et al., Identification of dihydroceramide desaturase as a direct in vitro target for fenretinide, J Biol Chem, 2011;286:24754-24764.
[8] Cingolani, F, Casasampere, M, Sanllehi, P, et al., Inhibition of dihydroceramide desaturase activity by the sphingosine kinase inhibitor SKI II, J Lipid Res, 2014;55:1711-1720.
[9] Othman, A, Rütti, MF, Ernst, D, et al., Plasma deoxysphingolipids: a novel class of biomarkers for the metabolic syndrome?, Diabetologia, 2012;55:421–431.
[10] Othman, A, Benghozi, R, Alecu, I, et al., Fenofibrate lowers atypical sphingolipids in plasma of dyslipidemic patients: A novel approach for treating diabetic neuropathy?, Journal of clinical lipidology, 2015;9:568-575.
[11] Steiner, R, Saied, EM, Othman, A, et al., Elucidating the chemical structure of native 1-deoxysphingosine, J Lipid Res, 2016;57:1194-1203.
[12] Ternes, P, Franke, S, Zahringer, U, et al., Identification and characterization of a sphingolipid delta 4-desaturase family, J Biol Chem, 2002;277:25512-25518.
[13] Omae, F, Miyazaki, M, Enomoto, A, et al., DES2 protein is responsible for phytoceramide biosynthesis in the mouse small intestine, Biochem J, 2004;379:687-695.
[14] Enomoto, A, Omae, F, Miyazaki, M, et al., Dihydroceramide:sphinganine C-4-hydroxylation requires Des2 hydroxylase and the membrane form of cytochrome b5, Biochem J, 2006;397:289-295.
[15] Pruett, ST, Bushnev, A, Hagedorn, K, et al., Biodiversity of sphingoid bases ("sphingosines") and related amino alcohols, J Lipid Res, 2008;49:1621-1639.
[16] Weiss, B and Stoffel, W, Human and murine serine-palmitoyl-CoA transferase--cloning, expression and characterization of the key enzyme in sphingolipid synthesis, Eur J Biochem, 1997;249:239-247.
[17] Hanada, K, Hara, T, Nishijima, M, et al., A mammalian homolog of the yeast LCB1 encodes a component of serine palmitoyltransferase, the enzyme catalyzing the first step in sphingolipid synthesis, J Biol Chem, 1997;272:32108-32114.
[18] Renkonen, O and Hirvisalo, EL, Structure of plasma sphingadienine, J Lipid Res, 1969;10:687-693.
[19] Fabrias, G, Munoz-Olaya, J, Cingolani, F, et al., Dihydroceramide desaturase and dihydrosphingolipids: debutant players in the sphingolipid arena, Prog Lipid Res, 2012;51:82-94.
[20] Alecu, I, Tedeschi, A, Behler, N, et al., Localization of 1-deoxysphingolipids to mitochondria induces mitochondrial dysfunction, J Lipid Res, 2017;58:42-59.

# 3 Chapter 3: Online extraction using Turbulent Flow Chromatography

*Regula Steiner*

## 3.1 Abstract

For applications of lipidomics to a large sample size, an automated high throughput analysis and well-defined workflows are essential. Sample preparation is one of the most critical steps in this process, as it can introduce biases. Therefore, a fast and robust sample preparation process is needed, which optimally covers a broad range of analytes varying in solubility, polarity and abundance. We evaluated the automated Thermo TLX online extraction system using turbulent flow chromatography, which bypasses manual sample preparation steps to speed up the preparation time. We established a TLX extraction protocol for various sphingolipid species and additionally, compared it to established manual liquid-liquid extraction procedures, like those of Folch, Bligh and Dyer, as well as a recently published single-phase methyl-tert-butyl-ether extraction protocol. We show that, although the TLX system allowed for robust extraction of various sphingolipid classes, the over-all lipid recovery is much lower compared to the liquid-liquid based extraction methods, varying between 12 % and 93 % for the different sphingolipid classes.

## 3.2 Introduction

Novel biomarkers need validation and replication in large population-based studies, with sample numbers ranging from hundreds to several thousands. To analyze such large numbers of samples, an automated high throughput analysis and well-defined workflows are desired. For lipid analysis, sample preparation is the first and most critical step, as it can significantly influence the number, abundance and types of extracted lipid species in a specimen [1]. The primary aim of the sample preparation is to enrich the analytes of interest and remove interfering impurities, such as proteins or salts [2]. Chromatographic separation techniques usually do not tolerate the presence of proteins during analysis as they interact with the analytical column, interfere with the retention of the analytes, and might form precipitates, which block the flow through the column. Furthermore, proteins interfere with most of the detectors and can lead to ion suppression [3], which can be seen as a competition for ionization between molecules introduced into the MS source at the same time, and thereby reduces the signal for the analyte of interest.

In lipidomics, several sample preparation strategies have been used. Proteins can be precipitated by the use of organic solvents, or analytes can be extracted using liquid-liquid extraction or solid phase extraction [2]. However, none of the described precipitation techniques results in complete protein removal or is optimal for all metabolites of interest [4]. Therefore, each extraction method has to be chosen separately according to the individual analytical needs. For protein precipitation, organic solvents such as methanol (MeOH), ethanol (EtOH), acetonitrile (ACN), acetone, or a combination thereof are used [4, 5]. For the extraction of lipids, the protocols from Bligh and Dyer [6] or Folch [7] are considered as the gold standards, however, relatively new optimized protocols using methyl-tert-butyl-ether or other ether-based solvent systems have also been developed recently [8].

Sample preparation methods improve the quality of the analysis, but also pose the risk to lose certain analytes during the extraction. Also, most of these techniques require evaporation and reconstitution steps, which can lead to the loss of analytes or an increase in

ion suppression. In addition and in general, manual extraction is more time-consuming and lowers sample throughput significantly [1].

The workflow in our lab currently includes a manual two-step liquid-liquid extraction [9-13]. This extraction step, as well as the semi-manual analysis of the identified metabolites, greatly limits the analytical throughput and the number of samples, which can be analyzed within a reasonable time. To circumvent these limitations, we wanted to establish an TLX based extraction method which allows the extraction of a great variety of lipid classes and species.

Turbulent flow chromatography is a novel technique for sample preparation, which was initially established for the analysis of small molecules [14] and metabolites [15]. The technique allows complete automation, as the samples can be serially injected into and extracted by the chromatographic system. This minimizes manual sample preparation steps and allows high throughput analysis [16, 17].

The set-up requires a turbo flow extraction column with relatively large particle size, installed in series before the analytical column. Low molecular weight analytes diffuse into the pores of the extraction column and are retained, while lager matrix components are washed out of the column by a high turbulence flow (Figure 3-1). After elution, the retained analytes are directly loaded onto the analytical column for LC-MS analysis [18-20].

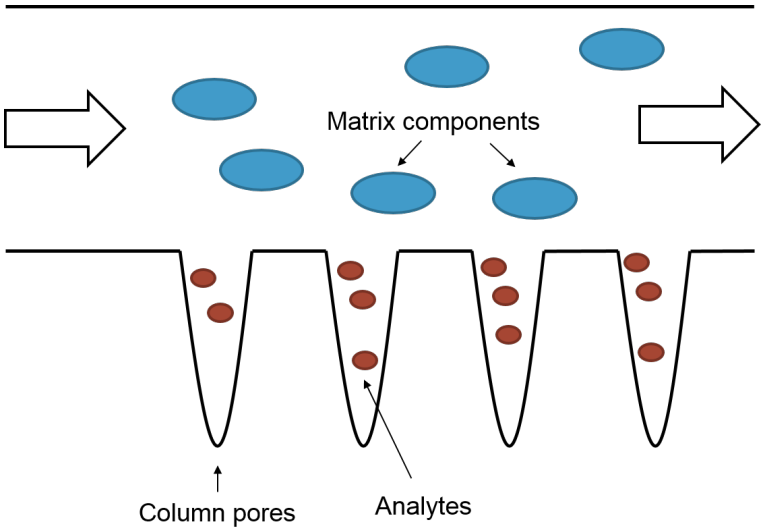


Figure 3-1: A turbulent flow extraction column consists of large pores, where the sample is run through with high flow. (Small particle size) analytes will diffuse into pores and are therefore retained, while (big size) matrix components will be flushed trough the column without retention.

The extraction of analytes with turbulent flow chromatography is performed in a five steps process. In the first step, the sample is loaded onto the extraction column, while the analytical column is preconditioned with the loading solvent. Therefore, the extraction column is connected to the loading pump and waste, whereas the analytical column is autonomous and connected to the eluting pump (Figure 3-2 a). In the second step, the sample is eluted backward from the extraction column by attaching a loop filled with elution solvent and thereby changing the direction of flow. The sample is loaded onto the analytical column by setting the two columns in line. The solvent streams of loading and elution pumps are therefore combined (Figure 3-2 b). As a third step, the separation on the analytical column starts by applying the eluent from the elution pump, which is directly connected to the analytical column. To establish the chromatographic separation in an autonomous system the, extraction column is disconnected from the analytical system (Figure 3-2 c). In the forth step, the extraction column is washed with a strong organic solvent. At the same time, the gradient on the analytical column is set to reach a maximum of 100 % elution mobile phase, and the analytical column is washed with 100 % elution solvent. Next, the loop on the extraction system needs to be refilled again with the eluting solution, while the analytical column is set back to starting conditions for re-equilibration (Figure 3-2 c).

In the fifth step, the refilled loop is disconnected from the extraction column and the extraction, but also the analytical column is re-equilibrated for a next run (Figure 3-2 a).

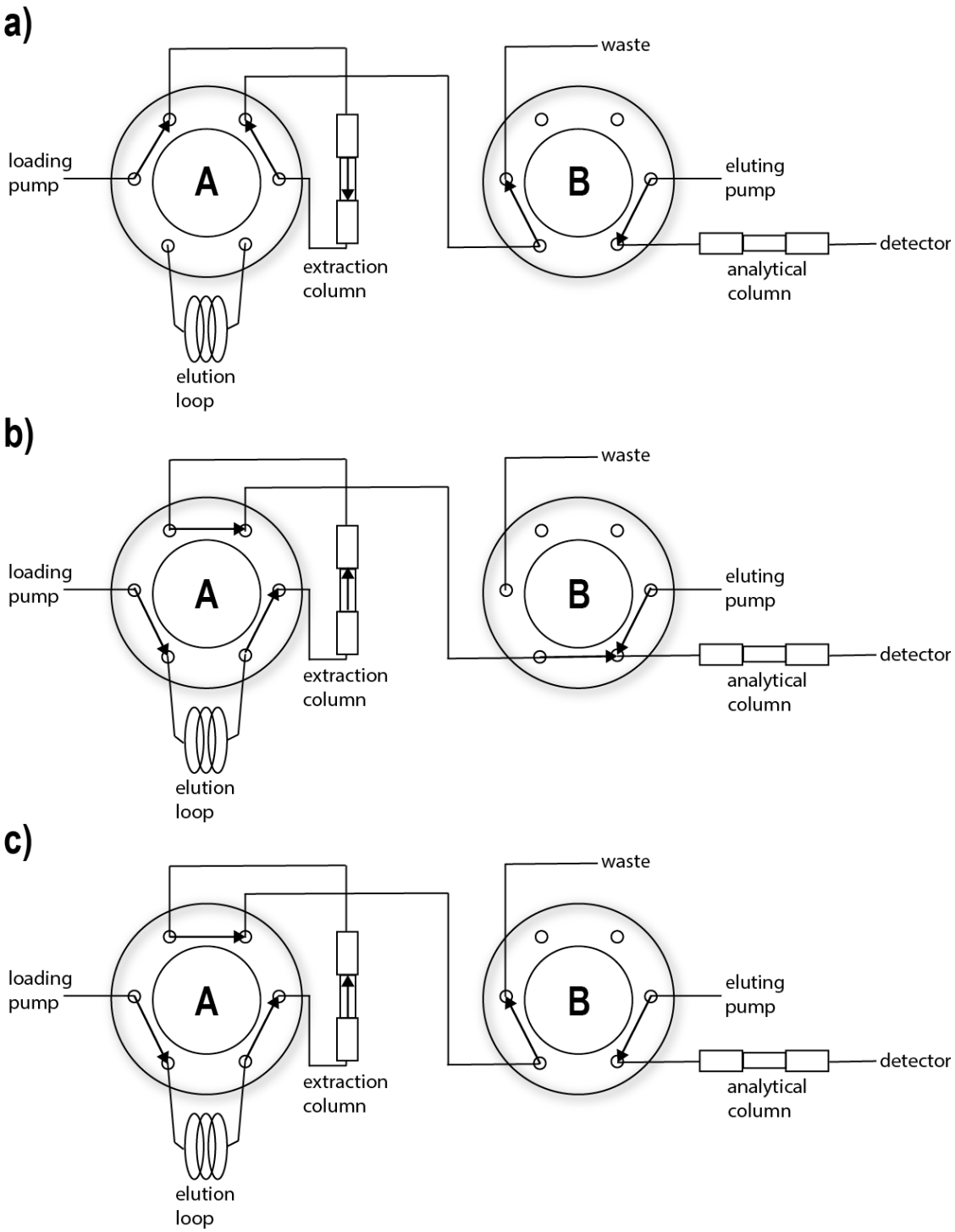


Figure 3-2: a) Valve A: Extraction column connected to loading pump and waste for loading sample or re-equilibrating extraction column. Valve B: Analytical column connected to the eluting pump and the detector for LC-run. b) Valve A: Extraction column elution by changing flow direction and connecting additional loop with eluting solvent. Valve B: Analytical column set in line with extraction column to load the sample onto analytical column. c) Valve A: Loop was filled again with the eluting solvent for the next run. Valve B: Chromatographic separation is started on analytical column.

## 3.3 Materials and methods

A TLX system (Thermo Fisher Scientific, Reinach, Schweiz) with two accela pumps (loading and eluting) was used. For extraction, a TurboFlow XL C8 0.5 x 50 mm (Thermo Fisher Scientific, Reinach, Schweiz) was used. Unless stated otherwise, all solvents and reagents were purchased from Sigma-Aldrich Chemie GmbH (Buchs, Switzerland). Methanol was obtained from Honeywell specialty chemicals (Seelze GmBH, Germany). All lipid standard were purchased from Avanti Polar Lipids (Alabaster, USA).

### 3.3.1 Liquid chromatography

For chromatographic separation an Accucore C30 column (2.6 µm, 150 × 2.1 mm, Thermo Fischer Scientific) was used. The following mobile phases were used:

Eluting A: water / acetonitrile 80 / 20 v/v with 10 mM ammonium acetate and 0.1 % formic acid, eluting B: isopropanol / acetonitrile 90 / 10 v/v with 10 mM ammonium acetate and 0.1 % formic acid and eluting C: methanol. The gradient profile is shown in Table 3-1.

Table 3-1: Chromatographic details for LC separation on C30 Accucore column. ‡

| Step | Grad | time [min] | Flow | % A | % B | % C |
|---|---|---|---|---|---|---|
| Load | Step | 1.5 | 0.3 | 70 | 20 | 10 |
| Elute | Ramp | 17 | 0.3 | | 100 | |
| Wash | Step | 7 | 0.3 | | 100 | |
| Re-cond | Ramp | 1 | 0.3 | 70 | 20 | 10 |
| Re-equ | Ramp | 4 | 0.3 | 70 | 20 | 10 |

## 3.3.2 Mass spectrometry

Samples were analyzed on a Q Exactive (Thermo, Reinach, BL, Switzerland) using a heated electrospray ionization (HESI) interface. For mass spectral detection, the following parameters were set on the HESI source: spray voltage 3.5 kV, a vaporizer temperature of 300 °C, sheath gas pressure 20 AU, aux gas 8 AU and a capillary temperature of 320 °C. The detector is set to an $MS^2$ method using a $top^{10}$ approach with a 140k resolution for full

‡ Mobile phase A consists of water / acetonitrile 80 / 20 v/v with 10 mM ammonium acetate and 0.1 % formic acid, mobile phase B consists of isopropanol / acetonitrile 90 / 10 v/v with 10 mM ammonium acetate and 0.1 % formic acid and mobile phase C is 100 % methanol.

spectrum and 17.5k for $MS^2$, where a full scan is followed by fragmentation spectra of the ten most intense ions per full scan with stepped collision energy between 25 and 30. For the selection of ion fragmentation, a dynamic exclusion filter was applied which excludes ions after fragmentation for 20 seconds.

### 3.3.3 Method development

#### Standards used for method development

For method development, a set of different synthetic sphingoid bases and ceramides were used (Table 3-2). All standards were used at a concentration of 2 µM.

Table 3-2: Synthetic standards used for online extraction method development. [§]

| Sub-Class | Species |
|---|---|
| Sphingoid bases | SPH d17:1 |
| | SPH d17:0 |
| | $D_7$-SPH d18:1 |
| | $D_7$-SPH d18:0 |
| | SPH d18:1 |
| | SPH d18:0 |
| | SPH t18:0 |
| | SPH m17:1 |
| | $D_5$-SPH m17:0 |
| | SPH m18:0 |
| | $D_3$-SPH m18:0 |
| | SPH m18:1 |
| | SPH d20:1 |
| | SPH d20:0 |
| | SPH d18:2 |
| Ceramides | Cer d18:1 / 12:0 |
| | Cer d18:1 / 14:0 |
| | Cer d18:1 / 17:0 |
| | Cer d18:1 / 18:1 |
| | Cer d18:1 / 20:0 |
| | Cer d18:1 / 22:0 |
| | Cer d18:1 / 24:0 |
| | Cer d18:1 / 24:1 |
| | Cer d18:0 / 12:0 |

[§] All standards were mixed and used with a final concentration of 2 µM.

| | |
|---|---|
| | Cer d18:0 / 24:0<br>Cer m18:0 / 12:0<br>Cer m18:0 / 24:1<br>Cer m18:1 / 16:0<br>Cer m18:1 / 24:1 |

**Turbulent flow column selection and loading solvent evaluation**

Nine different turbulent flow columns (Table 3-3) obtained from Thermo Scientific (Reinach BL, Switzerland) were tested for optimal retention of sphingoid bases and ceramides. All nine columns were tested in combinations with three different mobile phases:

- water with 0.1 % formic acid (pH 3)
- water with 10 mM ammonium acetate (pH 6)
- water with 10 mM ammonium acetate, adjusted to pH 8 with ammonium hydroxide.

Methanol was used for elution during the column selection and solvent evaluation step.

Table 3-3: Turbulent flow columns and characteristics. Information adapted from Thermo Scientific TurboFlow Method Development Guide.

| **Column** | **Properties** |
|---|---|
| C18 | C18 bonded silica, very high hydrophobicity |
| C18-P | C18 bonded silica, high hydrophobicity |
| C8 | C8 bonded silica, high hydrophobicity |
| Fluoro | Alkyl fluoro bonded silica, slight hydrophobicity |
| Cyclone | Styrene / divinyl benzene copolymer bead, very high hydrophobicity |
| Cyclone-P | Styrene / divinyl benzene copolymer bead with polar modification, high hydrophobicity |
| CycloneMCX | Styrene / divinyl benzene copolymer with sulfonic acid modification, moderate hydrophobicity |
| CycloneMCX2 | Styrene / divinyl benzene copolymer with sulfonic acid modification, moderate hydrophobicity, lower ion exchange capacity than CycloneMCX |
| CycloneMAX | Styrene / divinyl benzene copolymer with quaternary ammonium, moderate hydrophobicity |

Each column was tested using the three different water mobile phases (pH 3, pH 6 and pH 8) for optimal retention, minimal breakthrough, maximally sharp elution, and minimal loss during the wash phase. Breakthrough is observed when part of the sample travels with the injection band through the column without interacting with the stationary phase.

A short chromatographic method on the extraction column was used to evaluate and optimize the different steps of the online extraction (Table 4).

Table 3-4: Chromatographic setting for method development for online extraction method.

| Step | Time [min] | Flow [mL/min] | % A | % B | Loop |
|---|---|---|---|---|---|
| 1. Load | 30 | 1.5 | 100 | | out |
| 2. Elute | 60 | 0.3 | 100 | | in |
| 3. Wash | 60 | 1.5 | | 100 | in |
| 4. Loop fill | 60 | 1.5 | 100 | | in |
| 5. Equilibrate | 60 | 1.5 | 100 | | in |

- Step 1: The standard mix (10 µL) was injected into the turbulent flow column (mobile phase A) at a high flow rate (30 sec, 1.5 mL/min).
- Step 2: The retained metabolites were eluted by connecting the loop, which was filled with methanol (1 min, 0.3 mL/min).
- Step 3: The column was washed with methanol (B) for one minute at 1.5 mL/min
- Step 4: The loop was refilled with methanol (B) for one minute at 1.5 mL/min.
- Step 5: After disconnecting the loop, the column was re-equilibrated for one minute with water mobile phase at 1.5 mL/min flow.

Mass spectra were recorded for 4.5 minute to evaluate the retention capacity for all synthetic standards. To ensure a constant flow trough the detector, the flow of the loading pump (used for the online extraction column) was combined with the flow of the eluting pump and the combined flow was kept at 1.5 mL/min. The combined flow was divided into waste and detector using a T connector.

**Sample elution and transfer**

Further, the optimal percentage of organic solvent (methanol, ethanol, and acetonitrile) in the elution was assessed by testing conditions with 20, 40, 60, 80, 90 and 100 % of organic solvent against water containing 0.1 % formic acid as mobile phase. Therefore, the loop was filled with the corresponding solvent composition during the loop-filling step (Step 4, Table 3-4). The method was optimized for total extraction where the total amount of organic solvent

should stay as low as possible to avoid a breakthrough of the analytes on the analytical column.

The transfer of the sample to the analytical column during the second elution step was optimized for flow during transfer and the time needed for a complete transfer in the corresponding flow rate. Therefore, flow rates of 0.1 mL/min, 0.2 mL/min, 0.3 mL/min, 0.4 mL/min and 0.5 mL/min during elution (Step 2, Table 3-4) were tested and the corresponding time for complete transfer was measured.

### 3.3.4 Protocol for online turbulent flow extraction

The following mobile phases were used:
Loading A: 0.1 % formic acid in water, Loading B: Methanol, Loading D: Acetonitrile / Isopropanol / Methanol 1/1/1 v/v/v

Eluting A: Water / Acetonitrile 80/20 v/v with 10mM ammonium Acetate and 0.1 % formic acid and Eluting B: Isopropanol / Acetonitrile 90/10 v/v with 10mM ammonium Acetate and 0.1 % formic acid and Eluting C: MeOH.

See further details of solvent composition, gradient, and flow in Table 3-5.

Table 3-5: Chromatographic details for the online extraction method using a TLX system with loading and eluting pumps and a C8 TLX turbulent flow column (connected to loading pump) and an analytical Accucore C30 column (connected to the eluting pump). **

| Step | time [min] | Loading pump | | | | | Eluting Pump | | | | |
|---|---|---|---|---|---|---|---|---|---|---|---|
| | | Flow | % A | % B | % D | Loop | Flow | Grad | % A | % B | % C |
| Load on TLX | 0 | 1.5 | 100 | | | out | 0.3 | step | 70 | 20 | 10 |
| Elute to LC | 0.5 | 0.1 | | 100 | | in | 0.2 | step | 70 | 20 | 10 |
| LC gradient | 1.5 | 0.0 | | 100 | | in | 0.3 | ramp | | 100 | |
| Wash TLX and LC | 18.5 | 0.5 | | | 100 | in | 0.3 | step | | 100 | |
| Loop fill TLX, start cond. LC | 25.5 | 1.5 | | 100 | | in | 0.3 | ramp | 70 | 20 | 10 |
| Loop fill TLX, re-equilibrate LC | 26.5 | 1.5 | | 100 | | in | 0.3 | step | 70 | 20 | 10 |
| Re-equilibrate TLX and LC | 28.5 | 1.5 | 100 | | | out | 0.3 | step | 70 | 20 | 10 |
| End | 30.5 | 1.5 | 100 | | | out | 0.3 | step | 70 | 20 | 10 |

### 3.3.5 Method validation

#### Linearity

For method validation, linearity of the measured area under the peak and concentration was measured using the TLX system.

A standard mix of 65 lipids, including species from various classes of sphingolipids, phospholipids, and cholesteryl esters in five different concentrations were tested for the concentration dependent linearity of the signal. To achieve an optimal detection range, lipid standards varying 50 fold in concentration from 0.1 to 5 µM were used. The details for the standards used are depicted in table 4.

Table 3-6: Synthetic lipid species included in standard mix for online extraction method validation

| Sub-Class | Species |
|---|---|
| Sphingoid bases | SPH d17:1<br>SPH d17:0<br>$D_7$-SPH d18:1<br>$D_7$-SPH d18:0 |

** Mobile Phases on the loading pump are A: 0.1 % formic acid in water, B: Methanol, D: Acetonitrile / Isopropanol / Methanol 1/1/1 v/v/v. On the eluting pump, mobile phases are A: Water / Acetonitrile 80 / 20 v/v with 10mM ammonium Acetate and 0.1 % formic acid and B: Isopropanol / Acetonitrile 90 / 10 v/v with 10mM ammonium Acetate and 0.1 % formic acid and C: MeOH.

| **Sub-Class** | **Species** |
|---|---|
| | SPH d18:1 |
| | SPH d18:0 |
| | SPH t18:0 |
| | SPH d20:1 |
| | SPH d20:0 |
| | SPH d18:2 |
| 1-Deoxy sphingoid bases | m17:1 |
| | $D_5$-m17:0 |
| | m17:0 |
| | m18:0 |
| | $D_3$-m18:0 |
| | m18:1 |
| Spingosine-1-phosphate | S1P d18:1 |
| | S1P d17:1 |
| | S1P d17:0 |
| | $D_7$-S1P d18:1 |
| Ceramides | Cer d18:1 / 12:0 |
| | Cer d18:1 / 14:0 |
| | Cer d18:1 / 17:0 |
| | Cer d18:1 / 18:1 |
| | Cer d18:1 / 20:0 |
| | Cer d18:1 / 22:0 |
| | Cer d18:1 / 24:0 |
| | Cer d18:1 / 24:1 |
| | Cer d18:0 / 12:0 |
| | Cer d18:0 / 16:0 |
| | Cer d18:0 / 24:0 |
| | $D_7$-Cer d18:1 / 16:0 |
| | $D_7$-Cer d18:1 / 24:0 |
| 1-Deoxyceramides | Cer m18:0 / 12:0 |
| | Cer m18:0 / 24:1 |
| | Cer m18:1 / 12:0 |
| | Cer m18:1 / 16:0 |
| | Cer m18:1 / 24:1 |
| | Cer m17:0/16:0 |
| | Cer m17:1/16:0 |
| | Cer m17:0/24:1 |
| | Cer m17:1/24:1 |
| Sphingomyelins | SM 18:1 / 24:0 |

| Sub-Class | Species |
|---|---|
| | SM 18:1 / 24:1 |
| | SM 18:0 / 12:0 |
| | SM 18:1 / 12:0 |
| | SM 18:1 / 16:0 |
| | $D_9$-SM 18:1 / 18:1 |
| | GluCer 18:1 / 8:0 |
| | GluCer 18:1 / 16:0 |
| | GluCer 18:1 / 24:1 |
| Glucosylceramides | $D_5$-GluCer 18:1 / 18:1 |
| Phospholipids | PC 16:0 / 18:2 |
| | PC 14:0 / 14:0 |
| | PC 24:0 / 24:0 |
| | LPC 16:0 |
| | LPC 17:0 |
| | PE 14:0 / 14:0 |
| | PE 18:0 / 18:0 |
| | LPE 17:1 |
| | PG 16:0 / 16:0 |
| | PG 17: 17:0 |
| | PA 14:0 / 14:0 |
| | PA 17:0 / 17:0 |
| Cholesteryl esters | $D_7$-ChE 16:0 |

**Recovery**

A mix of 65 different lipid species (Table 3-6) was injected with and without the use of the TLX column. Recovery was calculated for all lipid species (5 µM concentration), by calculating the percentage of the area measured with the TLX column applied to the area measured with bypassing the online extraction.

**Online extraction in comparison to manual liquid-liquid extraction**

Different lipid extraction methods were compared for the extraction of lipids from plasma samples. Four different volumes (3 µL, 5 µL, 10 µL and 20 µL) of pooled plasma from healthy donors were used. Volume was filled up to 20 µL with PBS for all samples. Internal standards were added to the samples ($D_7$-SPH 18:0, $D_7$-SPH 18:1, Cer d18:0 / 12:0, Cer 18:1 / 12:0, 1-deoxyCer m18:0 / 12:0, 1-deoxyCer 18:1 / 12:0, HexCer 18:1 8:0, SM 18:1 / 12:0 and $D_7$-

S1P d18:1) and the sphingolipidome was analyzed by the different extraction methods. Recovery was evaluated for 20 µL plasma samples. The Bligh and Dyer protocol was used as a reference extraction method for relative comparison.

For Folch-based extraction, 1 mL of methanol/chloroform (2/1 v/v) was added to the samples. Samples were extracted at 37 °C for 1 hour using an Eppendorf Thermo shaker at 1400 rpm. After the addition of 0.5 mL of chloroform, samples were vortexed for 20 seconds, followed by addition of 200 µL of alkaline water and again vortexed for 20 seconds. Finally, the samples were centrifuged at 16000 rpm for 5 min for phase separation. The aqueous phase was aspirated and the organic phase dried under a stream of $N_2$ after washing with alkaline water.

For ether-based extraction, 1 mL of EtOAc / 2-propanol (85/15 v/v) was added to the samples. After vortexing for 20 seconds, 0.5 mL of water and 50 µL of concentrated formic acid were added. Samples were extracted at 37 °C for 20 min using the Eppendorf Thermo shaker at 1400 rpm. Finally, the samples were centrifuged at 16000 rpm for 5 min for phase separation. The organic phase was transferred to a fresh tube and dried under a stream of $N_2$.

For the Bligh- and Dyer-based protocol, 375 µL of methanol/chloroform (2/1 v/v) was added to the sample and vortexed for 20 seconds. Afterwards, 125 µL of chloroform were added and vortexed again for 20 seconds. Then 125 µL of water were added, and samples were shaken for 20 min at 37 °C in an Eppendorf Thermo shaker with 1400 rpm. Finally, samples were centrifuged at 16000 rpm for 5 min for phase separation. The organic phase was transferred into another tube and the water phase was re-extracted with 250 µL of chloroform. Both organic phases were combined, and samples were dried under a stream of $N_2$.

For the MMC protocol, 1mL of methanol / MTBE / chloroform (MMC) 1.33/1/1 v/v/v was added to the sample and the sample was vortexed for 20 seconds. The mixture was agitated for 20 min in an Eppendorf Thermo shaker at 37 °C at 1400 rpm. The protein precipitate was pelleted by centrifuging for 5 min at 16000 rpm at 24 °C, and 1 mL of the supernatant was transferred to another tube. The solvent was dried under a stream of $N_2$.

For analysis with LC-MS, the samples were re-suspended in 100 µL methanol and transferred to MS vials and 25 µL injected into the LC system.

For online extraction, different protein precipitation solvents were used. As most of the lipids are bound to lipoproteins [21-23], these proteins need to be denatured to release the lipids for quantification with LC-MS. Therefore, plasma proteins were precipitated with methanol, acetonitrile or a mix of methanol/acetonitrile 1/1 (v/v). The organic solvent was added in a 1:5 plasma to solvent ratio. 100 µL of the solution was added to 20 µL plasma, vortexed for 20 seconds and extracted at 37 °C for one hour. The samples were centrifuged at 16000 rpm for 5 min and the supernatant was transferred into the MS vials. For LC-MS analysis, 25 µL of the samples were directly injected into the turbulent flow column.

## 3.4 Results

### 3.4.1 Method development

Nine different extraction columns with different column chemistry were tested. This included the C18 or C8 bonded silica with different modifications, alkyl fluoro bonded silica, styrene/divinylbenzene copolymer bead with and without polar change or cationic/anionic exchange. For each column, three different loading solvents, varying in pH from 3 to 8 were evaluated.

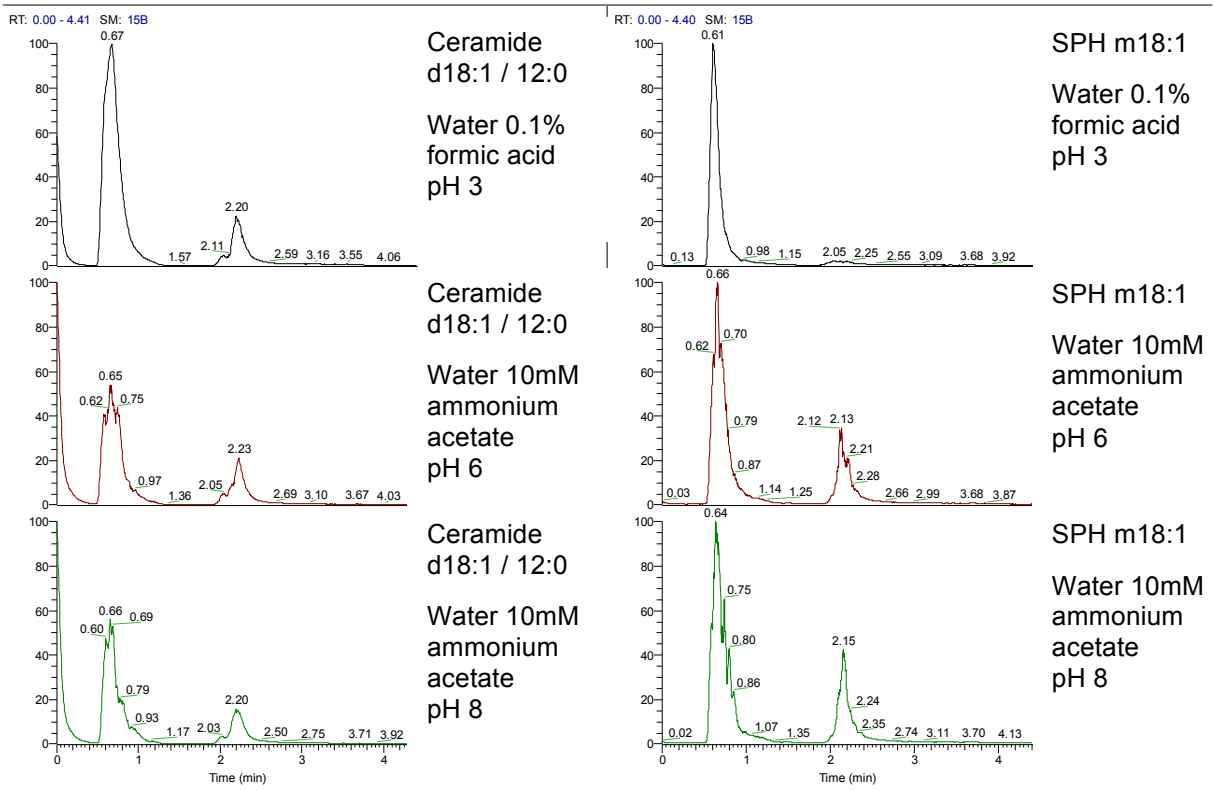


Figure 3-3: Loading solvents were evaluated on a C8 XL column for ceramides and sphingoid bases. Chromatograms for $C_{12}$ ceramide (Cer d18:1 / 12:0) and a 1-deoxysphingoid base (SPH m18:1) are depicted as an example. The C8 XL column was evaluated with three different loading mobile phases, water containing 0.1 % formic acid (pH 3) or 10 mM ammonium acetate (pH 6) and water with 10 mM ammonium acetate adjusted to pH 8 with ammonium hydroxide. Best retention was achieved on C8 XL column using water with 0.1 % formic acid.

Breakthrough happens when not all lipids were retained by the column. This breakthrough is typically seen in a pre-peak directly after sample injection. The retained lipids were eluted from the column within 0.5 minutes in a narrow peak. If retention was too high, a second peak eluting at 2.2 minutes is seen during the column wash step (Figure 3-3). For ceramides, a breakthrough was observed for all the tested columns and for all three different mobile phases. The best retention of sphingoid bases and ceramides was obtained using the C8 XL column with water and 0.1% formic acid (pH 3) as loading mobile phase (Figure 3-3). No breakthrough and very low elution during the washing step were seen for sphingoid bases and a minor breakthrough and elution during washing were seen for ceramides compared to the other mobile phases. These conditions were chosen for further method development.

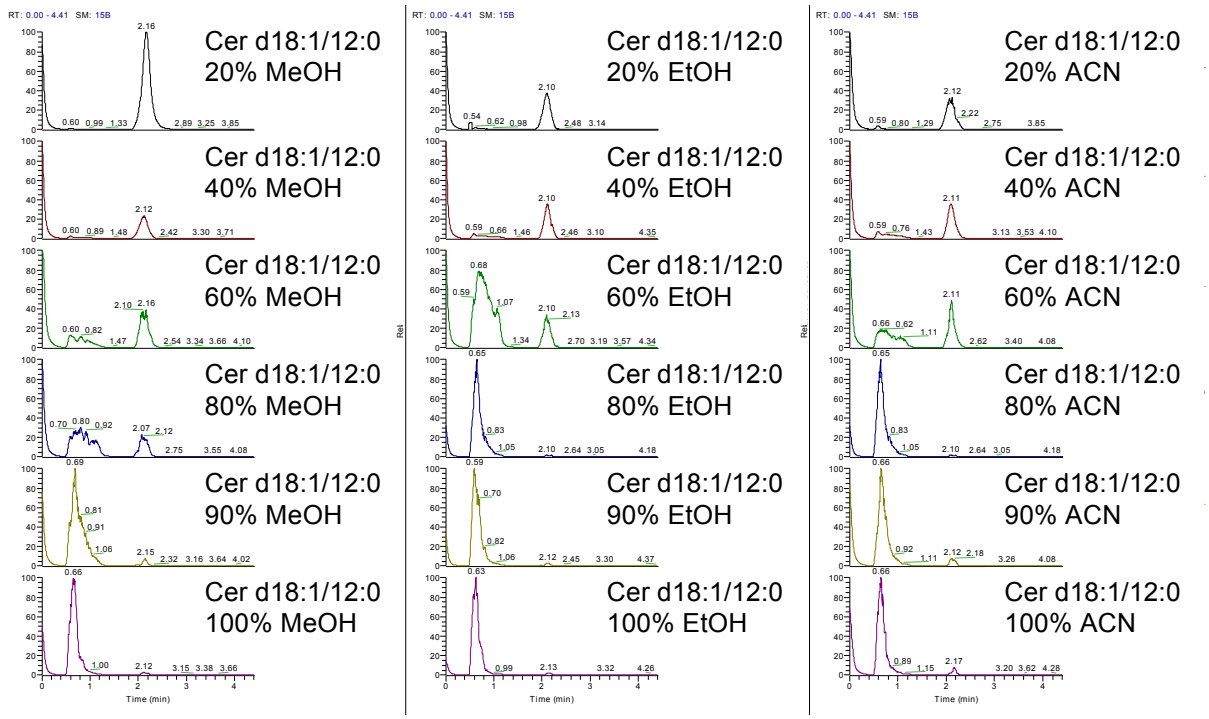


Figure 3-4: Elution solvent (ethanol (EtOH), methanol (MeOH) and acetonitrile (ACN)) was evaluated for sphingoid bases and ceramides. Organic solvents, methanol, ethanol and acetonitrile were tested in mixture with water 0.1 % formic acid in 20 %, 40 %, 60 %, 80 %, 90 % and at 100 % organic solvent. Ceramide Cer d18:1 / 12:0 was eluted at 0.7 minutes with eluting solution or if incomplete elution occurred at 2.1 min during the washing step. Maximal elution was measured with 100 % methanol or ethanol.

Next, the optimal elution solvent was defined. Methanol, ethanol and acetonitrile were tested for maximal elution of sphingolipids with minimal use of organic solvent. Best elution results for sphingoid bases and ceramides were reached on the C8 XL using 100 % ethanol or 100 % methanol for elution. With a lower percentage of organic solvent, the elution was not complete. This is shown for the elution of Cer d18:1 / 12:0 (Figure 3-4). Finally, 100 % methanol was chosen as the eluent because methanol had less influence on the peak shape and resolution on the analytical column compared to ethanol.

After selecting the appropriate elution solvent, the elution flow and time was adjusted. For this, flow rates between 0.1 mL/min and 0.5 mL/min were tested and the time for complete elution was measured for all flow rates (Figure 3-5).

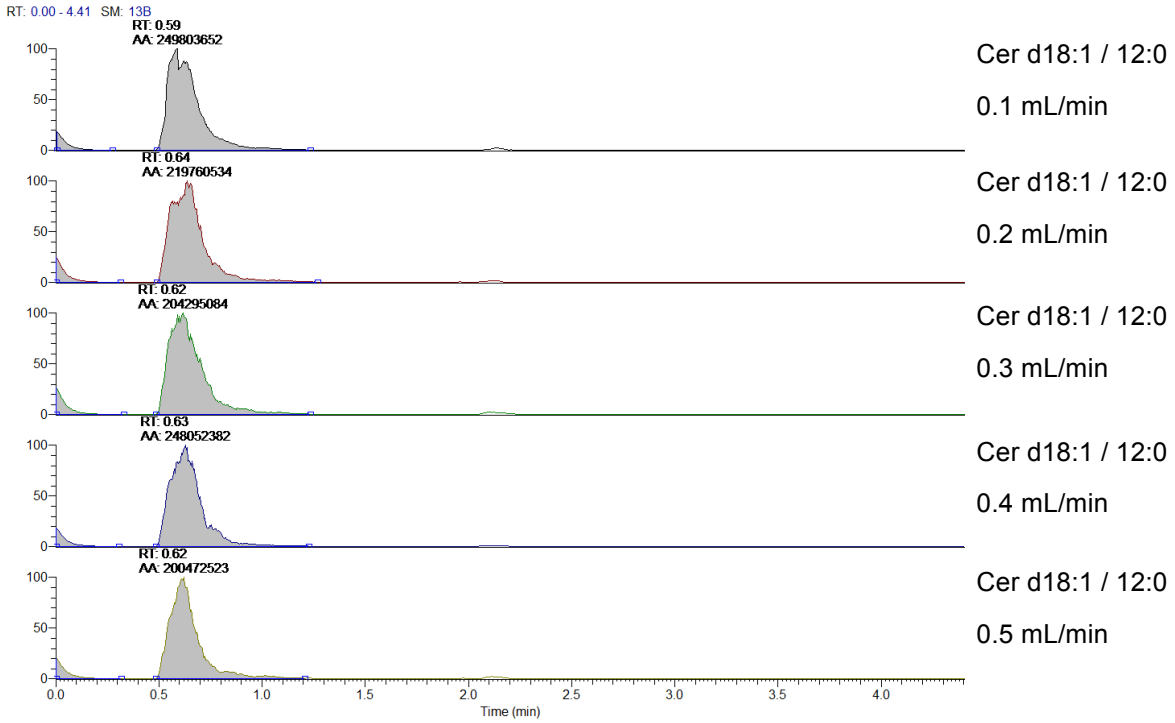


Figure 3-5: Elution time and flow rate were evaluated for sphingoid bases and ceramides. Flow rates between 0.1 mL/min and 0.5 mL/min were tested and the corresponding elution time measured. For all five tested flow rates, elution time was 30 seconds and elution efficiency did not differ between the tested conditions.

We did not observe any significant difference between the flow rates for elution efficiency and transfer time (Figure 3-5). Maximal elution was reached within 30 seconds for all flow rates. We therefore chose a minimal transfer flow of 0.1 mL/min to minimize the organic solvent transferred to the analytical column thereby decreasing the risk for a breakthrough on the analytical column. Transfer time was set to 60 seconds to ensure complete elution.

### 3.4.2 Method validation

**Linearity of extraction efficiency using of online extraction**

The linearity of the extraction efficiency of all different sphingolipid classes, phospholipids, and cholesteryl ester was measured using the TLX system. Synthetic standards were injected and extracted on the TLX column and the linearity verified by comparing $R^2$ values (Figure 3-6).

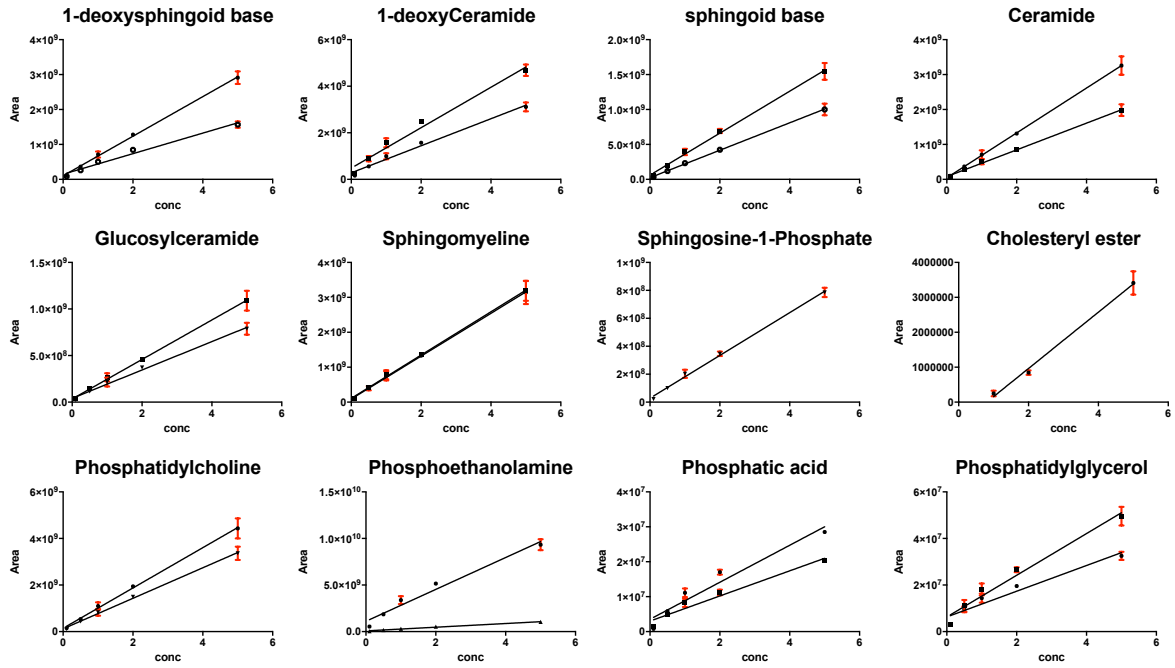


Figure 3-6: Linear regression of different sphingolipids, phospholipids and cholesteryl ester after TLX extraction in 0.1, 0.5, 1, 2 and 5 µM concentration.

For most of the analyzed lipid species, we obtained a linear relationship with an $R^2$ >0.95. Linearity was less pronounced for phosphatidylglycerol ($R^2$ >0.91) and for Phosphatidic acid the curve was not linear ($R^2$ = 0.75) (Table 3-7).

Table 3-7: Linearity ($R^2$) and relative recoveries (%) of indicated lipid species.

| **Sub-Class** | **Species** | **Linearity ($R^2$)††** | **Rel. Recovery [%]‡‡** |
|---|---|---|---|
| Sphingoid bases | SPH d18:2 | 0.9919 | 32.6 |
| | SPH d17:1 | 0.9909 | 32.1 |
| | SPH d17:0 | 0.9897 | 46.0 |
| | SPH t18:0 | 0.9849 | 49.7 |
| | $D_7$-SPH d18:1 | 0.9886 | 38.2 |
| | SPH d18:1 | 0.9875 | 37.2 |
| | $D_7$-SPH d18:0 | 0.9842 | 44.3 |
| | SPH d18:0 | 0.9860 | 43.5 |
| | SPH d20:1 | 0.9773 | 40.0 |
| | SPH d20:0 | 0.9738 | 43.3 |
| 1-Deoxy sphingoid bases | SPH m18:1 | 0.9901 | 36.3 |

†† Linearity was determined by calculation of linear coefficients of correlation (see Figure 3-6)

‡‡ Recoveries were assessed at a concentration of 5 µM.

| Sub-Class | Species | Linearity ($R^2$)†† | Rel. Recovery [%]‡‡ |
|---|---|---|---|
| | SPH m17:1 | 0.9886 | 35.2 |
| | $D_5$-SPH m17:0 | 0.9836 | 42.6 |
| | SPH m17:0 | 0.9834 | 42.0 |
| | $D_3$-SPH m18:0 | 0.9672 | 47.6 |
| | SPHm18:1 | 0.9679 | 48.3 |
| Ceramides | Cer d18:1 / 12:0 | 0.9875 | 64.7 |
| | Cer d18:0 / 12:0 | 0.9841 | 46.3 |
| | Cer d18:1 / 14:0 | 0.9789 | 64.3 |
| | $D_7$-Cer 18:1 / 16:0 | 0.9842 | 49.9 |
| | Cer d18:1 / 18:1 | 0.9881 | 52.7 |
| | Cer d18:0 / 16:0 | 0.9867 | 52.3 |
| | Cer d18:1 / 17:0 | 0.9834 | 55.9 |
| | Cer d18:1 / 20:0 | 0.9777 | 47.8 |
| | Cer d18 1:24:1 | 0.9757 | 46.3 |
| | Cer d18:1 / 22:0 | 0.9803 | 46.3 |
| | $D_7$-Cer d18:1 / 24:0 | 0.9645 | 43.6 |
| | Cer d18:1 / 24:0 | 0.9684 | 41.0 |
| | Cer d18:0 / 24:0 | 0.9851 | 25.8 |
| 1-Deoxyceramides | doxCer m18:1 / 12:0 | 0.9729 | 67.9 |
| | doxCer m18:0 / 12:0 | 0.9671 | 71.0 |
| | doxmetCer m17:1 / 16:0 | 0.9804 | 51.9 |
| | doxCer m18:1 / 16:0 | 0.9736 | 54.8 |
| | doxmetCer m17:0 / 16:0 | 0.9829 | 41.3 |
| | doxmetCer m17:1:24:1 | 0.9753 | 43.4 |
| | doxCer m18:1 / 24:1 | 0.9638 | 47.3 |
| | doxmetCer m17:0 / 24:1 | 0.9587 | 46.1 |
| | doxCer m18:0 / 24:1 | 0.9712 | 43.9 |
| Sphingomyelins | SM 18:1 / 12:0 | 0.9794 | 48.3 |
| | SM d18:0 / 12:0 | 0.9828 | 47.3 |
| | SM 18:1 / 16:0 | 0.9804 | 43.4 |
| | $D_9$-SM d18:1 / 18:1 | 0.9767 | 45.4 |
| | SM 18:1 / 24:1 | 0.9778 | 27.6 |
| | SM:d18 1:24 0 | 0.9806 | 23.1 |
| Glucosylceramides | GluCer d18:1 / 8:0 | 0.9749 | 56.4 |
| | GluCer d18:1 / 16:0 | 0.9810 | 48.1 |
| | $D_5$-GluCer d18:1 / 18:1 | 0.9809 | 62.7 |
| | GluCer d18:1 / 24:1 | 0.9760 | 48.4 |
| Phospholipids | LPC 16:0 | 0.9817 | 44.1 |

| Sub-Class | Species | Linearity ($R^2$)†† | Rel. Recovery [%]‡‡ |
|---|---|---|---|
| | LPC 17:0 | 0.9808 | 38.1 |
| | PC 14:0 / 14:0 | 0.9824 | 44.3 |
| | PC 16:0 / 18:2 | 0.9833 | 42.4 |
| | PC 24:0 / 24:0 | 0.9547 | 8.7 |
| | LPE 17:1 | 0.9532 | 76.1 |
| | PE 14:0 / 14:0 | 0.9870 | 63.9 |
| | PE 18:0 / 18:0 | 0.9723 | 49.1 |
| | PA 14:0 / 14:0 | 0.9206 | 53.0 |
| | PA 17:0 / 17:0 | 0.7574 | 32.7 |
| | PG 16:0 / 16:0 | 0.9160 | 55.2 |
| | PG 17:0 / 17:0 | 0.9469 | 42.1 |
| Cholesteryl ester | $D_7$ ChE 16:0 | 0.9748 | 3.9 |
| Sphingosine-1-phosphate | S1P d17:1 | 0.9847 | 84.9 |
| | S1P d17:0 | 0.9803 | 94.0 |
| | $D_7$-S1P d18:1 | 0.9784 | 88.1 |
| | S1P d18:1 | 0.9911 | 93.6 |

**Recovery for online extraction**

Recovery for the individual species was determined by comparing the signal intensity of directly injected standards with those after liquid-liquid or TLX extraction (Table 3-7).

Recovery was tested for 5 µM concentration of the standards. Although online TLX extraction was linear among the sphingolipids and phospholipid classes, the total recovery of injected standard ranged between 39.2% and 90.2% depending on the different sphingolipid and phospholipid classes. The best recovery was obtained for sphingosine-1-phosphate (average recovery of 90.2 %)

PC 24:0 / 24:0 and D7-cholesteryl ester 16:0 were not retained by the C8 TLX column, resulting in a recovery below 10 %.

A poor recovery might be acceptable for the further analysis, if the loss of lipid is linear throughout different concentrations, but it increases the lower limit of quantification in the method. A method with poor recovery is then applicable for highly abundant analytes.

### TLX extraction compared to manual liquid-liquid extraction

Using a human plasma sample, the recovery of the TLX extraction methods was compared to four widely used liquid-liquid extraction protocols. Recoveries were compared in relation to the Bligh and Dyer method (100 %).

We tested three precipitation solvents (methanol, acetonitrile and methanol / acetonitrile mixture) prior to online extraction for the release of lipid bound in plasma lipoproteins.

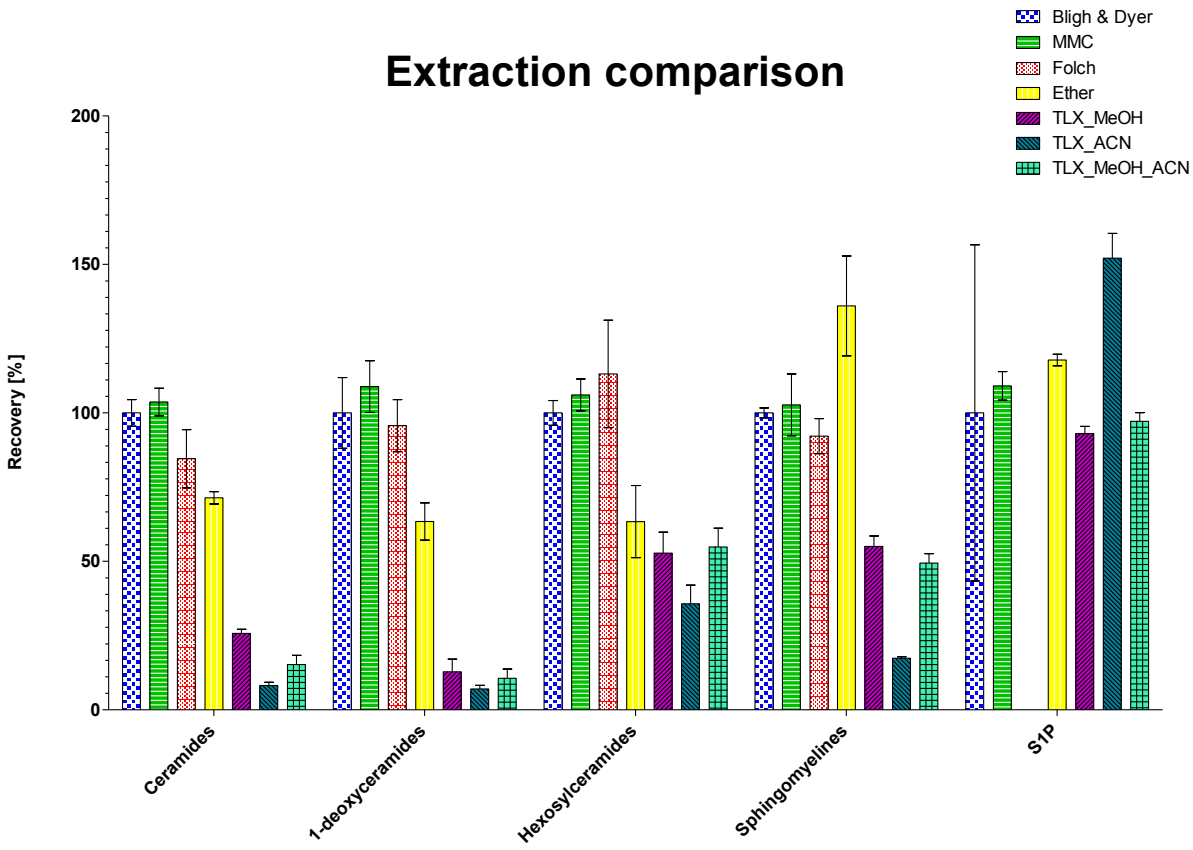


Figure 3-7: Recovery for sphingolipid classes with turbulent flow online extraction (TLX) compared to the Bligh & Dyer (set as 100%), MMC protocol, Folch, or acidic ether protocol. For TLX, three different precipitation solvents for sample preparation were used (TLX_MeOH: Methanol, TLX_ACN: Acetonitrile, TLX_MeOH_ACN: Methanol / Acetonitrile 1/1 v/v). Recovery in Bligh & Dyer protocol was set to 100% for comparison.

The MMC protocol showed the best overall coverage for all sphingolipid classes. In general, the protocols from Folch and Bligh & Dyer and the MMC single-phase extraction protocol reached comparable recoveries for all the different sphingolipid classes. The MMC protocol showed overall the best coverage for all sphingolipid classes. The ether-based protocol was lower in recovery for (1-deoxy)ceramides and hexosylceramides, but better for sphingomyelins and S1P compared to the Bligh & Dyer protocol. The MMC protocol showed

the least variation, especially for S1P. Therefore, in comparison to the manual extraction with the Bligh and Dyer protocol, MMC shows superior results.

The three tested precipitation solvents for online extraction resulted in different recoveries. Whereas recovery for methanol and methanol/acetonitrile (1/1 v/v) was comparable for all sphingolipid classes, recovery after acetonitrile precipitation was lower for N-acetylated sphingolipids and higher for S1P. This is caused by the incompatibility of the precipitation solvents with the retention of lipids on the turbulent flow extraction column. The best recovery of the three different precipitations solvents was seen for methanol.

Table 3-8: Recovery [%] for sphingolipid classes extracted with different extraction protocols compared to Bligh & Dyer protocol as reference. TLX_MeOH: Methanol, TLX_ACN: Acetonitrile, TLX_MeOH_ACN: Methanol / Acetonitrile 1/1 v/v [§§]

| Mean Recovery [%] | Ceramides | 1-deoxy-ceramides | Hexosylceramides | Sphingomyelins | S1P |
|---|---|---|---|---|---|
| Folch | 84.56 | 95.71 | 113.13 | 92.18 | - |
| MMC | 103.66 | 108.85 | 106.05 | 102.71 | 109.09 |
| Ether | 71.39 | 63.41 | 63.38 | 136.02 | 117.81 |
| TLX_ACN | 8.18 | 7.06 | 35.70 | 17.38 | 152.11 |
| TLX_MeOH | 25.76 | 12.84 | 52.79 | 55.01 | 93.04 |
| TLX_MeOH_ACN | 15.23 | 10.62 | 54.83 | 49.41 | 97.18 |

In comparison to liquid-liquid extraction, online extraction showed poor recovery for most of the sphingolipid classes. Only for S1P, online extraction gave comparable results (with a recovery around 93 % for methanol precipitation) to manual Bligh and Dyer extraction. For other lipid species, recoveries were below 55 %.

[§§] Next to liquid-liquid extraction protocols (Folch and Bligh & Dyer), a single phase MMC protocol was used. Online extracton with turbulent flow chromatography (TLX) was compared to other extraction protocols. For online extraction, three different precipitation solvents were tested.

## 3.5 Discussion

Compared to manual liquid-liquid extraction (e.g. Bligh and Dyer) or the single phase extraction MMC [8], TLX extraction has several advantages: 1. shorter sample preparation protocol with less manual steps, 2. no need for sample drying and 3. no sample reconstitution before analysis. This should lead to a less lipid loss from the sample, and allow high throughput approaches needed for general lipidomic studies [1]. However, with regard to the recovery, the other liquid-liquid extraction and the single-phase MMC protocols were superior to the TLX method in our hands. For the TLX extraction with methanol precipitation, recoveries ranged between 12.0 % and 93 % (for different lipid classes) compared to Bligh and Dyer extraction method, in turn yielded similar recoveries as other manual extraction methods. S1P showed the highest recovery (93 % for methanol precipitation with TLX extraction compared to Bligh and Dyer).

This difference in recovery using TLX extraction for certain lipid classes seems to be associated with the difference in polarity. Recovery was better for polar lipid species such as S1P and low for relatively apolar ceramides and 1-deoxyceramides.This might be because ceramides are mostly bound to lipoproteins, whereas S1P is also transported by albumin in plasma. In this context, it is interesting that several turbulent flow applications for the extraction of small molecule analytes have been reported, with the aim to reduce phospholipids during extraction to reduce the effect of ion suppression during the MS analysis [24, 25]. Michapopoulos et. al. [16] compared turbulent flow chromatography against protein precipitation in a metabolomics context and found that turbulent flow is a stable approach compared to protein precipitation, but extracted phospholipids were reduced by up to 60 % of their concentration [16].

A critical aspect for the use of the TLX turbulent flow chromatography technology in lipidomics is, that in contrast to polar metabolites, lipids are hydrophobic and not transported free in plasma but as part of lipoproteins (HDL, LDL, VLDL etc) or other lipid binding proteins, notably albumine. Lipoproteins are spherical particles with a size of 7-70 nm [26] and might therefore be lost during turbulent flow extraction [16], as due to time limitations, they do not

cross the boundary layer, whereas smaller molecules do this relatively efficiently and are therefore retained by the turbulent flow column. Thus larger molecules such as proteins go directly to waste and the smaller molecules are adsorbed to the retentive stationary phase contained within the turbulent flow column [16]. Even though proteins are supposed to precipitate before injection into the turbulent flow column, a complete precipitation and release of bound lipids from these proteins is not achieved, with solvent ratios to 1:5 of solvents we used [5]. The solvent ratios cannot be further increased, which would help in the protein precipitation. But this would increase the loss of lipids during loading step because of breakthrough of lipids, which are not retained by the turbulent flow column because of organic solvent present. These effects contribute to the lower recovery with the turbulent flow extraction protocol.

In conclusion, the TLX extraction protocol offers an automatic, fast, one-step sample preparation protocol, however at the cost of much lower recoveries of lipids in plasma compared to the established liquid-liquid extraction protocols. The use of the TLX method in lipidomics might therefore be justified for a quick and general qualitative comparison of samples where recovery and exact quantification is not essential. However, the need for a preceding protein precipitation (MeOH or ACN) makes the manual extraction effort more time-consuming and almost comparable to those of single-phase extraction procedures like the MMC protocol. In conclusion, the TLX extraction technology for lipidomic analysis is not advantageous compared to other, more established protocols.

## 3.6 References

[1] Vuckovic, D, Current trends and challenges in sample preparation for global metabolomics using liquid chromatography-mass spectrometry, Anal Bioanal Chem, 2012;403:1523-1548.
[2] Zhou, J and Yin, Y, Strategies for large-scale targeted metabolomics quantification by liquid chromatography-mass spectrometry, Analyst, 2016;141:6362-6373.
[3] Chang, MS, Ji, Q, Zhang, J, et al., Historical review of sample preparation for chromatographic bioanalysis: pros and cons, Drug Develop Res, 2007;68:107-133.
[4] Bruce, SJ, Tavazzi, I, Parisod, V, et al., Investigation of human blood plasma sample preparation for performing metabolomics using ultrahigh performance liquid chromatography/mass spectrometry, Anal Chem, 2009;81:3285-3296.
[5] Polson, C, Sarkar, P, Incledon, B, et al., Optimization of protein precipitation based upon effectiveness of protein removal and ionization effect in liquid chromatography-tandem mass spectrometry, J Chromatogr B Analyt Technol Biomed Life Sci, 2003;785:263-275.
[6] Bligh, EG and Dyer, WJ, A rapid method of total lipid extraction and purification, Can J Biochem Physiol, 1959;37:911-917.
[7] Folch, J, Lees, M and Sloane Stanley, GH, A simple method for the isolation and purification of total lipides from animal tissues, J Biol Chem, 1957;226:497-509.
[8] Pellegrino, RM, Di Veroli, A, Valeri, A, et al., LC/MS lipid profiling from human serum: a new method for global lipid extraction, Anal Bioanal Chem, 2014;406:7937-7948.
[9] Steiner, R, Mostafa, E, Othman, A, et al., Elucidating the chemical structure of native 1-deoxysphingosine, J Lipid Res, 2016.
[10] Sutter, I, Park, R, Othman, A, et al., Apolipoprotein M modulates erythrocyte efflux and tubular reabsorption of sphingosine-1-phosphate, J Lipid Res, 2014;55:1730-1737.
[11] Sutter, I, Velagapudi, S, Othman, A, et al., Plasmalogens of high-density lipoproteins (HDL) are associated with coronary artery disease and anti-apoptotic activity of HDL, Atherosclerosis, 2015;241:539-546.
[12] Sutter, I, Klingenberg, R, Othman, A, et al., Decreased phosphatidylcholine plasmalogens--A putative novel lipid signature in patients with stable coronary artery disease and acute myocardial infarction, Atherosclerosis, 2016;246:130-140.
[13] Penno, A, Reilly, MM, Houlden, H, et al., Hereditary sensory neuropathy type 1 is caused by the accumulation of two neurotoxic sphingolipids, J Biol Chem, 2010;285:11178-11187.
[14] Couchman, L, Jones, DJ and Moniz, CF, The use of turbulent flow chromatography for rapid, on-line analysis of tryptic digests, Rapid Commun Mass Spectrom, 2015;29:2140-2146.
[15] Tecleab, AG, Schofield, RC, Ramanathan, LV, et al., A Simple and Sensitive Method for Quantitative Measurement of Methylmalonic Acid by Turbulent Flow Chromatography and Tandem Mass Spectrometry, J Chromatogr Sep Tech, 2016;7.
[16] Michopoulos, F, Edge, AM, Theodoridis, G, et al., Application of turbulent flow chromatography to the metabonomic analysis of human plasma: comparison with protein precipitation, J Sep Sci, 2010;33:1472-1479.
[17] Bousova, K, Senyuva, H and Mittendorf, K, Multiresidue automated turbulent flow online LC-MS/MS method for the determination of antibiotics in milk, Food Addit Contam Part A Chem Anal Control Expo Risk Assess, 2012;29:1901-1912.
[18] Gorga, M, Insa, S, Petrovic, M, et al., Analysis of endocrine disrupters and related compounds in sediments and sewage sludge using on-line turbulent flow chromatography-liquid chromatography-tandem mass spectrometry, J Chromatogr A, 2014;1352:29-37.
[19] Lim, HK, Chan, KW, Sisenwine, S, et al., Simultaneous screen for microsomal stability and metabolite profile by direct injection turbulent-laminar flow LC-LC and automated tandem mass spectrometry, Anal Chem, 2001;73:2140-2146.
[20] Mueller, DM, Duretz, B, Espourteille, FA, et al., Development of a fully automated toxicological LC-MS(n) screening system in urine using online extraction with turbulent flow chromatography, Anal Bioanal Chem, 2011;400:89-100.
[21] Wiesner, P, Leidl, K, Boettcher, A, et al., Lipid profiling of FPLC-separated lipoprotein fractions by electrospray ionization tandem mass spectrometry, J Lipid Res, 2009;50:574-585.
[22] Scherer, M, Bottcher, A, Schmitz, G, et al., Sphingolipid profiling of human plasma and FPLC-separated lipoprotein fractions by hydrophilic interaction chromatography tandem mass spectrometry, Biochim Biophys Acta, 2011;1811:68-75.
[23] Dashti, M, Kulik, W, Hoek, F, et al., A phospholipidomic analysis of all defined human plasma lipoproteins, Scientific reports, 2011;1:139.
[24] Michopoulos, F, Edge, AM, Hui, YT, et al., Extraction methods for the removal of phospholipids and other endogenous material from a biological fluid, Bioanalysis, 2011;3:2747-2755.

[25] Mazzoni, M, Polesello, S, Rusconi, M, et al., Liquid chromatography mass spectrometry determination of perfluoroalkyl acids in environmental solid extracts after phospholipid removal and on-line turbulent flow chromatography purification, J Chromatogr A, 2016;1453:62-70.
[26] Tsubakio-Yamamoto, K, Sugimoto, T, Nishida, M, et al., Serum adiponectin level is correlated with the size of HDL and LDL particles determined by high performance liquid chromatography, Metabolism, 2012;61:1763-1770.

# 4 Chapter 4: Lipidomics Method Development

*Regula Steiner*

## 4.1 Abstract

Lipidomics is defined as the study of the structure and function of the complete set of lipids (the so called lipidome) in a given cell or organism as well as the interactions with other lipids, proteins and metabolites in healthy and pathological conditions. (Un)targeted lipidomics not only provides a comprehensive overview of lipid metabolism and its physiological function but also allows the identification of diagnostic biomarkers in different disease conditions liked to lipid metabolism. Dyslipidaemia is linked to a significant number of diseases, like atherosclerosis, diabetes or cancer with an increasing number of affected patients worldwide.

Within this project we aimed to unify and further expand these existing LC-$MS^2$ based methods towards a more comprehensive and untargeted lipidomics approach. The method allows a detailed analysis of sphingolipids including ceramides, sphingomyelin, glycosphingolipids and sphingosine-1-phosphates, glycerolipids including gylcerophospholipids and their lyso-forms, as well as neutral acylglycerols cholesterols, neutral glycerolipids and free fatty acids in an LC-$MS^2$ run of 25 minutes. A reversed phase chromatographic separation on a Accucore C30 column and a data dependent acquisition with high-resolution accurate mass spectrometry were used for separation and detection of lipid species. For semi-quantitative data analysis, Lipid search™ was evaluated, which showed some problems of over-identification for atypical sphingolipids. Furthermore, a Trace finder™ quantification method was implemented for the quantification of typical but also low abundant atypical sphingolipids. The newly developed method allows accurate and precise highthroughput analysis for both biomarker discovery and validation in human body fluids as well as for the recording of dynamic lipid changes in cells and tissues from expermental models.

## 4.2 Introduction

The number of patients suffering from metabolic diseases is increasing worldwide. Although several risk factors for diabetes or cardiovascular diseases are known, it is still difficult to predict the individual risk for developing a metabolic disease or to diagnose metabolic diseases at a subclinical stage. An increasing number of patients with metabolic diseases demands novel biomarkers which allows an early diagnosis and risk prediction as well as the monitoring of therapeutic and lifestyle interventions [2].

A comprehensive analysis of lipids is an important tool to understand disease mechanisms, make diagnoses and prognoses, and evaluate therapeutic efficacy [3, 4]. The term "metabolomics" typically describes an unbiased approach to analyse the whole set of metabolites and metabolic changes in biological systems. As a sub-speciality, lipidomics focuses specifically on the profiling of lipids [4]. Mass spectrometry based tools are currently the most widely used technique for lipid profiling and quantification [5].

Lipids are highly diverse and the most abundant metabolites in human plasma, followed by carbohydrates (sugars), free amino acids and nucleic acids [6]. Lipids are defined as hydrophobic or amphipathic small molecules, which are soluble in organic solvents but not or only to limited degree in water [7]. They originate partly or entirely from the condensation of fatty acids with other molecules such as glycerols or sphingoid bases. They are classified as simple lipids if they are built of maximally two building blocks (a combination of fatty acids or sphingoid base) or as complex if they are made from three components (e.g., by the addition of a head group) [7]. By these building blocks, lipids are sub-classified into different classes. The major classes are fatty acids, glycerolipids (conjugation of one to three fatty acid to a glycerol backbone), glycerophospholipids (conjugation of one or two fatty acids to a glycerol backbone and a phosphate containing head group), sphingolipids (conjugation of a fatty acid to a sphingoid base backbone with or without headgroup), isoprenoids, saccharolipids and polyketides [6-8]. Of these individual lipid classes, sphingolipids are the most heterogeneous group and encompassing the biggest number of different species [9]. Sphingolipids are

involved in various biological processes like senescence, inflammation, and apoptosis and are relevant for diseases like Alzheimer's, diabetes and atherosclerosis [10, 11].

Lipids of the different classes are typically analysed using a combination of chromatographic separation (LC) combined with tandem mass spectrometry ($MS^2$). The combination of these two techniques allows to separate and annotate not only the different lipid classes but also to identify individual lipid species. Particularly isobaric lipids can be separated by liquid chromatography and structurally defined using high resolution accurate mass spectrometry (HARMS) with or without the fragmentation of the molecules ($MS^2$) [12].

The high resolution of HARMS allows to determine the exact mass of lipid molecules and to resolve molecules with very similar mass but different atomic composition. High-resolution accurate mass instruments are typically equipped with Orbitrap or Time of Flight (TOF) detectors. With $MS^2$, selected lipid ions can be further fragmented and characterized gaining information about the building blocks, like fatty acid chain length of conjugated head groups [13]. Table 4-1 shows an overview of various lipid classes and their typical fragmentation pattern.

Additionally, high-resolution accurate mass instruments typically offer the option of data dependent acquisition (DDA) features. In the DDA mode, fragmentation data is not obtained from pre-defined ions (as in multiple reaction monitoring in triple quadrupole instruments) but the fragmented ions are dynamically selected from full scan data within the individual samples. Typically, a fixed number of the most abundant ions per scan are identified and selected for fragmentation. These fragmentation data provide information about building block composition and help in identifying and annotating individual lipid species. Although this technique has a bias towards the identification of more abundant lipid species, it also opens the possibility of untargeted discoveries and the identification of new species [13].

The exact annotation of lipids is a critical step in lipidomics analysis [14]. The first step is to assign a measured feature to a specific lipid class. Lipid classes differ in their building block composition, their ionization properties and main fragment ions (for example differences in

the head group) which allows the assignment of specific lipid species. The second step is the annotation of the building block composition (for example the chain length of a fatty acid group and the number of double bonds within the different fatty acid groups). This annotation is typically more critical as the mass and elemental composition of two isomers within a lipid class can be identical (isobaric) although the distribution of double bonds or chain length is different. For such an annotation, a clear fragmentation spectrum is required to conclude more than the total chemical composition of a molecule i.e a ceramide with a total $[M+H]^+$ = 650.6445 *m/z* can be annotated as Cer d42:1. The use of fragmentation information allows to distinguish it as Cer d18:0 / 24:1 or d18:1 / 24:0. In reporting of data, it has to be stated to which extent an annotation was proven [14].

Table 4-1: Main ion with information about most abundant adduct to be formed is shown. Additionally, specific fragmentation pattern for different lipid classes is displayed. Table was adapted from Murphy et. al.[12]

| Lipid sub-class | Main Ion | Fragment | Fragment | Fragment | Fragment | Structure |
|---|---|---|---|---|---|---|
| Free sphingoid base (SPH) | $[M+H]^+$ | $[M+H-H_2O]^+$ | $[M+H-H_2O]^+$ | | | 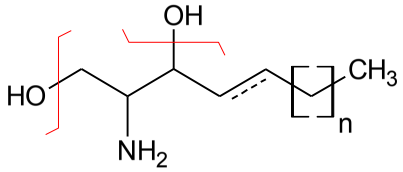 |
| Ceramide (Cer) | $[M+H]^+$ | $[M+H-H_2O]^+$ | $[M+H-2H_2O]^+$ | $[M+H-FA-H_2O]^+$ | $[M+H-FA-2H_2O]^+$ | 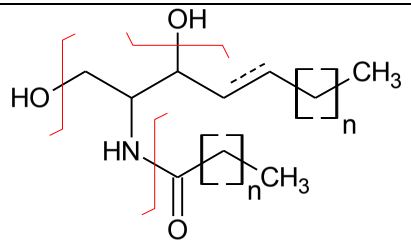 |
| Hexosylceramide (HexCer) | $[M+H]^+$ | $[M+H-H_2O]^+$ | $[M+H-Hex-H_2O]^+$ | $[M+H-FA-Hex]^+$ | $[M+H-FA-Hex-H_2O]^+$ | 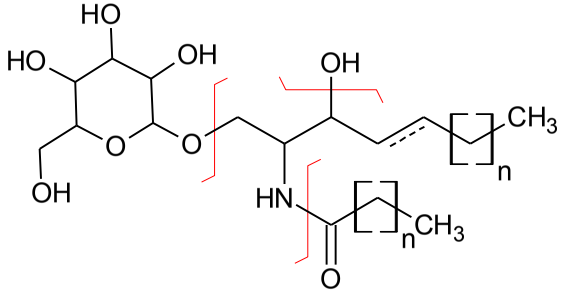 |
| Sphingomyelin (SM) | $[M+H]^+$ | $[PhC]^+$ | $[M+H-PhC-H_2O]^+$ | $[M+H-FA-PhC]^+$ | $[M+H-FA-PhC-H_2O]^+$ | 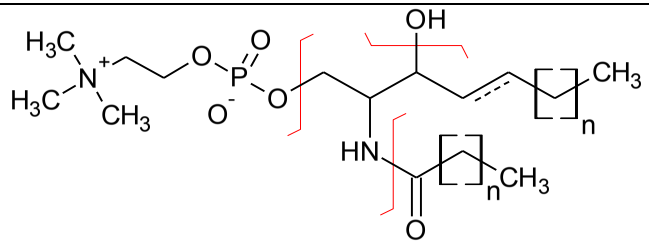 |

| Lipid sub-class | Main Ion | Fragment | Fragment | Fragment | Fragment | Structure |
|---|---|---|---|---|---|---|
| 1-Deoxy free sphingoid base (1-deoxySB) | $[M+H]^+$ | $[M+H-H_2O]^+$ | | | | 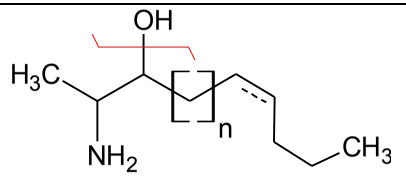 |
| 1-Deoxyceramide (1-deoxyCer) | $[M+H]^+$ | $[M+H-H_2O]^+$ | $[M+H-FA]^+$ | $[M+H-FA-H_2O]^+$ | | 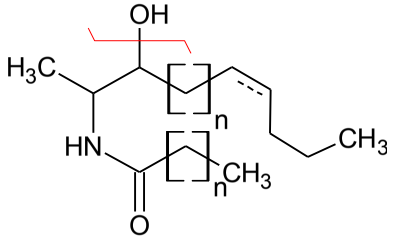 |
| Sphingosine-1-phosphate (S1P) | $[M+H]^+$ | $[M+H-H_2O]^+$ | $[M+H-Phos]^+$ | $[M+H-Phos-H_2O]^+$ | | 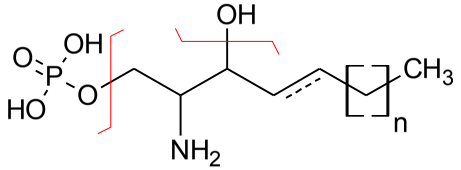 |
| Lyso-Phosphatidylcholine (LPC) | $[M+H]^+$ | $[M+H-PhC]^+$ | $[PhC]^+$ | | | 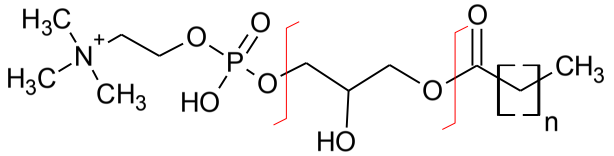 |
| Phosphatidylcholine (PC) | $[M+H]^+$ | $[M+H-PhC]^+$ | $[M+H-FA_{sn1}-PhC]^+$ | $[M+H-FA_{sn2}-PhC]^+$ | $[PC]^+$ | 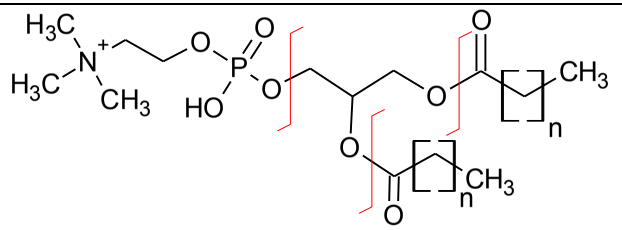 |

| Lipid sub-class | Main Ion | Fragment | Fragment | Fragment | Fragment | Structure |
|---|---|---|---|---|---|---|
| Lyso-Phosphatidic Acid (LPA) | $[M+NH_4]^+$ | $[M+H-PhA]^+$ | $[PhA]^+$ | | | 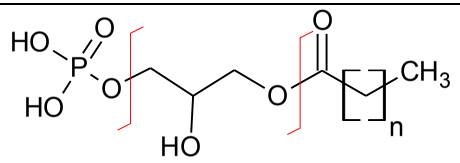 |
| Phosphatidic Acid (PA) | $[M+NH_4]^+$ | $[M+H-PhA]^+$ | $[M+H-FA_{sn1}-PhA]^+$ | $[M+H-FA_{sn2}-PhA]^+$ | | 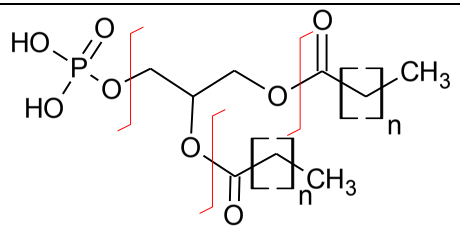 |
| Lyso-Phosphoethanolamine (LPE) | $[M+H]^+$ | $[M+H-PE]^+$ | | | | 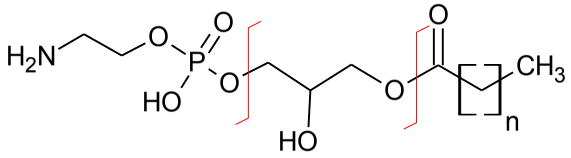 |
| Phosphoethanolamine (PE) | $[M+H]^+$ | $[M+H-PhE]^+$ | $[M+H-FA_{sn1}-PhE]^+$ | $[M+H-FA_{sn2}-PhE]^+$ | | 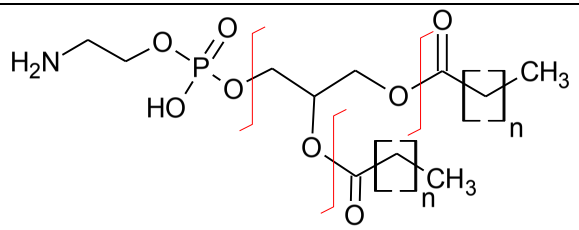 |
| Lyso-Phosphatidylglycerol (LPG) | $[M+NH_4]^+$ | $[M+H-PhG]^+$ | | | | 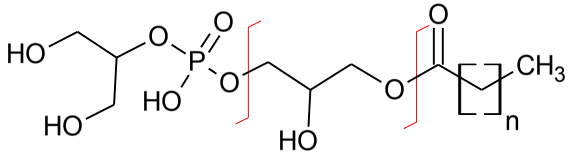 |

| Lipid sub-class | Main Ion | Fragment | Fragment | Fragment | Fragment | Structure |
|---|---|---|---|---|---|---|
| Phosphatidylglycerol (PG) | $[M+NH_4]^+$ | $[M+H-PhG]^+$ | $[M+H-FA_{sn1}-PhG]^+$ | $[M+H-FA_{sn2}-PhG]^+$ | | 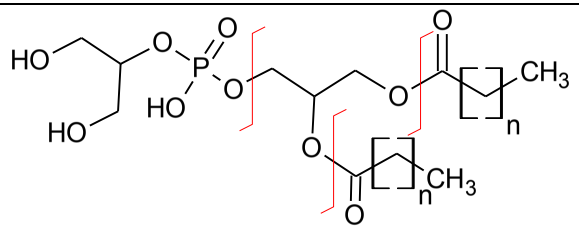 |
| Lyso-Phosphoinositol (LPI) | $[M+NH_4]^+$ | $[M+H-PhI]^+$ | | | | 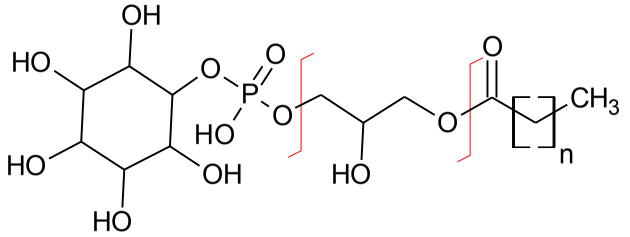 |
| Phosphoinositol (PI) | $[M+NH_4]^+$ | $[M+H-PhI]^+$ | $[M+H-FA_{sn1}-PhI]^+$ | $[M+H-FA_{sn2}-PhI]^+$ | | 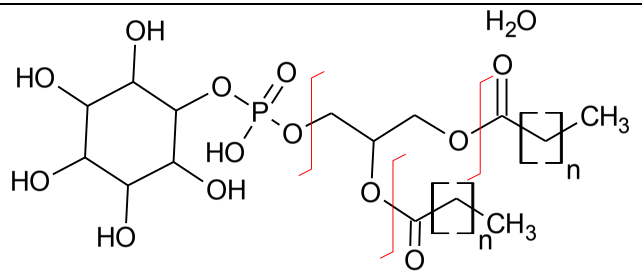 |
| Lyso-Phosphatidylserine (LPS) | $[M+H]^+$ | $[M+H-PhS]^+$ | | | | 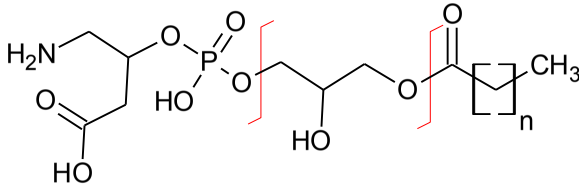 |

| Lipid sub-class | Main Ion | Fragment | Fragment | Fragment | Fragment | Structure |
|---|---|---|---|---|---|---|
| Phosphatidylserine (PS) | $[M+H]^+$ | $[M+H-PhS]^+$ | $[M+H-FA_{sn1}-PhS]^+$ | $[M+H-FA_{sn2}-PhS]^+$ | | 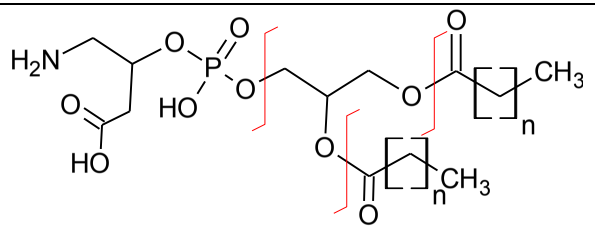 |
| Cholesterol | $[M+H-H_2O]^+$ | | | | | 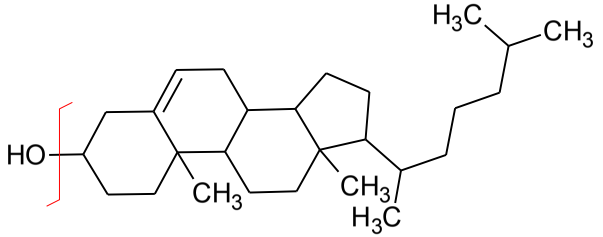 |
| Cholesteryl Ester (CE) | $[M+NH_4]^+$ | $[M+H-FA-H_2O]^+$ | | | | 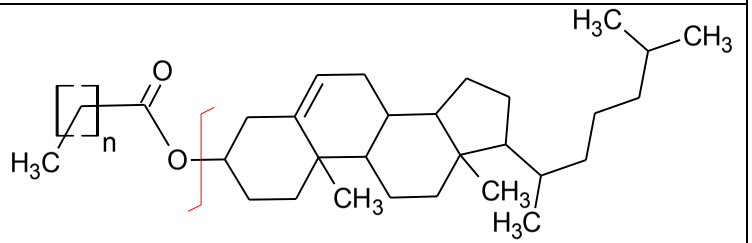 |
| Free fatty acid (FFA) | $[M-H]^-$ | -COOH | | | | 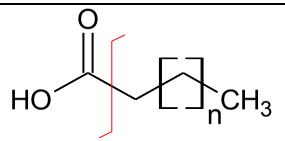 |
| Monoacylglycerol (MG) | $[M+Na]^+$ | $[M+H-C_3H_7O_3]^+$ | | | | 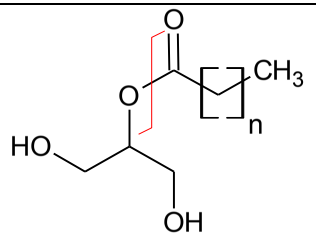 |

| Lipid sub-class | Main Ion | Fragment | Fragment | Fragment | Fragment | Structure |
|---|---|---|---|---|---|---|
| Diacylglycerol (DG) | $[M+Na]^+$ | $[M+H-FA_{sn1}]^+$ | $[M+H-FA_{sn2}]^+$ | | | 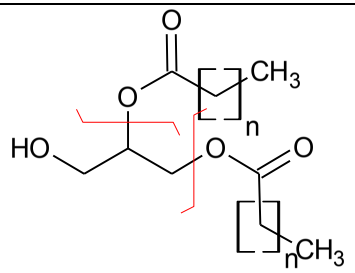 |
| Triacylglycerol (TG) | $[M+NH_4]^+$ | $[M+H-FA_{sn1}]^+$ | $[M+H-FA_{sn2}]^+$ | $[M+H-FA_{sn3}]^+$ | | 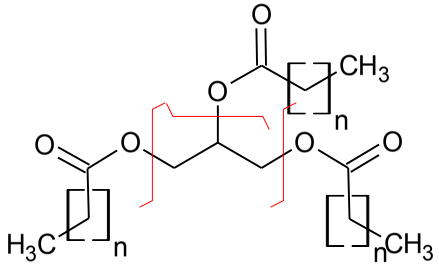 |

In our previous methods, lipid classes like glycophospholipids, or sphingolipids or even single lipid species like sphingosine-1-phosphate were each analysed by individual methods. The aim of this project was to combine and further expand our existing LC-$MS^2$ based methods into a more comprehensive unified lipidomics approach, covering apolar and polar lipids. The goal was to cover a great variety of lipid classes optimally in conjunction with related metabolites of the central energy and carbohydrate metabolism. The method shall allow to investigate dynamic changes in metabolic pathways in response to internal and external stimuli and to distinguish between healthy and pathological conditions for the identification of new biomarkers and novel therapeutic targets. The significance and clinical relevance of novel biomarkers is then typically validated in larger population based studies. Therefore a well-defined and (semi) automated high throughput workflow is essential to be able to analyse large numbers of clinical samples. In this respect, we also expanded our analytical workflow by the introduction of two software tools (Lipid Search ™ and TraceFinder™), which allow the semi automated analysis of lipidomics data.

## 4.3 Material and Methods

Unless stated differently, all solvents and reagents were purchased from Sigma-Aldrich Chemie GmbH (Buchs, Switzerland) excluding methanol, which was obtained from Honeywell specialty chemicals (Seelze GmBH, Germany). All lipid standards were obtained from Avanti polar lipids (Alabaster, USA).

### 4.3.1 Liquid chromatography

Initially, a C18 Uptispere (120 Å, 5 µm, 125 × 2 mm) column (Interchim, Montluçon, France) and the following mobile phases were used: Eluting A: water / acetonitrile 80 / 20 v/v with 10 mM ammonium acetate and 0.1 % formic acid and eluting B: isopropanol / acetonitrile 80 / 20 v/v with 10 mM ammonium Acetate and 0.1 % formic acid. See further details of solvent composition and flow in Table 4-2.

Table 4-2: Chromatographic details for LC separation on C18 Uptispere column. [***]

| Step | Grad | time [min] | Flow | % A | % B |
|---|---|---|---|---|---|
| Load | Step | 1.5 | 0.3 | 70 | 30 |
| Elute | Ramp | 17 | 0.3 | | 100 |
| Wash | Step | 7 | 0.3 | | 100 |
| Re-cond | Ramp | 1 | 0.3 | 70 | 30 |
| Re-equ | Step | 4 | 0.3 | 70 | 30 |

As we observed persisting resolution problems, the column was replaced by an Accucore C30 column (2.6 µm, 150 × 2.1 mm, Thermo Fischer Scientific). In combination with small adaptations in the mobile phases, the resolution could be improved. Finally, the following mobile phases were used:

Eluting A: water / acetonitrile 80 / 20 v/v with 10 mM ammonium acetate and 0.1 % formic acid and eluting B: isopropanol / acetonitrile 90 / 10 v/v with 10 mM ammonium acetate and 0.1 % formic acid and eluting C: methanol. The gradient profile is shown in Table 3-1.

Table 4-3: Chromatographic details for LC separation on C30 Accucore column. [†††]

| Step | Grad | time [min] | Flow | % A | % B | % C |
|---|---|---|---|---|---|---|
| Load | Step | 1.5 | 0.3 | 70 | 20 | 10 |
| Elute | Ramp | 17 | 0.3 | | 100 | |
| Wash | Step | 7 | 0.3 | | 100 | |
| Re-cond | Ramp | 1 | 0.3 | 70 | 20 | 10 |
| Re-equ | Ramp | 4 | 0.3 | 70 | 20 | 10 |

### 4.3.2 Mass spectrometry method

Samples were analyzed on a Q Exactive (Thermo, Reinach, BL, Switzerland) using a heated electrospray ionization (HESI) interface. For mass spectral detection, the following parameters were set on the HESI source: spray voltage 3.5kV, vaporizer temperature of

[***] Mobile phase A consists of water / acetonitrile 80 / 20 v/v with 10 mM ammonium acetate and 0.1 % formic acid and mobile phase B consists of isopropanol / acetonitrile 80 / 20 v/v with 10 mM ammonium acetate and 0.1 % formic acid.
[†††] Mobile phase A consists of water / acetonitrile 80 / 20 v/v with 10 mM ammonium acetate and 0.1 % formic acid, mobile phase B consists of isopropanol / acetonitrile 90 / 10 v/v with 10 mM ammonium acetate and 0.1 % formic acid and mobile phase C is 100 % methanol.

300°C, sheath gas pressure 20 AU, aux gas 8 AU and capillary temperature of 320 °C. The detector was set to an $MS^2$ method using a data dependent acquisition with $top^{10}$ approach, fragmenting the 10 most intense ions per full scan with stepped collision energy between 25 and 30. A 140000 resolution was used for the full spectrum and a 17500 for $MS^2$. For the selection of ions to be fragmented, a dynamic exclusion filter was applied which will exclude the same ions from fragmentation for 20 seconds.

Spectrum was recorded using a heated electrospray ionization and was in positive and negative mode to reach the best coverage for all lipid classes. Table 4-1 shows an overview of the lipid classes analysed as well as the particular adduct used for quantification and fragments identification.

### 4.3.3 Synthetic external standards

Linearity was tested on the C18 column using a mix of Phospholipids in different level (see Table 4-4) including an internal standard for all classes.

Table 4-4: Composition of Phospholipid calibration mix. ‡‡‡

| | **Concentration [µM]** | | | | | |
|---|---|---|---|---|---|---|
| Species | PC 16:0/18:2 | SM 18:1/16:0 | LPC 16:0 | PE 18:0/18:0 | Cer 18:1/14:0 | PG 16:0/16:0 |
| MW | 758,1 | 703,0 | 495,6 | 748,1 | 509,9 | 745,0 |
| Cal1 | 0,82 | 0,89 | 2,52 | 2,01 | 2,45 | 1,68 |
| Cal2 | 1,65 | 1,78 | 5,04 | 4,01 | 4,90 | 3,36 |
| Cal3 | 3,30 | 3,56 | 10,09 | 8,02 | 9,81 | 6,71 |
| Cal4 | 6,60 | 7,11 | 20,18 | 16,04 | 19,61 | 13,42 |
| Cal5 | 9,89 | 10,67 | 30,26 | 24,06 | 29,42 | 20,14 |
| Cal6 | 13,19 | 14,22 | 40,35 | 32,08 | 39,23 | 26,85 |

Our external standard consisted of 65 isotope labelled or non-natural lipid species (5µM each, Table 3-6).

‡‡‡ For linearity test, a calibration Mix of phospholipids was used. Per class, an internal standard and a calibrator compound was measured in specified concentrations. All lipid standards were purchased from Avanti polar lipid (Alabaster, USA)

In some experiments the commercial isotopic labelled lipidomics standard mixture "splash LipidoMix" (Avanti polar lipids, Alabaster, USA) was used for further glycolipids and glycophospholipid species (Table 4-5).

Table 4-5: Composition of splash LipidoMix (Avanti Polar Lipids, Alabaster, USA)

| Lipid Species | Concentration [µg/mL] |
|---|---|
| 15:0-18:1($D_7$) PC | 160 |
| 15:0-18:1($D_7$) PE | 5 |
| 15:0-18:1($D_7$) PS | 5 |
| 15:0-18:1($D_7$) PG | 30 |
| 15:0-18:1($D_7$) PI | 10 |
| 15:0-18:1($D_7$) PA | 7 |
| 18:1($D_7$) LPC | 25 |
| 18:1($D_7$) LPE | 5 |
| 18:1($D_7$) Chol Ester | 350 |
| 18:1($D_7$) MG | 2 |
| 15:0-18:1($D_7$) DG | 10 |
| 15:0-18:1($D_7$)-15:0 TG | 55 |
| 18:1($D_9$) SM | 30 |
| Cholesterol ($D_7$) | 100 |

The complete standard mix consisted of total 65 different lipid species was tested for linearity over a concentrations range of 0.1 to 5µM (concentrations: 0.1, 0.5, 1, 2 and 5 µM). Linearity was confirmed by calculating $R^2$ for each lipid species.

### 4.3.4 Internal standards

The use of internal standards controls for the loss during the extraction, differences in ionization and matrix effects. Each lipid class is represented by one or more non-natural, synthetic internal standard which were included in the extraction buffer. Optimally, internal standards are isotopically labeled lipids which have exactly the same chemical properties for extraction, chromatography and ionization as their native counterparts. However, as isotope labelled standards are not available for all lipid classes in our analytical profile, we also used lipid species with non-natural fatty acid composition. The lipid classes and the corresponding internal standards are summarized in Table 4-6.

Table 4-6: Internal standards used for extraction and quantification of lipidomics samples. §§§

| Lipid class | Internal standard | Concentration |
|---|---|---|
| (1-deoxy)Sphinganine | $D_7$-SPH d18:0 | 100pmol/sample |
| (1-deoxy)Sphingosine | $D_7$-SPH d18:0 | 100pmol/sample |
| (DH)ceramide | Cer d18:0 / 12:0 | 100pmol/sample |
| Ceramide | Cer d18:1 / 12:0 | 100pmol/sample |
| 1-Deoxy(DH)ceramide | Cer m18:0 / 12:0 | 100pmol/sample |
| 1-Deoxyceramide | Cer m18:1 / 12:0 | 100pmol/sample |
| Hexsosylceramide | GluCer d18:1 / 12:0 | 100pmol/sample |
| Sphingomyelin | SM d18:1 / 12:0 | 100pmol/sample |
| Sphingosine-1-phosphate | $D_7$-S1P d18:1 | 50pmol/sample |
| Cholesterol | $D_7$-Cholesterol | 500pmol/sample |
| Cholesteryl ester | $D_7$-CE 16:0 | 200pmol/sample |
| Phosphocholine | PC 14:0 / 14:0, PC 24:0 / 24:0 | 100pmol/sample |
| Lyso-Phosphocholine | LPC 17:0 | 100pmol/sample |
| Phosphatic acid | PA 17:0 / 17:0 | 100pmol/sample |
| Phosphoethanolamine | PE 14:0 / 14:0 | 100pmol/sample |
| Lyso-Phosphoethanolamine | LPE 17:1 | 100pmol/sample |
| Phosphoglycerol | PG 17:0 / 17:0 | 100pmol/sample |
| Free fatty acid | $D_3$-FA 16:0 | 10nmol/sample |

For quantification of the lipid species, the area under the peak (AUC) of each compound and internal standard is calculated. The AUC for lipids of each class is then normalized to the AUC of the respective internal standard, which was added in a known concentration. The concentration of the lipid species is therefore calculated via the following equation:

$$\text{Concentration} = \frac{AUC\ Analyte * conc\ IS}{\text{AUC IS} * \text{Sample volume}}$$

### 4.3.5 Sample extraction

Extraction started from either 20 µL of serum/plasma, 20 µL of tissue in PBS (1mg/dL) or a cell pellet consisting of 1-3 Mio cells suspended in 20 µL PBS. Extraction was done according to the MMC protocol described by Pellegrino et al. [15]. The samples were extracted

§§§ Per lipid class, one internal standard is added to a sample in the specified amount of internal standard. Internal standard is used to control for losses during extraction and calculate the concentration of specific lipid species. All lipid standards were purchased from Avanti polar lipids (Alabaster, USA)

in 2 mL Eppendorf tubes by adding 1 mL of a methanol / MTBE / chloroform (MMC 1.33/1/1 v/v/v) mixture containing the respective internal standards. The mix was vortexed for 20 seconds and agitated for 20 min in a thermo shaker (Eppendorf) at 37 °C at 1400 rpm. Precipitated proteins were pelleted by centrifuging for 5 min at 16000 rpm at 24 °C. The supernatant (1 mL) was transferred into a separate tube and the solvent dried under a stream of $N_2$. For analysis, the sample was re-suspended in 100 µL methanol and transferred to a PP-MS vial. Of each samples, 25 µL were injected.

For quality control, a standard sample was created, by pooling 5µL of each sample in an extra tube. From the pool, 2.5 µL, 5 µL, 10 µL, and 20 µL were aliquoted into a new tube and filled with PBS to 20 µL. These QC samples were treated the same way as other samples for extraction.

### 4.3.6 Semi-automated analysis evaluation

For a qualitative analysis of the raw data, we used the tool Xcalibur Qual Browser (Thermo) and for quantitative analysis the software tool TraceFinder™ (Thermo). In TraceFinder™, a method was implemented covering sphingolipid species including the corresponding fragment information.

For the sphingolipid subclasses (e.g. ceramides, hexosylceramides, sphingomyelins, etc.), the full mass and the presences of an indicative set of fragments was used as the signatures. Each lipid species was identified with an accurate mass accuracy for the full mass of < 5ppm and the presence of the determining fragments. The main ions for full mass and the fragmentation details per lipid class are summarised in Table 4-1. The combination of exact full mass, an indicative fragmentation spectrum and the retention time (RT), allows the annotation to a specific lipid metabolite. In most cases, this combination also allowed to identify isomeric and isobaric species.

### 4.3.7 Lipid Search ™ evaluation

The standard mix (2 µM each, Table 3-6) was measured in triplicates in positive and negative mode and the dataset was analysed using the software tool “Lipid Search ™”. All lipids were

aligned and filtered with the following filter criteria: S/N >10, no oxidized lipids, the area ratio of sample to blank > 1.5 and retention time between 5 and 26 min, area relative standard deviation < 30 and peak height > 5E6 and peak area > 1E6.

### 4.3.8 Quality Control and statistics

For each batch of samples, a set of quality control was included to control for accuracy and precision of the batch but also to check the linearity of all analytes measured.

Quality control (QC) samples are a pool of each sample of a batch measured in 1:8, 1:4, 1:2 and 1:1 dilution and measured at least three times within each batch.

The QC allowed to calculate the linearity of the analysis for each of the lipid species, for shifts in RT within the batch, the standard deviation and carry over and the ratios between blank and sample to check for impurities. The criteria to pass quality control within the normalized data are for linearity an $R^2$> 0.8, for precision a CV < 20% and a sample to blank ratio of >1.5. Lipid species, which did not fulfil these criteria, were excluded from the analysis.

### 4.3.9 Plasma samples from healthy donors

Six control plasma samples from healthy donors were extracted as described in 4.3.5 Sample extraction. The Sphingolipidome of these samples was analysed using the TraceFinder™ method for quantification of sphingolipid species.

### 4.3.10 Changes in sphingolipid metabolism with FB1, 4-HPR and myriocin

NIH3T3 cells were grown and maintained in DMEM (Sigma) with 10 % FBS (Fisher Scientific; FSA15-043) and 1 % penicillin / streptomycin (100 units per mL / 0.1 mg/mL, Sigma) at 37 °C and 5 % $CO_2$. Cells were treated for 24h with different inhibitors for sphingolipid metabolizing enzymes (myriocin (myr) [16-18], fumonisine B1 (FB1) [19-21] and fenretinide (4-HPR) [22, 23]) and harvested in PBS, counted and extracted as described (4.3.5 Sample extraction). Myrocin (Cayman Chemicals) in was used in 2.5 nM, Fumonisine B1 (FB1, Sigma) in 7 µM and Fenretinide [22] (4-HPR, Tocris Bioscience) in 2 µM. Levels of different sphingolipid classes were analyzed with TraceFinder™.

### 4.3.11 Method comparison

36 human plasma samples from the Hepadip cohort (randomly taken) were split and analysed for their total sphingolipid base profile after hydrolysis and in parallel whit a full sphingolipidomics approach.

Sphingoid base profile:

100 µL of each plasma were transfered to 2 mL Eppendorf tubes for acid base hydrolysis. 500 µL methanol including the internal standards $D_7$-sphingosine and $D_7$-sphinganine (Avanti Polar Lipids, Alabaster, AL) were added. Lipids were extracted for one hour under constant agitation at 37 °C in an Eppendorf Thermomixer. Samples were centrifuged at 16000 rpm for 5 min to pellet precipitated proteins, and 500 µL of the supernatant were transferred to a new tube. Lipids were hydrolyzed by adding 75 µL of methanolic HCl (1 M HCl and 10 M $H_2O$ in methanol) and incubated for 16 h at 65 °C. By adding 100 µL of KOH (10M), HCl was neutralized. 625 µL chloroform were added followed by 100 µL of 2M ammonium hydroxide and 0.5 mL alkaline water to reach phase separation. The sample was vortexed, centrifuged at 16000 rpm for 5 min, the upper phase discarded and the lower (organic) phase washed three times with alkaline water. The organic phase was finally dried under $N_2$ and stored at −20$^{o}$C until analysis.

Sphingoid bases were separated by RPLC on a C18-column (Uptispere 120 Å, 5 µm, 125×2 mm; Interchim, Montluçon, France) and analyzed on a TSQ Ultra (Thermo, Reinach, BL, Switzerland) using an atmospheric pressure chemical ionization (APCI) interface. Mobile phases consisted of A: ultra-pure $H_2O$ / methanol 1/1 v/v with 2.6 mM ammonium acetate and B: methanol. The gradient was set from 50 % B to 100 % B within 25 min followed by 5 min 100 % B and 5 min of equilibration with a flow rate of 0.3 mL/min. For mass spectral detection, the following parameters were set on the APCI source: discharge current of 4 µA, a vaporizer temperature of 450 °C, sheath gas pressure 20 AU, aux gas 5 AU and a capillary temperature of 200 °C. The measured area under the peak curve was normalized, and lipid

concentrations were calculated by comparison to $D_7$-sphingosine and quantification was reported in pmol per sample.

Lipidomics Analysis:

20 µL of plasma were extracted using the MMC protocol (4.3.5 Sample extraction) and measured using the C30-column based lipidomics method (3.3.1 Liquid chromatography).

## 4.4 Results: Method Development

### 4.4.1 Separation of lipid classes

We developed a novel LC-$MS^2$ lipidomics method for the analysing of a great number of lipid species. Figure 4-1 shows the chromatographic separation of some selected sphingolipid species included in the internal standard.

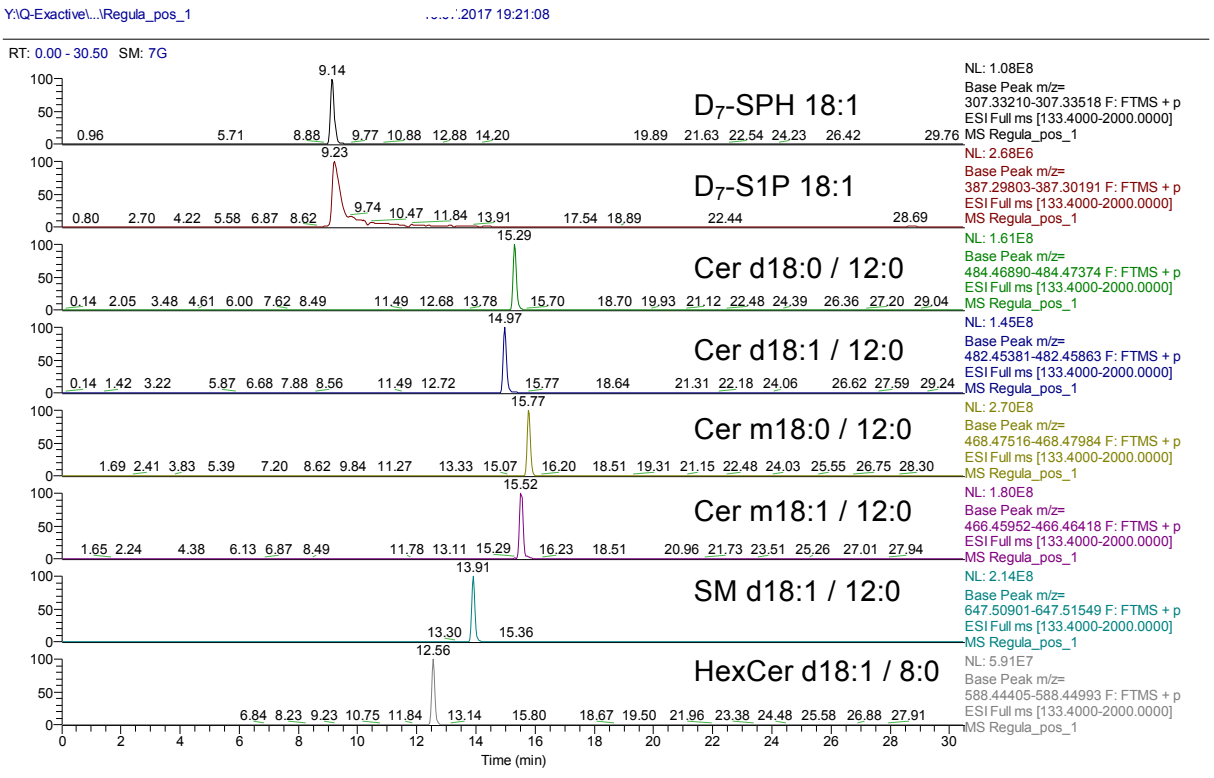


Figure 4-1: Chromatograms of different sphingolipid. Each chromatogram was acquired in positive mode. Internal standards are shown, which were spiked to a plasma from a healthy donor.

In reversed phase chromatography, separation is based on the hydrophobicity of the molecule. Lipids are separated based on the number of (hydrophobic) carbon atoms and the

presence of polar structures such as double bonds, sulfates or hydroxyl group. Therefore, free sphingoid bases elute earlier than ceramides which contain a N-linked fatty acid, whereas retention times of SPH d18:1 and S1P d18:1 do not differ much. Also, dihydroceramide Cer d30:0 elutes later than ceramide Cer d30:1 because of hydrophilic double bond whereas 1-deoxyceramide (Cer m30:1) elutes later than ceramide Cer d30:1, because of its missing $C_1$-hydroxyl group (Figure 4-1).

Figure 4-2 shows the separation of different phospholipid species included in the splash LipidoMix. The standard was spiked into and extracted from a control plasma sample. For LPG and LPS the native lipid present in plasma is shown.

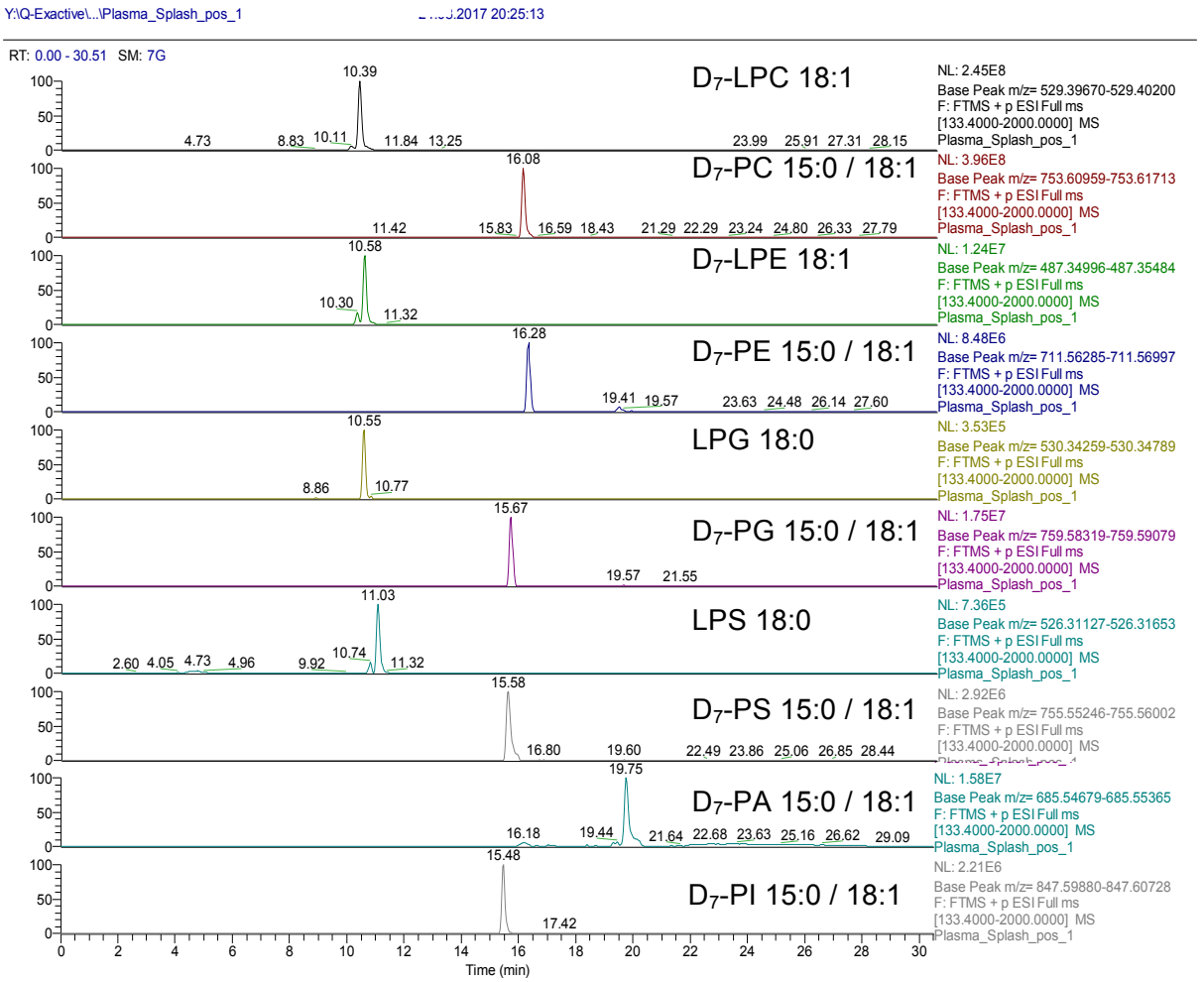


Figure 4-2: Chromatogram of different phospholipid. Each chromatogram was acquired in positive mode. Splash lipidoMix was spiked to a plasma from a healthy donor and for LPS and LPC a native species are shown.

The retention time of phospholipids on the C30 column is mostly determined by the number of carbons atoms and hydrophobic groups whereas the different polar head groups have

minor influence. Therefore, different phospholipid sub-classes (PC, PE, PG, PS) with the same numbers of carbons (e.g. 33:1) elute all in a narrow time window of about 30 seconds.

Figure 4-3 shows the chromatogram of free $D_7$-cholesterol which elutes within 15.9 min from the C30 column. It is ionized as $[M+H]^+$ but also as $[M+NH_4]^+$. But these two ions are low abundant compared to the in-source fragmented $[M-H_2O+H]^+$. The water loss represents the most abundant ion and which is also used for quantification.

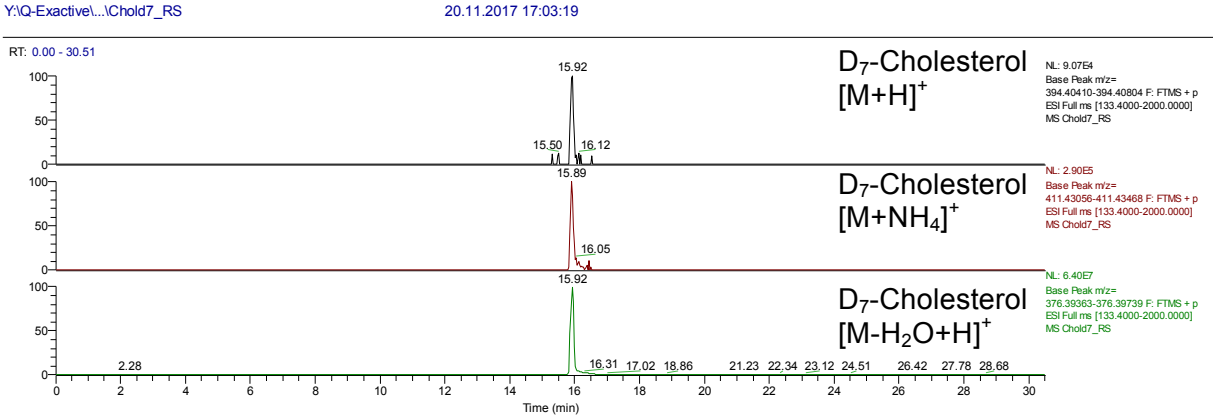


Figure 4-3: Chromatogram for free cholesterol with different ions with adducts ($[M+H]^+$ $[M+NH_4]^+$ and $[M-H_2O]^+$). The chromatogram was acquired in positive mode. Synthetic $D_7$-cholesterol was used as a standard. $[M-H_2O]^+$ is the most abundant ion present for free cholesterol.

Figure 4-4 displays the chromatogram of $D_7$-cholesteryl ester 16:0. The labelled synthetic standard was spiked to plasma from a healthy individual donor. Cholesteryl esters elute later than free cholesterol, because of the additional fatty acid attached to the cholesterol backbone. During ionization of cholesteryl esters, an in-source fragmentation occurs and more than 50 % of the molecules are fragmented to the free cholesterol fragment (minus water) by losing the fatty acid in the source during ionization.

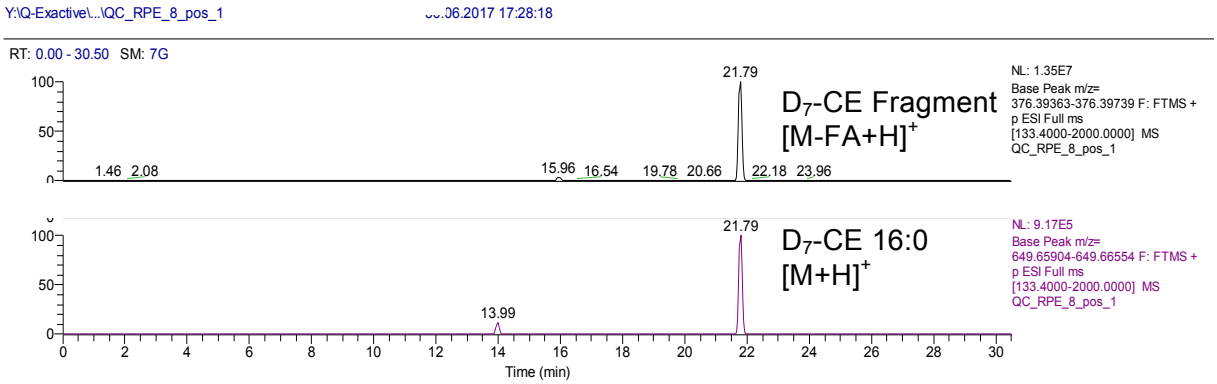


Figure 4-4: Chromatogram for cholesteryl ester with $[M+H]^+$ ion but also the in source fragmented ion (loss of the fatty acid). The Chromatogram was acquired in positive mode. Internal standards are shown, which were spiked to a plasma from a healthy donor.

Figure 4-5 shows the chromatogram of $D_3$-palmitic acid spiked into a control plasma sample. As fatty acids showed higher signal intensity in negative mode the shown chromatogram was acquired in negative mode.

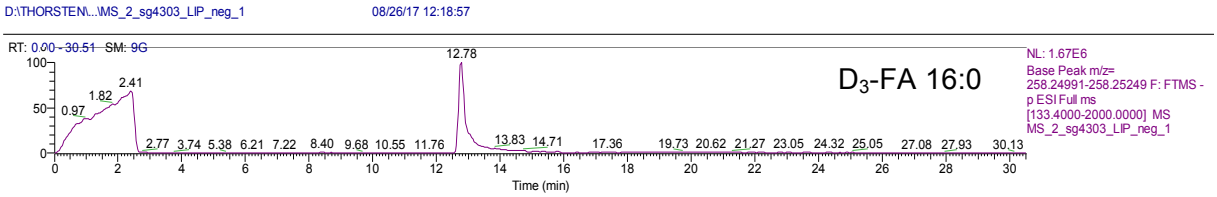


Figure 4-5: Chromatogram for free fatty acid palmitate. The chromatogram was acquired in negative mode. Internal standards are shown, which were spiked to a plasma from a healthy donor. The signal before 2.5 minutes is considered as noise, as the LC flow is directed into waist before 2.5 minutes.

In Figure 4-6 some examples of chromatograms of different glycerolipid classes are shown. To display the chromatographic resolution of glycerolipid classes, the splash LipidoMix was spiked to control plasma sample.

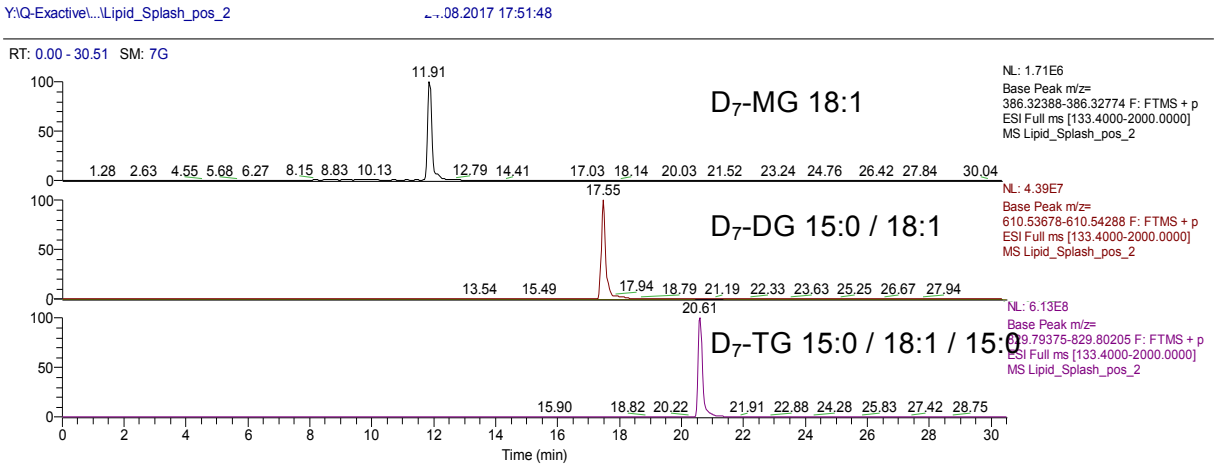


Figure 4-6: Chromatogram of different glycerolipid classes. The chromatogram was acquired in positive mode. Splash lipidoMix is shown, which was spiked to a plasma from a healthy donor. For LPS and LPC a native species is shown.

Glycerolipid sub-classes consist of one, two or three fatty acids conjugated to a glycerol backbone. Mono-acyl glycerols elute earlier than di- or triacyl glycerols. The retention time depends on the number of fatty acids, total carbon atoms and number of double bonds.

The here used C30 column allows the separation of a large number of lipid within a total runtime of 25 minutes using a gradient of organic solvents. The individual lipid species are well separated and show symmetric peak shapes without significant tailing. Using these conditions, it is possible to detect and quantify a wide variety of lipids species.

### 4.4.2 Semi-Automated data analysis with TraceFinder™

TraceFinder™ offers a software tool, which allows a targeted and quantitative analysis of MS datasets. A method was set up in TraceFinder™, allowing the comprehensive identification and quantification of typical and atypical sphingolipid species including isotope labelled lipids standards and isotopically labelled lipid metabolites.

First, a theoretical compound library was setup for sphingolipids. The nominal mass of sphingolipids, with $C_{16}$-$C_{20}$ sphingoid backbones with no, one or two double bonds in combination with fatty acids between $C_8$ and $C_{26}$ containing no or one double bond or as free base were calculated. Furthermore, head groups as choline, glucose or phosphate were also combined to all the possible theoretical combinations. Finally, also 1-deoxysphingolipids and

1-deoxymethylsphingolipids with $C_{18}$ or $C_{17}$ backbone respectively were added to the compound library. For all these theoretical masses, the parent masses with the respective $[M+H]^+$ adducts and fragmentation ions were calculated (Table 4-1).

Furthermore, the library was extended to isotopically labelled compounds, if isotopically labelled precursors such as $D_4$-L-alanine or $D_3N_{15}$-L-serine or isotopically labelled free bases (eg $D_7$-sphinganine, $D_7$-sphingosine, $D_3$-1-deoxysphinganine or $D_5$-1-deoxymethylsphinganine) were added to cells in metabolic conversion assays. This resulted in a compound library containing several thousand theoretical combinations of sphingolipids.

Retention times of all sphingolipids present in the external standard mix (Table 3-6) were determined using the newly developed C30 LC-$MS^2$ method (Table 3-1). From these known retention times, a theoretical retention time was estimated for other sphingolipids, applying a linear (logarithmic) correlation between retention time and number of carbons and double bonds in a sphingolipid.

Human plasma samples, but also HEK293 or NIH3T3 cell samples were than measured using the C30 LC-$MS^2$ method (see 3.3.1 Liquid chromatography and 4.3.2 Mass spectrometry method). In these samples, sphingolipids from the theoretical compound library were searched and identified using a TraceFinder™ search method and finally manually validated using Thermo Xcalibur Qual browser. All compounds with matching parent mass and confirming fragments (Table 4-1) and a retention time within a range of 30 sec to the estimated one, were included in a TraceFinder™ quantification method. Isobaric compounds were searched and identified in a separate step shown in the next paragraph. Overall, the method allowed the quantification of about 150 different sphingolipid species including the typically used internal standards.

### 4.4.3 Separation of isobars and isomers

Due to the building block like nature of lipids, lipid species are often occurring in isobaric or isomeric forms. Isobaric means they have the same nominal mass but different elemental composition (isobars) whereas isomeric means they have the same elemental composition,

but vary in the steric orientation, the composition of fatty acids or the position of a double bond. For example, a ceramide d42:1 can be Cer d18:0 / 24:1, Cer d18:1 / 24:0 or Cer d16:1 / 26:0. For these isomers, the elemental composition is the same but the steric structure is different (e.g. the double bond is either in the sphingoid backbone or in the fatty acid) which results in the same *m/z* but a different RT and different fragmentation pattern.

This often small difference allows to distinguish between individual isomers, e.g. Cer d18:0 / 24:1 and Cer d18:1 / 24:0 (Figure 4-7A). NIH3T3 cells were treated with 4-HPR [22], an inhibitor of dihydroceramide desaturase which leads to the accumulation of Cer d18:0 / 24:1 as the conversion to the primary metabolite Cer d18:1 / 24:1 is blocked.

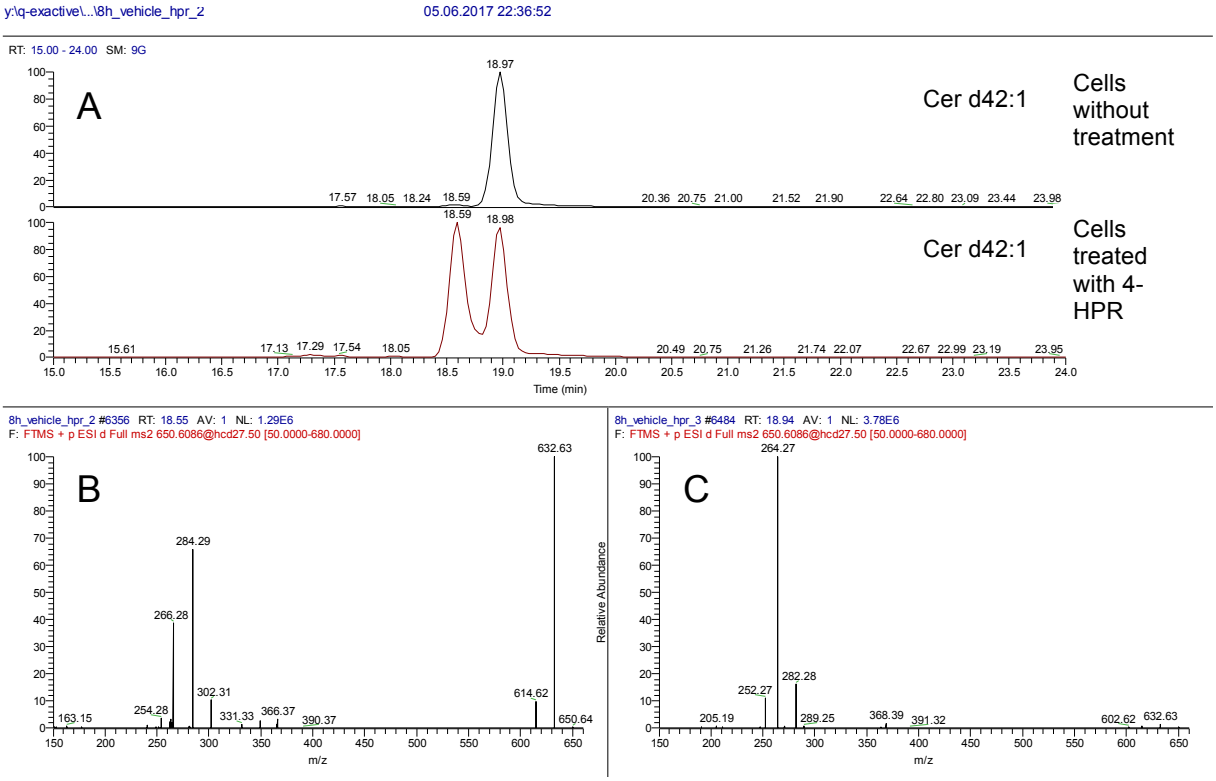


Figure 4-7: A: Chromatogram of Cer d42:1 from NIH3T3 cells treated with or without 4-HPR. B: Fragmentation pattern of Cer d18:0 / 24:1 (Peak at 18.59 min) C: Fragmentation pattern of Cer d18:1 / 24:0 (Peak at 18.98 min)

As seen in Figure 4-7A, there are two peaks with the full mass of Cer d42:1 eluting between 18.5 and 19.0 minutes. Without 4-HPR treatment, the peak at 18.59 minutes is very low abundant whereas the peak at 18.98 minutes is the major one. In the presence of 4-HPR, the peak at 18.59 increases to the same level as the peak at 18.98. However, the fragmentation

pattern of the two peaks at 18.59 and 19.98 are different, as seen in Figure 4-7B for the peak at 18.59 and Figure 4-7C for the peak at 18.98. From fragmentation pattern, the peak at 18.59 corresponds to Cer d18:0 / 24:1 and the peak at 18.98 to Cer d18:1 / 24:0. This also matches the biological interpretation of an accumulation of dihydroceramides in the presence of 4-HPR. In addition, the shift in RT is as expected as more polar compounds are eluting earlier in reversed phase chromatography. The *cis* double bond in the fatty acid moiety of Cer d18:0 / 24:1 seems to be more polar than the Δ4 *trans* double bond in the sphingoid base backbone of Cer d18:1 / 24:0. As a further example, Figure 4-8A shows the chromatogram of Cer d42:2 which could corresponds to Cer d18:1 / 24:1 (peak at 18.4 min) or Cer d18:2 / 24:0 (peak at 18.59 min). Also here, the fragmentation pattern is different for Cer d18:1 / 24:1 Cer d18:2 / 24:0 (Figure 4-8B and C).

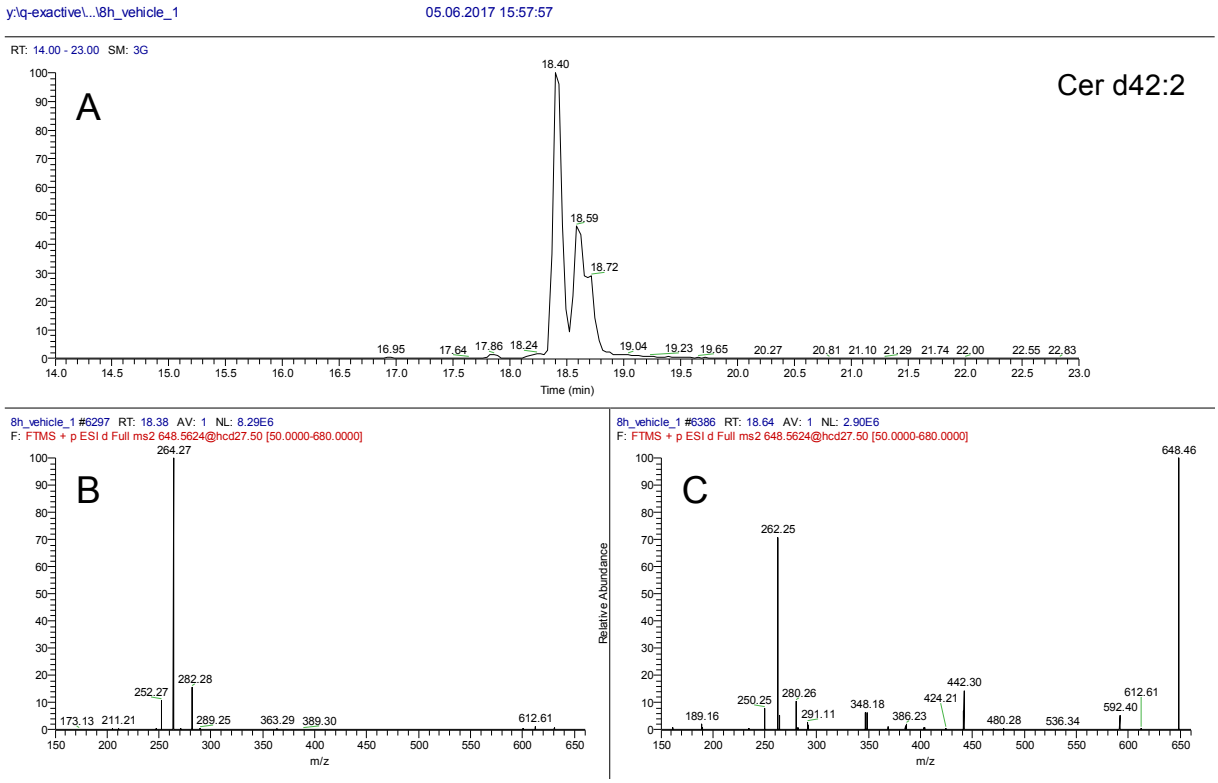


Figure 4-8: A: Chromatogram of Cer d42:2 from NIH3T3 cells without any treatment. B: Fragmentation pattern of Cer d18:1 / 24:1 (Peak at 18.4 min) C: Fragmentation pattern of Cer d18:2 / 24:0 (Peak at 18.59 min)

# 4.5 Results: Method validation

## 4.5.1 Linearity, Precision and Carry-over

### Uptispere C18 column

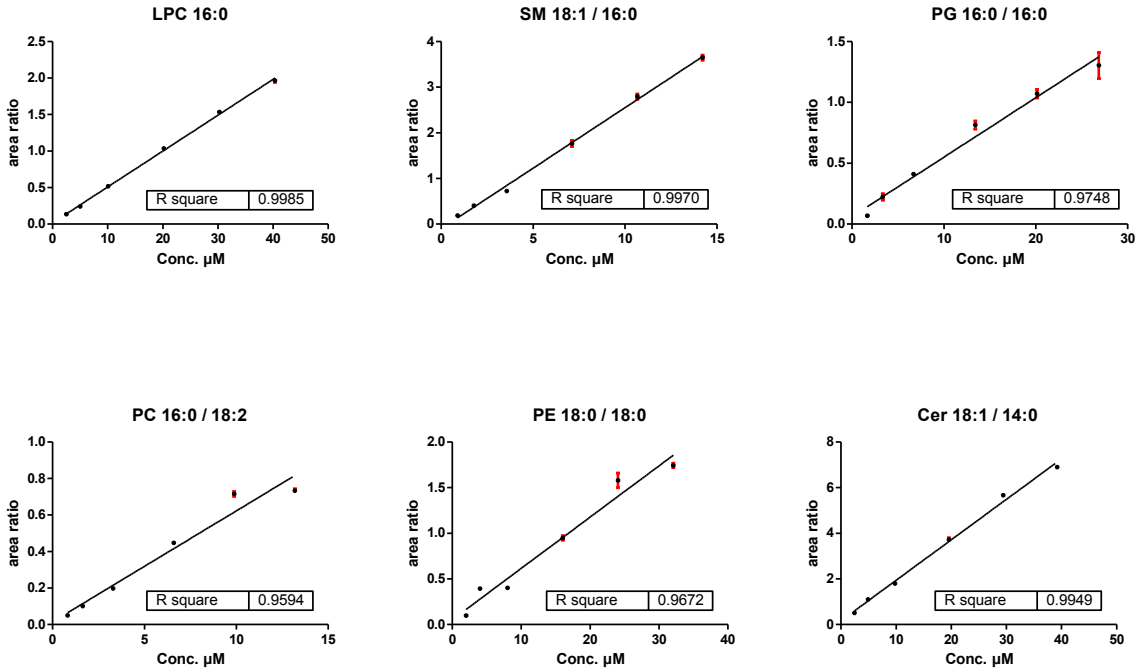


Figure 4-9: Calibration curves for different phospholipids to test linearity. Samples were dissolved in 100µL methanol with an injection volume of 25µL. All measured phospholipids show a linear correlation of concentration to measured ratio of AUC.

For all classes, the concentration of the calibrator shows a linear correlation to the area under the peak in the range specified in Table 4-4 with an $R^2 > 0.95$. The specific $R^2$ values are shown in Figure 4-9.

However we observed some persisting resolution problems, primarily for long chain sphingomyelins, S1P, and PC species. These species were eluting with long tailing over three minutes. Therefore, we replaced the C18 column with an Accucore C30 column.

### Accucore C30 column

The linearity of calibration curves, precision and carry-over for all different sphingolipids, phospholipids and cholesteryl ester are shown in Table 4-7.

Table 4-7: Linearity, imprecision and carry over of LC-MS Method with C30 column

| Sub-Class | Species | $R^2$**** | CV [%]†††† | Carry-over [%]‡‡‡‡ |
|---|---|---|---|---|
| Sphingoid Bases | SPH d18:2 | 0.9977 | 1.06 | 0.41 |
| | SPH d17:1 | 0.9978 | 1.43 | 0.76 |
| | SPH d17:0 | 0.9966 | 1.76 | 0.97 |
| | SPH t18:0 | 0.9965 | 1.28 | 0.95 |
| | $D_7$-SPH d18:1 | 0.9966 | 0.94 | 0.78 |
| | SPH d18:1 | 0.9970 | 1.00 | 0.84 |
| | $D_7$-SPH d18:0 | 0.9923 | 1.02 | 0.22 |
| | SPH d18:0 | 0.9909 | 0.20 | 0.27 |
| | SPH d20:1 | 0.9950 | 0.72 | 0.39 |
| | SPH d20:0 | 0.9951 | 1.73 | 0.11 |
| 1-Deoxysphingoid bases | m18:1 | 0.9856 | 1.84 | 0.30 |
| | m17:1 | 0.9866 | 2.16 | 0.34 |
| | $D_5$-m17:0 | 0.9735 | 0.75 | 0.41 |
| | m17:0 | 0.9779 | 1.02 | 0.38 |
| | $D_3$-m18:0 | 0.9336 | 1.45 | 0.33 |
| | m18:1 | 0.9297 | 2.05 | 0.43 |
| Ceramides | Cer d18:1 / 12:0 | 0.9901 | 1.45 | 0.08 |
| | Cer d18:0 / 12:0 | 0.9957 | 1.54 | 0.08 |
| | Cer d18:1 / 14:0 | 0.9553 | 2.22 | 0.16 |
| | $D_7$-Cer 18:1 / 16:0 | 0.9867 | 2.59 | 0.15 |
| | Cer d18:1 / 18:1 | 0.9686 | 2.25 | 0.14 |
| | Cer d18:0 / 16:0 | 0.9734 | 1.19 | 0.18 |
| | Cer d18:1 / 17:0 | 0.9698 | 1.48 | 0.21 |
| | Cer d18:1 / 20:0 | 0.9476 | 1.41 | 0.50 |
| | Cer d18 1:24:1 | 0.9412 | 2.55 | 0.62 |
| | Cer d18:1 / 22:0 | 0.9471 | 3.38 | 0.72 |
| | $D_7$-Cer d18:1 / 24:0 | 0.9262 | 1.37 | 0.69 |
| | Cer d18:1 / 24:0 | 0.9385 | 2.06 | 1.08 |
| | Cer d18:0 / 24:0 | 0.9867 | 4.44 | 0.76 |
| 1-Deoxyceramides | doxCer m18:1 / 12:0 | 0.9475 | 1.91 | 0.35 |
| | doxCer m18:0 / 12:0 | 0.8923 | 2.28 | 0.59 |
| | doxmetCer m17:1 / 16:0 | 0.9263 | 1.61 | 0.70 |
| | doxCer m18:1 / 16:0 | 0.9651 | 0.99 | 0.59 |

**** Linearity was determined by calculation of linear coefficients of correlation
†††† Impresicion was calculated by the relative coefficient of variation from measured triplicates.
‡‡‡‡ Carry-over was determined in blank methanol samples measured after 5 µM standard mix.

| | | | | |
|---|---|---|---|---|
| | doxmetCer m17:0 / 16:0 | 0.9709 | 0.98 | 0.59 |
| | doxmetCer m17:1:24:1 | 0.9171 | 1.53 | 1.44 |
| | doxCer m18:1 / 24:1 | 0.9366 | 1.85 | 1.52 |
| | doxmetCer m17:0 / 24:1 | 0.8719 | 1.92 | 1.71 |
| | doxCer m18:0 / 24:1 | 0.9100 | 1.35 | 1.48 |
| Sphingomyelines | SM 18:1 / 12:0 | 0.9777 | 3.17 | 0.15 |
| | SM d18:0 / 12:0 | 0.9769 | 1.27 | 0.15 |
| | SM 18:1 / 16:0 | 0.9625 | 1.23 | 0.23 |
| | $D_9$-SM d18:1 / 18:1 | 0.9497 | 2.23 | 0.27 |
| | SM 18:1 / 24:1 | 0.9776 | 1.12 | 0.29 |
| | SM:d18 1:24 0 | 0.9734 | 1.71 | 0.55 |
| Glucosylceramides | GluCer d18:1 / 8:0 | 0.9975 | 2.32 | 0.01 |
| | GluCer d18:1 / 16:0 | 0.9917 | 1.75 | 0.00 |
| | $D_5$-GluCer d18:1 / 18:1 | 0.9788 | 1.77 | 0.04 |
| | GluCer d18:1 / 24:1 | 0.9756 | 2.09 | 0.15 |
| Sphingosine-1-phosphate | S1P d17:1 | 0.9964 | 1.15 | 5.03 |
| | S1P d17:0 | 0.9977 | 3.19 | 7.84 |
| | $D_7$-S1P d18:1 | 0.9989 | 1.48 | 8.42 |
| | S1P d18:1 | 0.9991 | 0.80 | 8.50 |
| Phospholipids | LPC 16:0 | 0.9813 | 0.95 | 0.07 |
| | LPC 17:0 | 0.9859 | 1.42 | 0.06 |
| | PC 14:0 / 14:0 | 0.9731 | 2.89 | 0.25 |
| | PC 16:0 / 18:2 | 0.9538 | 1.81 | 0.35 |
| | PC 24:0 / 24:0 | 0.9658 | 9.49 | 6.94 |
| | LPE 17:1 | 0.9709 | 0.89 | 0.06 |
| | PE 14:0 / 14:0 | 0.9956 | 2.34 | 0.25 |
| | PE 18:0 / 18:0 | 0.9602 | 1.89 | 3.30 |
| | PA 14:0 / 14:0 | 0.9541 | 0.50 | 24.84 |
| | PA 17:0 / 17:0 | 0.8005 | 2.23 | 66.41 |
| | PG 16:0 / 16:0 | 0.7247 | 2.30 | 0.93 |
| | PG 17:0 / 17:0 | 0.8559 | 3.00 | 1.29 |
| Cholesteryl ester | $D_7$ ChE 16:0 | 0.9941 | 3.04 | 0.00 |

### 4.5.2 Semi-Automated Data analysis with Lipid search™

Lipid Search ™ is a software tool that allows the semi-quantitative annotation of lipid species based on a database with more than 1.5 million lipid ions and their predicted fragmentation pattern. The $MS^2$ datasets are automatically analysed by algorithms and identified based on product ion, precursor ion, and neutral loss scans.

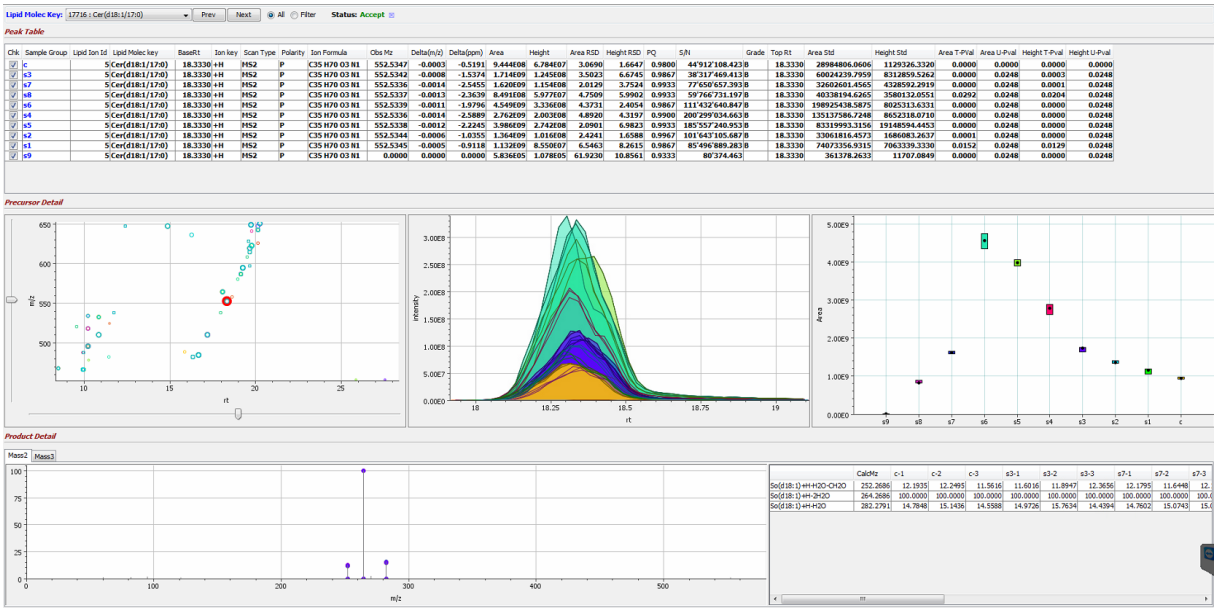

Figure 4-10: Lipid Search [TM] analysis software. Example of Cer 18:1 / 17:0 is shown. Alignment of a standard mix in different concentration from 0.02 to 10µM was done; samples were measured in triplicates in positive mode. Panels show samples and identified molecule, the alignment of all the samples, the area measured per sample group, the product spectra and the fragments used to identify the molecule.

In a first validation and proof of principle assay, we analysed whether the Lipid Search [TM] is capable to identify all lipid species included in the external standard mix. The software was capable to identify 59 out of 65 species in the standard. Six species were not identified. This included phytosphingosine (SPH t18:0) and the isotope labelled species $D_3$-SPH m18:0, $D_5$-SPH m17:0, $D_7$-Cer d18:1 / 16:0, $D_7$-Cer d18:1 / 24:0, $D_9$-SM 18:1 / 18:1, which is explained by the fact that the isotope labelled masses were not yet included in the Lipid Search [TM] database in this version (from Lipid Search[TM] version 4.2 on, the isotope labelled commercial SplashMix standard is included in the database). Also $D_7$-ChE 16:0, although present as deuterated form in the database, was not identified as no fragment spectrum was generated in the data dependent acquisition.

Four species were identified twice. For Cer 18:1 / 22:0, LPC 16:0 SM 18:1 / 12:0 and SM 18:1 / 24:1 this might be explained by the presence of a small pre-peak, which elutes shortly before the main peak (Figure 4-11).

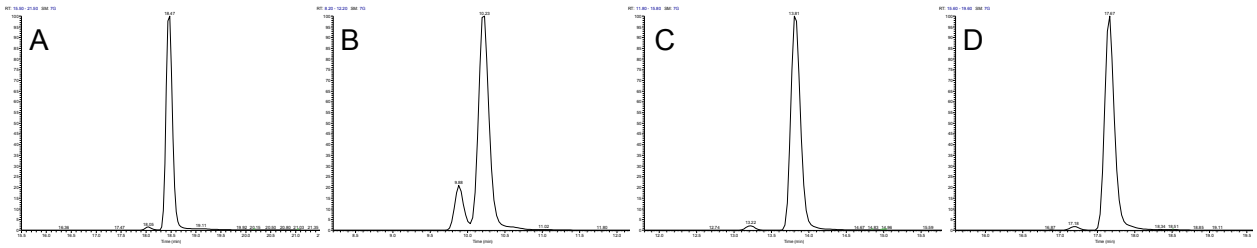


Figure 4-11 Chromatogram of twice identified species out of the 65 lipid standard mix (4.3.3 Synthetic external standards) in lipid search, which all show a small pre peak eluting before the main peak. A: Cer 18:1 / 22:0, B: LPC 16:0, C: SM 18:1 / 12:0, D: SM 18:1 / 24:1

As fifth example SPH d17:0 was identified twice. In this case is was a false-positive identification, as the SPH d17:0 main ion was identified as $[M\text{-}H_2O +H]^+$, which has the same elementary composition as SPH m17:1 $[+H]^+$. Interestingly, the Lipid Search ™ made this false-positive identification of SPH m17:1 in just one of the triplicate samples. In other samples, the ion was correctly annotated. Unfortunately, in the alignment, the correct identification of SPH m17:1 and the false positive SPH d17:0 were identified as separate patterns, and the peak was annotated twice although retention time, main area and the peak height of both species were identical for either ion (see Figure 4-12).

| LipidMolec | Class | BaseRt | MainIon | MainArea[c] | MainArea[s1] | MainHeight[c] | MainHeight[s1] |
|---|---|---|---|---|---|---|---|
| So(m17:1) | So | 9.438 | +H | 8.666E06 | 9.054E08 | 1.101E06 | 1.109E08 |
| So(d17:0) | So | 9.439 | +H-H2O | 8.666E06 | 9.007E08 | 1.101E06 | 1.109E08 |

Figure 4-12: SPH d17:0 false-positive identification in Lipid Search ™. SPH m17:1 was identified correctly as SPH m17:1 but also with false annotation as SPH d17:0-$H_20$.

Based on the theoretical isomers  also other misidentifications occurred:

- Cer d18:1 / 8:0 identified as Cer m18:2 8:0
- Cer d18:1 / 12:0 identified as Cer m18:2 12:0
- Cer d18:1 / 14:0 identified as Cer m18:2 14:0
- Cer d18:1 / 17:0 identified as Cer m18:2 17:0
- Cer d18:1 / 18:1 identified as Cer m18:2 18:1
- Cer d18:1 / 20:0 identified as d Cer m18:2 20:0
- Cer d18:1 / 22:0 identified as Cer m18:2 22:0 (two peaks, see Figure 4-11A)
- Cer d18:1 / 24:1 identified as Cer m18:2 24:1
- Cer d17:0 / 16:0identified as Cer m17:1 / 16:0
- GluCer d18:1 / 16:0 identified as Cer m18:2 16:0 (whit loss of head group)

Most of these misinterpreted species are not occurring in significant amounts in nature and were therefore excluded as false positive.

We also found an impurity in the GluCer d18:1 / 8:0 standard which turned out to also contain Cer d18:1 / 8:0

Deuterated ceramides are not included in the Lipid Search ™ database. Therefore, Lipid Search™ misidentified two deuterated standards. $D_7$-Cer d18:1 / 16:0 (or its $–H_2O$ ion) was identified as 1-deoxyCer m33:0 $[M+NH_4]^+$ and $D_7$-Cer d18: 1/ 24:0 (or its $–H_2O$ ion) as 1-deoxyCer m41:0 $[M+NH_4]^+$. However, the fatty acid composition could not be annotated, because Lipid Search ™ did not find the sphingoid base fragments for the 1-deoxyCer species (as this is a false annotation). Furthermore, the software identified a SPH d22:0, which seems to be a real positive result. It might be a contamination in one of the standards, from a synthesis artefact. In summary, Lipid Search ™ correctly identified and annotated 59 out of 65 lipids in the standard mix. Three lipids were not detected, because they were not present in the database, for $D_7$-ChE 16:0 (which is present in the database) the concentration was too low for data dependent fragmentation, which is required by the algorithm for identification. Two deuterated ceramides were detected but not correctly annotated by Lipid Search ™. 17 Lipids were identified twice. Four because of a pre-peak with the same mass and 13, because of a double identifications of the same ion. This double integration is an unsolved problem in Lipid Search ™.

The double identification is created because Lipid Search ™ first tries to identify a pattern (full scan data plus the corresponding fragmentation data) in the chromatogram, which fits best to a spectrum in the database and therefore it annotates the spectra in each sample. This creates a list of annotated patterns in the sample. In a second step, Lipid Search ™ aligns different measurements of the same sample, e.g. positive and negative mode of the sample but also data from measured (biological) replicates. If in one sample that was aligned, the pattern identification was incorrect, this creates two different annotations within the alignment. The alignment algorithm will now search for full scan data with the corresponding

ion in the other samples and integrate them in all the aligned samples, leading to two annotated species for the same peak. To improve the Lipid Search ™ algorithm, a control step should be implemented in the alignment step, which checks for peaks which are present in the aligned samples at the same retention time, where the same pattern was annotated differently and either implement an algorithm to choose the correct annotation or to ask the user which annotation fits better. This control step could avoid double identification of ion-patterns. This issue was reported to the Lipid Search ™ product manager at Thermo. So far, it is not possible to reliably filter these wrongly assigned peaks. Therefore, a manual validation is still necessary to validate the results.

### 4.5.3 Lipidome in plasma from healthy donors

Human plasma from six healthy individuals were extracted as described in 4.3.5 (Sample extraction) and analysed with TraceFinder™. The average sphingolipidome from the six samples is shown in Figure 4-13. Sphingomyelins inculde the most abundant species in plasma making up 92 % of the total plasma sphingolipidome. The second most abundant sphingolipids are ceramides with 4 % and hexosylceramides with 3 %. S1P species and 1-deoxyceramides are very low abundant making 0.3 % for S1P and 0.2 % for 1-deoxyceramides.

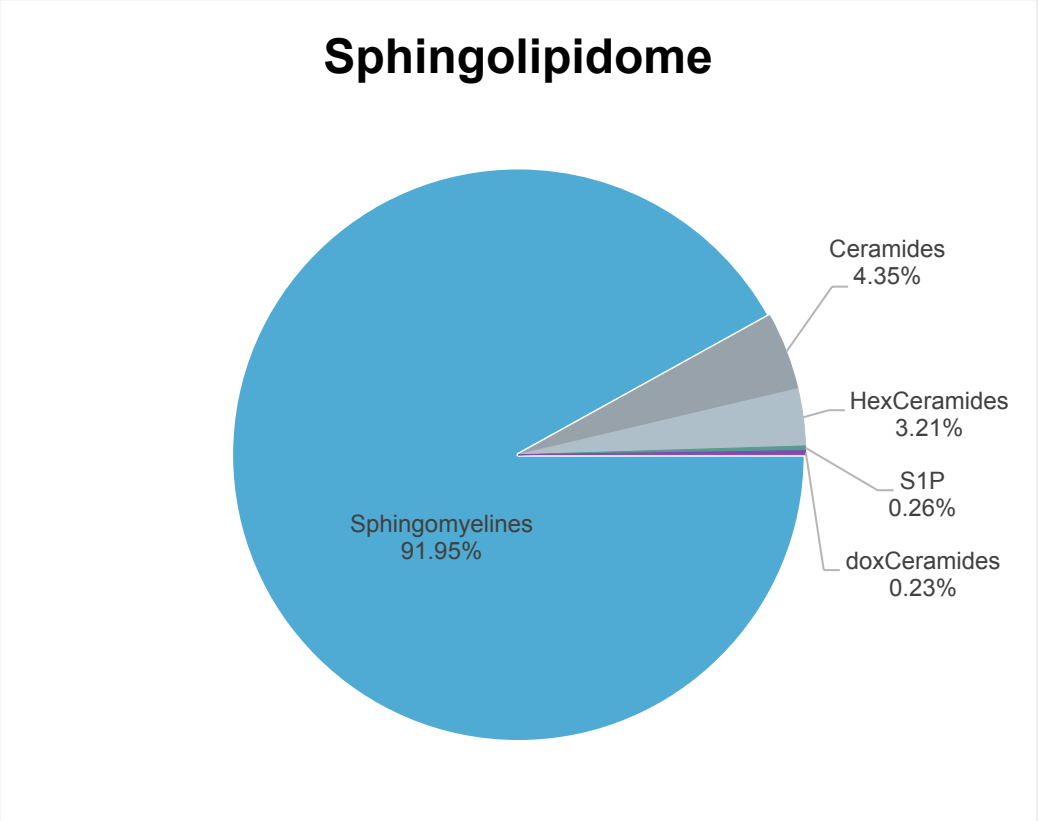


Figure 4-13: Six different plasmas from healthy donors were extracted and whole sphingolipidome was analyzed using the TraceFinder™ quantification software. The average value from the six samples per sphingolipid class is shown. HexCeramides represent hexosylceramides, doxCeramides 1-deoxyceramides and S1P stands for sphingosine-1-phosphate.

The distribution of the individual subspecies is shown in Figure 4-14. All species fulfilled the quality criteria and were normalized to internal standards of the respective sub-class.

The most abundant ceramide species in plasma is Cer d18:1 / 24:0 followed by Cer d18:1 / 22:0, Cer d18:1 / 24:1 and Cer d18:2 / 24:0. The same distribution of fatty acids was seen for dihydroceramide. For 1-deoxceramides, the most abundant species are the 1-deoxy(DH)Cer (m18:0 or m18:1) with 24:0, 24:1 or 22:0 fatty acids.

The most abundant hexosylceramide species were HexCer d18:1 / 24:0, HexCer d18:1 / 22:0, HexCer d18:1 / 24:1 and HexCer d18:2 / 16:0. Conentraction of Hex(DH)ceramides were very low and therefore did not meet the quality criteria.

Interestingly, in contrast to ceramides is the most abundant SM and (DH)SM species were d18:1 /16:0 and d18:0 / 16:0 respectively. Second most abundant species was SM d18:1 /

24:1 followed by SM d18:1 / 22:0, Cer and SM d18:1 / 24:0. This is due to the fact, that ceramide transport protein (CerT) prefers C16:0 fatty acid ceramide species, whereas C22:0 and C24:1 fatty acid ceramide species are transferred at ~40 % of the rate of the shorter fatty acid ceramides, and the transfer of C24:0 fatty acid ceramide is negligible. CerT is responsibly to transport ceramides from ER to Golgi, where sphingomyelins are formed from ceramides [24].

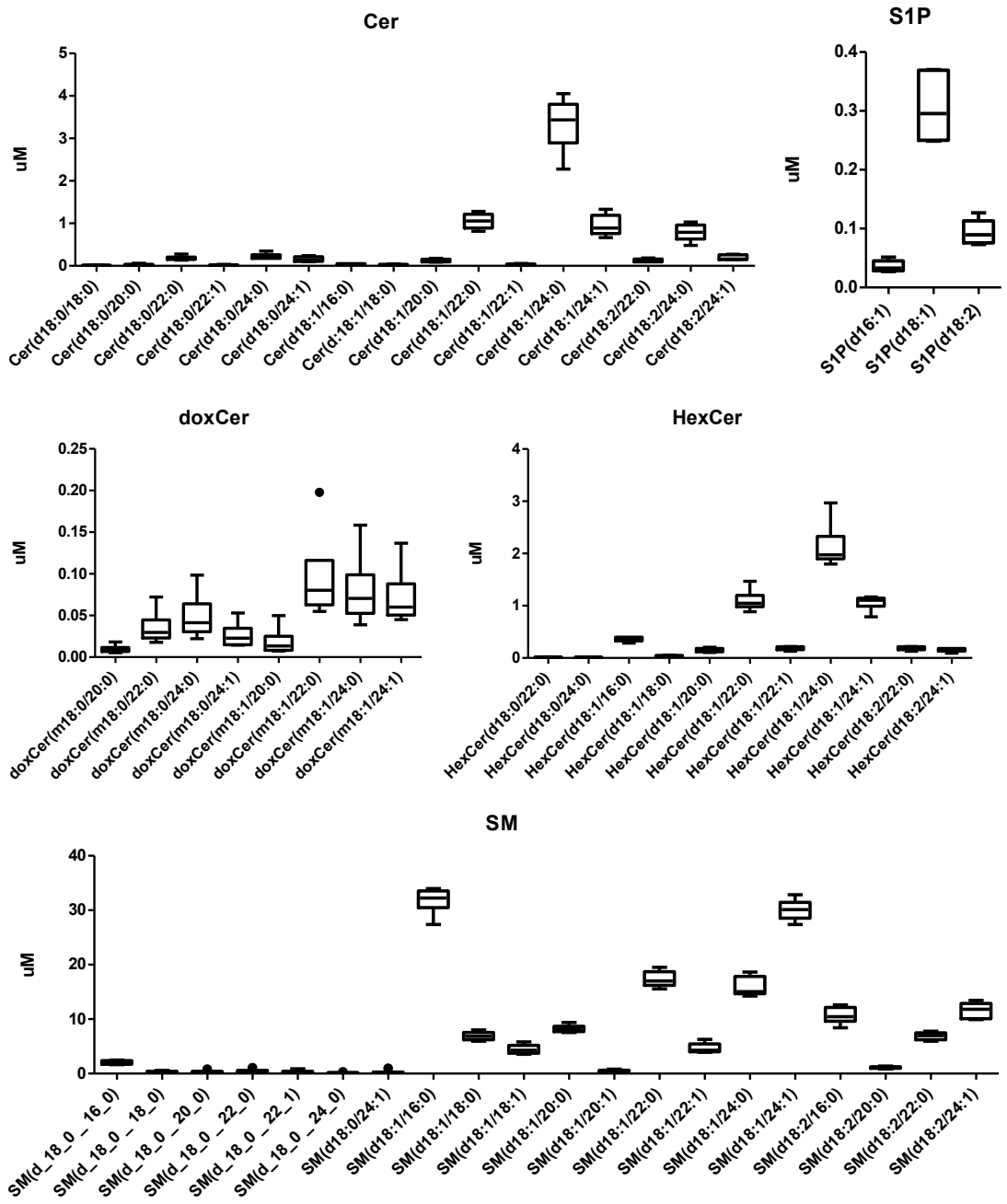


Figure 4-14: Sphingolipidome of plasma from healthy donors. Species were identified and quantified with spingolipid TraceFinder™ method. For each class of sphingolipids, the individual species are shown which fulfilled the quality criteria.

For reference values see the sphingolipidome measured by Samar R. Hammad [25] or Oswald Quehenberger [6].

### 4.5.4 Biological verification of the identified sphingolipid species

To verify that our method correctly identified the assigned sphingolipid species, we compared the sphingolipid profile in cells, which were treated with different inhibitors of the sphingolipid metabolic pathway. We used three well-established inhibitors of the pathway.

1. Myriocin is a potent inhibitor of SPT and blocks the *de novo* synthesis of sphingolipids. It is expected that total sphingolipid levels are decreased in the presence of myriocin compared to control.

2. Fumosin B1 ( FB1) is an inhibitor of the Ceramide Synthases (CerS). Inhibiting CerS blocks the conversion of sphinganine and sphingosine to (dihydro)ceramide and leads to the accumulation of the free sphingoid bases. As a consequence, (dihydro)ceramide but also complex sphingolipids like hexosylceramides and sphingomyelines should be decreased and free bases and S1P should be increased.

3. Inhibiting dihydroceramide desaturase 4-HPR should cause the accumulation of saturated sphingolipids like dihydroceramide, but also saturated hexosyl(DH)ceramides and (DH)sphingomyelins.

NIH3T3 cells were treated with the three inhibitors for 24 hours [§§§§]. Myriocin reduced the levels of all analysed species including 1-deoxyCer except for S1P d18:0. Total sphingolipids levels were reduced indicating a significant turnover and degradation of sphingolipids in the cells. FB1 had a minor effect on most species but increased significantly the free sphingoid bases and its phosphorylated forms (SPH d18:1, S1P d18:1). Interestingly, although by trend most species were slightly elevated in the presence of FB1, some species with an $C_{16}$ fatty acid (e.g. HexCer d18:0;16:0, HexCer d18:1;16:0, 1-deoxyCer d18:1;16:0) were rather reduced (Figure 4-15). 4-HPR caused increases of all saturated species except 1-deoxyCer. As demonstrated in Chapter 1, 1-deoxyceramides contains a (14*Z*) double bond and are therefore no substrate for DES1/2. Therefore, 4-HPR has no impact on the 1-deoxyCer formation (Figure 4-15C). 4-HPR also increased the saturated free sphingoid base

[§§§§] Cells were cultured, harvested and extracted by Gergely Karsai

sphinganine and sphinganine-1-phosphate, and decreased the desaturated free sphingoid bases and sphingosine-1-phosphate (Figure 4-15D).

In summary we observed a change in the sphingolipidome in response to inhibitor treatment. This strongly indicated that the sphingolipid species were identified correctly by our method. Surprisingly we observed that with the inhibition of FB1 all C16:0 acetylated species are decreased but it had only a minor effect on the other species. FB1 is known to inhibit in concentrations around 35 µM, in this experiment, 7 µM was used to avoid toxic effects of FB1 on the sensitive NIH3T3 cells. This might have resulted in an incomplete inhibition of the individual CerS isoforms.

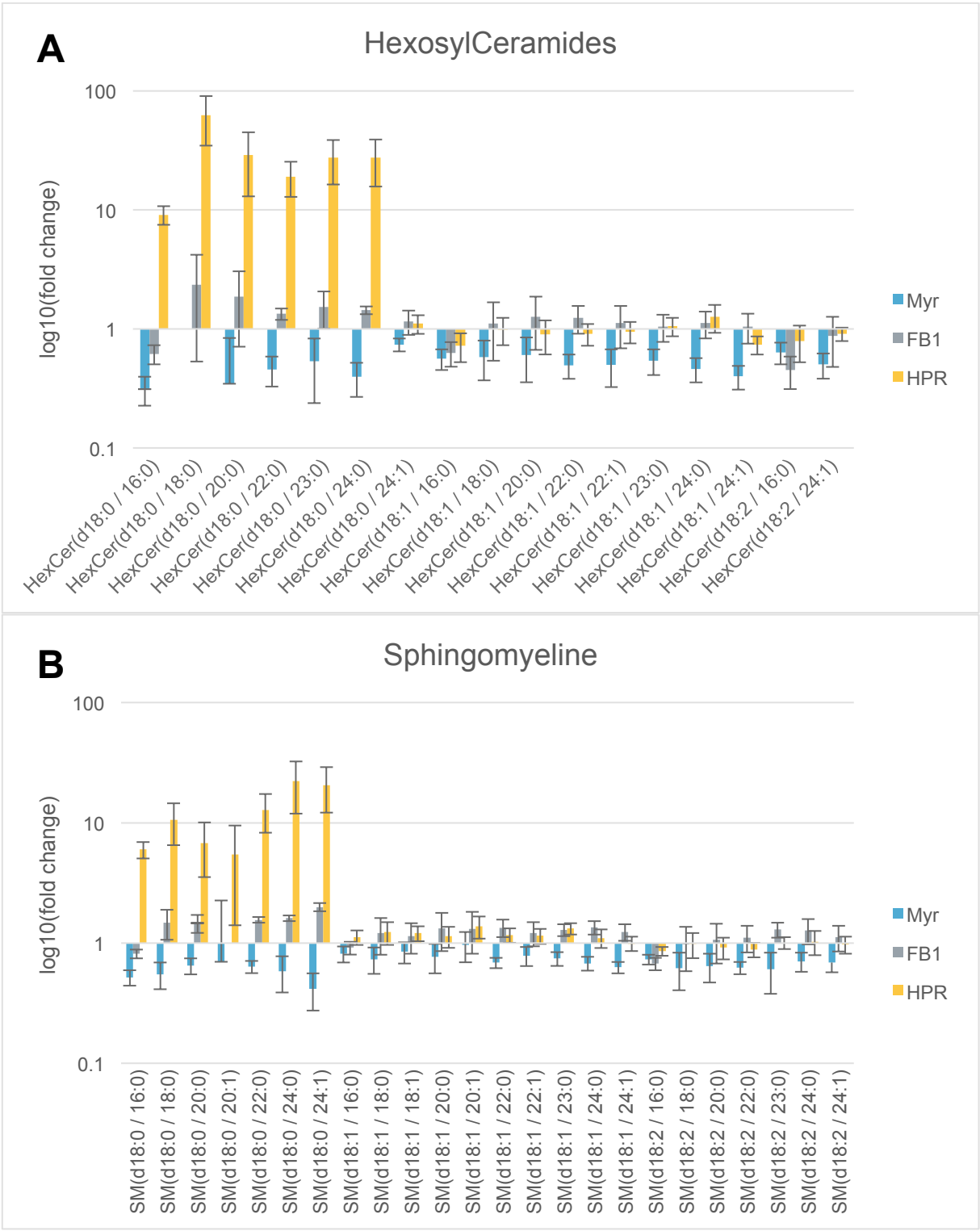
A
HexosylCeramides
log10(fold change)
100
10
1
0.1
Myr
FB1
HPR
HexCer(d18:0 / 16:0)
HexCer(d18:0 / 18:0)
HexCer(d18:0 / 20:0)
HexCer(d18:0 / 22:0)
HexCer(d18:0 / 23:0)
HexCer(d18:0 / 24:0)
HexCer(d18:0 / 24:1)
HexCer(d18:1 / 16:0)
HexCer(d18:1 / 18:0)
HexCer(d18:1 / 20:0)
HexCer(d18:1 / 22:0)
HexCer(d18:1 / 22:1)
HexCer(d18:1 / 23:0)
HexCer(d18:1 / 24:0)
HexCer(d18:1 / 24:1)
HexCer(d18:2 / 16:0)
HexCer(d18:2 / 24:1)
B
Sphingomyeline
log10(fold change)
100
10
1
0.1
Myr
FB1
HPR
SM(d18:0 / 16:0)
SM(d18:0 / 18:0)
SM(d18:0 / 20:0)
SM(d18:0 / 20:1)
SM(d18:0 / 22:0)
SM(d18:0 / 24:0)
SM(d18:0 / 24:1)
SM(d18:1 / 16:0)
SM(d18:1 / 18:0)
SM(d18:1 / 18:1)
SM(d18:1 / 20:0)
SM(d18:1 / 20:1)
SM(d18:1 / 22:0)
SM(d18:1 / 22:1)
SM(d18:1 / 23:0)
SM(d18:1 / 24:0)
SM(d18:1 / 24:1)
SM(d18:2 / 16:0)
SM(d18:2 / 18:0)
SM(d18:2 / 20:0)
SM(d18:2 / 22:0)
SM(d18:2 / 23:0)
SM(d18:2 / 24:0)
SM(d18:2 / 24:1)

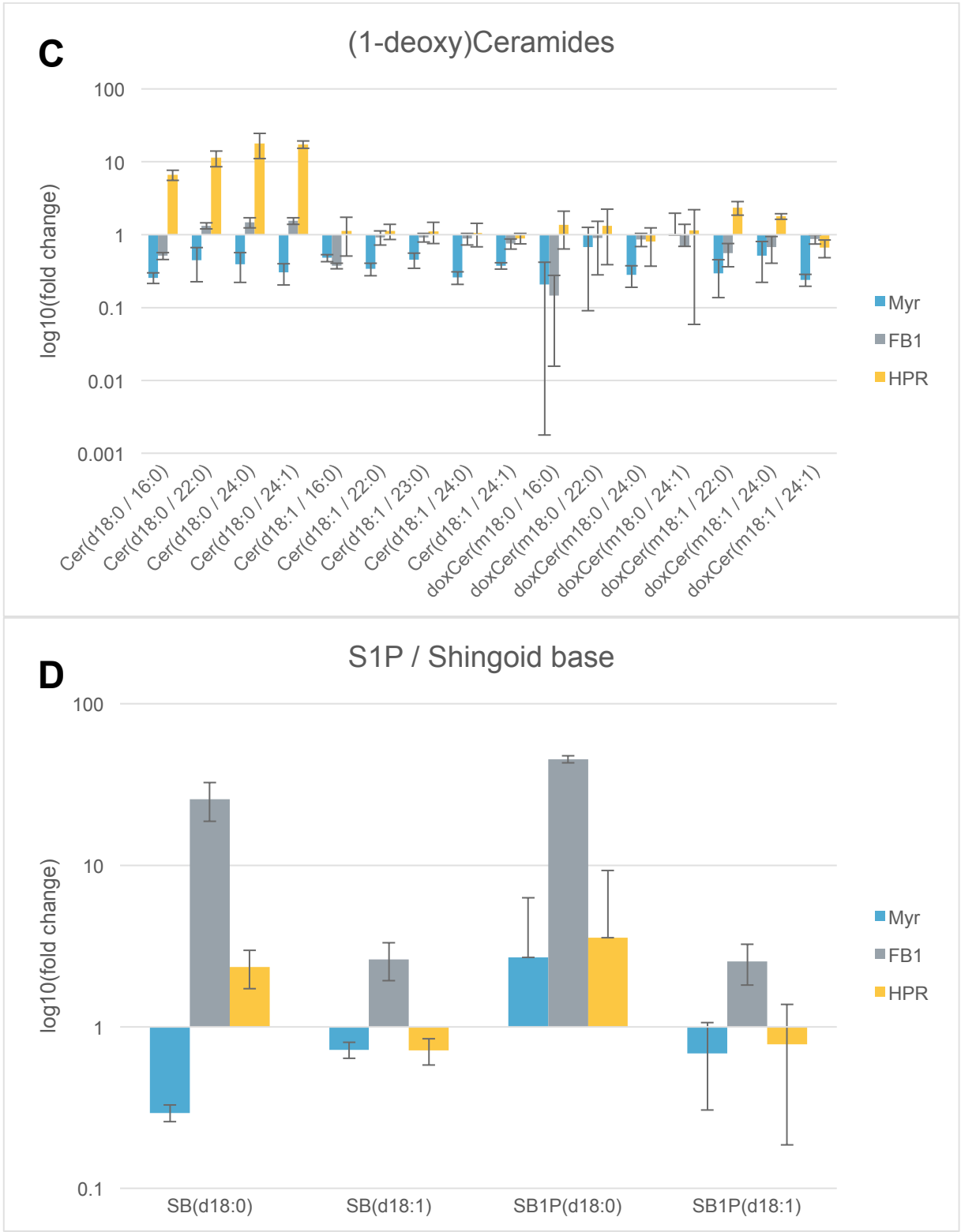


Figure 4-15: NIH3T3 cells were treated with myriocin (myr, SPT inhibitor), fumonisine B1 (FB1, ceramide synthase inhibitor) or fenretinide (4-HPR, dihydroceramide desaturase inhibitor) to interfere with the sphingolipid metabolism. Species are shown in as $\log_{10}$(fold changes) of inhibitor to ethanol control. A: Hexsosylceramides, B: Sphingomyelins, C. (1-deoxy)Ceramides, D: free base sphingolipids and S1P

### 4.5.5 Method comparison

In the past, sphingolipidome was determined in our lab with a method for the hydrolysed sphingoid bases. Therefore, we compared the sphingolipid profile measured with the established acid-base hydrolysed protocol with the newly developed sphingolipidomics approach. In 36 human plasma samples from the Hepadip cohort, the sphingoid base profile was measured after acid base hydrolysis and in parallel a full sphingolipidomics analysis was performed (see 3.3.1 Liquid chromatography and 4.3.2 Mass spectrometry method). With acid base hydrolysis, sphingoid bases are released and total levels reflect all sphingolipids, which were formed on the particular backbones. Hydrolysis provides a comprehensive readout of the SPT product spectrum and the total sphingolipid levels in a sample. However, after hydrolysis any information on the N-acyl chain or head groups is lost. We therefore compared the two methods to see how they perform in relation to each other. For comparison all $C_{18}$ based sphingolipids measured with the lipidomics approach were added up independently of the sub classes (e.g. all the d18:0, d18:1, d18:2 or m18:0 and m18:1 from all classes summed up) and compared to the $C_{18}$ sphingoid base levels obtained after hydrolysis ($C_{18}$ Sphinganine, $C_{18}$ Sphingosine, $C_{18}$ Sphingadiene, 1-deoxysphinganine and 1-deoxysphingosine).

For the measured d18:0 based sphingolipids, we saw a linear correlation between the hydrolysis method, whereas for the bases with one (d18:1) or two double bonds (d18:2), this correlation was not as strong (Figure 4-16). Interestingly, 1-deoxysphingolipids (m18:0 and m18:1) showed a much better correlation between the methods than the canonical $C_{18}$ sphingolipids (Figure 4-16). The general bias towards lower levels in the hydrolysis method might be due to incomplete hydrolysis.

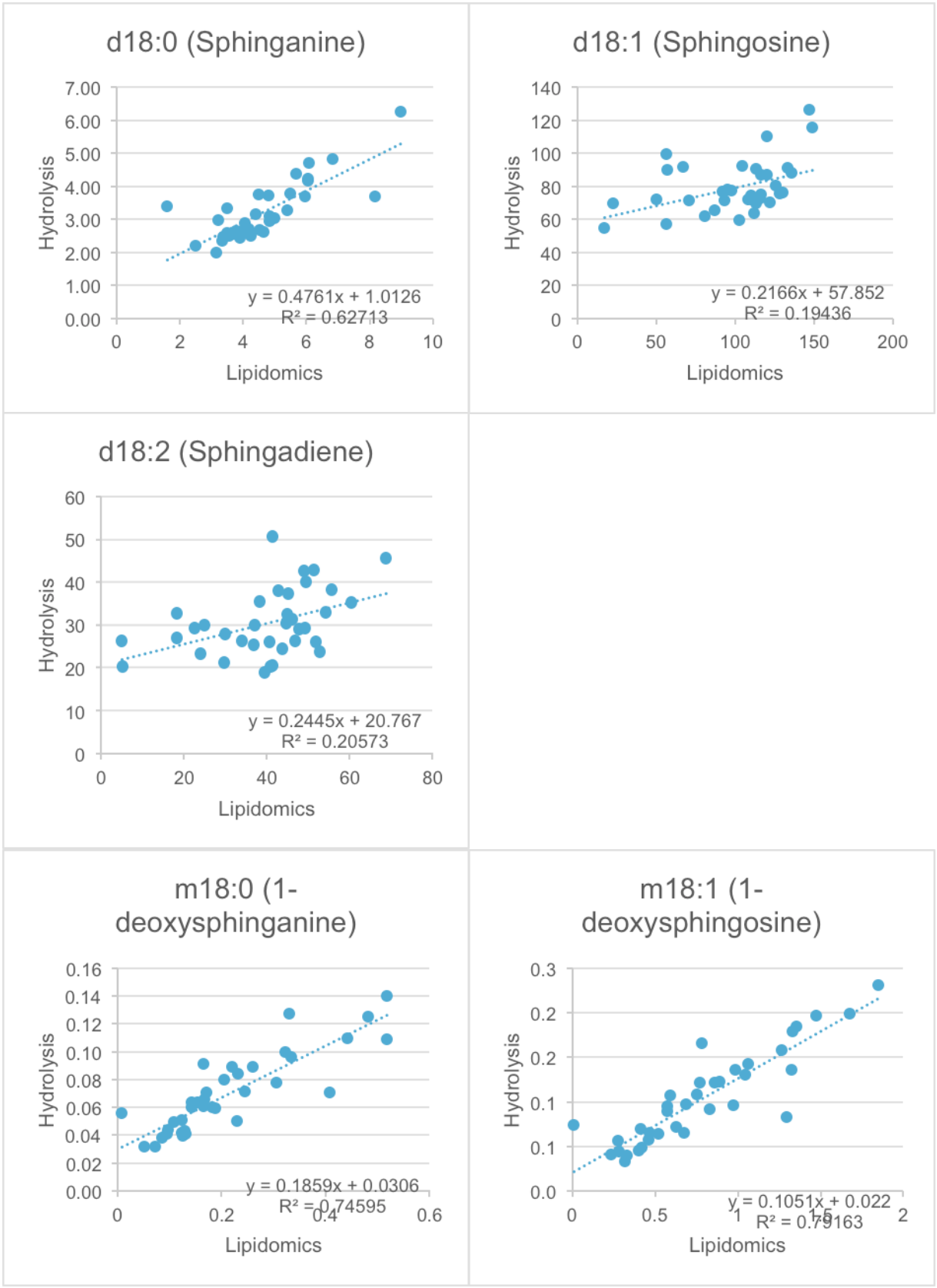


Figure 4-16: Correlation between (1-deoxy)sphingoid bases measured after acid base hydrolysis or as sum of the (1-deoxy)sphingoid bases in different sphingolipid classes (free base, sphingosine-1-phosphate, ceramides, 1-deoxyceramides, hexosylceramides and sphingomyelines) after sphingolipidomic analysis.

One possible reason for the observed differences could be, that the sphingoid bases were normalized either on $D_7$-SPH d18:0 or $D_7$-SPH d18:1 whereas in the lipidomics method uses a variety of different internal standards according to the class of the species (4.3.4 Internal standards). As these internal standards are often non-natural variant of FAs they do not necessarily elute at the same time as the quantified species – particularly not in reverse phase chromatography. This will affect the calculated concentration by introducing more variance.

Further, after hydrolysis, all the different sphingolipid species will elute as one sphingoid base peak, and therefore, sum up all the species to one peak. With this, also minor species contribute to the concentration, whereas in the lipidomics method, minor species might not be detected if they were below the detection limit. In addition, in the lipidomics methods, only the known species were included in the quantification, therefore, some species, which contribute to the hydrolysed peak, were presumably not included in the quantification of the lipidomics data.

Moreover, isobaric compounds were cleaved to different sphingoid bases during hydrolysis, whereas in the lipidomics method, isobars might overlap and therefore contribute to the quantification. This might explain the better correlation of saturated d18:0 compared to d18:1 and d18:2, because the additional double bond increases the possible number of isobaric species.

## 4.6 Discussion

Lipids represent a significant part of the metabolome. A technique to determine a comprehensive lipid profile becomes more and more important in systems biology but also in medicine. Lipidomics techniques provide a broad profile of biological lipid molecules and allow extensive pathway analysis and interpretation of their physiological role [5]. As a significant number of diseases are associated with changes in the lipid profile, lipidomics is an important tool to understand disease mechanisms, and search for biomarkers, which help in diagnostics of diseases, risk stratification and monitoring of therapeutic interventions [13].

In this work, we developed a quantitative data dependent acquisition LC-$MS^2$ method for different sub-classes of sphingolipids, such as free sphingoid bases, S1P, ceramides, hexosylceramides and sphingomyelins. The method allows the differentiation between different isomeric sphingolipid subspecies (e.g. Cer d18:0 / 24:1 vs. Cer d18:1 / 24:0) and is also unique as it includes atypical and low abundant sphingolipid species like atypical chain length sphingolipids and 1-deoxysphingolipids. Further, the method can be used to quantify glycerophospholipids, free cholesterol and cholersteryl esters. Additionally, also neutral glycerolipids and free fatty acids are separated and can be (semiquantitively) analysed.

With this lipidomics method, it is possible to map the metabolic pathways of individual lipid classes and particular species. The here established method showed a good separation and resolution of the various lipid classes. Sphingolipids, glycerophospholipids, S1P but also cholesterol species, free fatty acids and neutral gycerolipids could be reliably detected. It remains demanding to acquire a comprehensive lipid profile covering apolar to polar lipids but also very low and high abundant lipids in a broad dynamic range. In an earlier version of the method we started using a C18 instead of an C30 column. Using these conditions, we obtained a decent separation of the species but observed a significant peak tailing for some species, in particular for long chain PCs and S1Ps. Switching to C30 column and slight adaptations in the LC conditions solved these issues. The analysis time of our method is rather long (30min) and separated into two runs for positive and negative ionisation mode. Several other methods are reported in the literature, Basit et al [10] describes a reversed phase method using a C18 column for a rapid evaluation of 25 sphingolipid species within nine minutes, where free sphingoid bases, S1P species, (DH)ceramides, sphingomyeline and glucosylceramide are covered. Although dihydroceramides are covered, Basit and co-authors do not report (DH) species for sphingomyeline or glucosylceramide, nor do they report any minor N-acetyl fatty acid chain length like 20:0 or 22:0 for ceramide. Further, atypical 1-deoxysphingolipids were not included. Compared to the method published by Basit [10], the here presented method needs longer in LC separation, but covers more species.

Mi et al. [26] reported a similar method using RPLC with a C18 column, which covers the major sphingolipid classes and species, neither show low abundant species nor separates or quantifies isobaric species.

Scherer et al. [27] published a very rapid method of 4.5 minutes for the analysis of different sphingolipid classes using a HILIC column. As sphingolipids co-elute with the internal standard, matrix effects can be largely avoided, but isobaric species are not resolved in this approach. Furthermore, co-elution of species and an isotopic overlay of different species is possible and needs to be corrected by post-analysis calculation methods to avoid overestimation. This is due to the fact that isotopes of co-eluting desaturated species may overlap with saturated species. Especially in case of 1-deoxysphingolipids the $[M+H]^+$ ion of 1-deoxyceramides will overlap with $[M-H_2O+H]^+$ species of canonical dh-ceramides. With such a method, it is difficult to reliably identify and quantify minor 1-deoxysphingolipids.

Although a C30 stationary phase is much less used in untargeted profiling of lipidome, its potential has been demonstrated in separation of phospholipids and recently also for complex lipidomics studies [28, 29]. In a comparison of C18 and C30 columns by Narvaez-Rivas and co-authors [28], the C30 column showed the narrowest peaks, highest theoretical plate number, excellent peak capacity and retention time reproducibility. They also demonstrated, that the C30 column separates *cis* and *trans* isomeric lipid species.

Few authors do mention the measurement of 1-deoxysphingolipids like Shaner et al. [30] or Sullards et al. [31], but they do not comment on how to reliably identify or quantify these 1-deoxysphingolipids. As most of the natively occurring 1-deoxysphingolipids are present in their N-acetylated form, this might explain why these compounds were often overseen in general sphingolipid analysis, because their $[M+H]^+$ is overlapping with $[M-H_2O+H]^+$ of typical dh-ceramide species [32].

Most of the so far published sphingolipidomics methods are targeted approaches using a triple quadrupole mass spectrometer in multiple reaction monitoring (MRM) mode [25-27, 30, 31, 33]. MS analysis with MRM enables the detection of specific lipid species based on their

unique parent/fragment ion transitions. A MRM method provides highly selective and very sensitive determination of individual lipid species in the complex lipid mixture. However MRM requires prior knowledge about the fragmentation patterns of lipids analysed and a predefined list of species of interest. It is not possible to search for unknown species or to re-analyse data for further compounds. Recently, also methods using high-resolution accurate mass spectrometer (HRAMS) were published. Bilal et al. [34] showed a method to quantify sphingolipid with LC-HRAMS using full scan data for identification and quantification, with the limitation, that no fragmentation data is acquired and therefore, not used for identification of the lipid species [34].

In our work, we demonstrated the use of HRAMS with data dependent acquisition, where full scan but also fragmentation data is acquired, based on the signal intensity of the measured species. This is limiting the detection of low abundant species in the $MS^2$ level. On the other hand, it allows to search for unknown species and a re-analysis of data for new compounds of interest. Each run takes about 31 minutes. In combination with the MMC extraction protocol, this method provides a fast and comprehensive tool for lipidomics analysis.

After the acquisition of hundreds of $MS^2$ features, these need to be annotated to lipid classes and species. It is rather difficult to obtain exact annotation for all molecules, even in the limited categories of metabolites such as lipids, especially because of the huge number of isobars possible for lipids. Fragments of fatty acyl anions from the *sn- 1* and *sn- 2* positions and neutral loss of water or fatty acids are very important for identification of individual molecular species. Fragment ions of polar head groups or specific neutral loss from each class are also very important for identification of each different category of polar lipids. High coverage of detected fragments results in identification that is more accurate.

Lipid search [TM] offers an automated search engine that can indicate the most probable candidates for each $MS^2$ feature. The database consists of theoretical *m/z* values of lipid ions with different adducts for positive and negative mode and their fragment ions for different lipid classes. This database is theoretically constructed, calculating the fragment data for lipid

species. Patterns of ion fragmentation have been theoretically constructed and improved by using experimental data obtained from synthesized standards and various natural samples [35]. The implemented algorithm in Lipid Search ™ is based on a feature identification in different samples, where the best match is annotated to a measured feature. Afterwards, different samples can be aligned and the identified species will be overlaid and peaks are integrated over the whole sample set. This alignment produces a number of false positive identifications, where an quality check for double annotation of a specific ion feature is missing. For a high throughput approach, an automated annotation and quantification would be necessary. Lipid Search ™ provides such features, but because of a high percentage of false-positive annotation, a time-consuming validation process is needed which is not feasible yet for a high throughput analysis.

In summary, we developed a comprehensive method for the analysis of the total sphingolipidome, including the high abundant sphingolipid classes, but also the low abundant 1-deoxysphingolipid species. With this method, it is possible to analyse the sphingolipidome in different matrices and to follow metabolic changes in different (disease) conditions or treatments.

## 4.7 Protocol for lipidomics

The following protocol was developed and validated for whole sphingo- and phospholipidomics analysis.

### 4.7.1 Extraction

Cells, plasma or tissue sample, is aliquot to 20µL volume. For quality control, a pooled sample is mixed by taking 3µL of each sample to pool. The extraction buffer (methanol / chloroform / MTBE 4/3/3 v/v/v) is combined with internal standards for all lipid classes. From pool sample, four different quality control samples are aliquot by taking 1/8, ¼, ½, and 1 of the sample volume.

Samples and quality controls are mixed with 1mL of extraction buffer (containing an internal standard for all lipid classes), vortexed for 20 seconds and then shacked for 20 min at 37 °C with 1400 rpm. After samples are centrifuged at 24 °C for 5 min at room temperature, the supernatant is transferred to new Eppendorf tube and samples dried down under N2. Samples can be stored at -20 °C until measurement.

For LC-MS measurement, samples and quality controls are dissolved in 100µL methanol.

### 4.7.2 LC-MS

For chromatographic separation, an Accucore C30 (150 Å, 2.6 µm, 150 × 2.1 mm) column (Thermo Fischer Scientific, Reinach, Schweiz) is used. Mobile Phase A: Water / Acetonitrile 80 / 20 v/v and B: Isopropanol / Acetonitrile 90/10 v/v both containing 10mM ammonium Acetate and 0.1 % formic acid and C: Methanol. Samples are loaded with 70 % A, 20 % B, and 10 % C for 1.5 min and then separated for 17 min in a gradient to 100 % B and finally eluted for another 7 min at 100 % B. After the column is set back to start conditions and re-equilibrated for 5min. Samples are measured in singles in the positive and negative mode in a top 10 data dependent acquisition mode with heated electrospray ionization on a Q Exactive (Thermo Fisher). Quality controls are measured minimally in triplicates in positive and negative mode, distributed over the sequence, e.g., in the beginning, in the middle and at the end of the series.

### 4.7.3 Lipid identification

Samples are semi-automatically analysed, and lipids are annotated with Lipid Search ™ software (Thermo Fisher). Quality control samples are aligned in Lipid Search ™, and lipid annotation is validated with these samples.

The following filter criteria are applied to quality control samples:

- S/N threshold 10
- Area of QC 1/ Area blank >1.5
- Base Retention time > 5 min and < 26 min
- Relative standard deviation < 30 within QC triplicates
- Peak height in QC1 > 5e5

The aligned and filtered results are checked for:

- Peak shape: did it identify a real peak or just noise?
- Do the QC samples follow an increasing linear pattern?
- Did Lipid Search ™ find all internal standards added to the sample and do they show the same area within all QC samples?
- Were lipids identified more than once?
- Sort for RT: are their Lipids identified with same RT which could be the same molecule (e.g., d-species – H2O vs. m-species plus double bond)

Also, some known impurities of internal standards are excluded from results like Cer d18:1 / 8:0 (impurity coming from glucosylceramide 18:1 / 8:0 standard) or SPH d15:0 (Impurity coming from internal STD)

### 4.7.4 Lipid quantification

This search gives a list of molecules that have to be quantified in TraceFinder™. Parent Ion, fragments ions, identifies peaks and RT. TraceFinder™ integrates peak area. Results can be exported to excel.

Calculate Concentration of lipids by correction to the internal standard.

| **Lipid Sub-Class** | **Internal standard to correlate** |
|---|---|
| Dh-Cer | Cer d18:0 / 12:0 |
| Cer (also diene) | Cer d18:1 / 12:0 |
| Dh-1-deoxyCer | 1-deoxyCer m18:0 / 12:0 |
| 1-deoxyCer | 1-deoxyCer m18:1 / 12:0 |
| Sphinganine bases | $D_7$-SA |
| Sphingosine bases | $D_7$-SO |
| 1-Deoxybases | $D_7$-SO |
| HexCer | GlucosylCer d18:1 / 8:0 |
| SM | SM 18:1 / 12:0 |
| Free Cholesterol | $D_7$ cholesterol |
| ChE | $D_7$ ChE |

### 4.7.5 Data Validation

Exclude compounds with a duplicate area from further analysis, e.g., d18:0 / 24:1 and d18:1 / 24:0 (check which compound is correct with fragmentation data and delete duplicate).

Exclude compounds with CV % of QC 1 is higher than > 20 %

Eliminate compounds with $R^2$ of QC is smaller than < 0.8

Remove compounds with a ratio of Area Sample / Area blank (methanol) is lower than 1.5.

## 4.8 References

[1] Wenk, MR, Lipidomics: new tools and applications, Cell, 2010;143:888-895.
[2] Khot, UN, Khot, MB, Bajzer, CT, et al., Prevalence of conventional risk factors in patients with coronary heart disease, JAMA, 2003;290:898-904.
[3] German, JB, Gillies, LA, Smilowitz, JT, et al., Lipidomics and lipid profiling in metabolomics, Curr Opin Lipidol, 2007;18:66-71.
[4] Han, X, Lipidomics for studying metabolism, Nat Rev Endocrinol, 2016;12:668-679.
[5] Hu, T and Zhang, JL, Mass-Spectrometry-Based Lipidomics, J Sep Sci, 2017.
[6] Quehenberger, O and Dennis, EA, The human plasma lipidome, N Engl J Med, 2011;365:1812-1823.
[7] Fahy, E, Subramaniam, S, Brown, HA, et al., A comprehensive classification system for lipids, J Lipid Res, 2005;46:839-861.
[8] Fahy, E, Subramaniam, S, Murphy, RC, et al., Update of the LIPID MAPS comprehensive classification system for lipids, J Lipid Res, 2009;50 Suppl:S9-14.
[9] Quehenberger, O, Armando, AM, Brown, AH, et al., Lipidomics reveals a remarkable diversity of lipids in human plasma, J Lipid Res, 2010;51:3299-3305.
[10] Basit, A, Piomelli, D and Armirotti, A, Rapid evaluation of 25 key sphingolipids and phosphosphingolipids in human plasma by LC-MS/MS, Anal Bioanal Chem, 2015;407:5189-5198.
[11] Hla, T and Dannenberg, AJ, Sphingolipid signaling in metabolic disorders, Cell Metab, 2012;16:420-434.
[12] Murphy, RC and Axelsen, PH, Mass spectrometric analysis of long-chain lipids, Mass Spectrom Rev, 2011;30:579-599.
[13] Vaz, FM, Pras-Raves, M, Bootsma, AH, et al., Principles and practice of lipidomics, J Inherit Metab Dis, 2015;38:41-52.
[14] Liebisch, G, Vizcaino, JA, Kofeler, H, et al., Shorthand notation for lipid structures derived from mass spectrometry, J Lipid Res, 2013;54:1523-1530.
[15] Pellegrino, RM, Di Veroli, A, Valeri, A, et al., LC/MS lipid profiling from human serum: a new method for global lipid extraction, Anal Bioanal Chem, 2014;406:7937-7948.
[16] Breslow, DK, Collins, SR, Bodenmiller, B, et al., Orm family proteins mediate sphingolipid homeostasis, Nature, 2010;463:1048-1053.
[17] Miyake, Y, Kozutsumi, Y, Nakamura, S, et al., Serine palmitoyltransferase is the primary target of a sphingosine-like immunosuppressant, ISP-1/myriocin, Biochem Biophys Res Commun, 1995;211:396-403.
[18] Wadsworth, JM, Clarke, DJ, McMahon, SA, et al., The chemical basis of serine palmitoyltransferase inhibition by myriocin, J Am Chem Soc, 2013;135:14276-14285.
[19] Stockmann-Juvala, H and Savolainen, K, A review of the toxic effects and mechanisms of action of fumonisin B1, Hum Exp Toxicol, 2008;27:799-809.
[20] Merrill, AH, Jr., van Echten, G, Wang, E, et al., Fumonisin B1 inhibits sphingosine (sphinganine) N-acyltransferase and de novo sphingolipid biosynthesis in cultured neurons in situ, J Biol Chem, 1993;268:27299-27306.
[21] Desai, K, Sullards, MC, Allegood, J, et al., Fumonisins and fumonisin analogs as inhibitors of ceramide synthase and inducers of apoptosis, Biochim Biophys Acta, 2002;1585:188-192.
[22] Rahmaniyan, M, Curley, RW, Jr., Obeid, LM, et al., Identification of dihydroceramide desaturase as a direct in vitro target for fenretinide, J Biol Chem, 2011;286:24754-24764.
[23] Wang, H, Maurer, BJ, Liu, YY, et al., N-(4-Hydroxyphenyl)retinamide increases dihydroceramide and synergizes with dimethylsphingosine to enhance cancer cell killing, Mol Cancer Ther, 2008;7:2967-2976.
[24] Yamaji, T and Hanada, K, Sphingolipid metabolism and interorganellar transport: localization of sphingolipid enzymes and lipid transfer proteins, Traffic, 2015;16:101-122.
[25] Hammad, SM, Pierce, JS, Soodavar, F, et al., Blood sphingolipidomics in healthy humans: impact of sample collection methodology, J Lipid Res, 2010;51:3074-3087.
[26] Mi, S, Zhao, YY, Dielschneider, RF, et al., An LC/MS/MS method for the simultaneous determination of individual sphingolipid species in B cells, J Chromatogr B Analyt Technol Biomed Life Sci, 2016;1031:50-60.
[27] Scherer, M, Leuthauser-Jaschinski, K, Ecker, J, et al., A rapid and quantitative LC-MS/MS method to profile sphingolipids, J Lipid Res, 2010;51:2001-2011.
[28] Narvaez-Rivas, M and Zhang, Q, Comprehensive untargeted lipidomic analysis using core-shell C30 particle column and high field orbitrap mass spectrometer, J Chromatogr A, 2016;1440:123-134.

[29] Houjou, T, Yamatani, K, Imagawa, M, et al., A shotgun tandem mass spectrometric analysis of phospholipids with normal-phase and/or reverse-phase liquid chromatography/electrospray ionization mass spectrometry, Rapid Commun Mass Spectrom, 2005;19:654-666.
[30] Shaner, RL, Allegood, JC, Park, H, et al., Quantitative analysis of sphingolipids for lipidomics using triple quadrupole and quadrupole linear ion trap mass spectrometers, J Lipid Res, 2009;50:1692-1707.
[31] Sullards, MC, Liu, Y, Chen, Y, et al., Analysis of mammalian sphingolipids by liquid chromatography tandem mass spectrometry (LC-MS/MS) and tissue imaging mass spectrometry (TIMS), Biochim Biophys Acta, 2011;1811:838-853.
[32] Duan, J and Merrill, AH, Jr., 1-Deoxysphingolipids Encountered Exogenously and Made de Novo: Dangerous Mysteries inside an Enigma, J Biol Chem, 2015;290:15380-15389.
[33] Haynes, CA, Allegood, JC, Park, H, et al., Sphingolipidomics: methods for the comprehensive analysis of sphingolipids, J Chromatogr B Analyt Technol Biomed Life Sci, 2009;877:2696-2708.
[34] Bilal, F, Peres, M, Le Faouder, P, et al., Liquid Chromatography-High Resolution Mass Spectrometry Method to Study Sphingolipid Metabolism Changes in Response to CD95L, Methods Mol Biol, 2017;1557:213-217.
[35] Taguchi, R, Nishijima, M and Shimizu, T, Basic analytical systems for lipidomics by mass spectrometry in Japan, Methods Enzymol, 2007;432:185-211.

# 5 Chapter 5: Applications on Lipidomics method to biological samples

The newly established lipidomics method described in Chapter 4, was used for the following collaborative projects

1. Mutation in SGPL1 cause CMT Neuropathy

   S1P and sphingoid bases were profiled in samples of patients with a mutation in the gene encoding for sphingosine-1-phosphate lyase (SGPL1) and leading to peripheral sensory neuropathy. Lipid analysis allowed insights into changes in the S1P levels and potential disease mechanism.
2. Roux-en-Y gastric bypass (RYGB) as a therapy of morbid obesity

   Sphingolipidomic studies were performed in mice undergoing gastric bypass surgery to evaluate the effect of surgery on changes in (lipid) metabolism.
3. Regulation of sphingolipid metabolism through ORMDL3

   The sphingolipidome was determined in ORMDL3 knock-out mice as well as in mice with transgenic overexpression of human ORMDL3 to study the effect of ORMDL3 on metabolism and regulation of sphingolipids in the context of asthma.
4. Effect of ABCA1 and ABCG1 in age-related macula degeneration (ADM)

   Unbiased lipidomics was applied to a mouse model for age-related macular degeneration. Retina-specific Abca1/Abcg1 knock out mice were suspected to accumule lipids in their macula and features of ADM. Therefore, cholesteryl esters, retinyl esters, and sphingolipid were measured in eye samples of these mice.

Author contributions: Steiner R did all the sample extraction, lipid analysis and quantification, whereas the individual collaborators were responsible to obtain the samples for analysis.

## 5.1 S1P levels in Sphingosine-1-phosphate lyase deficient patient

*In collaboration with A.Jordanova (VIB, Antwerp, BE)*

*Results were published by Atkinson, D., Nikodinovic Glumac, J., Asselbergh, B., Ermanoska, B., Blocquel, D., Steiner, R., Estrada-Cuzcano, A., Peeters, K., Ooms, T., De Vriendt, E., Yang, X. L., Hornemann, T., Milic Rasic, V., Jordanova, A., Sphingosine 1-phosphate lyase deficiency causes Charcot-Marie-Tooth neuropathy, Neurology, 2017;88:533-542.*

Author contribution: Steiner R did the sphingolipid analysis.

In collaboration with the group of A. Jordanova (VIB, Antwerp, BE) we analysed the plasma lipid profile in two patients with an atypical form of axonal peripheral neuropathy, characterized by an acute or subacute onset and episodes of recurrent mono-neuropathy. Next genome sequencing revealed compound heterozygous mutations in the SGPL1 gene, which encodes sphingosine-1-phosphate lyase (SGPL). These mutations co-segregate with the described pathology and are absent in controls. One of the mutations (p.Ser361*) introduces a premature stop codon in the C-terminus and triggers nonsense-mediated decay of the mRNA transcript. The second one is a missense mutation (p.Ile184Thr) which possibly leads to proteasomal protein degradation [1]. SGPL1 catalyses the irreversible degradation of sphingolipids by the terminal cleavage of S1P into hexadecenal and ethanolamine phosphate [2] and thus provides the only exit route for the sphingoid bases from the *de novo* biosynthetic pathway. In addition, S1P is a potent agonist of five G-protein coupled receptors. Thus, SGPL1 expression and activity is essential for the maintenance of physiological levels of S1P and normal growth in mammals. In this context, we were interested to see whehter and how much these mutations cause alterations in the plasma sphingoid base and S1P profile of the patients. We thus determined sphingoid base and S1P profiles in patients and non-affected genetically related family members.

First, we sought to look at the total sphingoid base profiles in the patients. For this, lipids were extracted and acid-hydrolyzed to release free sphingoid bases as described previously [3-5]. It is noteworthy to mention here that this method releases sphingoid bases from all sphingolipids and thus, provides a comprehensive readout of the sphingoid backbone profile. However it does not provide any information on the levels or types of different subclasses of

sphingolipids. For details of the analysis, see 3.3.1 (Liquid chromatography) and 4.3.2 (Mass spectrometry method).

Second, we analysed S1P levels in plasma from the two patients, two unaffected family members and 24 unrelated control samples. Extraction of 50uL of plasma was performed using the MMC protocol, as described in 4.3.5 using $D_7$-S1P as the internal standard. For chromatographic separation, a C18-column-based method was used as described in 3.3.1.

The sphingolipid profiles were compared between the two index patients, the unaffected parents and three unrelated healthy control individuals. Total sphinganine was significantly lower in the patients compared to unaffected parents or unrelated controls (Figure 5-1A). In contrast, total sphingosine was not significantly different but by trend lower in the patient samples (Figure 5-1B). The ratio of sphingosine to sphinganine was significantly elevated in patients but not different between controls and parents (Figure 5-1C).

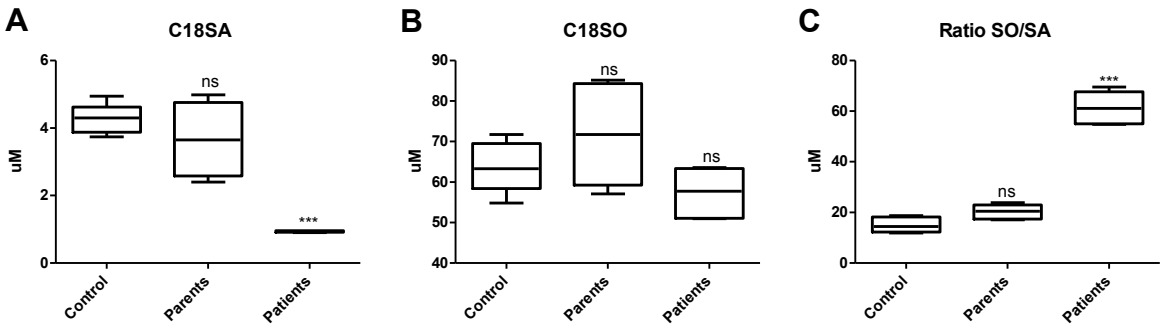


Figure 5-1: Sphingoid base profiles (hydrolyzed) from patients with mutations in the SGPL1 gene, the unaffected parents, and unrelated healthy controls. A: $C_{18}$-sphinganine (SA) levels, B: $C_{18}$ sphingosine (SO) levels and C: the ratio between $C_{18}$ sphingosine to sphinganine. ANOVA was performed to check for statistical differences. ***= $p<0.001$, ns = not significant

Plasma sphingosine-1-phosphate levels were increased in the patients compared to control and unaffected family members. S1P levels in the parents were significantly lower compared to the average of the 24 control samples (Figure 5-2A).

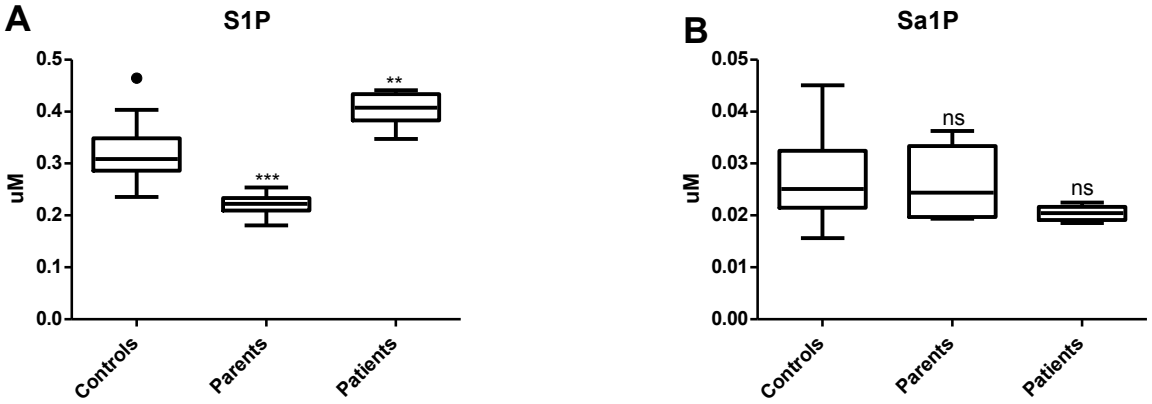


Figure 5-2: Sphingosine-1-phosphate profile from patients with mutations in the SGPL1 gene, the unaffected parents and unrelated healthy controls (n=24). A: $C_{18}$-sphingosine-1-phosphate levels and B: $C_{18}$ Sphinganine-1-phosphate levels. ANOVA test was performed to check for statistical differences. **= p<0.01, ***= p<0.001, ns = not significant

The significant decrease in sphinganine in patients could be due to a negative feedback loop of elevated S1P that inhibits the formation of sphinganine. As conversion from sphinganine to sphingosine is rather fast, we would expect to see its too. However, in view of the 15 times higher levels of sphingosine the conversion of 3 uM sphinganine into sphingosine caused only a small and not significant reduction in sphingosine levels.

The mutation in SPGL1 leads to a change in sphingoid base profile and an increase in plasma sphingosine-1-phosphate. The clinical data suggests that SGPL deficiency is associated with a distinct form of the Charcot-Marie-Tooth disease. This new association would extend the currently recognized clinical and genetic spectrum of inherited peripheral neuropathies. This data emphasizes the importance of SGPL1 and sphingolipid turnover in neuronal function [1]. This together with the other reports that link mutations in SGPL1 to other pathological conditions opens a new area of investigation for SGPL1 functions and hitherto unknown functions of the sphingosine-1-phosphate molecule itself. For example, Janecke et al. [6] describe two distinct mutations in SGPL1 (c.1513C>T; p.Arg505*) and c.934delC (p.Leu312Phefs*30)) which lead to a congenital nephrotic syndrome and congenital adrenal calcifications in human subjects. As expected, the levels of S1P and sphingosine were increased in the patient plasma as well as in fibroblasts derived from these patients [6]. On a similar note, Prasad et al. [7] describe a primary adrenal insufficiency syndrome and steroid-

resistant nephrotic syndrome caused by loss-of-function mutations in sphingosine-1-phosphate lyase. They identified four different homozygous mutations, c.665G>A (p.R222Q), c.1633_1635delTTC (p.F545del), c.261+1G>A (p.S65Rfs*6), and c.7dupA (p.S3Kfs*11), in eight investigated patients; some of them also showed other symptoms including ichthyosis, primary hypothyroidism, neurological symptoms, and cryptorchidism [7]. However, so far, the authors did not report the sphingolipid profiles in these patients. Lovric et al. [8] also reported nine different recessive mutations in SGPL1, which are associated with the steroid-resistant nephrotic syndrome, facultative ichthyosis, adrenal insufficiency, immunodeficiency, and neurological defects. All mutations resulted in reduced or absent SGPL1 protein and/or enzyme activity [8].

Also in some of the nephrotic syndrome patients, neurological symptoms were reported, but mostly in older patients, whereas the nephrotic symptoms already occurred in younger patients [7, 8]. It seems that different mutations in SGPL1 lead to various clinical symptoms and that there is a difference in the pathology of these different mutations.

## 5.2 Sphingolipidomics in mice undergoing bariatric surgery

*In collaboration with Erika Tarasco and Thomas Lutz, Institute of Veterinary Physiology University of Zürich*

Author contribution: Steiner R did the sphingolipid analysis.

Obesity (BMI>30 kg/m$^2$) is an increasing healthcare problem worldwide. In particular, visceral obesity is one of the leading factors for hypertension, insulin resistance, metabolic syndrome (MetS) and type 2 diabetes mellitus (T2DM), but also hypertriglyceridemia and low levels of high-density lipoprotein cholesterol (HDL) [9, 10]. Bariatric surgery and in particular the Roux-en Y gastric bypass (RYGB) is the most effective treatment for obesity regarding long-term maintenance of body-weight loss and in particular for the improvement of obesity-related comorbidities [11, 12]. Patients undergoing gastric bypass surgery show a reduction in appetite and an increase in glycaemic control. Dyslipidaemia and cardiovascular function improve rapidly after RYGB, independent of changes in body weight [13]. Further, patients show improvements in insulin resistance or even a complete remission from T2DM [14, 15].

Double transgenic mice expressing human CETP and the ApoE*3Leiden mutation (ApoE3L.CETP) were used for this study. The expression of the human Cholesteryl Ester Transfer Protein (CETP), which is usually not expressed in wild-type mice, mediates the transfer of cholesteryl ester from HDL to VLDL and LDL in exchange for triglycerides. ApoE3L.CETP mice present a human-like lipoprotein metabolism with higher concentrations of VLDL and LDL and relatively low concentrations of HDL when fed a 60 % high fat plus 0.25 % cholesterol diet (HFDC) [10, 16].

To test the effect of gastric bypass surgery, the mice were divided into three groups. One group obtained Roux-en-Y gastric bypass (RYGB) surgery whereas the control group underwent laparotomy - an abdominal section without any surgical intervention but with the same post-surgery treatment and wound healing processes. These control groups were subdivided into a body weight-matched group (BWm), which were under food restriction to match the same body weight as the RYGB group and the other control group could access food ad libitum (ShamAL). The body weight-matched group controls for the effects of weight

loss caused by gastric bypass because of the limited gastric capacity to monitor changes, which are caused by the weight loss and not by the gastric bypass itself.

A lipidomics profiling was done in 20 µL mouse plasma as described in Chapter 4, using the C18-column-based method. The following commercially available lipids (Avanti Polar Lipids, Alabaster USA) were used as internal standards: $D_7$-sphinganine, $D_7$-sphingosine, Cer d18:0 / 12:0, Cer d18:1 / 12:0, 1-deoxyCer m18:0 / 12:0, 1-deoxyCer m18:1 / 12:0, SM d18:1 / 12:0, GluCer d18:1 / 8:0, $D_7$-S1P, PA 17:0 / 17:0, PE 14:0 / 14:0, LPE 17:1, PG 17:0 / 17:0, PC 14:0 / 14:0, PC 24:0 / 24:0, LPC 17:0. Quality control samples were made as described in 4.3.8 and included in the analysis. For chromatographic separation and MS analysis, the C18-column-based method was used (see 3.3.1 and 4.3.2).

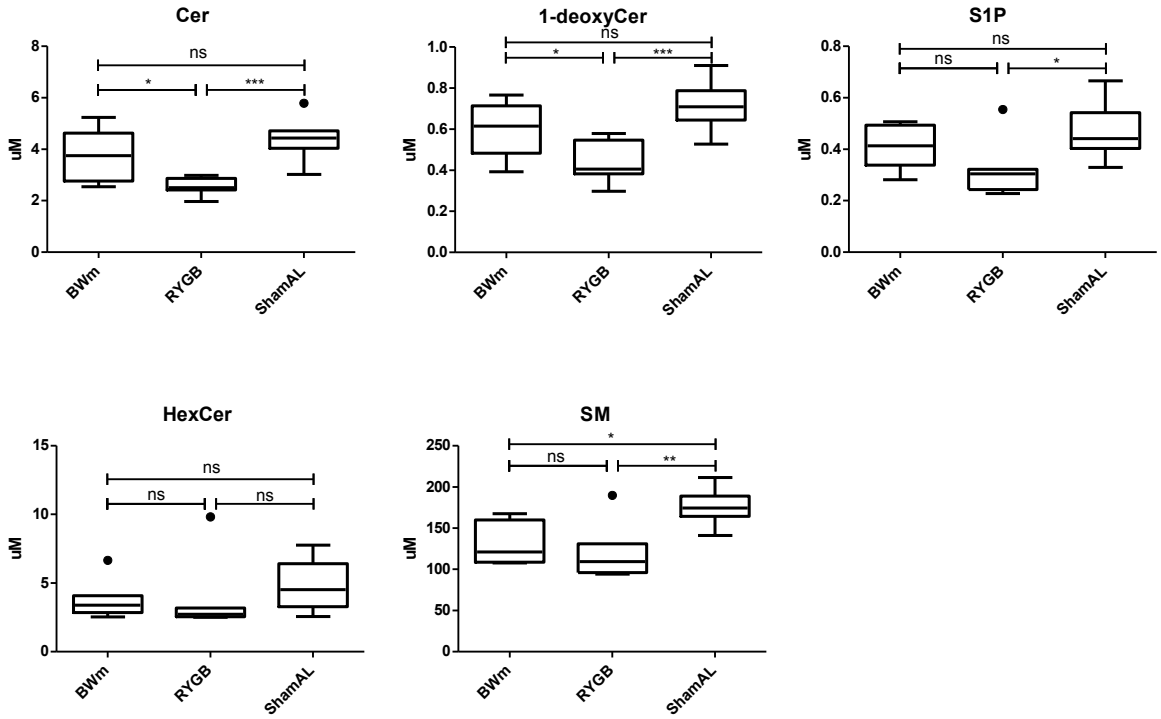


Figure 5-3: Sphingolipid profiles in mice after bariatric surgery. ANOVA statistical test was performed to check for differences. ***= p<0.001, **= p<0.001, *= p<0.05, ns = not significant. Cer: Ceramides, doxCer: 1-deoxyCeramides, S1P: Sphingosine-1-phosphate, HexCer: hexosylCeramides, SM: Sphingomyelin

The individual sphingolipid classes were calculated by summing up all the particular sphingolipid species belonging to each class (Figure 5-3). Compared to ShamAL group, Ceramides, 1-deoxyceramides, S1P and sphingomyelin, were significantly lower in the RYGB group. In contrast, hexosylceramides were not significantly different between these

two groups. Compared to the BWm group, only ceramides and 1-deoxyceramides were significantly reduced in the RYGB treated animals. If BWm group is compared to ShamAL, there was no significant reduction in ceramides seen.

From previous studies it is known that high-fat diet and obesity enhances the *de novo* sphingolipid metabolism [17]. Therefore, ShamAL mice on high fat diet were expected to have elevated sphingolipid levels. Here we showed, that gastric bypass has a significant effect on sphingolipid profiles in mice. The ceramide and 1-deoxyceramide levels are significantly lowered in mice, which underwent a gastric bypass surgery compared to the body weight-matched group, but also to the group without food restriction. However, ceramide levels are not changed with food restriction. Therefore, these changes in sphingolipid profile is not due to weight loss only, but specifically due to effect of gastric bypass surgery. Possibly, these changes in sphingolipid metabolism are responsible for the better metabolic outcomes of this surgical procedure compared to weight loss only [18]. Also in a human study done by Kayser et al., patients who underwent RYGB surgery, showed a change in sphingolipid profile [18]. Therefore, the benefit of RYGB surgery is to reverse the increase of sphingolipids due to high fat diet, which could not be seen with weight loss only.

## 5.3 Sphingolipidomics in ORMDL3 knock out mice

*In collaboration with Nincy Debeuf and Sophie Janssens, Gent University*

Author contribution: Steiner R did the sphingolipid analysis.

In yeast, ORM 1 and ORM 2 proteins are negative regulators of serine palmitoyl-transferase (SPT) which regulates *de novo* sphingolipid synthesis in response to multiple metabolic signals [19, 20]. Human genome encodes three proteins, ORMDL1-3, that share a significant sequence homology to the yeast ORM proteins. More importantly, genome-wide association studies (GWAS) identified single nucleotide polymorphisms at the ORMDL1-3 loci, which alter expression of these three genes. They have been shown to be strongly linked with the development of asthma in multiple ethnic populations [21-24]. These reports led to the hypothesis that perturbations in sphingolipid metabolism might be directly implicated in the development of asthma in humans. However, whether mammal orthologues ORMDL1-3 are also involved in SPT regulation is still a matter of debate [25-28], and the effect of ORMDL associated SNPs on SPT activity and its link to asthma remain unclear as well [29]. Ormdl3-knockout (Ormdl32/2) and transgenic (Ormdl3Tg/wt) mice were generated by collaborators at Gent University to study the role of ORMDL3 in the development of asthma and its role in the sphingolipid metabolism in general. The effect of ORMDL3 knockout and over-expression on sphingolipid levels was analysed in detail by quantification of sphingolipid profiles from plasma and mice tissues including lung, liver, white and brown adipose tissue as well as bronchial lavage fluid (BAL) [28]. Additionally, mice underwent asthmatic sensitization through exposure to house dust mite (HDM). HDM fecal pellets of *Dermatophagoides pteronyssinus* contain various allergens that belong to the major triggers of allergic asthma worldwide. This has led to the development of a clinically relevant mouse model based on the inhalation of HDM extracts to study the molecular mechanisms of allergic sensitization. In a first step, mice were sensitized (intra-tracheal treatment) with house dust mite (HDM) whereas control mice just received PBS treatment. Six to ten days after sensitization, mice were challenged again to reach the acute phase. Only the HDM sensitized mice develop asthma, whereas the PBS sensitized ones did not [30]. Mice were sacrificed after 14 days and lung, liver, white

adipose and brown adipose tissue were homogenized using 0.1 % Triton (TX100). The tissue was extracted at 4 °C for 1 hour and the insoluble debris was pelleted at 16000 rpm. The protein content of these lysates was determined using the Bradford protein assay. A lipidomics profiling was done in 20 µL mouse plasma, 20 µL of bronchial lavage fluid (BAL) or 20 µg of homogenate from each mouse tissue (lung, liver, white adipose and brown adipose tissue). The samples were extracted using the MMC protocol as described in 4.3.5. $D_7$-sphinganine, $D_7$-sphingosine, Cer d18:0 / 12:0, Cer d18:1 / 12:0, 1-deoxyCer m18:0 / 12:0, 1-deoxyCer m18:1 / 12:0, SM d18:1 / 12:0, GluCer d18:1 / 8:0, $D_7$-S1P, PA 17:0 / 17:0, PE 14:0 / 14:0, LPE 17:1, PG 17:0 / 17:0, PC 14:0 / 14:0, PC 24:0 / 24:0, LPC 17:0 were used as the internal standards. The C18-column-based method for chromatographic separation and MS analysis was used, as described in 3.3.1 and 4.3.2.

The individual sphingolipid groups were calculated by summing up all the particular sphingolipid species belonging to each group. The levels were compared between ORMDL3 knockout, ORMDL3 transgenic and wild-type animals with and without asthmatic challenge.

In general, sphingolipids were increased in the ORMDL3 knock out animals and decreased in the transgenic ORMDL3 overexpressing mice, but this was significantly different neither for all the different tissues nor between the asthmatic or non-asthmatic challenged groups. The most significant effect of ORMDL3 knock-out on sphingolipid levels was observed in plasma, followed by liver and the adipose tissues. In plasma, we observed a significant increase in ceramides and sphingomyelin levels for KO mice, whereas the Tg mice showed a significant decrease compared to the wild-type animals. Hexosylceramides, 1-deoxyceramides, and S1P followed the same trend in plasma (Figure 5-4). We also observed a similar increase in the liver derived tissue lysates although the increase was not as prominent and not significant (Figure 5-5). Interestingly, there was no significant change in sphingolipids seen in lung tissues (Figure 5-6) and BAL fluid (Figure 5-7).

In adipose tissues (BAT, Figure 5-8 and WAT, Figure 5-9), sphingomyelin and hexosylceramide as well as ceramides and S1P were not altered. However, 1-

deoxyceramides were increased in both BAT and WAT of ORMDL3 knockout mice, independently of the treatment with HDM, as they increased to the same extent in both the asthmatic and non-asthmatic mice. This elevation in 1-deoxyceramides is unusual, as in the adipose tissue, 1-deoxyceramides but not canonical ceramide levels increased whereas in the other tissues, ceramides and 1-deoxyceramides increased in parallel. This suggests, that 1-deoxysphingolipids were either formed more pronounced in adipose tissue compared to other tissues, or, that they accumulated in the fat tissue and therefore do not correlate anymore with canonical sphingolipid levels. Our data indicates that ORMDL3 expression in mice has a tissue specific function that alters lipids profiles differently in various tissues. It seems that ORMDL3 protein affects sphingolipid metabolism or regulation, and its deletion leads to an increase in sphingolipid levels whereas the overexpression leads to a decrease.

Previous studies which measured hydrolyzed sphingolipid profiles did not observe any general effect on sphingolipid levels ($C_{18}$ sphinganine (SA) and $C_{18}$ sphingosine (SO)), with the exception of small but significant increase in SA in ORMDL3 KO mice [28]. This could be due to the fact that overall sphingolipids in ORMDL3 knockout mice are generally similar to wild type mice and the hydrolysis method that cleaves sphingoid bases from all the sphingolipids thus masks the differences in ceramide levels, which arise as a result of loss in ORMDL3 function. This points to the possibility that ORMDL3 integrates the synthesis or levels of ceramides thus acting downstream of the SPT enzyme. This view is further corroborated by the fact that others and we have observed increased S1P levels in the plasma of ORMDL3 KO mice whereas these levels decrease in the transgenic mice (Figure 5-4 and Miller et al. [31]).

Additionally, it has been show that decreasing ORMDL3 expression in mammalian cells increased ceramide levels and whereas, modest increases in ORMDL3 expression decrease ceramide levels by reducing *de novo* synthesis [32]. However, high ORMDL3 levels had the opposite effect and significantly increased ceramide levels. This increase was mainly due to increased salvage/recycling of sphingolipids to ceramide and not to *de novo* biosynthesis [32].

Similarly, downregulation or overexpression of ORMDL3 in HEK293 cells alone did not affect ceramide levels, or the *de novo* biosynthesis [25, 28].

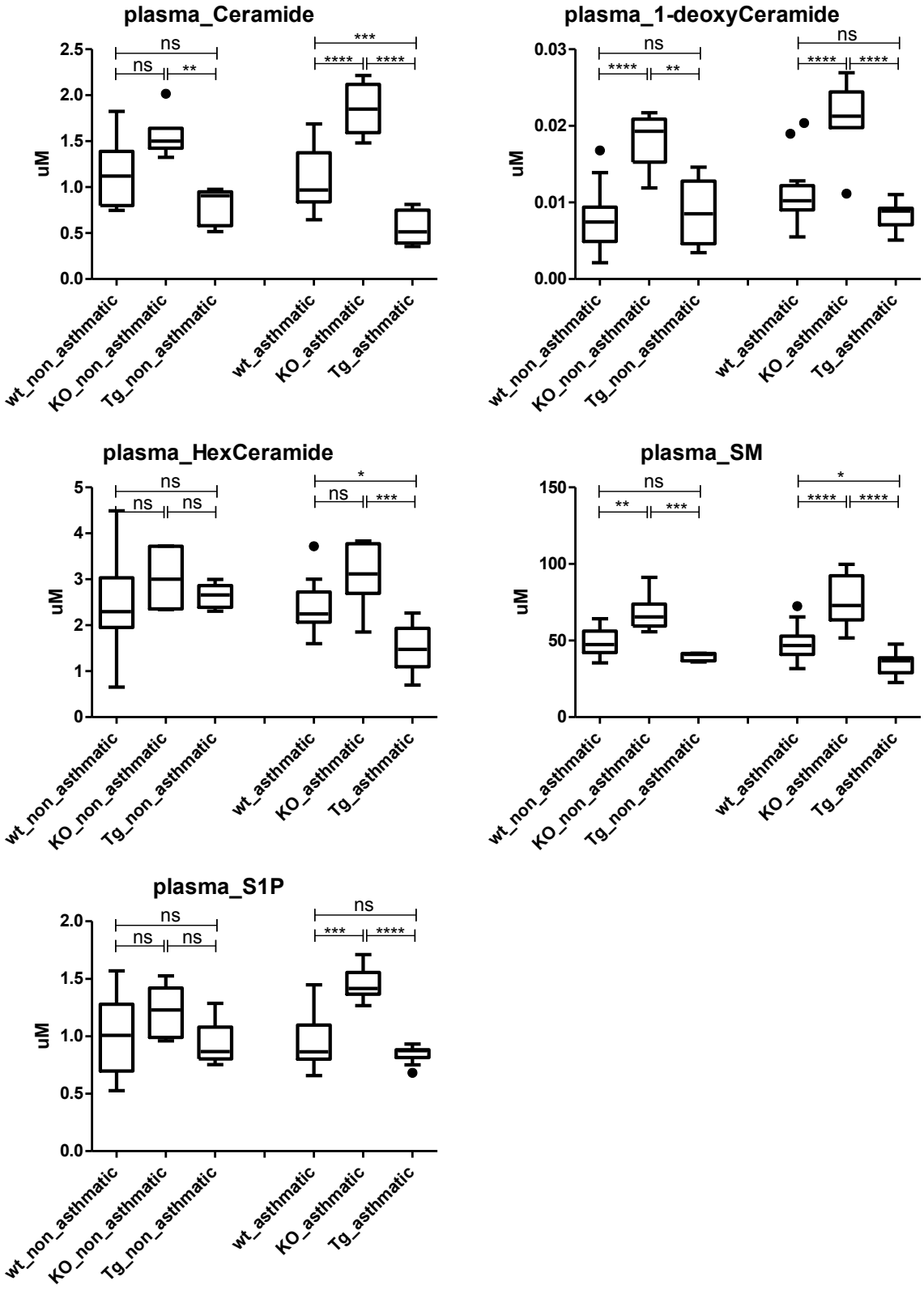


Figure 5-4: Sphingolipid profile in plasma of Ormdl3 (KO) and transgenic (Tg) mice compared to wild-type (wt) littermates. Mice were sacrificed without any asthmatic challenge or after exposure to house dust mite (HDM), which is considered as a model for allergic asthma. ANOVA statistical test was performed to check for differences. ***= p<0.001, **= p<0.01, *= p<0.05, ns = no significance.

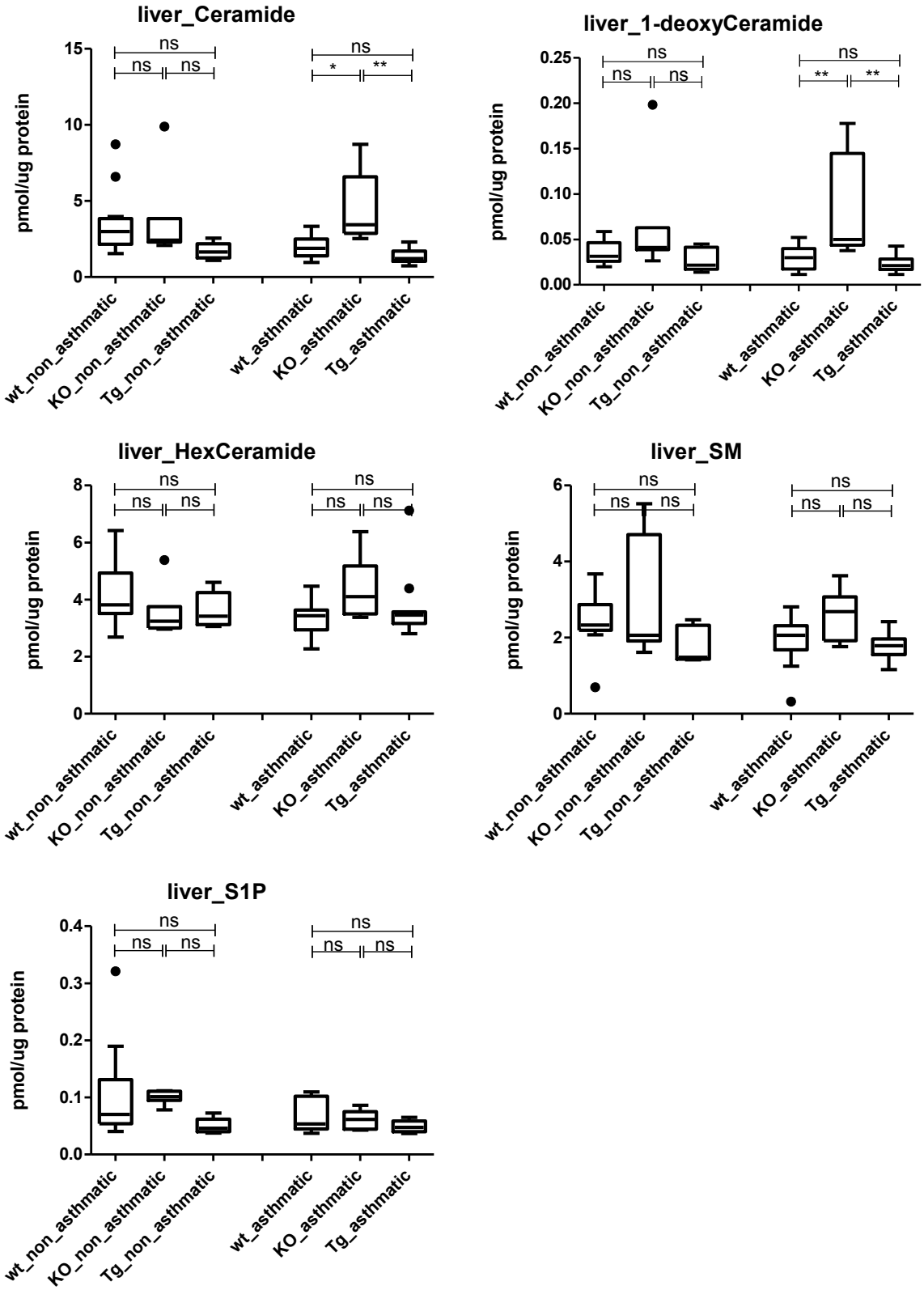


Figure 5-5: Sphingolipid profile in liver tissue of Ormdl3 (KO) and transgenic (Tg) mice compared to wild-type (wt) littermates. Mice were sacrificed without any asthmatic challenge or after exposure to house dust mite (HDM), which is considered as a model for allergic asthma. ANOVA statistical test was performed to check for differences. ***= p<0.001, **= p<0.01, *= p<0.05, ns = no significance.

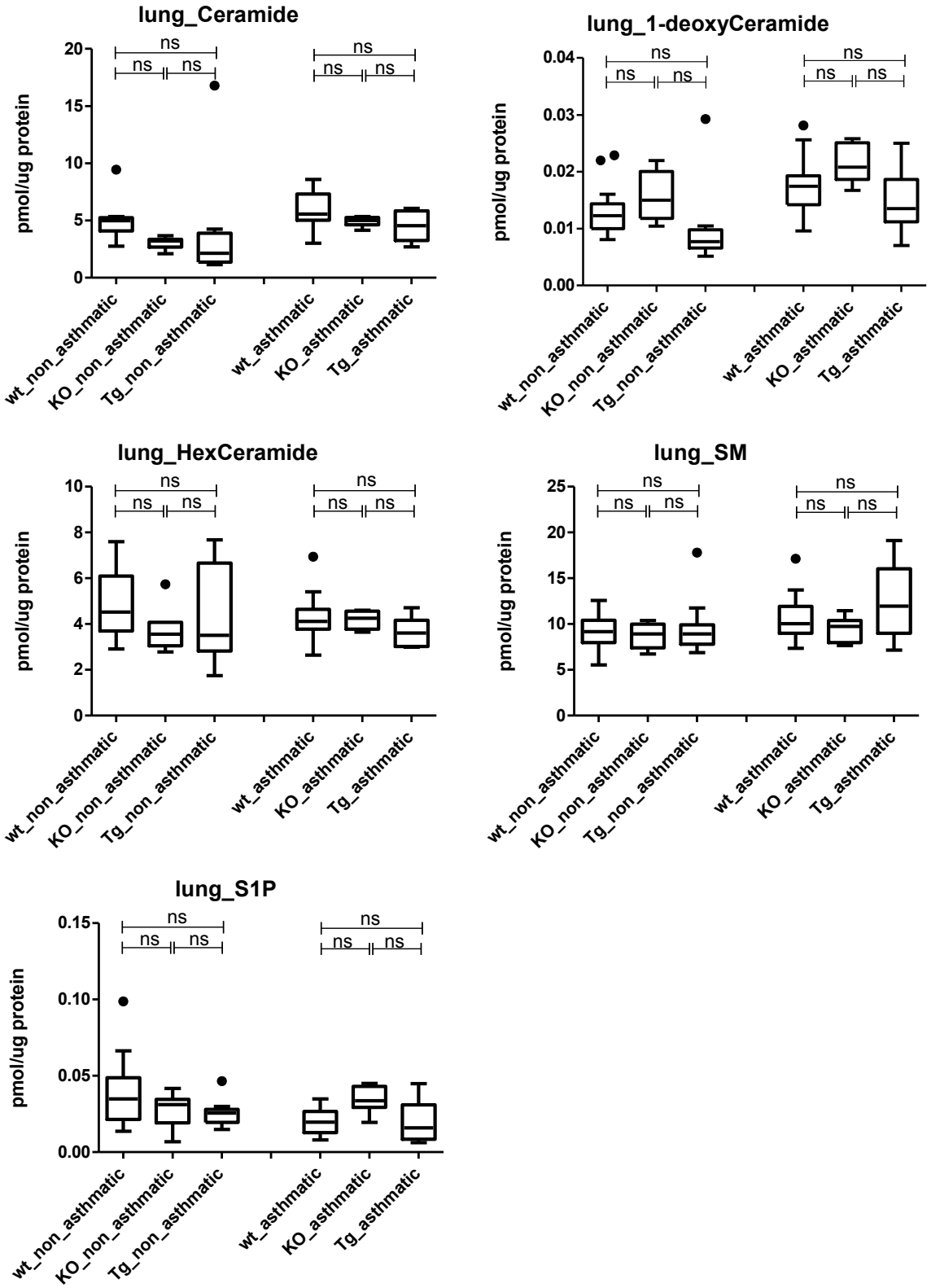


Figure 5-6: Sphingolipid profile in lung tissue of Ormdl3 (KO) and transgenic (Tg) mice compared to wild-type (wt) littermates. Mice were sacrificed without any asthmatic challenge or after exposure to house dust mite (HDM), which is considered as a model for allergic asthma. ANOVA statistical test was performed to check for differences. ***= p<0.001, **= p<0.01, *= p<0.05, ns = no significance.

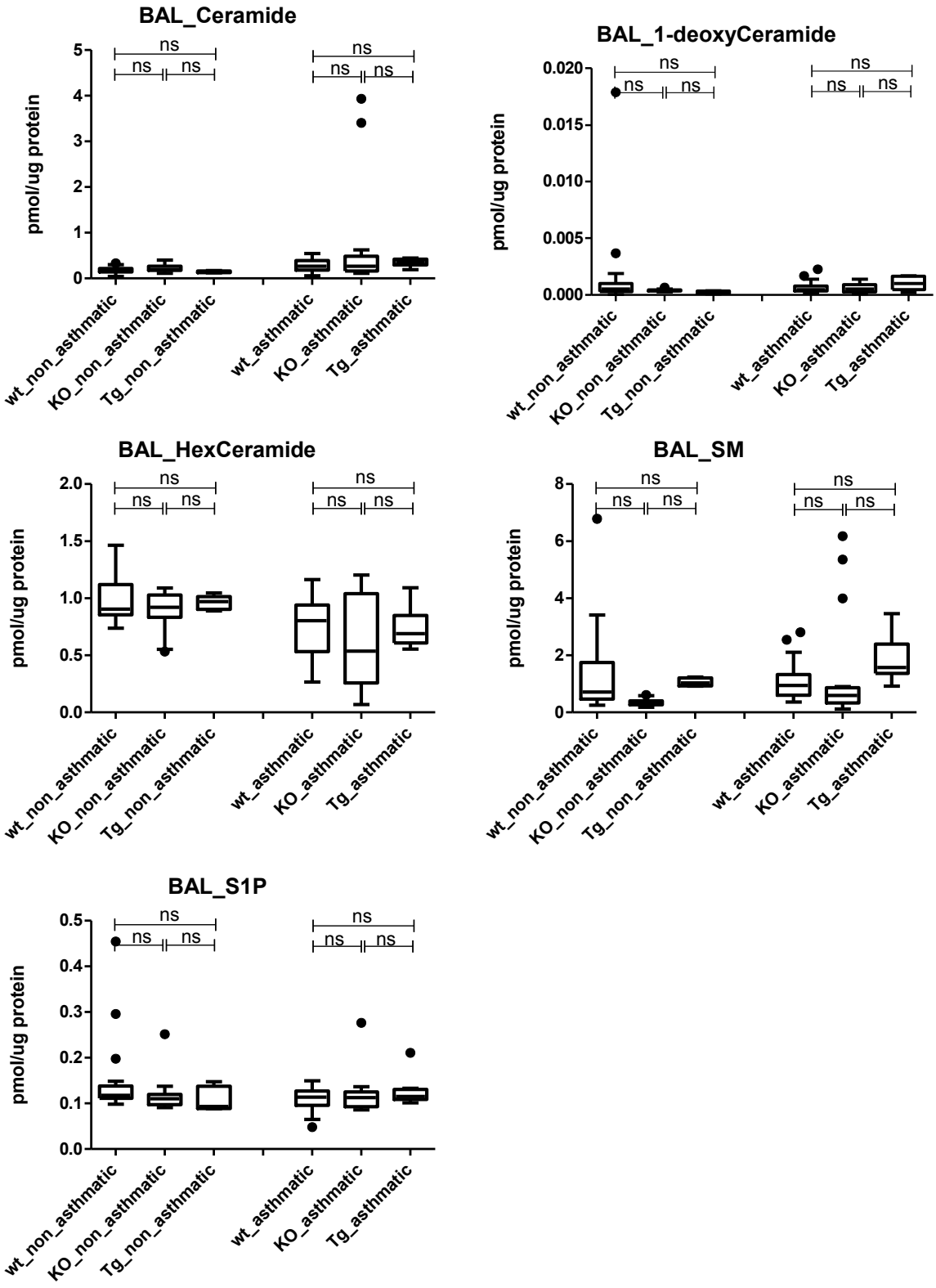


Figure 5-7: Sphingolipid profile in BAL fluid of Ormdl3 (KO) and transgenic (Tg) mice compared to wild-type (wt) littermates. Mice were sacrificed without any asthmatic challenge or after exposure to house dust mite (HDM), which is considered as a model for allergic asthma. ANOVA statistical test was performed to check for differences. ***= p<0.001, **= p<0.01, *= p<0.05, ns = no significance.

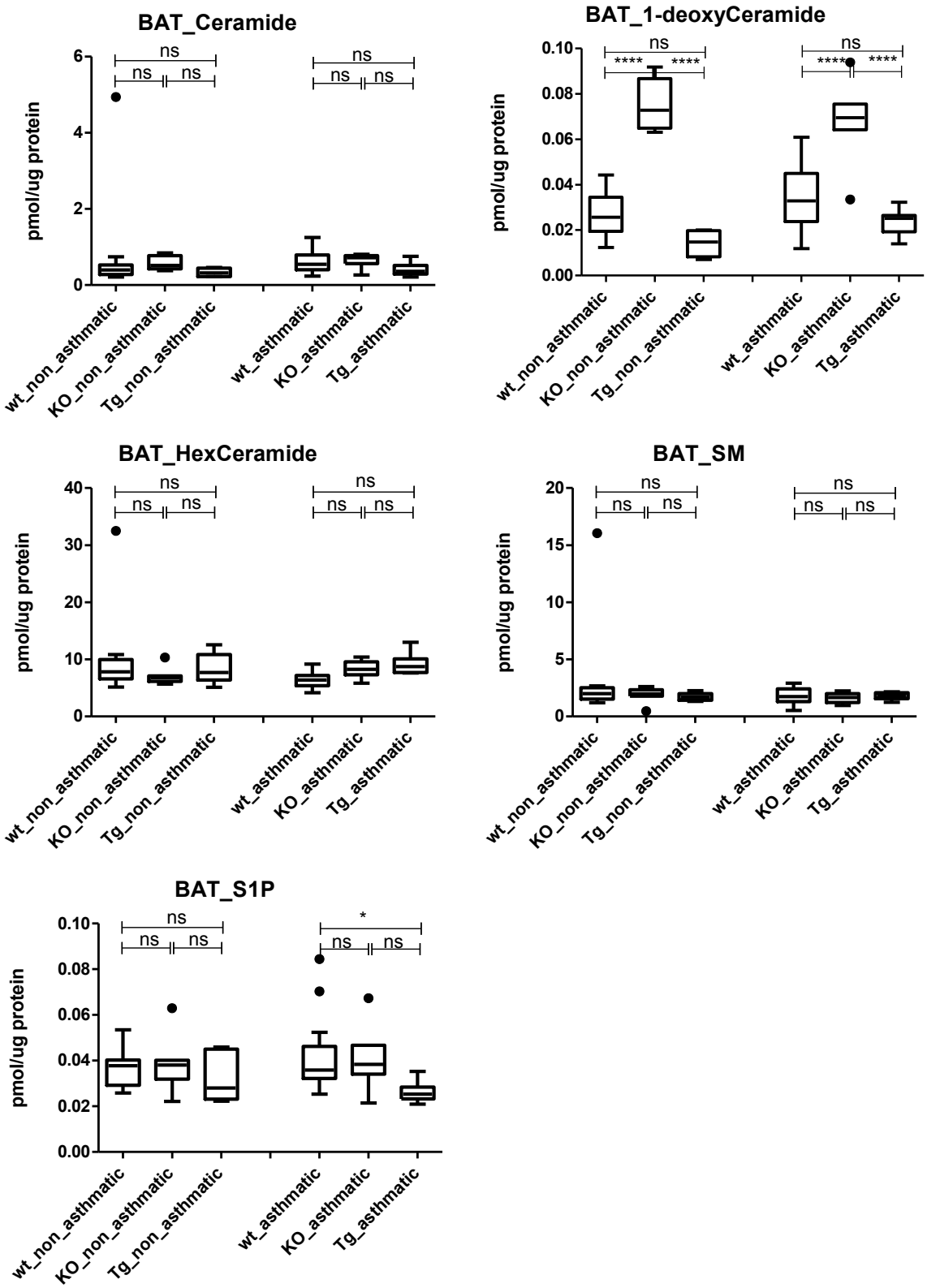


Figure 5-8: Sphingolipid profile in Brown adipose tissue (BAT) of Ormdl3 (KO) and transgenic (Tg) mice compared to wild-type (wt) littermates. Mice were sacrificed without any asthmatic challenge or after exposure to house dust mite (HDM), which is considered as a model for allergic asthma. ANOVA statistical test was performed to check for differences. ***= p<0.001, **= p<0.01, *= p<0.05, ns = no significance.

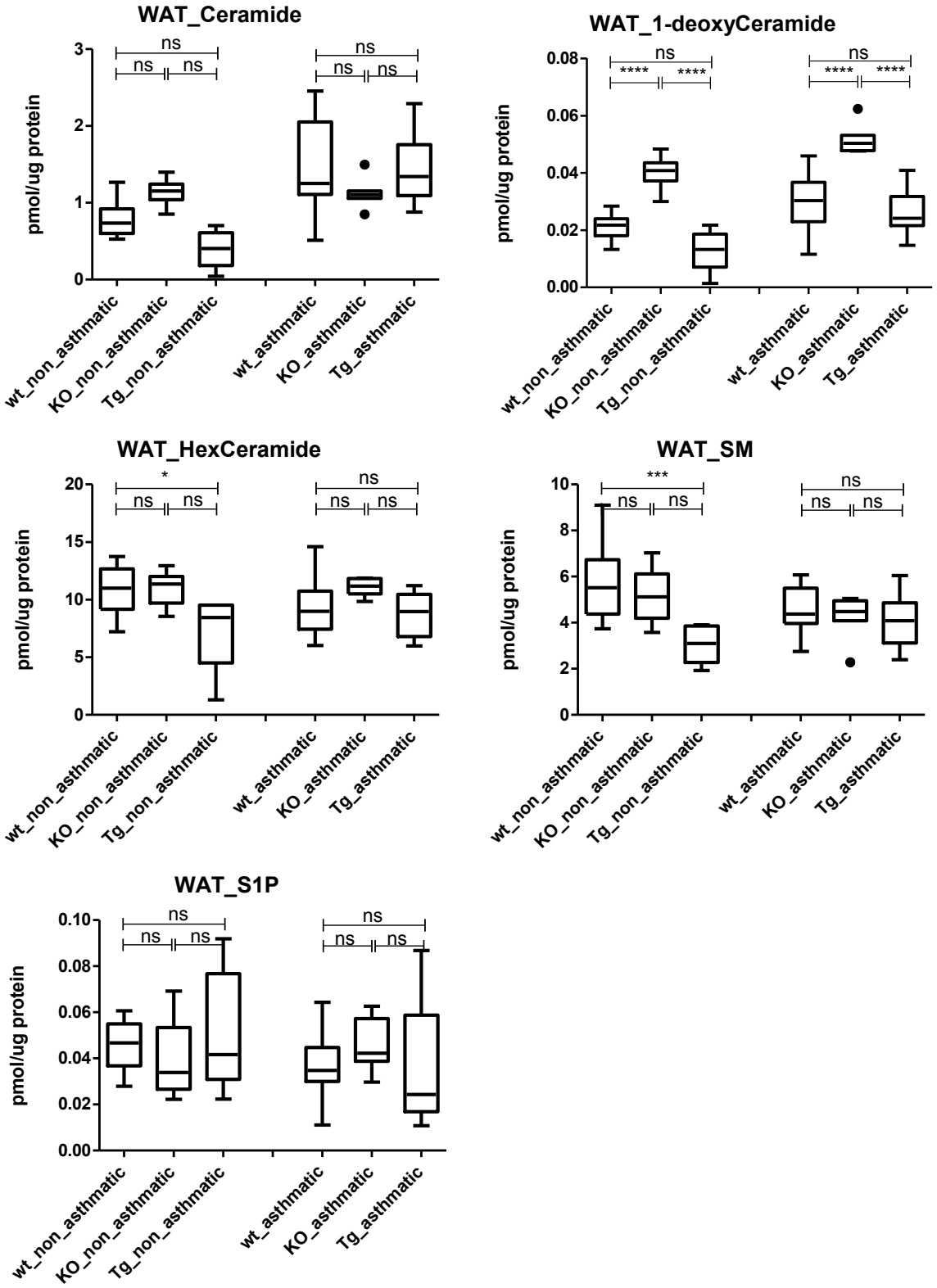


Figure 5-9: Sphingolipid profile in white adipose tissue (WAT) of Ormdl3 (KO) and transgenic (Tg) mice compared to wild-type (wt) littermates. Mice were sacrificed without any asthmatic challenge or after exposure to house dust mite (HDM), which is considered as a model for allergic asthma. ANOVA statistical test was performed to check for differences. ***= p<0.001, **= p<0.01, *= p<0.05, ns = no significance.

## 5.4 Lipidomics in mice with Abca1 and Abcg1 knock out in retina

*In collaboration with Federica Storti and Christian Grimm, Ophthalmology Department, University of Zurich*

Author contribution: Steiner R did the lipid analysis in the eye tissue.

Age-related macula degeneration (AMD) is caused by the accumulation of extracellular deposits known as drusen [33, 34]. Lipids and apo-lipoproteins accumulate with age on both sides of the retinal pigment epithelium (RPE) and form extracellular deposits associated with AMD. This process eventually destroys RPE cells and photoreceptors, which finally results in a progressive loss of vision and blindness [33]. Genes involved in the lipoprotein metabolism (ABCA1, APOE, CETP, LIPC) are genetically linked to AMD [35]. The RPE handles enormous amounts of lipids every day coming from the phagocytosis of the outer segments of photoreceptors. It, therefore, relies on efficient lipid metabolism, that coordinates both synthesis and turnover of the involved lipids. Lipids, such as cholesterol and phospholipids are abundant components of drusen [36]. Since ABCA1 and its partner ABCG1 mediate lipid efflux [37], the function of the ABCA1/G1 pathway in the RPE was investigated using a tissue-specific knockout (KO) mouse model. RPE-specific ABCA1-ABCG1 double KO mice were generated to investigate possible functional consequences for the retina in vivo [38, 39].

Already at six weeks of age, the RPE of KO mice was filled with lipid droplets, as seen by light and electron microscopy and Oil Red O staining. With age (>8 months) photoreceptors started to degenerate. To investigate the effect of the lack of the two genes in the RPE in the lipid profile, the lipidome of retinal tissue from ABCA1/G1 knock out mice to wild-type mice was compared.

ABCA1 and ABCG1 gene were selectively knocked out in retinal pigment epithelium (RPE) tissue in mice. Four KO mice and six WT controls were included. For each animal, neural retina, RPE, and remaining posterior eyecup were collected from the two pooled eyes. For preparation of protein lysates, tissues were homogenized using 0.1 % Triton (TX100). The tissue was extracted at 4 °C for one hour and the resulting lysate centrifuged at 16000 rpm for 5 min. 25 µg of RPE protein lysate and posterior eye cup and 50 µg of the neural retina

were transferred into a 2 mL Eppendorf tube. Tissue lysates were extracted using the MMC protocol described in 4.3.5. $D_7$-sphinganine, $D_7$-sphingosine, Cer d18:0 / 12:0, Cer d18:1 / 12:0, 1-deoxyCer m18:0 / 12:0, 1-deoxyCer m18:1 / 12:0, SM d18:1 / 12:0, GluCer d18:1 / 8:0, $D_7$-S1P, PA 17:0 / 17:0, PE 14:0 / 14:0, LPE 17:1, PG 17:0 / 17:0, PC 14:0 / 14:0, PC 24:0 / 24:0, LPC 17:0, $D_7$-cholesterol, $D_7$-CE 16:0 were used as the internal standards. For each analysis, a quality control series was prepared as described in 4.3.8. For LC-MS analysis, the C30-column-based method was used as described in 3.3.1 and 4.3.2.

To evaluate more comprehensively the types of lipids altered in the KO tissue, eye-specific retinyl esters were quantified in addition to the sphingolipids and cholesterol. Retinyl esters are part of the retinoid cycle, which is essential for photoreceptor function. 11-*cis*-retinal is a chromophore in the photoreceptor, which is converted to all-*trans*-retinal by the absorption of a photon of light through photo isomerization. All-*trans*-retinal is reduced to all-*trans*-retinol which diffuses into the RPE where it is esterified. These retinyl esters are stored in lipid droplet-like structures called retinosomes to prevent aggregation. The all-*trans*-retinyl esters are reconverted to 11-*cis*-retinol, which are then further oxidized to 11-*cis*-retinal in the RPE. 11-*cis*-retinal diffuses back into the photoreceptors [40]. Therefore, it was interesting to see, if the concentration of retinyl esters is also altered in ADM.

The linearity of the analysis of retinyl esters was confirmed with retinyl palmitate in a range between 2 nM and 2 µM (2, 20, 200 and 2000 nM).

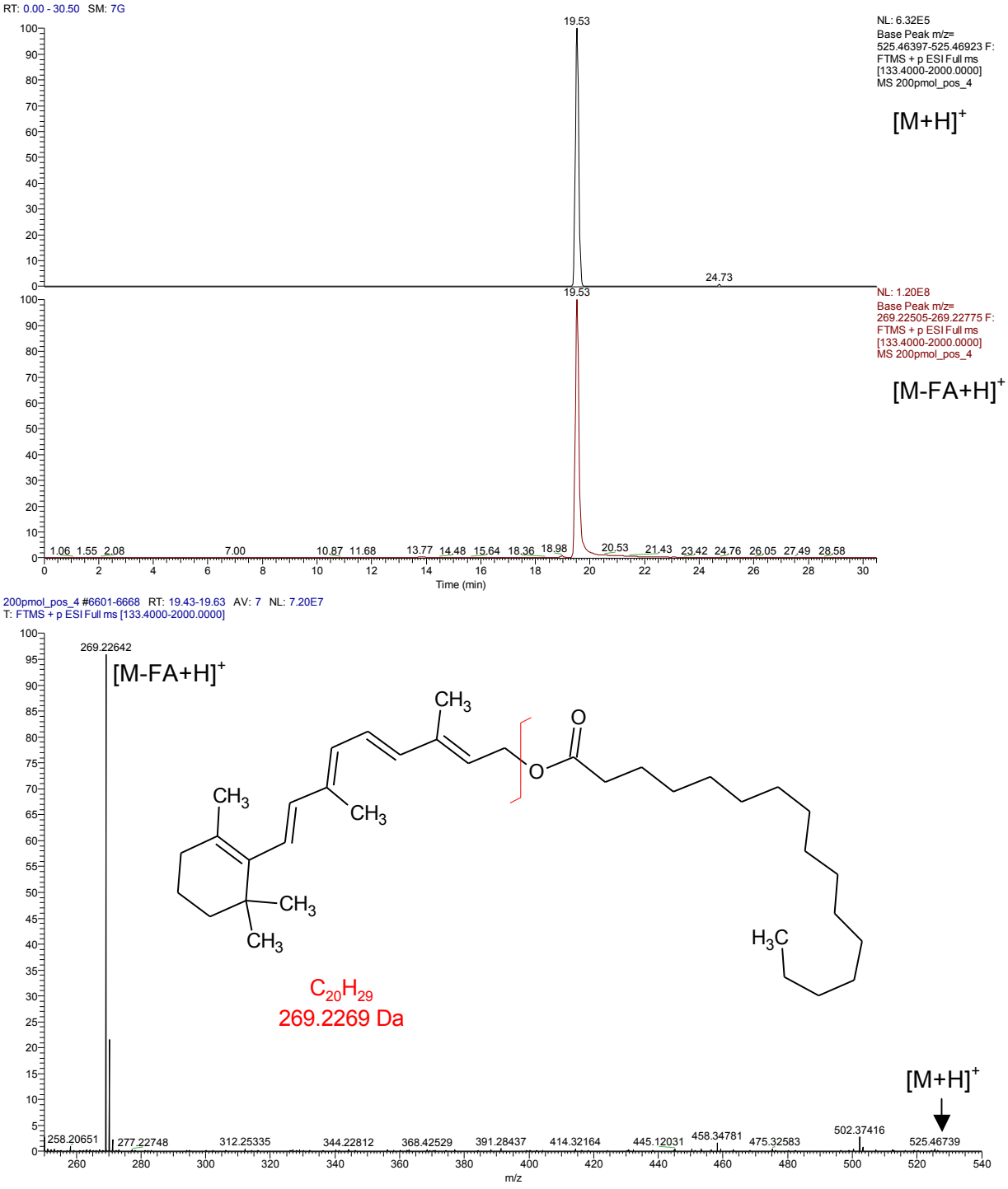


Figure 5-10: Retinyl palmitate with the fragment 269.2 caused by the loss of the fatty acid with in-source fragmentation.

Retinyl palmitate shows a significant in-source fragmentation losing the esterified fatty acid during ionization. The full mass ion was around 0.5 % (5.5 $e^6$ compared to 1.1 $e^9$ for 2 µM sample) of the total retinol. The chromatogram and fragmentation pattern is shown in Figure 5-10. Linearity was checked for the full mass $[M+H]^+$ ion, but also for the retinol-fragment

$[M\text{-}FA+H]^+$. Both showed a linear correlation between the concentration of the standard and the peak area.

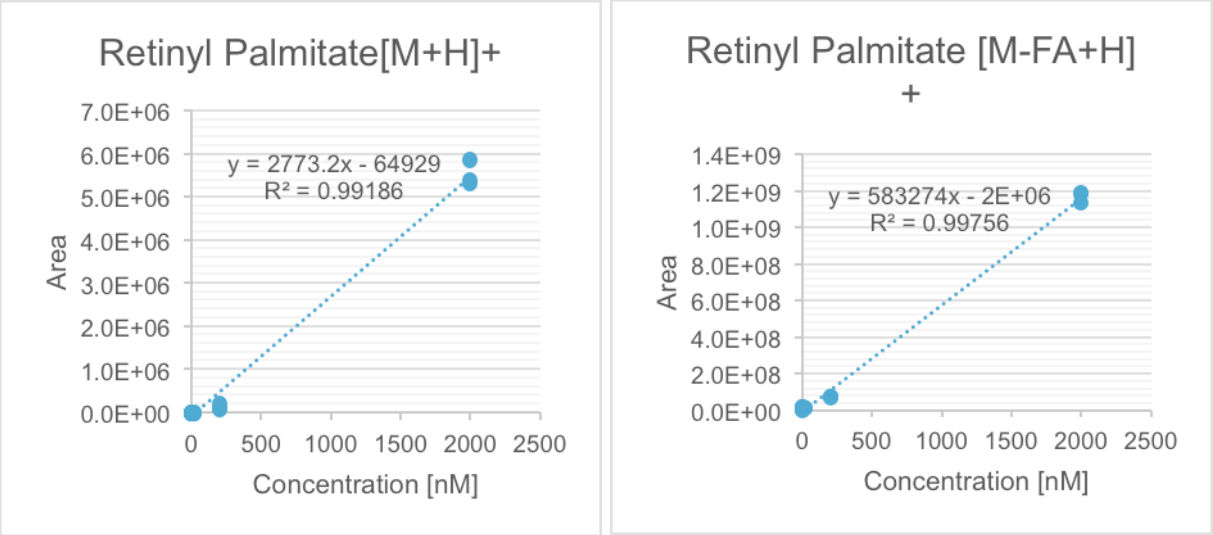


Figure 5-11: Linearity of retinyl palmitate. A: Quantification based on the full mass of retinyl palmitate on $[M+H]^+$ ion. B: Quantification based $[M\text{-}FA+H]^+$ because of ion-source fragmentation.

Free retinol and retinyl esters were analyzed in eye tissues. Due to the massive in-source fragmentation, total retinyl esters were quantified using the retinyl fragment with the mass of 269.2 Da. Because of missing internal standard, free retinol and retinyl esters were correlated to $D_7$-cholesteryl ester 16:0 the internal standard. Therefore, values are reported as the ratio of the area of free retinol or retinyl ester to the internal standard.

Cholesterol and cholesteryl ester were significantly elevated in all analyzed tissues of the ABCA1 and ABCG1 knock out mice (Figure 5-12 ). Retinyl esters (Figure 13) were significantly elevated in all tissues (retina, RPE and PEC) whereas free retinol was only elevated in RPE tissue (Figure 5-13). The most prominent change was seen in RPE tissue, which was expected as the knockout of ABCA1 and ABCG1 was RPE specific. The elevated lipid level in the retina, but also in the posterior eye-cup tissue can be explained by the incomplete separation of the three eye tissues during sample preparation. Therefore, the elevated level of cholesteryl esters in retina and posterior eye-cup might be from contamination of RPE tissue. There was no difference in the sphingolipid profile between wind type and knockout tissue (Figure 5-14).

There was a significant change in cholesteryl ester in all eye tissues of mice with ABCA1 and ABCG1 deletion in the retinal pigment epithelium. Also, retinyl esters were changed in RPE tissue. By contrast, sphingolipids were not altered by the knockout of ABCA1 and ABCG1. Cholesteryl ester accumulation probaby happens secondary to impaired cholesterol efflux and hence increased intracellualr levels of free cholesterol in the ABCA1 and ABCG1 deficient cells. To prevent ER stress and apoptosis induced by free cholesterol cells actuivate the cholesterol esterifiction by ACAT.

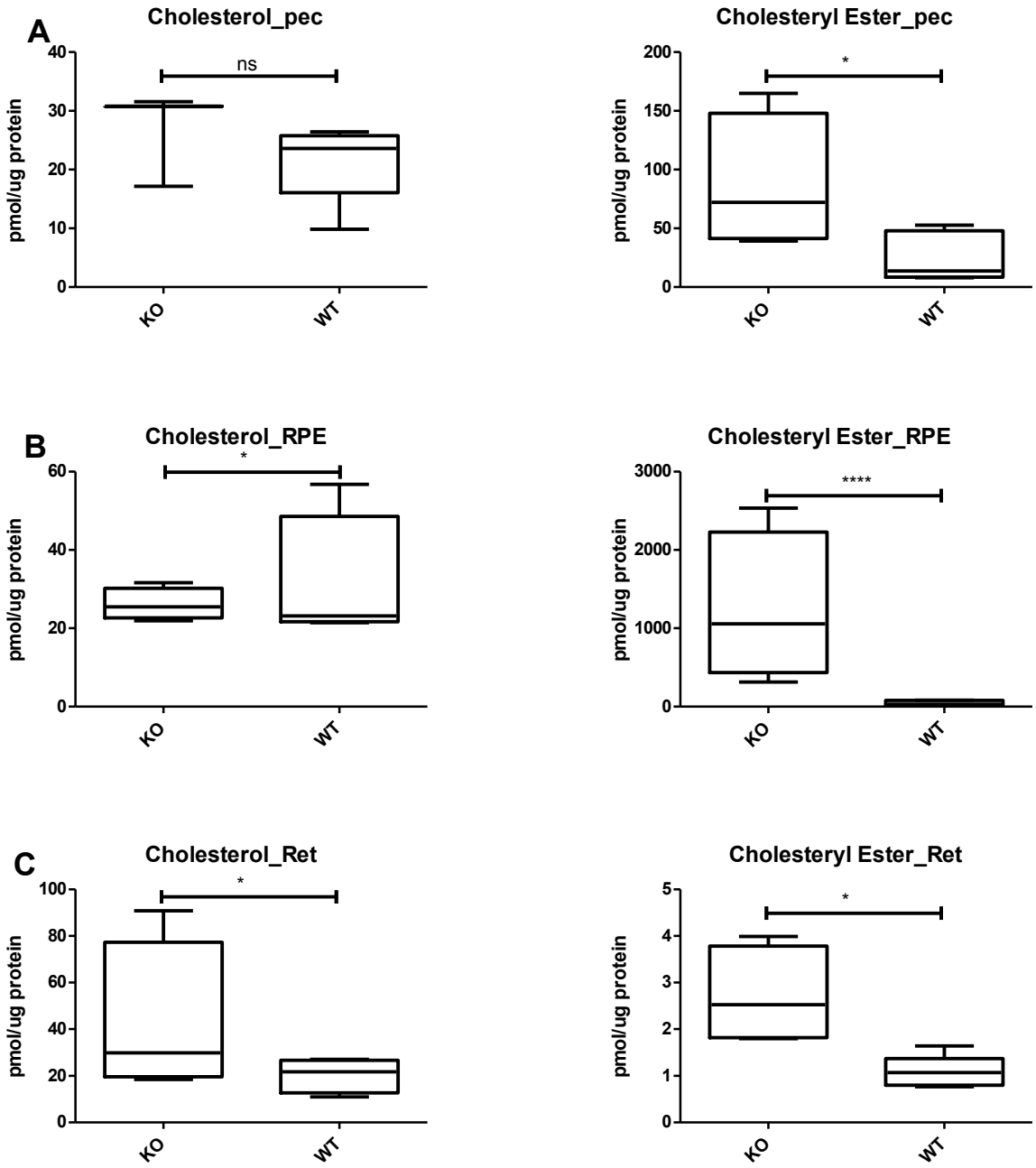


Figure 5-12: Free Cholesterol and cholesteryl esters were analyzed in A: posterior eye cup samples, B: RPE and C: neutral retina. Statistical significance was calculated using two-tailed *t*-test, where ***= p<0.001, **= p<0.001, *= p<0.05, ns = not significant.

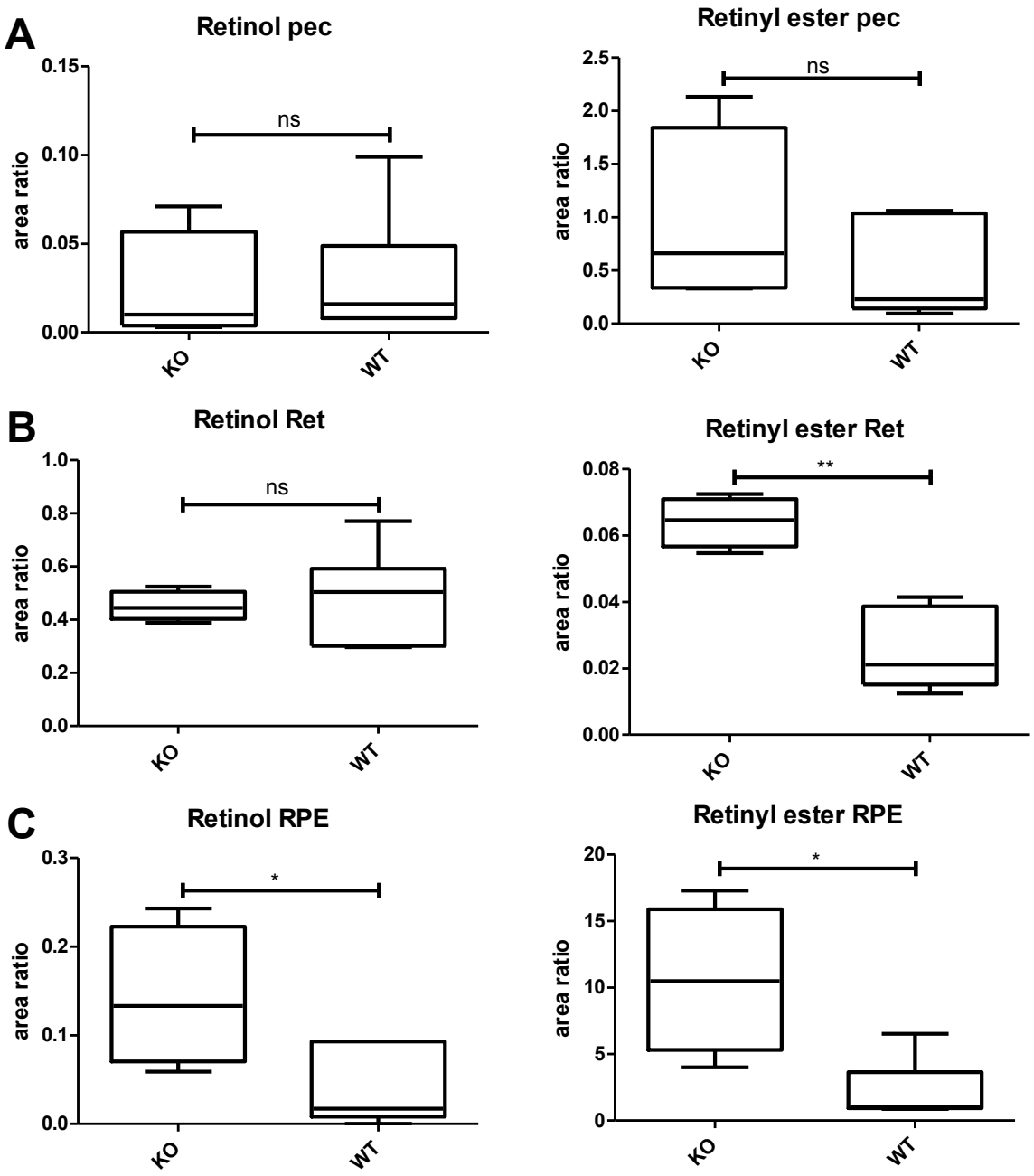


Figure 5-13: Free retinol and retinyl ester were analyzed in A: posterior eyecup samples, B: neutral retina and C: RPE. Statistical significance was calculated using two-tailed non-parametric *t*-test, where ***= p<0.001, **= p<0.001, *= p<0.05, ns = no significance.

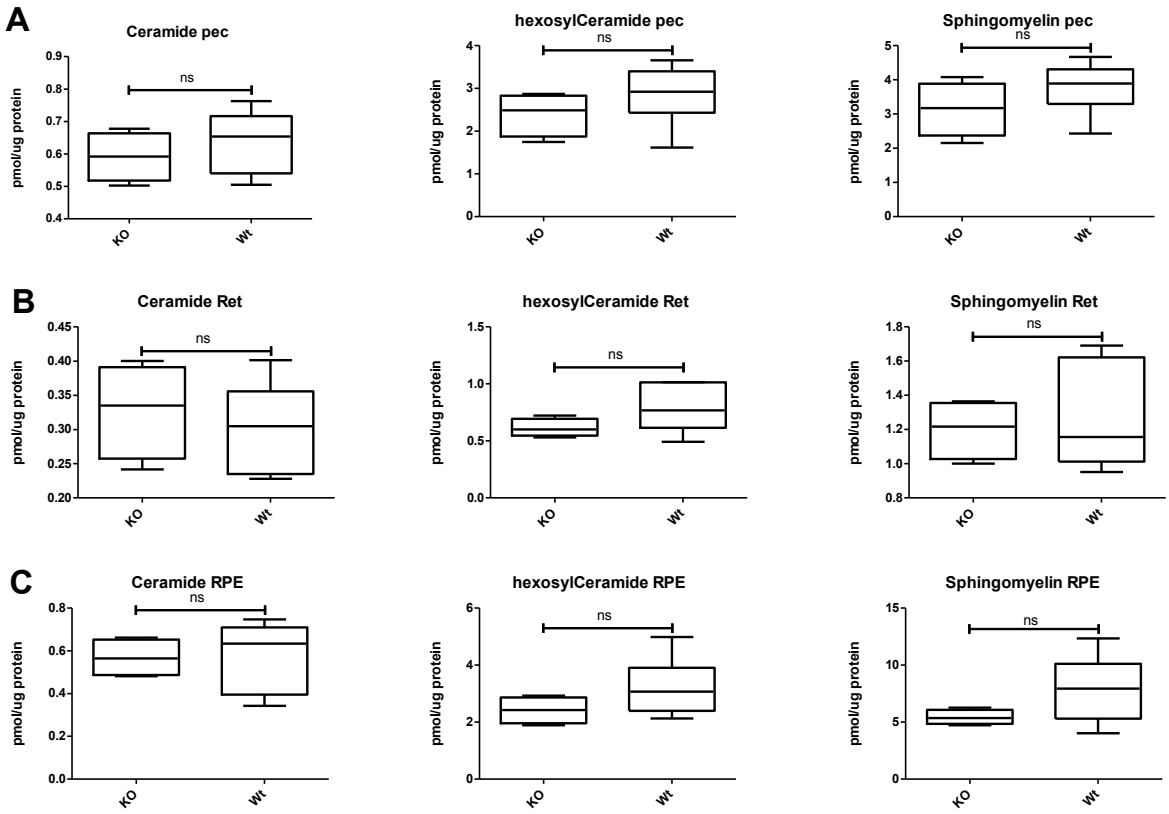


Figure 5-14: Sphingolipid classes were analyzed in A: posterior eyecup samples, B: neutral retina and C: RPE. Statistical significance was calculated using two-tailed non-parametric t-test, where ***= p<0.001, **= p<0.001, *= p<0.05, ns = no significance.

These results support an important role of the ABCA1/G1 lipid pathway for the function of RPE, which in turn supports the retina function. RPE cells lacking ABCA1 and ABCG1 may not be able to manage the physiological lipid load coming from the photoreceptors. Over time, RPE cells with lipid accumulation undergo cell death with the consequent photoreceptors loss. This suggest that the ABCA1/G1 pathway might contribute to impaired lipid handling in the RPE of AMD patients.

## 5.5 Conclusion

Various diseases are linked to disorders in lipid metabolism. Therefore, a comprehensive lipid analysis is needed to determine changes in disease conditions, map pathway connections, evaluate treatment efficacy or search for and validate novel biomarkers. We were able to establish and validate a lipidomics method towards application to mammalian cells, tissues and plasma. Lipid profiles were identified within a broad set of samples, involving plasma samples of tissues and cells humans and mice. With the measured lipid profiles, we supported the understanding of disease mechanisms in a neuropathy caused by rare mutations in association with sphingosine-1-phosphate lyase and in a mouse model of AMD, got more insight into the regulation of sphingolipid metabolism by ORMD3, and unravelled novel effects of gastric bypass surgery.

This method, therefore, offers a tool to analyse lipid profiles in a high throughput setting for many research questions.

## 5.6 References

[1] Atkinson, D, Nikodinovic Glumac, J, Asselbergh, B, et al., Sphingosine 1-phosphate lyase deficiency causes Charcot-Marie-Tooth neuropathy, Neurology, 2017;88:533-542.
[2] Serra, M and Saba, JD, Sphingosine 1-phosphate lyase, a key regulator of sphingosine 1-phosphate signaling and function, Adv Enzyme Regul, 2010;50:349-362.
[3] Othman, A, Rütti, MF, Ernst, D, et al., Plasma deoxysphingolipids: a novel class of biomarkers for the metabolic syndrome?, Diabetologia, 2012;55:421–431.
[4] Othman, A, Benghozi, R, Alecu, I, et al., Fenofibrate lowers atypical sphingolipids in plasma of dyslipidemic patients: A novel approach for treating diabetic neuropathy?, Journal of clinical lipidology, 2015;9:568-575.
[5] Steiner, R, Saied, EM, Othman, A, et al., Elucidating the chemical structure of native 1-deoxysphingosine, J Lipid Res, 2016;57:1194-1203.
[6] Janecke, AR, Xu, R, Steichen-Gersdorf, E, et al., Deficiency of the sphingosine-1-phosphate lyase SGPL1 is associated with congenital nephrotic syndrome and congenital adrenal calcifications, Hum Mutat, 2017;38:365-372.
[7] Prasad, R, Hadjidemetriou, I, Maharaj, A, et al., Sphingosine-1-phosphate lyase mutations cause primary adrenal insufficiency and steroid-resistant nephrotic syndrome, J Clin Invest, 2017;127:942-953.
[8] Lovric, S, Goncalves, S, Gee, HY, et al., Mutations in sphingosine-1-phosphate lyase cause nephrosis with ichthyosis and adrenal insufficiency, J Clin Invest, 2017;127:912-928.
[9] Kopelman, PG, Obesity as a medical problem, Nature, 2000;404:635-643.
[10] van den Hoek, AM, van der Hoorn, JW, Maas, AC, et al., APOE*3Leiden.CETP transgenic mice as model for pharmaceutical treatment of the metabolic syndrome, Diabetes Obes Metab, 2014;16:537-544.
[11] Scheen, AJ, De Flines, J, De Roover, A, et al., Bariatric surgery in patients with type 2 diabetes: benefits, risks, indications and perspectives, Diabetes Metab, 2009;35:537-543.
[12] Mokadem, M, Zechner, JF, Margolskee, RF, et al., Effects of Roux-en-Y gastric bypass on energy and glucose homeostasis are preserved in two mouse models of functional glucagon-like peptide-1 deficiency, Mol Metab, 2014;3:191-201.
[13] Osto, E, Doytcheva, P, Corteville, C, et al., Rapid and body weight-independent improvement of endothelial and high-density lipoprotein function after Roux-en-Y gastric bypass: role of glucagon-like peptide-1, Circulation, 2015;131:871-881.
[14] Ferrannini, E and Mingrone, G, Impact of different bariatric surgical procedures on insulin action and beta-cell function in type 2 diabetes, Diabetes Care, 2009;32:514-520.
[15] Letiexhe, MR, Desaive, C, Lefebvre, PJ, et al., Intact cross-talk between insulin secretion and insulin action after postgastroplasty recovery of ideal body weight in severely obese patients, Int J Obes Relat Metab Disord, 2004;28:821-823.
[16] van der Hoorn, JW, de Haan, W, Berbee, JF, et al., Niacin increases HDL by reducing hepatic expression and plasma levels of cholesteryl ester transfer protein in APOE*3Leiden.CETP mice, Arterioscler Thromb Vasc Biol, 2008;28:2016-2022.
[17] Choi, S and Snider, AJ, Sphingolipids in High Fat Diet and Obesity-Related Diseases, Mediators Inflamm, 2015;2015:520618.
[18] Kayser, BD, Lhomme, M, Dao, MC, et al., Serum lipidomics reveals early differential effects of gastric bypass compared with banding on phospholipids and sphingolipids independent of differences in weight loss, Int J Obes (Lond), 2017;41:917-925.
[19] Han, S, Lone, MA, Schneiter, R, et al., Orm1 and Orm2 are conserved endoplasmic reticulum membrane proteins regulating lipid homeostasis and protein quality control, Proc Natl Acad Sci U S A, 2010;107:5851-5856.
[20] Breslow, DK, Collins, SR, Bodenmiller, B, et al., Orm family proteins mediate sphingolipid homeostasis, Nature, 2010;463:1048-1053.
[21] Galanter, J, Choudhry, S, Eng, C, et al., ORMDL3 gene is associated with asthma in three ethnically diverse populations, Am J Respir Crit Care Med, 2008;177:1194-1200.
[22] Wu, H, Romieu, I, Sienra-Monge, JJ, et al., Genetic variation in ORM1-like 3 (ORMDL3) and gasdermin-like (GSDML) and childhood asthma, Allergy, 2009;64:629-635.
[23] Moffatt, MF, Gut, IG, Demenais, F, et al., A large-scale, consortium-based genomewide association study of asthma, N Engl J Med, 2010;363:1211-1221.
[24] Toncheva, AA, Potaczek, DP, Schedel, M, et al., Childhood asthma is associated with mutations and gene expression differences of ORMDL genes that can interact, Allergy, 2015;70:1288-1299.

[25] Kiefer, K, Carreras-Sureda, A, Garcia-Lopez, R, et al., Coordinated regulation of the orosomucoid-like gene family expression controls de novo ceramide synthesis in mammalian cells, J Biol Chem, 2015;290:2822-2830.
[26] Siow, DL and Wattenberg, BW, Mammalian ORMDL proteins mediate the feedback response in ceramide biosynthesis, J Biol Chem, 2012;287:40198-40204.
[27] Siow, D, Sunkara, M, Morris, A, et al., Regulation of de novo sphingolipid biosynthesis by the ORMDL proteins and sphingosine kinase-1, Advances in biological regulation, 2015;57:42-54.
[28] Zhakupova, A, Debeuf, N, Krols, M, et al., ORMDL3 expression levels have no influence on the activity of serine palmitoyltransferase, FASEB J, 2016;30:4289-4300.
[29] Ono, JG, Worgall, TS and Worgall, S, 17q21 locus and ORMDL3: an increased risk for childhood asthma, Pediatr Res, 2014;75:165-170.
[30] Debeuf, N, Haspeslagh, E, van Helden, M, et al., Mouse Models of Asthma, Curr Protoc Mouse Biol, 2016;6:169-184.
[31] Miller, M, Rosenthal, P, Beppu, A, et al., Oroscomucoid like protein 3 (ORMDL3) transgenic mice have reduced levels of sphingolipids including sphingosine-1-phosphate and ceramide, J Allergy Clin Immunol, 2017;139:1373-1376 e1374.
[32] Oyeniran, C, Sturgill, JL, Hait, NC, et al., Aberrant ORM (yeast)-like protein isoform 3 (ORMDL3) expression dysregulates ceramide homeostasis in cells and ceramide exacerbates allergic asthma in mice, J Allergy Clin Immunol, 2015;136:1035-1046 e1036.
[33] Lim, LS, Mitchell, P, Seddon, JM, et al., Age-related macular degeneration, Lancet, 2012;379:1728-1738.
[34] Zajac-Pytrus, HM, Pilecka, A, Turno-Krecicka, A, et al., The Dry Form of Age-Related Macular Degeneration (AMD): The Current Concepts of Pathogenesis and Prospects for Treatment, Adv Clin Exp Med, 2015;24:1099-1104.
[35] Curcio, CA, Johnson, M, Rudolf, M, et al., The oil spill in ageing Bruch membrane, Br J Ophthalmol, 2011;95:1638-1645.
[36] Curcio, CA, Presley, JB, Malek, G, et al., Esterified and unesterified cholesterol in drusen and basal deposits of eyes with age-related maculopathy, Exp Eye Res, 2005;81:731-741.
[37] Phillips, MC, Molecular mechanisms of cellular cholesterol efflux, J Biol Chem, 2014;289:24020-24029.
[38] Iacovelli, J, Zhao, C, Wolkow, N, et al., Generation of Cre transgenic mice with postnatal RPE-specific ocular expression, Invest Ophthalmol Vis Sci, 2011;52:1378-1383.
[39] Westerterp, M, Gourion-Arsiquaud, S, Murphy, AJ, et al., Regulation of hematopoietic stem and progenitor cell mobilization by cholesterol efflux pathways, Cell Stem Cell, 2012;11:195-206.
[40] Palczewski, K, Retinoids for treatment of retinal diseases, Trends Pharmacol Sci, 2010;31:284-295.

# 6 Conclusion and Outlook

In this work, we used liquid chromatography (LC) and mass spectrometry (MS) techniques to elucidate the structure of 1-deoxysphingosine, unravel the metabolism of 1-deoxymethsphingolipid, evaluated the turbulent flow chromatography for online extraction of sphingolipids and developed an LC-$MS^2$ method for the comprehensive analysis of the sphingolipidome covering regular sphingolipids (SL) but also minor and atypical sphingolipid species.

We showed, that the double bond position of native 1-deoxysphingosine (1-deoxySO) is at (14*Z*) position and not at (4*E*) like in canonical sphingosine, indicating that the metabolism of 1-deoxySO is distinct from the canonical sphingosine pathway. Further investigations need to be done to identify and characterize the responsible enzyme, which introduces the double bond in 1-deoxySO, but presumably also the second double bond in sphingadiene, a di-unsaturated downstream metabolite of sphingosine, containing an (4*E*) and (14*Z*) double bonds [1]. This provides novel insights into lipid metabolism and opens new possibilities for treatment for patients with HSAN1 or diabetes type 2, as the 1-deoxysphingolipid metabolism can possibly be targeted without affecting the canonical pathway [2-8].

This different location of the double bond in 1-deoxySO must be considered in the study of 1-deoxysphingolipids (1-deoxySL) in different contexts. In any case the accurate analysis of 1-deoxySL is mandatory, as commercially available 1-deoxySO, but also the corresponding 1-deoxyceramides contain a (4*E*) double bond rather than a (14*Z*) double bond. These two backbones have different biological effects in cell culture, but also behave differently upon LC-$MS^2$ analysis [9, 10].

After finding some differences in the metabolism of L-alanine based 1-deoxySL, we also investigated the metabolism of glycine based 1-deoxymethylsphingolioids (1-deoxymethylSL). This other group of atypical sphingolipids was found in human plasma and is also elevated in the context of HSAN1. However 1-deoxymethylSL were not studied in

detail so far and assumed to follow the pathway of either L-serine or atypical L-alanine based sphingolipids [8].

Although the metabolism of the three different amino acid based sphingolipids starts with the condensation of palmitoyl-CoA with L-serine, L-alanine or glycine by the enzyme serine-palmitoyl-transferase (SPT) [11, 12], we found several different branching points within the metabolic pathways for the different sphingolipids. After the formation of the initial sphingoid backbone, sphinganine, which can be N-acetylated to dihydroceramide [10], we found differences in the further desaturation to ceramide by dihydrosphingosine desaturase. For L-serine and glycine based sphingolipids, the desaturation at (4*E*) or (3*E*) respectively over DES1/2 is possible, which leads to the second major sphingoid backbone sphingosine [13]. For L-alanine based 1-deoxySL, we showed that, this desaturation does not occur, but a double bond is introduced at (14*Z*) by another different enzyme [14]. This reaction also occurs for L-serine or glycine based sphingolipids, but seems to be an alternative pathway of secondary desaturation for these lipids. Further, we showed, that the major downstream metabolite of 1-deoxymethylSA is a di-hydroxylated 1-deoxymethylSA species, which was not known before, and therefore, never quantified in any (disease) condition. This needs further investigation, as the role of this lipid in HSAN1 might have been underestimated so far [2-8].

In the second part of this doctoral work, we developed and validated a comprehensive LC-$MS^2$ method with automated online extraction for comprehensive and fast analysis of sphingolipids including the atypical ones, as well as other classes of lipids.

We showed that a turbo flow column for online extraction of lipids from biological samples is of limited use, as the online extraction showed poor recovery (12.0% to 93% for different lipid classes compared to Bligh and Dyer). We further compared a newly published single-phase extraction protocol using methyl-tert-buthyl-ether / methanol / chloroform (MMC) [17], which showed less variance at equal recovery rates for the different sphingolipid classes, also covering very low abundant sphingolipids. The need for protein precipitation with an organic solvent prior to online extraction with turbulent flow makes the manual extraction effort more

time-consuming and almost comparable to those of single-phase extraction procedures like the MMC protocol. In conclusion, the TLX extraction for lipidomics analysis is not advantageous compared to other, more established protocols. Therefore, the single phase MMC protocol was implemented for sphingolipidomics studies in this work.

We developed an LC-$MS^2$ method with data dependent acquisition to detect and quantify different groups of sphingolipids, including free sphingoid bases, S1P, ceramides, hexosylceramides and sphingomyelins, but also the low abundant 1-deoxysphingolipids. Further, we demonstrated, that also the C30 column retains glycerophospholipids, free cholesterol and cholersteryl esters and that also these classes can be separated with the developed LC conditions. Also these lipid classes show a linear correlation between concentration and signal intensity. Additionally, also neutral glycerolipids and free fatty acids were separated by the developed method.

For a validation the entire method was applied to various kinds of samples. Lipid profiles were analysed by LC-$MS^2$, lipid species identified by the library and finally semi-automatically quantified in a broad range of samples, including plasma samples of patients and knockout mice as well as tissues and cells. The lipid profiles helped to better understand disease mechanisms, in a neuropathy caused by rare mutations in sphingosine-1-phosphate lyase or in a murine AMD model generated by knock-out of ABCA1 and ABCG1 in the retinal pigment epithelium, get more insights into the regulation of sphingolipid metabolism by ORMDL3, or gastric bypass surgery.

For a further focus on low abundant and rather atypical lipids, the method could be extended with a targeted acquisition list of atypical lipid species as addition to the data dependent acquisition, which manly covers more abundant species. As many published sphingolipidomic methods mostly cover just the high abundant species, a specific focus on low abundant species reveals new insights in lipid metabolism. The method, therefore, offers a universal tool to analyse the lipid profile for high but also low abundant species in a high throughput setting and allows addressing many research questions.

## 6.1 References

[1] Renkonen, O and Hirvisalo, EL, Structure of plasma sphingadienine, J Lipid Res, 1969;10:687-693.
[2] Mwinyi, J, Bostrom, A, Fehrer, I, et al., Correction: Plasma 1-deoxysphingolipids are early predictors of incident type 2 diabetes mellitus, PLoS One, 2017;12:e0179313.
[3] Bertea, M, Rutti, MF, Othman, A, et al., Deoxysphingoid bases as plasma markers in Diabetes mellitus, Lipids Health Dis, 2010;9:84.
[4] Zuellig, RA, Hornemann, T, Othman, A, et al., Deoxysphingolipids, novel biomarkers for type 2 diabetes, are cytotoxic for insulin-producing cells, Diabetes, 2014;63:1326-1339.
[5] Othman, A, Bianchi, R, Alecu, I, et al., Lowering plasma 1-deoxysphingolipids improves neuropathy in diabetic rats, Diabetes, 2015;64:1035-1045.
[6] Kramer, R, Bielawski, J, Kistner-Griffin, E, et al., Neurotoxic 1-deoxysphingolipids and paclitaxel-induced peripheral neuropathy, FASEB J, 2015;29:4461-4472.
[7] Othman, A, Rutti, MF, Ernst, D, et al., Plasma deoxysphingolipids: a novel class of biomarkers for the metabolic syndrome?, Diabetologia, 2012;55:421-431.
[8] Penno, A, Reilly, MM, Houlden, H, et al., Hereditary sensory neuropathy type 1 is caused by the accumulation of two neurotoxic sphingolipids, J Biol Chem, 2010;285:11178-11187.
[9] Alecu, I, Othman, A, Penno, A, et al., Cytotoxic 1-deoxysphingolipids are metabolized by a cytochrome P450-dependent pathway, J Lipid Res, 2017;58:60-71.
[10] Duan, J and Merrill, AH, Jr., 1-Deoxysphingolipids Encountered Exogenously and Made de Novo: Dangerous Mysteries inside an Enigma, J Biol Chem, 2015;290:15380-15389.
[11] Weiss, B and Stoffel, W, Human and murine serine-palmitoyl-CoA transferase--cloning, expression and characterization of the key enzyme in sphingolipid synthesis, Eur J Biochem, 1997;249:239-247.
[12] Hanada, K, Hara, T, Nishijima, M, et al., A mammalian homolog of the yeast LCB1 encodes a component of serine palmitoyltransferase, the enzyme catalyzing the first step in sphingolipid synthesis, J Biol Chem, 1997;272:32108-32114.
[13] Ternes, P, Franke, S, Zahringer, U, et al., Identification and characterization of a sphingolipid delta 4-desaturase family, J Biol Chem, 2002;277:25512-25518.
[14] Steiner, R, Saied, EM, Othman, A, et al., Elucidating the chemical structure of native 1-deoxysphingosine, J Lipid Res, 2016;57:1194-1203.
[15] Folch, J, Lees, M and Sloane Stanley, GH, A simple method for the isolation and purification of total lipides from animal tissues, J Biol Chem, 1957;226:497-509.
[16] Bligh, EG and Dyer, WJ, A rapid method of total lipid extraction and purification, Can J Biochem Physiol, 1959;37:911-917.
[17] Pellegrino, RM, Di Veroli, A, Valeri, A, et al., LC/MS lipid profiling from human serum: a new method for global lipid extraction, Anal Bioanal Chem, 2014;406:7937-7948.

# 7 Acknowledgements

First of all I would like to thank Prof. Arnold von Eckardstein for allowing me to work in this lab at IKC. Thank you for your support, helpful feedback and advices throughout my PhD.

I am very grateful to my supervisor, Prof. Thorsten Hornemann, for the trust, openness, and enthusiasm that made this project possible. Thank you for giving me both the freedom and confidence to follow own ideas and the guidance to bring the project to a fruitful end.

I would also like to thank my committee members Prof. Michael Arand, Prof. Bruno Stieger and Prof. Nicola Zamboni and for their interest, helpful discussions, and support throughout the duration of my PhD.

Big thanks to all people in the lab who accompanied me during these years in the lab, for the great time we spent together both inside and outside the lab. This includes (in alphabetical order) Irina Alecu, Heiko Bode, Victoria Gruber, Simona Illev, Gergely Karsai, Museer Lone, Alaa Othman, Nina Steffen, Saranya Suriyanarayanan, Iryna Sutter, Yu Wei and Assem Zhakupova.

I would also like to say thanks to the other members of the IKC of the WAGI first floor: Lucia Rohrer, Vidya Velagapudi, Paolo Zanoni, Katrin Gebert, Silvija Radosavljevic, Anton Potapenko, Mustafa Yalcinkaya, Grigorios Panteloglou, Reda Hasballa, Hans Reiser, and Andrea Jäger. Thank you for the fun times we had, all the eating, joking, but also discussions and inputs during my PhD time.

I am very grateful to all my friends, but especially to my family, for all their love, time, care, support, and that they make me believe in myself and the gave me the confidence that I can reach everything in life.